

**Contribution of the tricellular tight junction
proteins, tricellulin and angulin-1,
to paracellular water permeability**

Inaugural-Dissertation
to obtain the academic degree
Doctor rerum naturalium (Dr. rer. nat.)

submitted to the Department of Biology, Chemistry, Pharmacy
of Freie Universität Berlin

by

Carlos Mario Ayala Torres

2020

The present thesis was performed at the Charité - Universitätsmedizin Berlin at the Institut für Klinische Physiologie under the supervision of Seniorprofessor Dr. med. Michael Fromm, Univ.-Prof. Dr. med. Jörg-Dieter Schulzke, and Priv.-Doz. Dr. rer. medic. Rita Rosenthal from October 2017 to December 2020.

1st reviewer: Seniorprofessor Dr. med. Michael Fromm

2nd reviewer: Prof. Dr. med. Rudolf Tauber

Date of defense: April 29th, 2021

To my parents and my sister

Acknowledgment

I would like to express my deepest appreciation to Seniorprofessor Dr. med. Michael Fromm and Univ.-Prof. Dr. med. Jörg Schulzke, my research supervisors. Thank you both for giving me the opportunity to be part of your research group.

I would like to express my deep gratitude to Dr. med. Michael Fromm, who convincingly guided and encouraged me to be professional and do the right thing even when the road got tough. Without his persistent help, the goal of this project would not have been realized. I would also like to extend my deepest gratitude to Dr. med. Jörg Schulzke for his valuable and constructive suggestions during the planning and development of this research work. His willingness to give his time so generously has been very much appreciated.

I am extremely grateful to Priv.-Doz. Dr. rer. medic. Rita Rosenthal, who was always there whenever I ran into a trouble spot or had a question about my research or writing. She consistently allowed this thesis to be my own work but steered me in the right direction whenever she thought I needed it. I will always carry you in my heart.

I would like to extend my sincere thanks to my supervisor of the Freie Universität Prof. Dr. med. Rudolf Tauber for his kind willingness to provide his expert opinion during the development of this thesis and for his participation in all thesis committee meetings, which were very valuable.

I would also like to extend my gratitude to Priv.-Doz. Dr. rer. nat. Susanne Krug, our meetings and conversations were vital in inspiring me to think outside the box, from multiple perspectives to perform a comprehensive and objective research. Furthermore, I would like to thank Prof. Dr. rer. nat. Dorothee Günzel and Priv.-Doz. Dr. rer. nat. Jörg Piontek for their excellent support and responsiveness in both academic and personal matters during the running of this project.

I would like to acknowledge my colleagues from the first and second cohort of PhD students of the GRK 2318 "TJ-Train" for their wonderful collaboration and support. My

special thanks to these wonderful friends and women scientists: Laura-Sophie Beier, Danielle Cardoso da Silva, Deborah Delbue, Carolin Grünhagen, Fábía Daniela Lobo da Fonseca de Sá, Jia-Chen E. Hu, and Caroline Hempel.

I would also like to extend my thanks to the principal investigators and technicians of the Institut für Klinische Physiologie for their help in offering me the resources to carry out this investigation. I am particularly grateful for the assistance given by Britta Jebautzke, In-Fah M. Lee, and Anja Fromm.

The contribution of the DFG (GRK 2318 “TJ-Train”, project A3) is truly appreciated. Without their support and funding, this project could not have reached its goal.

I wish to acknowledge the support and great love of my family, my father, Cesar Ayala; my mother, Maritza Torres; and my sister, Fernanda Ayala Torres. They kept me going on and this work would not have been possible without their involvement. In addition, I would like to thank Erik Skarle and his wonderful family for their love, patience and support. Finally, I could not have completed this dissertation without the encouragement of my best friends, Deborah Delbue, Danielle Cardoso da Silva, Alejandra Arias Salazar, Edgar Dolores, Andrea Chiappe Pulido, Ronald Gonzalez, Laura Carolina Pardo, Felix Wald, Caterin Arevalo, Paola Alejandra Pulido, Andres Felipe León, Lorena Novoa Aponte, and Sandra Milena Chingate, who provided stimulating discussions as well as happy distractions to rest my mind outside of my research.

Abstract

In epithelia, large amounts of water pass by transcellular and paracellular pathways, driven by the osmotic gradient built up by solutes' movement. The transcellular pathway has been molecularly characterized by the discovery of aquaporin membrane channels. Unlike this, the existence of a paracellular pathway for water through the tight junctions (TJ) was discussed controversially for many years until two molecular components of paracellular water transport, claudin-2, and claudin-15, were identified.

A main protein of the tricellular TJ (tTJ), tricellulin, was shown to be downregulated in ulcerative colitis leading to increased permeability to macromolecules. In addition to tricellulin, the family of angulin proteins is known to be able to recruit tricellulin to the tTJ. Recently, Gong and colleagues found that angulin-2 knockout increases water transport on isolated mouse kidney tubules, and its overexpression reduces the water transport in MDCK II cells. Whether or not tricellulin regulates water transport or angulin-1 also mediates a direct effect on water permeability independent of tricellulin, or act indirectly via tricellulin regulation, is unknown yet.

To answer our research question, two epithelial cell lines featuring properties of the tight and intermediate-tight epithelium, MDCK C7 and HT-29/B6, respectively, were stably transfected with shRNA targeting tricellulin or sgRNA along with CRISPR/Cas9 targeting angulin-1, proteins of the tTJ essential for the barrier against passage of solutes up to 10 kDa. Interestingly, tricellulin knockdown and angulin-1 knockout reduced the transepithelial resistance (TER) in both cell lines and increased 4-kDa FITC-dextran permeability, especially in HT-29/B6 cell line. In addition, the expression and location of different TJ proteins in control cells and in knockdown or knockout clones were investigated. In MDCK C7 cells, tricellulin knockdown and angulin-1 knockout downregulated the expression of some tight junction proteins, while on HT-29/B6 cells, the opposite effect was observed; some TJ proteins were upregulated.

Finally, water flux was induced by osmotic gradients using mannitol, 4-kDa, and 40-kDa dextran or albumin and measured in both cell lines. In MDCK C7 cells, tricellulin knockdown and angulin-1 knockout increased the water flux compared to that of vector

controls, indicating a direct role of tricellulin in regulating water permeability in a tight epithelial cell line; nevertheless, in HT-29/B6 cells, water flux was unchanged between the control and the tricellulin knockdown or angulin-1 knockout clones. We conclude that tricellulin and angulin-1, the latter acting indirectly via tricellulin displacement, increase water permeability at reduced expression only in MDCK C7 cells, i.e., in the tight epithelium.

Zusammenfassung

In Epithelien werden große Wassermengen über transzelluläre und parazelluläre Wege transportiert, angetrieben durch den osmotischen Gradienten, der durch die Bewegung der gelösten Stoffe aufgebaut wird. Der transzelluläre Weg ist durch die Entdeckung der Aquaporin-Membrankanäle molekular charakterisiert worden. Im Gegensatz dazu wurde die Existenz eines parazellulären Weges für Wasser durch die Tight Junctions (TJ) viele Jahre lang kontrovers diskutiert, bis zwei molekulare Komponenten des parazellulären Wassertransports, Claudin-2 und Claudin-15, identifiziert wurden.

Es wurde gezeigt, dass ein Hauptprotein der trizellulären TJ (tTJ), Tricellulin, bei Colitis ulcerosa herunterreguliert ist, was zu einer erhöhten Permeabilität für Makromoleküle führt. Zusätzlich zu Tricellulin ist bekannt, dass die Familie der Angulin-Proteine in der Lage ist, Tricellulin an die tTJ zu rekrutieren. Kürzlich fanden Gong und Kollegen, dass der Knockout von Angulin-2 den Wassertransport an isolierten Nierentubuli der Maus erhöht und seine Überexpression den Wassertransport in MDCK II-Zellen reduziert. Ob Tricellulin den Wassertransport reguliert oder Angulin-1 auch einen direkten, von Tricellulin unabhängigen Effekt auf die Wasserpermeabilität vermittelt, oder indirekt über die Tricellulin-Regulation wirkt, ist noch nicht bekannt.

Zur Beantwortung unserer Forschungsfrage wurden zwei Epithelzelllinien mit Eigenschaften des tighten und intermediär-tight Epithels, MDCK C7 bzw. HT-29/B6, stabil mit shRNA, die auf Tricellulin abzielt, oder sgRNA zusammen mit CRISPR/Cas9, die auf Angulin-1 abzielt, transfiziert, Proteine der tTJ, die für die Barriere gegen die Passage von gelösten Stoffen bis zu 10 kDa essentiell sind. Interessanterweise reduzierte das Knockdown von Tricellulin und Angulin-1 die TER in beiden Zelllinien und erhöhte die 4-kDa-FITC-Dextran-Permeabilität, insbesondere in der HT-29/B6-Zelllinie. Zusätzlich wurden die Expression und Lokalisation verschiedener TJ-Proteine in Kontrollzellen und in Knockdown- bzw. Knockout-Klonen untersucht. In MDCK-C7-Zellen wurde durch Tricellulin-Knockdown und Angulin-1-Knockout die Expression einiger Tight-Junction-Proteine herunterreguliert, während in HT-29/B6-Zellen der gegenteilige Effekt beobachtet wurde; einige TJ-Proteine wurden hochreguliert.

Schließlich wurde der Wasserfluss durch osmotische Gradienten mit Mannitol, 4-kDa- und 40-kDa-Dextran oder Albumin induziert und in beiden Zelllinien gemessen. In MDCK-C7-Zellen erhöhten Tricellulin-Knockdown und Angulin-1-Knockout den Wasserfluss im Vergleich zu den Vektor-Kontrollen, was auf eine direkte Rolle von Tricellulin bei der Regulierung der Wasserpermeabilität in einer dichten Epithelzelllinie hinweist; in HT-29/B6-Zellen war der Wasserfluss zwischen der Kontrolle und den Tricellulin-Knockdown- oder Angulin-1-Knockout-Klonen jedoch unverändert. Wir schlussfolgern, dass Tricellulin und Angulin-1, wobei letzteres indirekt über die Tricellulin-Verdrängung wirkt, die Wasserpermeabilität bei reduzierter Expression nur in MDCK-C7-Zellen, d.h. im tighten Epithel, erhöhen.

Table of contents

List of figures	XVII
List of tables	XIX
List of abbreviations	XXI
1. Introduction	23
1.1 Epithelium	23
1.2 Transport across epithelia	23
1.2.1 Transcellular pathway	24
1.2.2 Paracellular pathway	24
1.3 The tight junction (TJ)	25
1.3.1 Protein components of the TJ	25
1.3.2 Morphology of the bicellular tight junction (bTJ)	26
1.3.2.1 Claudins	27
1.3.2.2 Occludin	28
1.3.2.3 MarvelD3	29
1.3.2.4 Junctional adhesion molecules (JAM)	29
1.3.3 Morphology of the tricellular tight junction (tTJ)	29
1.3.3.1 Tricellulin	30
1.3.3.2 Angulin protein family	32
1.3.4 Adjacent tight-junctional proteins	32
1.4 Barrier properties: resistance, flux, and selective permeability	33
1.4.1 Electrical resistance, “leaky” and “tight” epithelia	33
1.4.2 Charge selectivity	35
1.4.3 Size selectivity	36
1.4.3.1 Paracellular pore pathway	36
1.4.3.2 Paracellular leak pathway	37
1.5 Water transport across the epithelia	41
1.5.1 Transcellular water pathway	41
1.5.1.1 Aquaporin channels	41
1.5.1.2 Urea transporter B	43
1.5.1.3 Cotransporters	44
1.5.2 Paracellular water pathway	45
1.5.2.1 Bicellular tight junction	46
1.5.2.2 Tricellular tight junction	48
1.5.3 Interaction between transcellular and paracellular water transport pathways	49
1.6 Purpose and objectives	50
1.6.1 Effect of the tricellular tight junction on paracellular water transport	51
2. Materials and methods	53
2.1 Materials	53
2.1.1 Devices	53

2.1.2	Consumable supplies	55
2.1.3	Chemicals and kits	56
2.1.4	Cultivation media	58
2.1.5	Buffers and solutions	58
2.1.6	Plasmids	60
2.1.7	Antibodies	62
2.1.8	Cell lines	65
2.1.9	Software	65
2.2	Cell biological methods	66
2.2.1	Cell culture	66
2.2.2	Transfection of cells	66
2.2.2.1	shRNA plasmids	67
2.2.2.2	sgRNA, CRISPR/Cas9, and HDR plasmids	68
2.2.3	Cryopreservation and thawing of cells	69
2.2.4	Cell passage	70
2.2.5	Immunofluorescence labeling and microscopy	70
2.2.6	Topology measurements	71
2.2.7	Freeze-fracture electron microscopy	72
2.3	Biochemical methods	72
2.3.1	Preparation of cell lysates	72
2.3.2	Determination of the protein concentration	72
2.3.3	Sodium dodecyl sulfate-polyacrylamide gel electrophoresis (SDS-PAGE)	73
2.3.4	Western blotting	73
2.4	Biophysical methods	74
2.4.1	Transepithelial electrical resistance measurements	74
2.4.2	Dilution potential measurements	74
2.4.3	Measurement of 4-kDa FITC-dextran flux	75
2.4.4	Measurement of transepithelial water transport	76
2.5	Statistics	78
3.	Results	81
3.1	Tricellulin knockdown (KD): MDCK C7 cells	81
3.1.1	Characterization of tricellulin KD in MDCK C7 cells	81
3.1.1.1	Effect on the transepithelial resistance (TER)	83
3.1.1.2	Analysis of permeability for sodium and chloride	84
3.1.1.3	Measurement of macromolecule permeability (4-kDa FITC-dextran)	85
3.1.2	Effects of tricellulin KD on endogenous proteins of MDCK C7 cells	86
3.1.3	Effects of tricellulin KD on the localization of other tight junction proteins	88
3.1.4	Effect of tricellulin KD on transepithelial water transport in MDCK C7 cells	90
3.2	Tricellulin knockdown (KD): HT-29/B6 cells	94
3.2.1	Characterization of tricellulin KD in HT-29/B6 cells	94
3.2.1.1	Effect on the transepithelial resistance	96
3.2.1.2	Analysis of permeability for sodium and chloride	96
3.2.1.3	Measurement of macromolecule permeability (4-kDa FITC-dextran)	97
3.2.2	Effects of tricellulin KD on other proteins of HT-29/B6 cells	98

3.2.3	Effects of tricellulin KD on the localization of other tight junction proteins of HT-29/B6 cells _____	100
3.2.4	Effect of tricellulin KD on transepithelial water transport in HT-29/B6 cells _____	103
3.3	Angulin-1 knockout (KO): MDCK C7 cells _____	106
3.3.1	Characterization of angulin-1 KO in MDCK C7 cells _____	106
3.3.1.1	Effect on the transepithelial resistance and macromolecule permeability _____	109
3.3.2	Effects of angulin-1 KO on other proteins of MDCK C7 cells _____	110
3.3.3	Effects of angulin-1 KO on tricellulin protein localization _____	112
3.3.4	Effect of angulin-1 KO on the ultrastructure of MDCK C7 cells _____	114
3.3.5	Effect of angulin-1 KO on transepithelial water transport in MDCK C7 cells _____	120
3.4	Angulin-1 knockout (KO): HT-29/B6 cells _____	124
3.4.1	Characterization of angulin-1 KO in HT-29/B6 cells _____	124
3.4.1.1	Effect on the transepithelial resistance and macromolecule permeability _____	126
3.4.2	Effects of angulin-1 KO on other proteins of HT-29/B6 cells _____	128
3.4.3	Effects of angulin-1 KO on tight junction protein localization _____	130
3.4.4	Effect of angulin-1 KO on the ultrastructure of HT-29/B6 cells _____	132
3.4.5	Effect of angulin-1 KO on transepithelial water transport in HT-29/B6 cells _____	136
4.	<i>Discussion</i> _____	139
4.1	Tricellulin _____	139
4.1.1	Tricellulin knockdown alters the expression and localization of tight junction proteins in MDCK C7 and HT-29/B6 cells _____	140
4.1.2	Tricellulin knockdown increases the ion permeability in MDCK C7 and HT-29/B6 cells _____	141
4.1.3	Tricellulin knockdown increases the macromolecule passage in MDCK C7 and HT-29/B6 cells _____	142
4.1.4	Water transport as driven by different osmotic gradients _____	143
4.1.5	Tricellulin knockdown increases transepithelial water transport only in MDCK C7 cells _____	145
4.2	Angulin-1/LSR _____	148
4.2.1	Angulin-1 knockout alters the expression and localization of other proteins in MDCK C7 and HT-29/B6 cells _____	148
4.2.2	Angulin-1 knockout did not alter the ultrastructure of the bicellular tight junction in MDCK C7 and HT-29/B6 cells _____	150
4.2.3	Angulin-1 knockout increases the ion permeability in MDCK C7 and HT-29/B6 cells _____	151
4.2.4	Angulin-1 knockout increases the macromolecule permeability only in HT-29/B6 cells _____	152
4.2.5	Angulin-1 knockout increases transepithelial water transport only in MDCK C7 cells _____	154
5.	<i>Conclusion and outlook</i> _____	157
6.	<i>References</i> _____	161
7.	<i>Appendices</i> _____	169
7.1	Appendix A: Tricellulin and angulin-1 expression (control cells) _____	169

7.2	Appendix B: Numerical data	171
7.3	Appendix C: Topology data	175
7.4	Appendix D: List of publications	183
7.4.1	Scientific articles	183
7.4.2	Presentations at scientific conferences	183
	<i>Declaration of Authorship</i>	185

List of figures

Figure 1-1. Transepithelial transport pathways and intercellular junctions..	24
Figure 1-2. The claudin family of transmembrane proteins.....	26
Figure 1-3. Tricellulin and angulin family proteins	30
Figure 1-4. Flow across a leaky and tight epithelium.....	35
Figure 1-5. A paracellular solute's view of a hypothetical tight junction comprising various claudins in homotypic and heterotypic interactions	36
Figure 1-6. Size selectivity in MDCK II, ZO-1/ZO-2 dKO, claudin quinKO, JAM-A KO, and claudin/JAM-A KO cells.....	38
Figure 1-7. Tricellulin as a regulator of the paracellular leak pathway.....	40
Figure 1-8. Distribution of aquaporins in the digestive system	42
Figure 1-9. Expression and localization of AQPs in the kidney.	43
Figure 2-1. Method for analyzing transepithelial water transport.	78
Figure 3-1. Expression and localization of tricellulin in MDCK C7 control and knockdown cells.	82
Figure 3-2. Functional analysis of tricellulin knockdown in MDCK C7 cells.	83
Figure 3-3. Functional analysis of tricellulin knockdown in MDCK C7 cells.....	85
Figure 3-4. Effect of tricellulin knockdown on permeability for 4-kDa FITC-dextran (FD4).	86
Figure 3-5. Claudin, occludin, angulin, and AQP expression in control and tricellulin knockdown MDCK C7 cells.	88
Figure 3-6. Localization of claudin-1 and claudin-4 in MDCK C7 control and tricellulin KD clones.....	90
Figure 3-7. Water flux in control and tricellulin knockdown MDCK C7 cells stimulated by an osmotic gradient on the apical side and on the basolateral side of the cell layer.....	92
Figure 3-8. Water flux in control and tricellulin knockdown MDCK C7 cells stimulated by an osmotic gradient of 5.5 mM 40-kDa dextran (100 mOsm) on the apical side of the cell layer.	93
Figure 3-9. Expression and localization of tricellulin in HT-29/B6 cells.....	95
Figure 3-10. Functional analysis of tricellulin knockdown in HT-29/B6 cells. Effect of tricellulin knockdown on transepithelial resistance.....	96
Figure 3-11. Functional analysis of tricellulin knockdown in HT-29/B6 cells. Effect of tricellulin knockdown on permeability for Na ⁺ and Cl ⁻	97
Figure 3-12. Functional analysis of tricellulin knockdown in HT-29/B6 cells. Permeability to 4-kDa FITC-dextran in control cells and tricellulin knockdown clones.....	98
Figure 3-13. Angulin, occludin, claudin, and AQP expression in control and tricellulin knockdown HT-29/B6 cells.....	100
Figure 3-14. Immunofluorescent staining of claudin-2, claudin-3 and angulin-1 in HT-29/B6 control and tricellulin KD cells.	103
Figure 3-15. Water flux in control and tricellulin knockdown HT-29/B6 cells stimulated by an osmotic gradient.	104
Figure 3-16. Water flux in control and tricellulin knockdown HT-29/B6 cells stimulated by an osmotic gradient of 2.5 mM albumin on the apical side of the cell layer.	105
Figure 3-17. Expression and localization analysis of angulin-1 in control and angulin-1 KO MDCK C7 cells	108
Figure 3-18. Functional analysis of angulin-1 knockout in MDCK C7 cells.....	110
Figure 3-19. Angulin family proteins, tricellulin, occludin, claudins, and AQP expression in angulin-1 knockout MDCK C7 cells.....	112
Figure 3-20. Effects of angulin-1 knockout on the localization of tricellulin and occludin.	114
Figure 3-21. Freeze-fracture electron microscopy of angulin-1 knockout MDCK C7 cells.....	116
Figure 3-22. Morphometric analysis of TJ ultrastructure of angulin-1 knockout MDCK C7 cells.	119
Figure 3-23. Water flux in angulin-1 knockout MDCK C7 cells.....	121
Figure 3-24. Partial characterization of an angulin-1 knockout MDCK C7 clone with a reduction in the expression of tricellulin.	123
Figure 3-25. Expression and localization of angulin-1 knockout in HT-29/B6 cells.....	125
Figure 3-26. Functional analysis of angulin-1 knockout in HT-29/B6 cells.....	127

Figure 3-27. Angulin, tricellulin, occludin, claudin, and AQP expression in angulin-1 knockout HT-29/B6 cells.....	130
Figure 3-28. Localization of TJ proteins in angulin-1 knockout HT-29/B6 cells. Immunofluorescence analyses of HT-29/B6 control and angulin-1 KO cells.....	132
Figure 3-29. Freeze-fracture electron microscopy. Photos were taken at x51000; Bars: 200 nm.	133
Figure 3-30. Morphometric analysis of TJ ultrastructure of angulin-1 knockout HT-29/B6 cells.	136
Figure 3-31. Water flux in angulin-1 knockout HT-29/B6 cells stimulated by an osmotic gradient	137
Figure 4-1. Water flux as a function of the level of tricellulin expression in MDCK C7 cells driven by an osmotic gradient of 37 mM 4-kDa dextran (100 mOsm).....	146
Figure 4-2. Comparison of angulin-1 knockout effect on permeability for 4-kDa FITC-dextran (FD4) under isosmotic and osmotic gradient conditions	153
Figure 5-1. Synopsis of tricellulin and angulin-1 effects on osmotically driven water transport in HT-29/B6 cells.....	158
Figure 5-2. Synopsis of tricellulin and angulin-1 on osmotically driven water flux in MDCK C7 cells..	159
Figure 5-3. Summarizing scheme of water, ion, and macromolecule passage via the tricellular tight junction on epithelial cell lines with different tightness.....	160
Figure 7-1. Endogenous expression of tricellulin in the epithelial cell lines using in this study.	169
Figure 7-2. Endogenous expression of angulin-1 in the epithelial cell lines using in this study.	170
Figure 7-3. Cell geometry analysis. Neighboring cell analysis in tricellulin knockdown	176
Figure 7-4. Cell geometry analysis. Neighboring cell analysis in angulin-1 knockout.....	178

List of tables

Table 1-1. <i>Water-transport properties of cotransporters, uniporters, and channels.</i>	44
Table 2-1. <i>Devices.</i>	53
Table 2-2. <i>Consumables supplies.</i>	55
Table 2-3. <i>Chemicals and kits.</i>	56
Table 2-4. <i>Cultivation media.</i>	58
Table 2-5. <i>Buffers and solutions.</i>	58
Table 2-6. <i>shRNA plasmids.</i>	60
Table 2-7. <i>sgRNA, CRISPR/Cas9 and HDR plasmids.</i>	61
Table 2-8. <i>Antibodies.</i>	62
Table 2-9. <i>Cell lines.</i>	65
Table 2-10. <i>Osmolality of the HEPES-buffered solutions using a freezing point depression osmometer.</i>	77
Table 3-1. <i>Angulin-1 isoforms and exons that are targeted by the three sgRNA.</i>	106
Table 7-1. <i>Characteristics of MDCK C7 tricellulin knockdown clones and the corresponding controls.</i>	171
Table 7-2. <i>Characteristics of HT-29/B6 tricellulin knockdown clones and the corresponding control.</i>	172
Table 7-3. <i>Characteristics of MDCK C7 angulin-1 knockout clones and the corresponding controls.</i>	173
Table 7-4. <i>Characteristics of HT-29/B6 angulin-1 knockout clones and the corresponding controls.</i>	174
Table 7-5. <i>Morphometric comparison of MDCK C7 and HT-29/B6 cells as models for tight and intermediate-tight epithelia before and after tricellulin knockdown.</i>	175
Table 7-6. <i>Morphometric comparison of MDCK C7 and HT-29/B6 cells as models for tight and intermediate-tight epithelia before and after angulin-1 knockout.</i>	177
Table 7-7. <i>Macros for segmentation of epithelial cells depending on the resolution of the fluorescence images obtained.</i>	179

List of abbreviations

Abbreviations

Abbreviations	Meaning
°C	Degree Celsius
AJ	Adherens junction
Amp	Ampicillin
BSA	Bovine serum albumin
bTJ	Bicellular tight junction
CAR	Coxsackie and adenovirus receptor
Cldn	Claudin
CLMP	CAR-like membrane protein
CRISPR	Clustered regularly interspaced short palindromic repeats
Da	Dalton
DAPI	4', 6'-diamidino-2-phenylindole
Dlg1	Drosophila disc large tumor suppressor
DMEM	Dulbecco's modified eagle's medium
DMSO	Dimethyl sulfoxide
dNTP	Deoxyribonucleotide triphosphate
DTT	Dithiothreitol
ECL	Extracellular loop
EDTA	Ethylenediaminetetraacetic acid
EF	Extracellular fracture-face
ESAM	Endothelial cell-selective adhesion molecule
FD4	4-kDa FITC-dextran
FFEM	Freeze-Fracture Electron Microscopy
FITC	Fluorescein isothiocyanate
HEPES	4-(2-hydroxyethyl)-1-piperazineethanesulfonic acid
JAM	Junctional adhesion molecule
JAM-L	JAM-like protein
KD	Knockdown
KO	Knockout
LSM	Confocal Laser Scanning Microscopy
MDCK C7	Madin-Darby Canine Kidney – Clone 7 Canis lupus familiaris (dog, <i>Canis familiaris</i>) Breed/subspecies: Cocker spaniel
PAGE	Polyacrylamide gel electrophoresis
PBS	Phosphate buffered saline
PCR	Polymerase chain reaction
PSD-95	Post synaptic density protein

P/S	Penicillin–Streptomycin
rpm	Rounds per minute
RPMI 1640	Medium Roswell Park Memorial Institute 1640
RT	Room temperature
SDS	Sodium dodecyl sulfate
shRNA	Short hairpin RNA
STED	Stimulated emission depletion microscopy
TBS-T	Tris saline buffer and tween-20
TC	Tricellular contact
TER	Transepithelial resistance
TEMED	Tetramethylethylenediamine
TJ	Tight junction
TRIC	Tricellulin
tTJ	Tricellular tight junction
wt	Wild type
ZO	Zonula occludens protein

1. Introduction

1.1 Epithelium

Tissue functionality is assured by the accurate regulation of its barriers, i.e., the epithelium and the endothelium (Schnoor and Parkos, 2008). While the endothelium lines the vasculature and ensures tissue supply with nutrients and oxygen, the epithelium creates the barrier between tissues and the outward environment, thus protecting organs from invading damaging agents. Both epithelium and endothelium form a cellular monolayer that is connected and more or less sealed by a junctional complex. The junctional complex consists of tight junctions (TJ) that regulate the permeability of the monolayer and subjacent adherens junctions (AJ) that mediate intercellular adhesive interactions (Ivanov and Naydenov, 2013; Van Itallie and Anderson, 2014) (Figure 1-1d). Epithelial cells also form desmosomes that are located more basally and further strengthen adhesive interactions (Figure 1-1d). All these junctions are composed of several transmembrane proteins and cytosolic adaptor molecules that connect the adhesion molecules to the cytoskeleton. Desmosomes are connected to cytokeratins, whereas TJ and AJ are connected to actin. The connection of TJ and AJ to the actin cytoskeleton is critical for barrier functionality (Garcia-Ponce et al., 2015; Ivanov et al., 2010). In addition, the epithelial membrane acts as a selectively permeable polarized membrane (different proteins in the apical and basolateral membrane), which determines which substances will be able to enter the epithelium (Suzuki, 2013). Therefore, the epithelium allows the absorption of nutrients while providing a physical barrier to the permeation of proinflammatory molecules, such as pathogens, toxins, and antigens, from the luminal environment into the underlying mucosal tissues and circulatory system (Buckley and Turner, 2018).

1.2 Transport across epithelia

The transport of molecules across the epithelial layer occurs through two major pathways: the transcellular pathway (i.e., across the cell membranes and protein carrier/receptor-mediated transport) and the paracellular pathway (i.e., between the spaces through adjacent cells). The sum of both pathways represents total transepithelial transport (Figure 1-1a).

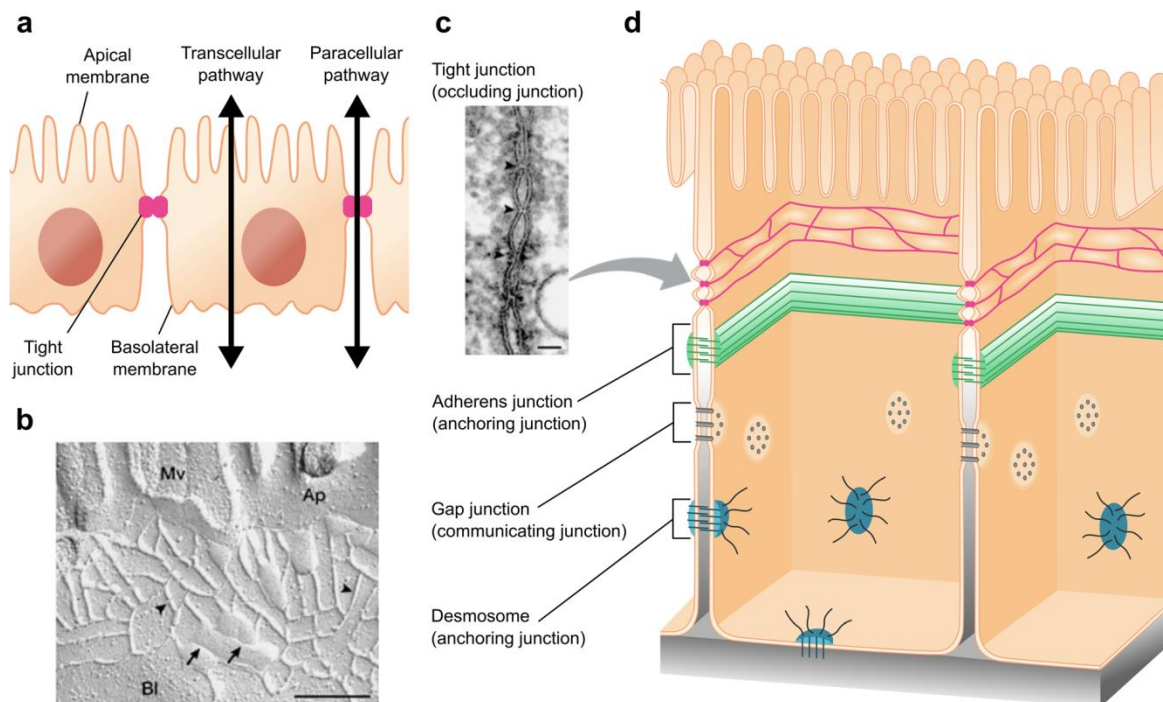


Figure 1-1. Transepithelial transport pathways and intercellular junctions. **(a)** Paracellular and transcellular pathways across an epithelial layer. **(b and c)** Structure and localization of TJ strands, including **(b)** freeze-fracture electron microscopic image (scale bar, 200 nm) and **(c)** ultrathin sectional view (scale bar, 50 nm). Mv: Microvilli; Ap: Apical membrane; Bl: Basolateral membrane. **(d)** Schematic representation of the intercellular space and the junctional protein complex. It was adapted from (Yeste et al., 2018).

1.2.1 Transcellular pathway

The transcellular route for hydrophilic molecules, for example, ions and nutrients including sugars, amino acids, peptides, fatty acids, minerals, and vitamins, is governed by the profile of membrane pumps, carriers, and channels expressed in a particular cell type (Suzuki, 2013). The passive movement across the lipid component of the membrane is limited for uncharged and hydrophilic molecules. The profile of transport proteins differs among epithelia, which explains their unique functions. Individual transporters show a polarized distribution to the apical or basolateral membrane surface as the basis for directional transport (Figure 1-1a) (Anderson and Van Itallie, 2009).

1.2.2 Paracellular pathway

The paracellular pathway is associated with transport through the intercellular space between the adjacent epithelial cells (Figure 1-1a). It is regulated by an apical junctional complex, which is composed of tight junctions (TJs), adherence junctions (AJs), and

desmosomes (Figure 1-1c and 1-1d) (Buckley and Turner, 2018; Suzuki, 2013). The TJs encircle the apical ends of the lateral membranes of epithelial cells (Figure 1-1b and 1-1c), and it is this structure that determines the selective paracellular permeability to solutes and water (Buckley and Turner, 2018; Suzuki, 2013). The AJ, along with desmosomes, provides strong adhesive bonds between the epithelial cells and also aids intercellular communication but does not determine paracellular permeability.

1.3 The tight junction (TJ)

The tight junction provides both a barrier to potentially harmful molecules and a pathway for the permeation of ions, solutes, and water. Paracellular transport through the TJs is passive, driven by electrochemical gradients, and demonstrates channel-like properties such as electric conductance, charge-, and size-selectivity (pore and leak pathways) similar to those found in membrane ion channels (Buckley and Turner, 2018; Suzuki, 2013).

1.3.1 Protein components of the TJ

The tight junction comprises several transmembrane proteins, including claudins, TJ-associated marvel proteins (TAMP), and angulins. Also, the junctional adhesion molecules (JAM) belong to the tight junction, although their barrier function is not fully understood (Günzel and Fromm, 2012). Numerous other proteins are related to or interact with the tight junction like zonula occludens (ZOs), cingulin, and several others, which interact with each other, as well as with the cytoskeleton, and form a complex architecture (Figure 1-2). Only the “true” tight junction proteins are integral membrane proteins that extend into the paracellular spaces between the cells. Cingulin and ZOs are cytoskeletal linker proteins, which interact with the cytoplasmic peripheral membrane proteins, occludin, claudins, and JAMs to form strong cross-links and interact with the membrane cytoskeleton composed of F-actin and myosin (Figure 1-2) (Varadarajan et al., 2019). Together with intracellular signaling proteins, tight junction proteins activate many cellular processes to maintain barrier integrity. Tight junction complexes are the rate-limiting factor for paracellular permeability; they are programmed to quickly open and seal the barrier in the case of damage and additional signals. They form a highly dynamic entity that undergoes a series of regulations to improve or modulate the integrity of the intestinal barrier through the continuous transmission of signals to its individual components

(Chelakkot et al., 2018). There are two types of TJ arrangements, the bicellular tight junction (bTJ) and the tricellular tight junction (tTJ) (Friend and Gilula, 1972).

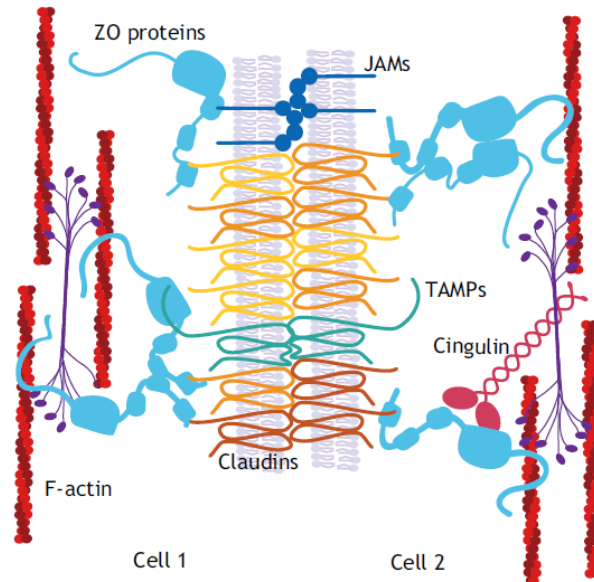


Figure 1-2. The claudin family of transmembrane proteins (yellow and orange), oligomerize into strands and mesh with their counterparts on neighboring cells to selectively regulate passage through the paracellular space. Whereas “pore-forming” claudins facilitate ion flux by forming size- and charge-specific pores, “barrier-forming” claudins primarily restrict it (Günzel and Yu, 2013). Together with claudin strands, junctional adhesion molecules (JAMs, dark blue) also help limit macromolecule flux (Otani et al., 2019). TJ-associated MARVEL proteins (TAMPs, green), such as occludin, tricellulin, and MarvelD3, play various roles in signaling, barrier development, and TJ strand morphology (Raleigh et al., 2010; Krug et al., 2009a; Cording et al., 2013). ZO proteins (light blue) facilitate the formation of a dense plaque of proteins associated with TJs (Otani et al., 2019; Beutel et al., 2019). A ZO protein can multimerize with itself and other ZO proteins and can bind claudins, JAMs, TAMPs, F-actin (red), scaffolding proteins (e.g., cingulin, pink), and signaling molecules (Shen et al., 2011). It was adapted from (Varadarajan et al., 2019).

1.3.2 Morphology of the bicellular tight junction (bTJ)

Key components for the structural and functional properties of the bicellular TJ of mammals are the claudin family, occludin, marvelD3, and junctional adhesion molecules (JAMs) (Anderson and Van Itallie, 2009; Mineta et al., 2011; Günzel and Yu, 2013). All TJ proteins mentioned above, except JAMs, contain four transmembrane domains with N- and C-terminal cytoplasmic tails, two extracellular loops, and a short intracellular loop. Expression of these proteins varies among different tissues, and the pattern of a given set

of claudins determines the properties of the intercellular seal formed by TJ strands (see Chapter 1.4) (Furuse et al., 1999).

1.3.2.1 Claudins

The discovery of claudins in 1998 significantly forward-thinking our understanding of the TJ barrier as it was first demonstrated that claudins have the ability to form strands and confer cell-to-cell adhesion (Tsukita and Furuse, 1998). There are several isoforms of claudin, each having potentially different roles, and a fine balance between them is needed to maintain paracellular integrity. Alterations in the claudin levels can affect the barrier integrity differently depending on the type of claudin isoform (Chelakkot et al., 2018).

Claudins are tetraspan proteins consisting of a family with at least 27 members whose molecular weight ranges from 20 to 28 kDa (Mineta et al., 2011; Overgaard et al., 2011). The claudin proteins are characterized by a conserved amino acid motif in the first extracellular loop (W-GLW-C-C). These first extracellular loops are highly conserved, range from 41 to 55 residues, and appear to contribute to TJ ion selectivity and barrier function. Site-directed mutagenesis of specific residues within the first extracellular loop of claudins can reverse the TJ pore's charge selectivity, while the inclusion of both acidic and basic residues in that region can reduce permeability to both cations and anions. The second loops, which are also highly conserved, range from 10 to 21 residues and appear to be more involved in homotypic and heterotypic adhesion and are also the site of *Clostridium perfringens* enterotoxin binding in claudin-3 and -4 (Colegio et al., 2002; Colegio et al., 2003). The claudin cytoplasmic tails range from 21 to 44 residues and are the least well-conserved regions. Except for claudin-12, all claudin cytoplasmic tails end in PDZ binding motifs, which bind PDZ domains in the cytoplasmic scaffolding proteins ZO-1 and MUPP1, and other proteins. PDZ-mediated interactions of claudins with ZO-1 and ZO-2 are required for efficient delivery to the TJ, although this may not be universally true (Van Itallie and Anderson, 2006).

Leaving aside its structure and talking a little more about its function, it appears that each claudin protein has its unique property of ion permeability: the claudins making paracellular cation channels include claudin-2, -10b, -12, -15, -16, and -21; the claudins

making paracellular anion channels include claudin-4, -7, -8, -10a, and -17 and the barrier-forming claudins include claudin-1, -3, -4, -5, -8, -11, -14, and -19 (Günzel and Fromm, 2012; Günzel and Yu, 2013; Rosenthal et al., 2017b). For claudin-4, -7, -8, and -16, a sealing or channel-forming function has not been unequivocally determined (Heinemann and Schuetz, 2019). Notably, the measurement of claudin permeability depends upon the background of the endogenous claudins expressed in the epithelium. Because the TJ's transport property is determined by the combination of all the claudin proteins present in the cells, studying any individual claudin will need to take into account the permeabilities of the remaining claudins (Anderson and Van Itallie, 2009; Nakamura et al., 2019).

1.3.2.2 Occludin

Although occludin was the first transmembrane TJ component discovered almost three decades ago, its physiological functions' full scope has remained controversial (Furuse et al., 1993). Occludin belongs to the TJ-associated marvel protein (TAMP) family, as well as MarvelD3 and tricellulin, based on their sequence homology within the shared marvel domain (MAL and related proteins for vesicle trafficking and membrane link) (Cording et al., 2013); nonetheless, the three-dimensional structures of TAMPs are unknown. Occludin is a protein with approximately 65 kDa, bearing four transmembrane domains and not showing any sequence similarity with claudins (Mariano et al., 2011). Its C-terminus contains a coiled-coil domain that is involved in a redox-sensitive dimerization of occludin and the association of ZO-1 (Cording et al., 2015; Buschmann et al., 2013).

According to *in vivo* experiments, occludin-deficient mice possess morphologically normal TJs, despite the various complex phenotypes including chronic inflammation and hyperplasia of the gastric epithelium, calcification in the brain, testicular atrophy, loss of cytoplasmic granules in striated duct cells of the salivary gland, and thinning of the compact bone (Kitajiri et al., 2014). These phenotypes cannot be explained in terms of barrier dysfunction of TJs and suggest that occludin may be involved in epithelial differentiation as well (Mariano et al., 2011). Thus, occludin is involved in maintaining the barrier function *in vivo* (Raleigh et al., 2011). In addition, occludin does not regulate basal permeability to macromolecules in epithelial sheets. Neither lack nor re-expression of occludin had a consistent impact on macromolecule permeability. Therefore, occludin is likely not directly involved in the passage of macromolecules across epithelial barriers.

Instead, it appears to mediate responses to environmental changes in epithelium and thus may have a more regulatory function (Richter et al., 2019; Zhou et al., 2020).

1.3.2.3 MarvelD3

MarvelD3 was identified as the latest member of TAMP member (Steed et al., 2009), which is expressed as two isoforms that show a broad tissue distribution (Steed et al., 2009). MarvelD3 has an extended N-terminal and a short C-terminal tail, and it was found at both bicellular and tricellular TJs of Caco-2 intestinal epithelial monolayers as well as murine jejunum, hepatocytes, and renal tubules (Cording et al., 2013). Like occludin, regular MarvelD3 expression is not essential for tight junction formation (Steed et al., 2009). Nevertheless, knockdown of MarvelD3 affects the paracellular barrier properties of tight junctions by mechanisms that still have to be identified (Steed et al., 2009).

1.3.2.4 Junctional adhesion molecules (JAM)

The third class of integral membrane proteins comprises members of the immunoglobulin superfamily and can be subdivided into a group consisting of JAM proteins and a group consisting of CAR, CLMP, ESAM, and JAM-4/JAM-L. To date, at least three JAM isoforms have been described (JAM-1, -2, and -3, or JAM-A, -B, and -C, respectively), which are expressed differentially in epithelial and endothelial cells, but also cells devoid of TJ strands like leukocytes (Heinemann and Schuetz, 2019). In contrast to claudins and occludin, JAMs are single-pass transmembrane proteins of approximately 40 kDa, with a transmembrane domain and an extracellular portion folded into two immunoglobulin-like domains. JAMs are concentrated at TJs, where they associate laterally with the claudin-based backbone of TJ strands in epithelial cells. They appear to be clustered at intercellular contacts, playing a role in TJs formation and endothelial cell polarity, as well as in paracellular permeability (Otani et al., 2019; Mariano et al., 2011).

1.3.3 Morphology of the tricellular tight junction (tTJ)

Tricellular TJs (tTJs) are generated within tricellular contacts (TCs) in the mammalian epithelial cell sheet and comprise multiple transmembrane proteins (e.g., angulin-1, angulin-2, angulin-3, and tricellulin; Figure 1-3) (Ikenouchi et al., 2005; Higashi et al., 2013; Anderson and Van Itallie, 2009; Wade and Karnovsky, 1974). Here, the elements of adjacent bTJ strands join and extend in a basal direction forming a vertical central tube-

like space at the tricellular contacts of assumedly 1 μm in length and 10 nm in diameter (Staehelin, 1973; Higashi and Miller, 2017). These central tubes are critical points for the TJ barrier integrity and are sealed by the transmembrane proteins mentioned above.

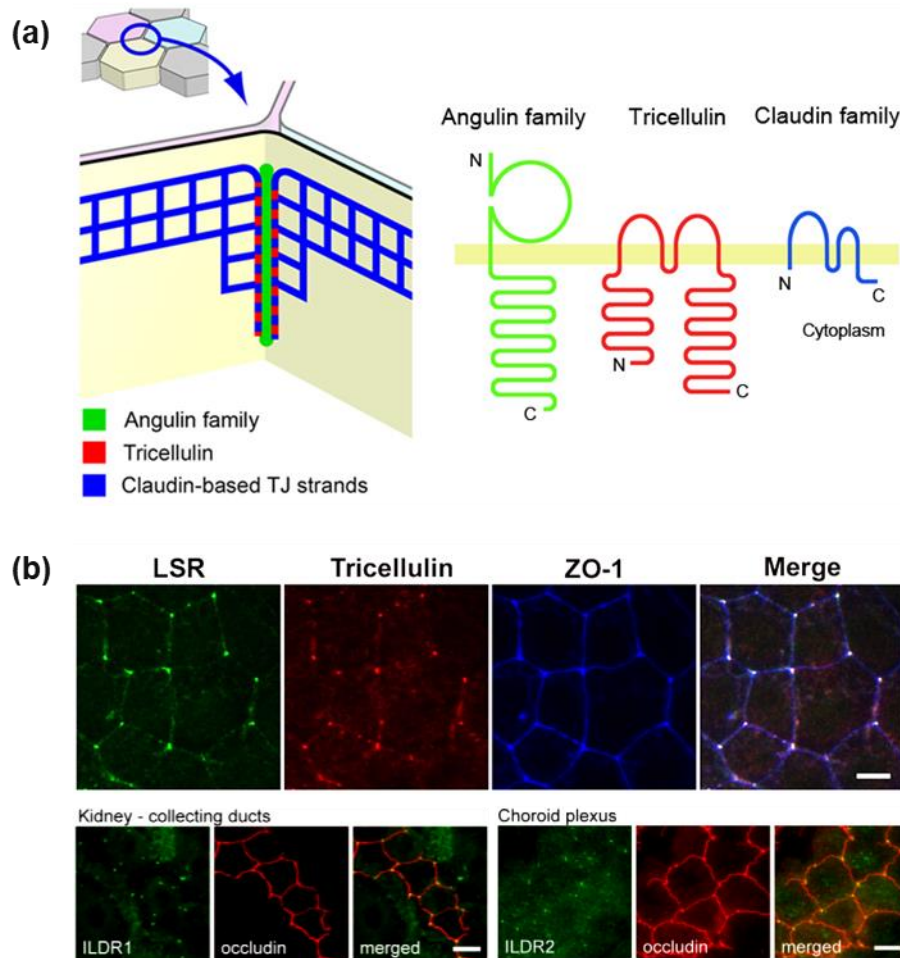


Figure 1-3. Tricellulin and angulin family proteins. **(a)** Membrane-spanning model of tricellulin, angulins, and claudins (Masuda et al., 2011). **(b)** Immunofluorescence staining images of tricellulin and angulin-1/LSR in EpH4 mouse mammary epithelial cells (upper panel (Masuda et al., 2011)) and angulin-2/LSR in kidney collecting ducts and angulin-3/ILDR2 in choroid plexus (lower panel (Higashi et al., 2013)). Bars: 10 μm .

1.3.3.1 Tricellulin

Tricellulin, also known as MarvelD2, is a member of the MARVEL protein family. In mature tissues, tricellulin strongly localizes at the tricellular cell-cell contacts where the TJ network is extended basolaterally, whereas it is also present to a lesser extent in bicellular junctions yielding a typical punctate pattern (Figure 1-3). Tricellulin is an essential tTJs component, ensuring their proper formation, maintenance, and barrier function both *in*

vivo and *in vitro* (Ikenouchi et al., 2005; Lohmann et al., 2020). Four isoforms of human tricellulin have been described so far (Riazuddin et al., 2006): TRIC-a is the most lengthened form (558 aa) and is meant in this as well as in other studies when simply termed “tricellulin”. It contains seven exons and has a C-terminal ELL sequence with an overall identity of 32% (51% similarity) to occludin. Despite this homology, occludin and tricellulin are differentially phosphorylated in their C-terminal tails. Mutations of TRIC-a lead to nonsyndromic deafness, DFNB49. The isoform TRIC-a1 lacks the exon three, and TRIC-b is a shorter isoform (458 aa) of tricellulin lacking the occludin-ELL. The occurrence of TRIC-b is hypothesized in basal cell layers of keratinocyte cultures. TRIC-c (442 aa) is predicted to be a two-transmembrane domain protein with an alternatively spliced exon two (Riazuddin et al., 2006).

Tricellulin has extended cytoplasmic N- and C-terminal domains, with the C-terminal tail exhibiting homology to the occludin C-terminus. It has been shown that the C-terminus binds to ZO-1 (Riazuddin et al., 2006) and is vital for the basolateral translocation of tricellulin and its binding to the lipolysis-stimulated lipoprotein receptor (LSR/angulin-1). Angulin-1 builds a landmark for tricellular TJs, and the N-terminal domain of tricellulin appears to be involved in directing tricellulin to tricellular contacts.

Tricellulin severely influences TJ organization not only at tricellular contacts but also at the level of bicellular TJs (Cording et al., 2013). The knockdown of tricellulin results in redistribution of occludin at bicellular TJs, i.e., tear-drop shaped accumulation of occludin close to tricellular TJs. Therefore, it is assumed that tricellulin and occludin may at least partially compensate for each other. On the other hand, after overexpression, tricellulin is also strongly detectable at bicellular contacts. Remarkably, mutations in the cytoplasmic C-terminal domain of tricellulin, which were most often truncations that disrupted ZO-1 binding, caused deafness without creating a syndrome involving other organs. This limited distribution of disease does not reflect the absence of tricellulin expression in other tissues, suggesting that another protein may compensate for tricellulin loss (Cording et al., 2013).

1.3.3.2 Angulin protein family

The angulin protein family comprises angulin-1 (also known as lipolysis-stimulated lipoprotein receptor [LSR]), angulin-2 (also known as immunoglobulin [Ig]-like domain-containing receptor [ILDR1]), and angulin-3 (also known as ILDR2, LISCH-like, or C1orf32) (Figure 1-3) (Higashi et al., 2013; Masuda et al., 2011). Angulins have a single transmembrane domain, an amino-terminal extracellular Ig-like domain, and a carboxyl-terminal cytoplasmic domain (Masuda et al., 2011). The angulin subtypes are expressed complementarily in many epithelial cell types, although angulin-1/LSR and angulin-2/ILDR1 are co-expressed in some regions. Previous studies using cultured epithelial cells showed that tricellulin and angulins are required for the full barrier function of epithelial cells with high transepithelial electrical resistance. Importantly, angulins recruit tricellulin to TCs through direct or indirect interaction between the cytoplasmic domain of angulins and the C-terminal cytoplasmic domain of tricellulin (Higashi et al., 2015). It has recently been revealed that angulin-2 is the causative gene for a familial nonsyndromic deafness, DFNB42 (MIM 609646) (Higashi et al., 2013). Angulin-3 was reported to be a candidate modifier of susceptibility to type-2 diabetes (Higashi et al., 2013). Angulin proteins 2 and 3, but not angulin-1, are involved in alternative pre-mRNA splicing via binding to splicing factors transformer 2 protein homolog alpha (TRA2A), transformer 2 protein homolog beta (TRA2B), and serine/arginine-rich splicing factor 1 (SRSF1) which are also SR protein family members (Liu et al., 2017). Sugawara and colleagues recently described that in MDCK II tricellulin KO cells, angulin-1 was localized at TCs extending along the apicobasal axis. The plasma membrane contacts, and the central sealing elements were maintained, but the central sealing elements lacked connection of short TJ strands. In addition, they found that in MDCK II angulin-1 KO cells, a paracellular gap was observed at TCs in horizontal ultrathin sections and freeze-fracture replicas, the vertical TJ strands at TCs were separated and did not form the central sealing elements, concluding that the epithelial barrier function was impaired in angulin-1 KO cells, but not in tricellulin KO cells (Sugawara et al., 2020).

1.3.4 Adjacent tight-junctional proteins

The interface between the transmembrane proteins and most cytoplasmic components is formed by a set of scaffolding proteins with multiple PDZ domains. PDZ domains, named for the proteins PSD-95, large discs, and ZO-1, are protein binding modules that

recognize target sequences at the extreme C-termini of transmembrane proteins. PDZ-proteins at the TJ include the ZO-MAGUK proteins ZO-1, ZO-2, and ZO-3; the MAGUK relatives MAGI-1, MAGI-2, and MAGI-3; a protein with 13 PDZ called MUPP-1; and the three conserved cell polarity protein complexes; namely the Par-aPKC complex, Crb3 (Crumbs) complex, and the Scribble-Lgl-Dlg complex which are crucial to maintaining balanced communication and proper barrier function. The Crumbs complex co-localizes to tight junctions with the Par-aPKC complex, which are stabilized via mutually antagonistic phosphorylations with the basolateral Scribble complex (Heinemann and Schuetz, 2019; O'Leary et al., 2021). Following assembly of the adherens junction, the ZO-1 and ZO-2 coordinate the polymerization of the claudin proteins to the TJ strands. In addition to the role for ZO proteins in TJ assembly, recent work has defined a role of these proteins, particularly ZO-1, in barrier regulation. ZO-1, but not ZO-2, knockdown in MDCK layers increased paracellular permeability of large solutes, such as the leak pathway (Figure 1-7) (Otani et al., 2019). Although charge selectivity was not examined, ZO-1 knockdown did not affect the paracellular flux of small polyethylene glycols, suggesting that pore pathway barrier function was intact (Otani et al., 2019).

1.4 Barrier properties: resistance, flux, and selective permeability

The characteristics of the selectively permeable TJ barrier vary widely among different epithelia, within different cell types of a single tissue, and respond to physiological and pathophysiological stimuli. Thus, while the paracellular barrier is most often assessed by electrical conductance, its reciprocal transepithelial electrical resistance, or transepithelial flux of small fluid phase markers, such as mannitol, measurement of only one or two of these parameters provides a half-finished picture of overall barrier function (Johnson, 2012; Shen et al., 2011).

1.4.1 Electrical resistance, “leaky” and “tight” epithelia

The transepithelial resistance (TER) represents the sum of two ion-conductive pathways, the paracellular and the transcellular one. The TER is a reciprocal indicator of the summed-up permeability of all involved ions and their concentrations (e.g., increased TER indicates decreased ion permeability). This parameter is used to monitor the cell barrier

integrity during experiments and roughly judge the tightness of epithelial and endothelial tissues for ions (Yeste et al., 2018; Johnson, 2012; Shen et al., 2011).

By definition, a “leaky epithelium” is defined by a ratio of paracellular resistance over transcellular resistance below one ($R^{\text{para}} / R^{\text{trans}} < 1$), while a “tight epithelium” is defined by a ratio of paracellular over transcellular resistance above one ($R^{\text{para}} / R^{\text{trans}} > 1$) (Diamond, 1974). Measurements of R^{para} and R^{trans} have been established by the method of two-path impedance spectroscopy (Krug et al., 2009b).

Practically, most leaky epithelia possess highly ion-permeable tight junctions so that their TER is low. On the other hand, most tight epithelia possess tight junctions of rather low or almost no ion permeability and a lesser density of ion-conductive membrane transporters; therefore, their TER is very high. Along these lines, the two epithelial cell lines used in this study, HT-29/B6 and MDCK C7, have been characterized and classified as “medium-tight” and plain “tight”, respectively (Krug et al., 2014).

Functionally, tight epithelia are characterized by the ability to maintain high electrochemical gradients produced by active transcellular transport without considerable back-leak through the tight junction (Figure 1-4). This configuration allows producing highly concentrated (or highly diluted) luminal content, as in the distal nephron, which can produce urine with osmolarity several times higher (or lower) than plasma. In contrast, “leaky” epithelia can move large amounts of solutes and water in an isosmotic way (Figure 1-4).

As a general rule, in organs forming tubular-shaped epithelia like nephron, intestine, and ducts of sweat or salivary glands, the proximally located segments are covered by leaky epithelia, and the functionally distal segments are covered by tight epithelia (Günzel and Fromm, 2012). An excellent example of that is the human gastrointestinal tract, which secretes and then reabsorbs about 10 L of fluid each day (Anderson and Van Itallie, 2009). While the small intestine is covered by leaky epithelia, especially the distal part of the colon is covered by tight epithelia, steep electrochemical gradients can be produced to reabsorb ions water and to form solid stool (Anderson and Van Itallie, 2009).

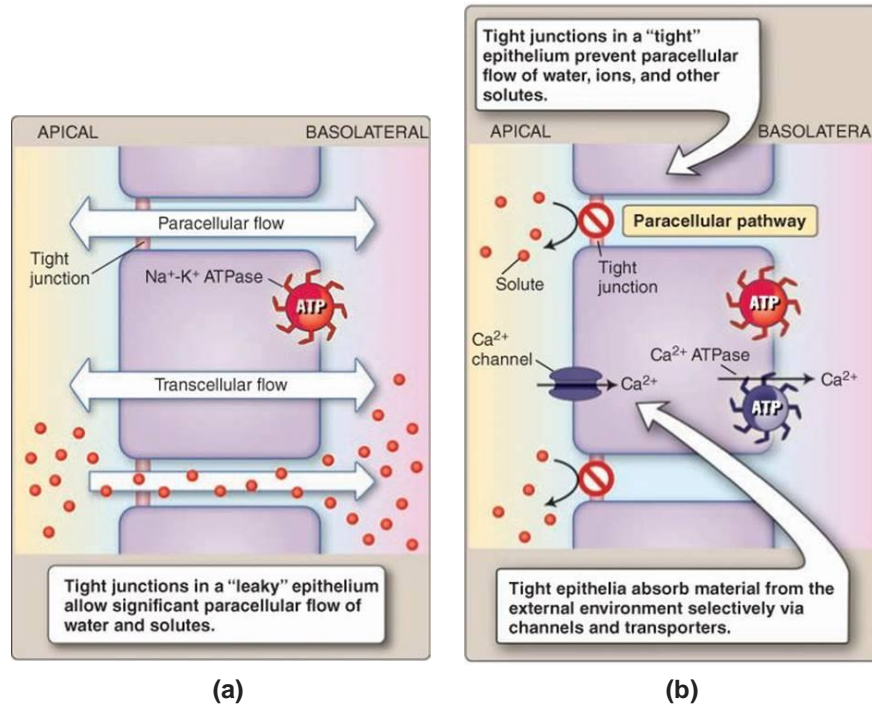


Figure 1-4. Flow across a leaky and tight epithelium. **(a)** The tight junction in a “leaky” epithelium (e.g., proximal renal tubule) is highly permeable and allows ions to pass the TJ by channel-forming claudins. All TJs, either “leaky” or “tight”, are not much permeable to other solutes like sugars, amino acids, etc.; nevertheless, water passes through relatively easily. Leakiness prevents an epithelium from creating strong ion concentration gradients between external and internal surfaces but are capable of transporting a large number of solutes and water, in part via the paracellular pathway. **(b)** Tight junctions in “tight” epithelia effectively bar paracellular flow of solutes and water, and they allow these epithelia to generate high concentration gradients, but only lower transport rates. It was adapted from (Preston, 2013).

1.4.2 Charge selectivity

Study of leaky epithelia revealed another interesting and variable property, namely that tight junctions (TJs) have ionic charge selectivity. Charge selectivity is most relevant in leaky tight junctions, where higher amounts of ions flow (Anderson and Van Itallie, 2009). Experimentally, ion charge selectivity is determined as the ratio of cation to anion permeability. Almost the TJs of most leaky epithelia show a preference for Na⁺ over Cl⁻, and the permeability ratio (expressed as PNa⁺/PCl⁻) ranges from about 10 to 0.1 among different epithelia and experimental cultured cell models. This represents only a modest ability to distinguish compared with membrane ion channels (Anderson and Van Itallie, 2009). Charge selectivity is a characteristic feature of paracellular barriers and is essential for creating transepithelial gradients that direct passive paracellular transport (Figure 1-5).

For instance, in the kidney, charge selectivity of the pore pathway varies along the length of the nephron, and such variance is critical to the physiology of tubular reabsorption (Shen et al., 2011). Nonetheless, paracellular permeability differences between nephron segments are relatively fixed, except for the stimuli that modify synthesis and turnover of tight junction proteins over extended intervals (Shen et al., 2011).

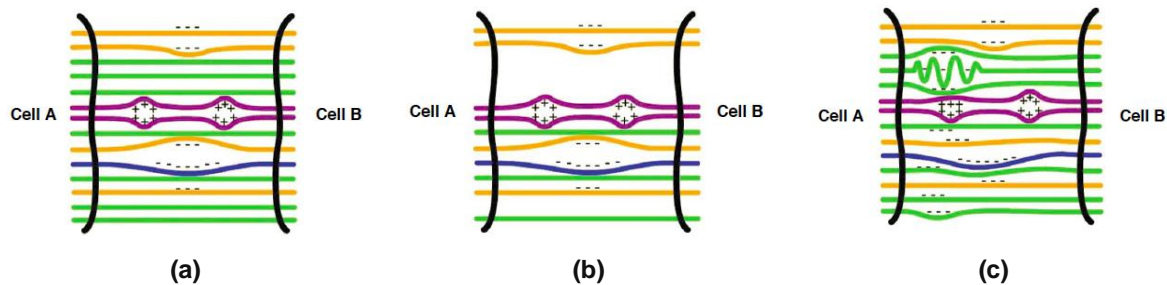


Figure 1-5. A paracellular solute's view of a hypothetical tight junction comprising various claudins in homotypic and heterotypic interactions (Mullin et al., 2005). Claudin protein alignment in pairs can create aqueous pores at points where similar charge alignment results in strand repulsion **(a)**. Pores created by such charge repulsion would support the passage of specific solutes based on their charge and size. This model oversimplifies but serves to highlight two types of changes of permeability. In the event of downregulation of a specific claudin **(b)**, the decreased expression of neutrally charged claudin-X creates opportunities for the increased paracellular flow of moderately large electrolytes and nonelectrolytes between wider separations of claudin strands. Another possibility **(c)** is that events such as the phosphorylation in claudin-Y creates steric changes in the intercellular loops, resulting in claudin-Y misalignment. The claudin-Y homotypic interactions then produce, in turn, pores created by interstrand repulsion of similar charges. As in **(b)**, the net result is decreased transepithelial resistance or increased nonelectrolyte flux, or both. It was adapted from (Mullin et al., 2005).

1.4.3 Size selectivity

In addition to charge selectivity, the TJ discriminates between solutes based on size. This barrier's function is complex, with at least two mechanisms of trans-tight junction flux: a pore pathway and a leak pathway (Johnson, 2012; Shen et al., 2011).

1.4.3.1 Paracellular pore pathway

TJ selectivity is regulated through claudin pores, channels formed by the extracellular domains of claudins, that conduct ions and small molecules based on size and charge (diameter of $\leq 8 \text{ \AA}$ (Van Itallie et al., 2008)). Paracellular permeability through claudin pores is commonly stated to as the "pore pathway". Selectivity is based on the

composition of pore-forming claudins (both cation and anion pores) and barrier-forming claudins, restricting the flux of small solutes (Figure 1-5 and 1-6). TJs' barrier properties can change in response to various stimuli by "claudin switching", e.g., by replacing a pore-forming claudin with a barrier-forming claudin. Owing to the large number of highly selective pores, the pore pathway is characterized by its high capacity and high selectivity (Varadarajan et al., 2019).

1.4.3.2 Paracellular leak pathway

A second pathway, known as the "leak pathway", allows larger molecules to cross TJs, although with less selectivity and a much lower capacity than the pore pathway. To date, there are three possible routes that larger molecules can use to cross the epithelium:

1) The predominant theory is that leak pathway flux occurs due to the breaking and annealing of claudin strands, which may be influenced by intermolecular associations between claudins, occludin, ZO-1, and the actin cytoskeleton; for example, loss of occludin is associated with a ~ 62.5 Å barrier defect suggests a model of leak associated with large paracellular channels (Buschmann et al., 2013). On the other hand, despite a lack of structural understanding, components of the signal transduction machinery that regulates leak pathway permeability have been studied extensively. The most well-characterized of these is myosin light chain kinase (MLCK), which regulates paracellular permeability during physiological, Na^+ -nutrient cotransport. Expression of constitutively-active MLCK is sufficient to increase leak pathway permeability *in vitro* and *in vivo*. The interaction with ZO-1 may be central to MLCK-dependent leak pathway regulation because ZO-1, but not occludin, binds directly to F-actin (Zuo et al., 2020). Consistent with this idea, the actin-binding region of ZO-1 is required for *in vitro* barrier regulation by MLCK. Moreover, ZO-1 knockdown increases the leak pathway permeability of epithelial monolayers (Figure 1-6) (Liang and Weber, 2014).

2) The second potential leak pathway regulator, JAM-A, is sufficient to limit the flux of macromolecules in the absence of claudin strands, suggesting that JAMs serve as a stop-gap measure to protect barrier integrity when claudin strands are disrupted or newly forming (Figure 1-6) (Varadarajan et al., 2019).

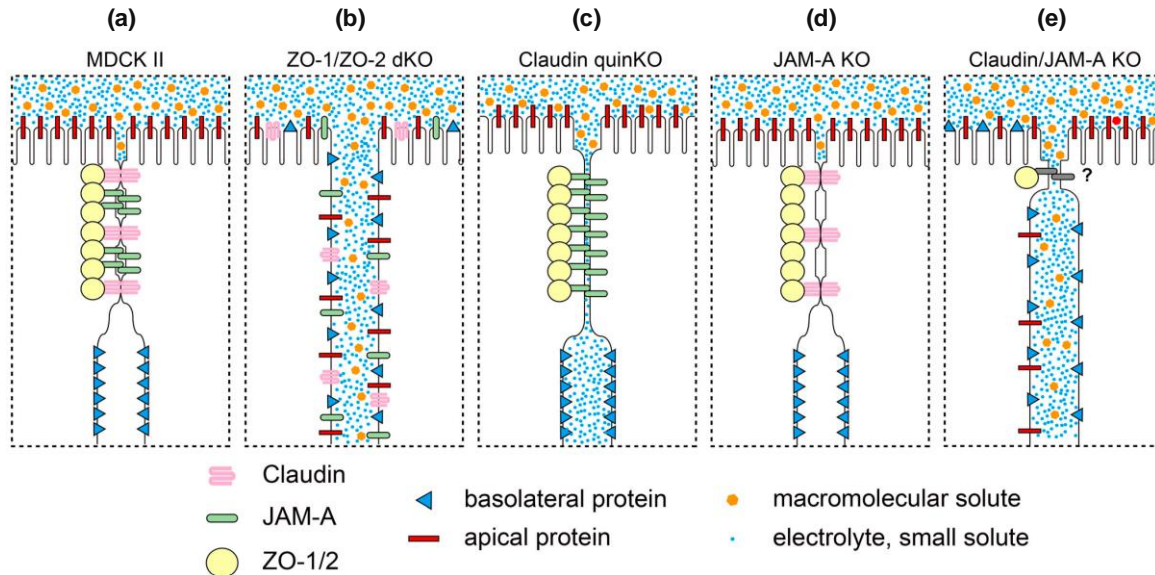


Figure 1-6. Size selectivity in MDCK II, ZO-1/ZO-2 dKO, claudin quinKO, JAM-A KO, and claudin/JAM-A KO cells. **(a)** In MDCK II cells, claudins and JAM-A are concentrated at the TJs with ZO-1/ZO-2. The membranes are closely connected to each other, and kissing points are formed, and paracellular diffusion of electrolytes and macromolecules is banned. Epithelial polarity is maintained. **(b)** In ZO-1/ZO-2 dKO cells, claudins and JAM-A are diffusely localized, and membrane associations and kissing points are lost. Intercellular space is widened, and electrolytes and macromolecules diffuse across the paracellular space. Epithelial polarity is disorganized. **(c)** In claudin quinKO cells, JAM-A and ZO-1/2 are concentrated at the apical junctions, and membrane associations are formed despite the lack of kissing points. Although electrolytes can diffuse across the paracellular space, the paracellular diffusion of macromolecules is prohibited. No epithelial polarity defects are observed. **(d)** In JAM-A KO cells, claudins and ZO-1/2 localize to TJs, and kissing points are formed. The epithelial barrier and polarity are not perturbed. **(e)** In claudin quinKO/JAM-A KO cells, ZO-1 can localize to apical junctions, but discontinuity is observed. Intercellular space is widened, although focal membrane associations are observed in some cases. Electrolytes and macromolecules can diffuse across the paracellular space, and epithelial polarity is disorganized in some regions. It was adapted from (Otani et al., 2019).

3) The third possible regulator that has been postulated is the central tube in the tTJ owing to its large dimension (~10 nm in diameter). Compatible with this hypothesis, knockdown of angulin-1 in the mouse mammary gland Eph4 epithelial cells significantly increased the permeability of macromolecules ranging in sizes from 0.9 to 9.0 nm in diameter (equivalent to 300 – 40000 Da in molecular weight) (Higashi et al., 2013; Sugawara et al., 2020). On the other hand, when tricellulin was overexpressed at low levels in the MDCK II cells (only at the tTJ), impeded the permeation of macromolecules with sizes from 1.3-4.6 nm in diameter (900 – 10000 Da in molecular weight) but showed no effect on molecules smaller than 1.3 nm in diameter (<900 Da in molecular weight)

(Krug et al., 2009a). Nevertheless, when tricellulin is overexpressed in bTJs and tTJs, the permeabilities to ions and midsize to large solutes decreased (Krug et al., 2009a). In contrast, in tTJs tricellulin overexpression did not alter permeability to ions but strongly diminished the permeability to macromolecules of 4-10 kDa. The presence of redundant mechanisms to regulate the leak pathway highlights the importance of restricting macromolecules' flux via the leak pathway (Varadarajan et al., 2019).

In summary, in leaky epithelia, many channel-forming claudins within the bTJ account for most ion conductance because tTJs are too rare to contribute significantly. In contrast, in tight epithelia, bTJ pathways for ion passage are rare, so the ion conductance of the tTJ becomes an essential contributor to overall flux (Figure 1-7). Especially under pathological conditions, changes in the composition of the tTJ may lead to severe defects affecting the macromolecular barrier and the ionic barrier in tight epithelia.

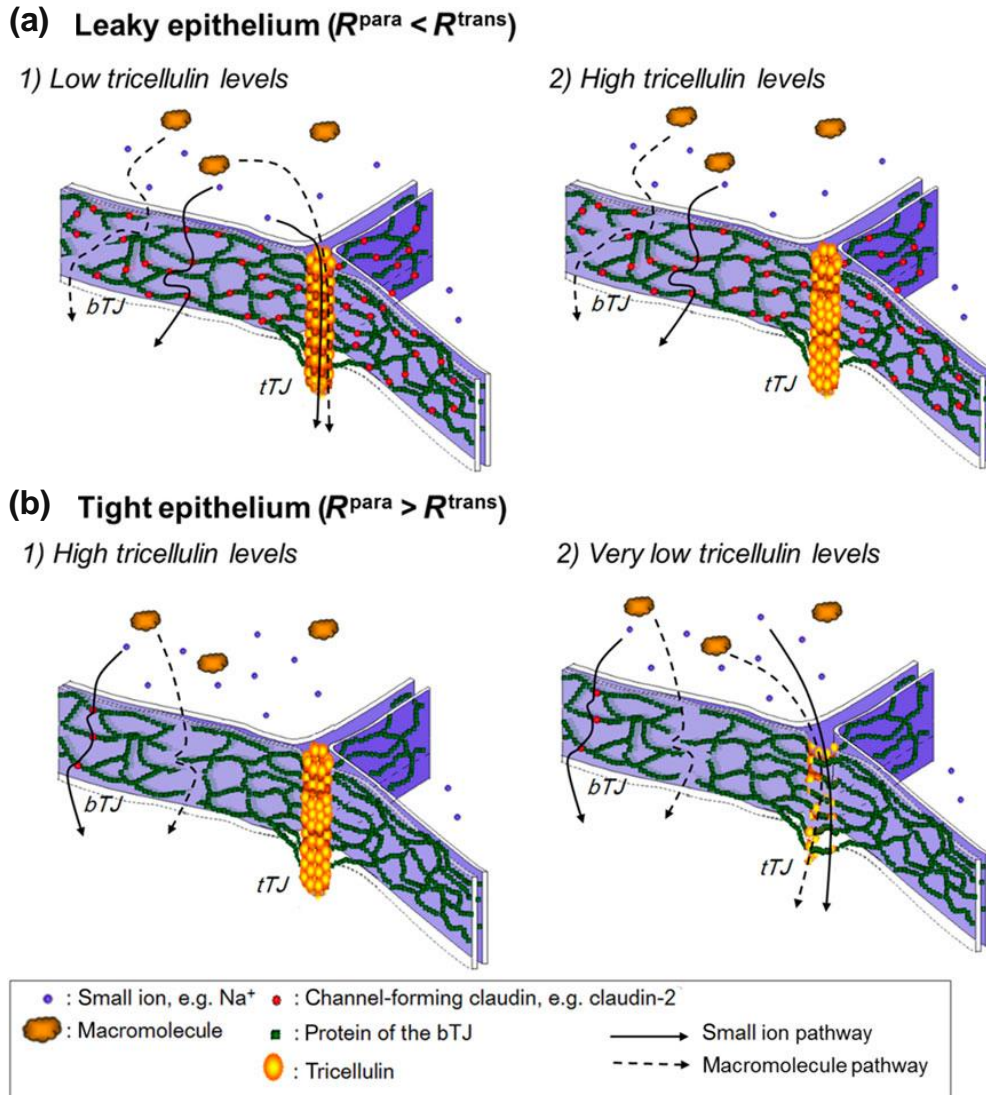


Figure 1-7. Tricellulin as a regulator of the paracellular leak pathway. **(a) Leaky epithelia.** (1) Low tricellulin levels: tTJs allow ionic passage but are too rare to contribute because ions predominantly pass via abundant paracellular claudin channels located in the bTJ. Macromolecules can pass via rare, reversible, and coincidental strand breaks or the comparably frequent tTJ. (2) High tricellulin levels: The tTJ is virtually sealed. For ions, the main route via bTJ claudin channels is unaffected, leaving TER unchanged, while for macromolecules, the main pathway is closed. Only the rare events of strand breaks may allow paracellular macromolecule passage. **(b) Tight epithelia.** (1) High tricellulin levels: The tTJ is nearly completely sealed to both macromolecule and ion passage. Additionally, ion-conductive claudin channels are low, leading to a low ion permeability and thus a high TER. (2) Very low tricellulin levels: The tTJ is open, now not only being of importance for macromolecule passage but also for being the predominant route for ion passage. Under these conditions, the tTJ makes a considerable contribution to ion permeability and TER changes. It was adapted from (Krug, 2017).

1.5 Water transport across the epithelia

1.5.1 Transcellular water pathway

Water transport through cell membranes is so intricate that there are still some debates. There are two general transcellular water transport mechanisms: water is either transported through aquaporins (AQPs) driven by the transmembrane difference in water osmosis or transported through various carriers that transport specific solutes organic molecules across the cell membrane but also act as water transporters. The most representative non-AQP water channel is urea transporter B (UT-B) (Yang and Verkman, 2002; Ogami et al., 2006) and the SGLT1 cotransporter, which temporarily form a continuous water channel through the transporter that allows the water to penetrate the protein (Adelman et al., 2014).

1.5.1.1 Aquaporin channels

Aquaporins (AQPs) are a family of highly selective transmembrane channels that mainly transport water across the cell, and some facilitate low-molecular-weight solutes. AQPs consist of 13 members (AQP0–AQP12) in mammals and are widely distributed in various tissues and organs (He and Yang, 2019). According to their primary structure, they have been classified into three subfamilies: 1) Water-selective AQPs or orthodox aquaporins include AQP0, AQP1, AQP2, AQP4, AQP5, AQP6, and AQP8. 2) Aquaglyceroporins are permeable to water and some small uncharged solutes, such as glycerol and urea, this subfamily includes AQP3, AQP7, AQP9, and AQP10. For instance, AQP3, AQP8, and AQP9 have been demonstrated to transport hydrogen peroxide (H₂O₂) in mammalian cells. 3) The third subfamily, named superaquaporins, including AQP11 and AQP12, has low homology at its amino acid level with other classical AQPs (He and Yang, 2019). Cells expressing AQPs on their plasma membrane have an ~5- to 50-fold higher osmotic water permeability than membranes that do not. AQP-expressing cells generally contain several thousand or more AQPs per μm^2 of the membrane compared with ten or fewer ion channels per μm^2 of the membrane (Verkman, 2011). Due to a broad spectrum of pathophysiological function in balancing water homeostasis, modulating intracellular signaling, and regulating cell proliferation and oxidative stress response, AQPs have been proven to participate in renal diseases, dermatosis, bowel disease, and cancer (He and Yang, 2019).

- **The digestive system**

Secretion and absorption, two of the digestive system's primary functions, both require fluid transfer across cellular membranes. Daily secretion in the form of saliva, gastric juices, intestinal mucous, bile, and pancreatic juice comprise a total volume of approximately 7.5 L of fluid in the human digestive system; approximately 9 L of fluid is absorbed daily (Day et al., 2014). The digestive system is a major site of fluid movement and has a comprehensive AQP expression profile within its organ network. A polarized AQP expression pattern suggests that an organized transcellular route for water is an essential role of AQPs in facilitating high secretion and absorption rates (Day et al., 2014). However, and in contrast to the kidney, AQPs in the intestine are considered not quantitatively abundant enough to do the full job; therefore, SGLT1 may play a major role (Zeuthen et al., 2016). The general distribution of AQPs in the digestive system is summarized in Figure 1-8.

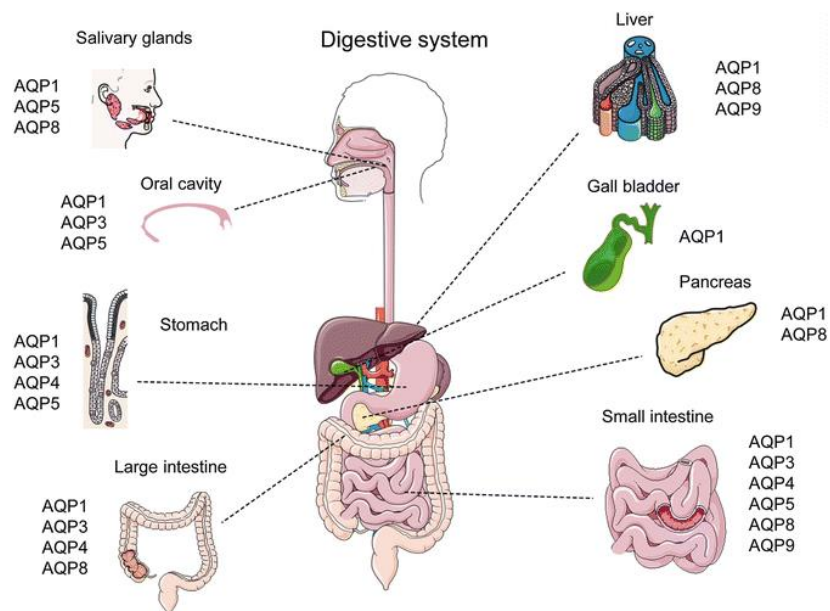


Figure 1-8. Distribution of aquaporins in the digestive system (Zhu et al., 2017). AQP1, AQP5, and AQP8 are expressed in salivary glands. AQP1, AQP3, and AQP5 are present in the oral cavity. In the stomach, AQP1 is expressed in the endothelial cells of capillaries and small vessels; AQP3 is expressed in the basolateral membrane of surface mucous cells; AQP4 is expressed in the basolateral membrane of parietal cells, and AQP5 is present at the apical membrane of parietal cells. Small intestine expresses AQP1, AQP3, AQP4, AQP5, AQP8, and AQP9. Large intestine expresses AQP1, AQP3, AQP4, and AQP8. In the liver AQP1, AQP8, and AQP9 are expressed. AQP1 is diversely expressed in gallbladder, bile duct and pancreas, while AQP8 is present in the pancreas as well.

- **The renal system**

Kidney AQPs form a highly organized system that facilitates water homeostasis maintenance (Day et al., 2014). To be more precise, eight AQPs are expressed in different segments and various cells of the kidney to maintain normal urine concentration function, tissue development, and substance metabolism (AQP1, AQP2, AQP3, AQP4, AQP5, AQP6, AQP7, and AQP11) (He and Yang, 2019). The general distribution of AQPs in the renal system is summarized in Figure 1-9.

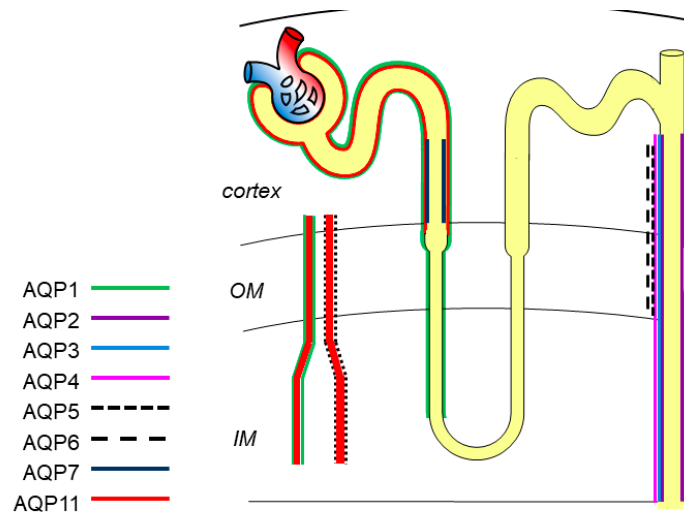


Figure 1-9. Expression and localization of AQPs in the kidney. AQP1 is located in the proximal tubule, descending thin limbs of Henle, and vasa recta; AQP2, AQP3, AQP4, AQP5, and AQP6 are in the collecting duct; AQP7 and AQP11 are expressed in the proximal tubule (He and Yang, 2019).

1.5.1.2 Urea transporter B

The urea transporter B (UT-B) is widely expressed in many tissues, such as the kidney, colon, small intestine, brain, liver, pancreas, among others. UT-B is a homotrimer, and each protomer contains a urea conduction pore with a narrow selectivity filter. The transport of water and urea are weakly temperature-dependent, and mostly inhibited by the urea transport inhibitors, but not inhibited by the AQP inhibitors HgCl_2 . In summary, the fact that urea and water share the same pathway through the pore of UT-B also indicates that UT-B acts as a water channel (Huang et al., 2017; Yang and Verkman, 2002; Ogami et al., 2006).

1.5.1.3 Cotransporters

Some cotransporters transport not only their specific substrates but also water. The water transport by cotransporters may well be significant because of the large number of cotransporters per cell and their considerable unit water permeability (Huang et al., 2017; Zeuthen, 2010; Zeuthen, 2002; Zeuthen et al., 2016; Zeuthen and MacAulay, 2012). The cotransport of water is independent of the osmotic gradient and even occurs in the presence of adverse osmotic gradients (Huang et al., 2017; Loo et al., 1996). Some cotransporters are summarized in Table 1-1.

- **Sodium-glucose transporters (SGLT)**

The human SGLT family is a group of twelve members (Hu et al., 2013). Except for SGLT1-5 co-transporting for sugars, they include Na⁺ cotransporters for myo-inositol, iodide, short-chain fatty acids, and choline. As a multifunctional protein, SGLT1 works as a water channel and transporter, which couples' water and glucose. The passive osmotic permeability of the hSGLT1 plays an important role in the final achievement of isotonic transport, and the water cotransport (4 L of water with 1 M of glucose) in the human small intestine plays a vitally important role in reuptake (total 9 L per day) (Huang et al., 2017; Meinild et al., 1998; Tappenden, 1999). SGLT1 has three modes in isotonic water transport: First, water influx is directly correlated with Na⁺ and glucose in the ratio of 260H₂O/2Na⁺/1glucose with no delay in humans. Second, it acts as a water channel. Last, it generates an osmotic driving force that is employed by other pathways (Huang et al., 2017; Loo et al., 1996). In accordance with the above, Zeuthen *et al.* concluded that in the mouse small intestine SGLT1 accounted for two-thirds of the passive water flow across the gut (Zeuthen et al., 2016).

Table 1-1. Water-transport properties of cotransporters, uniporters, and channels.

Protein	Substrates	Number of water molecules transported per turnover (Zeuthen, 2010)	Osmotic water permeability per transporter (10⁻¹⁴ cm³.s⁻¹) (Zeuthen, 2010)
K-Cl cotransporter (KCC4)	K ⁺ /Cl ⁻	500	NA
Na-K-Cl cotransporter	Na ⁺ /K ⁺ /2Cl ⁻	590	NA

(NKCC1)			
Monocarboxylate transporter (MCT1)	H ⁺ /lactate	500	NA
GABA transporter (GAT-1)	2Na ⁺ /Cl ⁻ /GABA	330	0.7
Na ⁺ -coupled glutamate transporter (EAAT1)	2Na ⁺ /H ⁺ /K ⁺ /glutamate	440	0.2
Na ⁺ -dicarboxylate cotransporter (NaDC-1)	2Na ⁺ /dicarboxylate	175	1.5
Glucose transporter (GLUT1)	Glucose	40	0.2
Glucose transporter (GLUT2)	Glucose	40-110	0.1
UT-B	Urea	ND	7.3
AQP-1	H ₂ O	NA	4.0

NA: not applicable, ND: not determined.

1.5.2 Paracellular water pathway

Whether or not the TJ at all is permeable to water was highly controversial for a long time. Across both epithelium and endothelium, significant water permeability remains when transcellular water channels are removed from the plasma membrane (Fischbarg, 2010; Steward et al., 1990). Furthermore, claudins can convey the paracellular solute transport, but at least two claudins, claudin-2 and claudin-15, can also mediate paracellular water flux.

A computational study analyzing the water and ion permeability of a claudin pore suggested that, in physiological solutions, ions drag a shell of water molecules with them through pores (Laghaei et al., 2016). Several channels with diameters from 3.8 to 8.0 Å were simulated, and it was shown that the relation between water flux and pore size is not linear. The number of water molecules passing the pores decreases with decreasing pore size between 5.0 and 8.0 Å, whereas water permeability of a pore ≤ 5 Å seems to be independent of the pore diameter and very low (Laghaei et al., 2016).

1.5.2.1 Bicellular tight junction

- **Cation and water channel-forming claudins: claudin-2 and claudin-15**

Similar to claudin-2, claudin-15 was identified as a cation-selective channel-forming claudin. The tight junction protein claudin-2 is predominantly expressed in leaky epithelia, such as the proximal tubule and small intestine, which are characterized by high paracellular ion permeability (Amasheh et al., 2002). Endogenous expression of claudin-15 was predominantly found in the gut, with the highest abundance in the small intestine, but claudin-15 is also present in colon segments. Nevertheless, claudin-15 is not expressed in the kidney tubule system (Tamura et al., 2011).

The function of claudin-2 was analyzed in overexpression studies, and it was found to be permeable to cations but not to anions or larger, uncharged molecules, such as mannitol, lactulose, or 4-kDa dextran (Amasheh et al., 2002). *In vivo* studies on claudin-2 knockout mice revealed the involvement of claudin-2 in paracellular water permeability, especially in the proximal tubule, with strong claudin-2 expression (Wilmes et al., 2014). Muto *et al.* found a decreased net transepithelial reabsorption of Na⁺, Cl⁻, and water in isolated proximal tubules of claudin-2-deficient mice (Muto et al., 2010). On the other hand, overexpression of claudin-15 in the anion-selective cell line LLC-PK1 increased in cation permeability, whereas overexpression in the cation-selective cell line MDCK II had no effect (Colegio et al., 2002; Van Itallie et al., 2003). Studies on claudin-15-deficient mice show that they develop megaintestine and revealed that claudin-15 is essential for Na⁺ homeostasis in the small intestine, which guarantees effective glucose and galactose reuptake through the sodium-glucose symporter SGLT1 (Tamura et al., 2011).

Regarding water transport, monovalent cations pass the claudin-2 pore in a partially dehydrated form and the cation and water fluxes are coupled and share a common pore (Rosenthal et al., 2017a; Rosenthal et al., 2010). Na⁺ flux through the claudin-2 pore induces water flux, and conversely, the osmotic gradient-induced water flux causes Na⁺ movement through the claudin-2 pore (Rosenthal et al., 2017a; Rosenthal et al., 2010). In contrast, Na⁺ and water's concomitant passage through the claudin-15 pore does not occur since cations pass the claudin-15 pore in a more strongly hydrated form compared to the claudin-2 pore (Rosenthal et al., 2019). The presence of a partially hydrated ion like Na⁺ could impair or even inhibit additional water passage. Additionally, osmotic water flux

through claudin-15 induced by mannitol could impede the passage of Na⁺ through claudin-15 (Rosenthal et al., 2019). Thus, claudin-15 allows the passage of either Na⁺ or water, but not a simultaneous passage of both as found for claudin-2 (Luettig et al., 2015; Rosenthal et al., 2017a; Rosenthal et al., 2019).

- **Ion channel-forming claudins: e.g., claudin-10a and -10b and claudin-17**

The tight junction protein claudin-10 exists in two major isoforms, claudin-10a and claudin-10b. Overexpression of these isoforms in MDCK II and MDCK C7 cells without endogenous claudin-10 expression reveals that claudin-10a acts as an anion channel, whereas claudin-10b forms a cation channel (Milatz and Breiderhoff, 2017). On the other hand, claudin-17 was identified as an anion channel-forming tight junction protein by overexpression as well as knockdown experiments. Overexpression in MDCK C7 cells without endogenous claudin-17 resulted in increased permeability for anions, including Cl⁻, HCO₃⁻, and small organic anions, and knockdown in LLC-PK1 cells resulted in a decrease of anion permeability (Krug et al., 2012).

Analysis of osmotically driven water flux in the claudin-10a, -10b or -17–expressing cell line MDCK C7 revealed no alteration in water permeability compared with the corresponding vector controls. Although the Na⁺ permeability of claudin-10b is comparable to claudin-2, claudin-10b is not permeable to water (Rosenthal et al., 2010). Besides, the finding that claudin-17 has a similar or even larger pore diameter than claudin-2 and is impermeable to water indicates that other, currently unknown parameters of the pore structure provide or prevent permeability water. It is possible that specific amino acids within the first extracellular loop, which is known to form the pore, form a hydrophobic gate, and contribute to the missing water permeability of this claudin.

- **Barrier-forming claudins: e.g., claudin-1 and claudin-3**

Claudin-1 and claudin-3 are expressed ubiquitously in most body tissues (Günzel and Fromm, 2012). Overexpression or knockdown of claudin-1 and claudin-3 in different cells indicated that claudin-1 acts as a profound barrier for ions (Milatz et al., 2010; Inai et al., 1999).

Claudin-1 in the epidermis is essential to the skin barrier, either directly or indirectly, is crucial for sealing the epidermis against ions, larger molecules, and water. However, water flux measurement revealed no significant difference in water permeability between keratinocytes from wild-type and claudin-1-deficient mice. Similarly, knockdown of claudin-1 in human keratinocytes did not alter the permeability to water, although here, the permeability to ions, fluorescein, and 4- and 40-kDa FITC-dextran was increased (Kirschner et al., 2013). It is not yet known whether the overexpression of claudin-1 would further strengthen the water barrier in the TJs. In summary, claudin-1 forms a water barrier, but a loss of claudin-1 does not impair the water barrier of the tight junction (Rosenthal et al., 2017b).

On the other hand, overexpression of claudin-3 in the low-resistance cell line MDCK II revealed that claudin-3 seals the tight junction against ions of either charge and against uncharged solutes, such as fluorescein and 4-kDa FITC-dextran. Surprisingly, overexpression of claudin-3 did not cause increased sealing of the tight junction against water flux (Milatz et al., 2010). It is not yet known whether the downregulation of claudin-3 would weaken the water barrier within the TJs. In summary, an increase of claudin-3 abundance within the tight junctions of claudin-2-expressing cells augments the seal against ions and other solutes, but not against water (Rosenthal et al., 2017b).

1.5.2.2 Tricellular tight junction

The tricellular tight junction is found where three cells meet and where three bicellular tight junction strands converge. The tricellular tight junction is thought to be important for the paracellular permeability of ions and water in epithelial tissues because the regular bicellular tight junctions cannot seal the tricellular corners. In fact, the tricellular tight junction is made of two types of proteins, tricellulin, and angulins, which are different from the components of the bicellular tight junction. Unlike the bicellular tight junction that is only permeable for small ions and molecules with a diameter of $\leq 8 \text{ \AA}$, the tricellular tight junction can allow the passage of macromolecules with sizes up to 100 \AA in diameter.

- **Angulin-2/ILDR1**

Angulin-2/ILDR1 is localized to tricellular tight junctions of the distal tubules in the mouse kidney. Gong and coworkers described that the angulin-2 knockout mice developed

phenotypes similar to a hereditary human disease, diabetes insipidus, which included polydipsia, polyuria and renal concentrating defect (Gong et al., 2017). Surprisingly, the renal tubular epithelium that was impermeable to water in wild-type mice became highly permeable to water in angulin-2 knockout mice. Outstandingly, molecular analyses revealed normal gene expression profiles and subcellular localization patterns for the TJ structural components, claudins, tricellulin, and ZO-1, in the knockout mouse kidney (Gong et al., 2017). More importantly, the transcellular water pathway remained intact when the paracellular water pathway was perturbed. Besides, in cultured renal epithelial cells, normally lacking the expression of angulin-2, overexpression of angulin-2 reduces the paracellular water permeability (Gong et al., 2017). These results have provided evidence that the tTJ contains a paracellular water pathway, which is usually inhibited by angulin-2 and is independent of the transcellular water pathway. In contrast to the Gong findings, Hempstock *et al.* concluded that angulin-2 KO mice have no detectable water transport abnormalities. In addition, they found that in the colon and the kidney of angulin-2 KO mice, another tTJ protein, angulin-1, changes its expression pattern, and this change in tissue localization of angulin-1 compensates for the loss of angulin-2 and maintains the barrier function of the epithelia (Hempstock et al., 2020).

1.5.3 Interaction between transcellular and paracellular water transport pathways

The potential physiological interactions between the transcellular and paracellular pathways of water transport were evaluated by deletion of aquaporin 5 (AQP5), the major transcellular water transporter in salivary acinar cells (Kawedia et al., 2007). It was found that the paracellular transport of 4-kDa FITC-dextran (FD4) was affected, which is transported through the paracellular but not the transcellular pathway (Kawedia et al., 2007). Besides, an increase in the number of tight junction strands of both AQP5^{+/+} and AQP5^{-/-} male mice after pilocarpine stimulation was found. Furthermore, expression of occludin, and claudin-3 and -7, critical proteins that regulate the permeability of the tight junction barrier, were significantly decreased in AQP5^{-/-} compared with AQP5^{+/+} salivary glands (Kawedia et al., 2007). In conclusion, Kawedia *et al.* revealed the existence of a gender-influenced molecular mechanism involving AQP5 that allows transcellular and paracellular paths of water transport to act in conjunction. Nevertheless, the quantitative contribution of each pathway to total fluid transport remains to be established.

1.6 Purpose and objectives

A highly specialized and thus most interesting part of the overall TJ is formed by the tricellular TJ, where three or more cells meet. Its major components are tricellulin and angulin-1 (LSR), -2 (ILDR1), and -3 (ILDR2).

The permeation property of tTJ, therefore, remains a major mystery, especially concerning water transport. Its major component is tricellulin, a tetraspan protein that plays a critical role in sealing the tTJ against medium-sized and large molecules (Krug et al., 2009a; Higashi and Miller, 2017). Furthermore, although tricellulin is ubiquitously expressed in epithelial tissues, no other clinical manifestations were co-segregated with hearing loss in two DFNB49 families with tricellulin mutations (Nayak et al., 2013). Recently, in our research group, Krug and colleagues found that in the early stages of ulcerative colitis, tricellulin is downregulated, and this would be of clinical importance because it may be increasing the macromolecule and water permeability of the intestinal epithelia and thus contributes to leak-flux diarrhea (Krug et al., 2018). In addition to tricellulin, the angulin protein family is also part of tTJ. The angulins play a regulative role and act as precursors in tTJ formation, and the phenotypes caused by angulin deficiencies are diverse and severe. Angulin-1-deficient mice exhibit embryonic lethality with blood-brain barrier failure (Sohet et al., 2015), while angulin-2-deficient mice show polyuria and polydipsia arising from renal concentrating defects in addition to hearing loss (Higashi et al., 2015; Gong et al., 2017). Most exciting, in pilot experiments, it was found that overexpression of tricellulin in MDCK II, epithelial cells with low endogenous tricellulin content, seals against paracellular water flux, similar to that found with angulin-2.

This doctoral thesis aimed to clarify the contribution of tricellulin and angulin-1 to epithelial water permeability, which may lead to new insights concerning overall transport characteristics in epithelia with different tightness. With these findings, we wanted to address the physiological mechanisms associated with increased epithelial water permeability due to changes in tricellulin or angulin-1 expression. To this end, the research used the following strategy:

1.6.1 Effect of the tricellular tight junction on paracellular water transport

To gain insights into the role of tricellulin and angulin-1 in the paracellular water pathway, we investigated the effect of the partial reduction of tricellulin and complete removal of angulin-1 inside of the TJ environment of HT-29/B6 cells (human colon adenocarcinoma cell line) and MDCK C7 cells (canine kidney cell line), two epithelial cell lines with different tightness. The knockdown and knockout cells were evaluated regarding the expression and localization of the endogenous proteins and the tight junction morphology and paracellular permeability for ions, macromolecules, and water. The results may improve understanding of whether the tricellular TJ, specifically tricellulin and angulin-1, may or may not establish a new-size independent paracellular pathway for water permeation. In addition, the results may improve understanding of whether angulin-1 can regulate the water permeability of tTJ similarly as does angulin-2 or whether it is indirectly associated with the expression or localization of tricellulin.

2. Materials and methods

2.1 Materials

2.1.1 Devices

All devices, the version and the supplier are listed in Table 2-1.

Table 2-1. Devices.

Device	Version	Supplier
Centrifuge	PerfectSpin 24R Refrigerated Microcentrifuge	PEQLAB Biotechnology GmbH, Germany
	Universal 320R	Hettich, Wehingen, Germany
CO ₂ incubator	Model CB-60 170 260	Binder GmbH, Tuttlingen, Germany
Electric pipetting device	Pipetboy acu	INTEGRA Biosciences, Zizers, Switzerland
Freezing Container	CoolCell® LX	Corning Inc., NY, USA
Heating block	AccuBlock™ Digital Dry Bath	Labnet International, Inc. NJ, USA
Inverted microscope	Olympus CK2	Olympus Optical Co. (Europa) GmbH, Hamburg, Germany
Lab Water System	Arium® pro UV Ultrapure Water System	Sartorius, Göttingen, Germany
	SAFE 2020	Thermo Electron Corporation, Waltham, MA, USA
Laminar Flow Workbench	LaminAir HB2472	Heraeus Instruments, Hanau, Germany
	HERA safe	Thermo Electron Corporation, Waltham, MA, USA
Laser-Scanning Microscope	LSM 780	Carl Zeiss Microscopy GmbH, Jena, Germany
Magnetic stirring	Ikamag® REO/RCT	Merck, Darmstadt, Germany
Micropipette	10, 100, 200 and 1000 µL	Eppendorf, Hamburg,

		Germany
Microplate reader	Tecan Infinite M200 PRO (Absorbance 96 well plates)	Tecan Trading AG, Switzerland
	Tecan Sunrise (Absorbance 96 well plates)	Tecan Trading AG, Switzerland
Mini centrifuge	Sprout	Thermo Fisher Scientific Inc., Waltham, MA, USA
Objective 63x Immersion oil	Plan-Apochromat 63x/1.4 Oil DIC M27	Carl Zeiss Microscopy GmbH, Jena, DE
Osmometer	Osmomat 3000	Gonotec®, Berlin, Germany
pH meter	HI 9017 microprocessor	Hanna Instruments, Kehl, Germany
Power supply	Blotting device 200/2.0	Bio-Rad Laboratories GmbH, Munich, Germany
Resistance measuring device	--	Institut für Klinische Physiologie, CBF, Charité Berlin, Germany
Scale	--	Musahl Waagenservice GmbH, Berlin, Germany
Shaker	Rocking platform VWR	VWR International GmbH, Vienna, Austria
	Rocking platform WT12	Biometra, Göttingen, Germany
	Rocking platform WT17	Biometra, Göttingen Germany
Vortex device	LSE™ Vortex mixer	Corning Inc., NY, USA
Water bath	GFL 1083	Burgwedel Biotech GmbH, Rheinland-Pfalz, Germany
	B4E5	Medingen, Dresden, Germany
	SW20C (Shaking)	JULABO GmbH, Seelbach, Germany
Water transport device	--	Institut für Klinische Physiologie, Charité, Berlin, Germany

2.1.2 Consumable supplies

Consumable supplies are listed in Table 2-2.

Table 2-2. Consumables supplies.

Consumable supplies	Supplier
25 cm ² -tissue culture flask	Corning Inc., NY, USA
75 cm ² -tissue culture flask	Corning Inc., NY, USA
15 mL PPN tube	Corning Inc., NY, USA
50 mL PPN tube	Greiner Bio-One GmbH, Frickenhausen, Germany
6-well-tissue culture plate (10 cm ² per well)	Corning Inc., NY, USA
12-well-tissue culture plate (4 cm ² per well)	Corning Inc., NY, USA
24-well-tissue culture plate (2 cm ² per well)	Corning Inc., NY, USA
96-well microplates for BCA assays	Corning Inc., NY, USA
Biosphere filter tips 10, 200, 1000 µL	SARSTEDT AG & CO. KG, Nümbrecht, Germany many
Cell culture dish (35x10 mm)	SPL, Life Sciences
Stirring rod 120 mm	SARSTEDT AG & CO. KG, Nümbrecht, Germany
CryoPure Tubes 1.6 mL	SARSTEDT AG & CO. KG, Nümbrecht, Germany
Gel-Blotting-papers, Whatman® 3MM	Carl Roth, Karlsruhe, Germany
Microscope slides	Menzel/Glaser, Braunschweig, Germany
Microtiter plate 96 wells (Round bottom)	SARSTEDT AG & CO. KG, Nümbrecht, Germany
Serological Pipet (5, 10 and 25 mL)	Corning Incorporated, NY, USA
Polyscreen (R) PVDF transfer membrane	PerkinElmer, Boston, MA, USA
SafeSeal tube 1.5 mL	SARSTEDT AG & CO. KG, Nümbrecht, Germany
Safe-Lock tubes 0.5 mL	Eppendorf AG, Hamburg, Germany
Surgical disposable scalpels	B Braun™, Thermo Fisher Scientific
Syringe 20 mL	BD Discardit™ II, Spain
Tissue culture dish (100x20 mm)	Corning Incorporated, NY, USA
Transwell filters (Millicell-HA, 0,6 cm ²)	MilliporeSigma, Darmstadt, Germany

2.1.3 Chemicals and kits

Chemicals and kits are listed in Table 2-3.

Table 2-3. Chemicals and kits.

Chemicals	Supplier
1,4 Dithiothreitol (DTT)	Sigma-Aldrich Chemie GmbH, Steinheim, Germany
4-(2-hydroxyethyl)-1-piperazineethanesulfonic acid (HEPES)	Sigma-Aldrich Chemie GmbH, Schnelldorf, Germany
4', 6-diamidino-2-phenylindole (DAPI)	Sigma-Aldrich Chemie GmbH, München, Germany
4-kDa dextran (Lot: 181176 and 200190)	Serva, Heidelberg, Germany
4-kDa FITC-dextran (FD4)	TdB Consultancy, Uppsala, Sweden
β -Mercaptoethanol	Clontech, Heidelberg, Germany
Ammonium persulfate (APS)	Sigma-Aldrich, Schnelldorf, Germany
AquaResist	VWR International GmbH, Vienna, Austria
BCA-Protein Assay (Reagents A and B)	Pierce, Rockford, Illinois, USA
Bovine serum albumin (BSA)	Biomol GmbH, Hamburg, Germany
Calcium chloride, dihydrate	Carl Roth GmbH, Karlsruhe, Germany
Carbogen	Linde AG, München, DE
cOmplete mini, EDTA free, Protein Inhibitor Cocktail	Roche, Basel, Switzerland
DMSO (cell culture quality)	Carl Roth GmbH, Karlsruhe, Germany
Dulbecco's PBS with Mg^{2+}/Ca^{2+}	Gibco, Waltham, Massachusetts, U.S.
Dulbecco's PBS without Mg^{2+}/Ca^{2+}	Gibco, Waltham, Massachusetts, U.S.
Emersion oil for microscopy	VWR International GmbH, Darmstadt, Germany
Ethanol 100%	Fisher scientific, UK/Acros organics, Belgium T.J. Baker, Poland
Ethanol 80%	Chemsolute, TH Geyer, Renningen, Germany
Fetal Bovine Serum (FBS)	Gibco, ThermoFisher Scientific, Berlin, Germany
Glucose	Carl Roth GmbH, Karlsruhe, Germany
Glycine	Carl Roth GmbH, Karlsruhe, Germany
Hydrochloric acid (32%)	Merck, Darmstadt, Germany
Lipofectamine-Reagent (shRNA transfection)	Invitrogen, Karlsruhe, Germany
Lipofectamine-Reagent (CRISPR/Cas9 transfection)	Santa Cruz Biotechnology, Inc., Heidelberg, Germany

Magnesium chloride, hexahydrate	Carl Roth GmbH, Karlsruhe, Germany
Mannitol	Sigma-Aldrich, Schnelldorf, Germany
Methanol	Merck, Berlin, Germany
Milk powder (Blotting grade blocker non-fat dry milk)	Carl Roth, Karlsruhe, Germany
N,N,N',N'-Tetramethylethylenediamine (TEMED)	ThermoFisher Scientific, Waltham, MA, USA
PageRuler Plus Prestained Protein Ladder	ThermoFisher Scientific, Waltham, MA, USA
Paraformaldehyde 16%	Electron microscopy sciences, Hatfield, PA, USA
Penicillin/Streptomycin (P/S)	Corning, Manassas, VA, USA
Polyacrylamide mix (30%)	Carl Roth GmbH, Karlsruhe, Germany
Potassium chloride	Carl Roth GmbH, Karlsruhe, Germany
ProTaq [®] MountFluor	Biocyc, Luckenwalde, Germany
Puromycin (Hydrochloride)	Cayman Chemical Company, Michigan, USA
Resolving Gel Buffer Tris-HCl 1.5M, pH 8.8	Bio-Rad Laboratories GmbH, Munich, Germany
SOC medium	Invitrogen, Karlsruhe, Germany
Sodium azide	Carl Roth GmbH, Karlsruhe, Germany
Sodium chloride	Carl Roth GmbH, Karlsruhe, Germany
Sodium dihydrogen phosphate, monohydrate	Carl Roth GmbH, Karlsruhe, Germany
Sodium Dodecyl Sulfate (SDS)	Carl Roth GmbH, Karlsruhe, Germany
Sodium hydrogen carbonate	Carl Roth GmbH, Karlsruhe, Germany
Sodium hydroxide	Fisher scientific, UK/Acros organics, Belgium
Sodium phosphate dibasic, dodecahydrate	Carl Roth GmbH, Karlsruhe, Germany
Stacking Gel Buffer Tris-HCl 0.5M, pH 6.8	Bio-Rad Laboratories GmbH, Munich, Germany
SuperSignal [™] West Pico PLUS Luminol/Enhancer solution	ThermoFisher Scientific, Waltham, MA, USA
SuperSignal [™] West Pico PLUS Stable peroxide solution	ThermoFisher Scientific, Waltham, MA, USA
Tris-Base	Carl Roth GmbH, Karlsruhe, Germany
Tris-Hydrochloride	Carl Roth GmbH, Karlsruhe, Germany
Triton X-100	Roche, Basel, Switzerland
Trypsin/EDTA	Biochrom, Berlin, Germany
Tween-20	Fisher scientific, UK/Acros organics, Belgium
Water for molecular biology	MilliporeSigma, Darmstadt, Germany
Water for cell culture	MilliporeSigma, Darmstadt, Germany

Water (HPLC Gradient Grade)	J.T. Baker, Gliwice, Poland
-----------------------------	-----------------------------

2.1.4 Cultivation media

Table 2-4 comprises the cultivation media for eukaryotic cells, as well as their composition.

Table 2-4. Cultivation media.

Cultivation medium	Composition	Supplier
Gibco MEM (1X) GlutaMAX™ (Minimum Essential Medium + Earle's salts)	Earle's salts L-glutamine 10% (v/v) FBS 1% (v/v) penicillin (100 U/mL) 1% streptomycin (100 µg/mL) 1.5 µg/mL puromycin	ThermoFisher Scientific, Waltham, MA, USA
Gibco RPMI Medium 1640 (1X) GlutaMAX™	10% (v/v) FBS 1% (v/v) penicillin (100 U/mL) 1% streptomycin (100 µg/mL) 1.5 µg/mL puromycin	ThermoFisher Scientific, Waltham, MA, USA
Transfection medium: MEM (1X) GlutaMAX™ or RPMI Medium 1640 (1X) GlutaMAX™	10% (v/v) FBS	ThermoFisher Scientific, Waltham, MA, USA
Plasmid Transfection Medium	--	Santa Cruz Biotechnology, Inc., Heidelberg, Germany

2.1.5 Buffers and solutions

All buffers and solutions as well as the composition are listed in Table 2-5.

Table 2-5. Buffers and solutions.

Buffers and solutions	Composition
<i>Immunofluorescence labeling</i>	
Blocking buffer	PBS (pH 7.4) 5% goat serum 1% BSA 0.05% Tween 20 0.01% Triton X-100

Washing buffer	PBS (pH 7.4) 1% BSA
<i>Protein extraction</i>	
Cell lysis extraction buffer	10 mM Tris-HCl pH 7.5 150 mM NaCl 0.5% Triton X-100 0.1% SDS protease inhibitor (1 tablet per 10 mL)
<i>SDS-PAGE</i>	
SDS running buffer	25 mM Tris (pH 8.3) 192 mM glycine 0.1% (w/v) SDS
5x SDS loading buffer	500 mM Tris-HCl (pH 6.8) 10% (w/v) SDS 50% (v/v) glycerol 500 mM DTT 0.001% (w/v) bromophenol blue
Separation gel (12%)	0.35 M Tris (pH 8.8) 12% acrylamide mix 0.1% SDS 0.1% ammonium persulfate 0.1% TEMED
Stacking gel	0.125 M Tris (pH 6.8) 5.1% acrylamide mix 0.1% SDS 0.1% ammonium persulfate 0.1% TEMED
<i>Western blotting</i>	
Transfer buffer	25 mM Tris (pH 8.3) 192 mM glycine 10% (v/v) methanol
TBS-T buffer	10 mM Tris (pH 7.4) 137 mM NaCl 0.001% (v/v) Tween-20
Blocking solution	1% PVP-40 0.05% Tween-20
<i>Dilution potential</i>	
Standard-Ringer (Eisenman)	21 mM NaHCO ₃ 119 mM NaCl 5.4 mM KCl 1.2 mM CaCl ₂ 1.0 mM MgCl ₂ 10 mM D(+)-glucose

	3 mM HEPES (pH 7.8)
	21 mM NaHCO ₃
	238 mM Mannitol
	5.4 mM KCl
Mannitol-Ringer (Eisenman)	1.2 mM CaCl ₂
	1.0 mM MgCl ₂
	10 mM D(+)-glucose
	3 mM HEPES (pH 7.8)
<i>Transepithelial water transport</i>	
	134.6 mM NaCl
	2.4 mM Na ₂ HPO ₄ .12H ₂ O
	0.6 mM NaH ₂ PO ₄ .H ₂ O
	5.4 mM KCl
HEPES-buffered solution	1.2 mM MgCl ₂ .6H ₂ O
	1.2 mM CaCl ₂ .2H ₂ O
	10 mM D(+)-glucose
	10.6 mM HEPES (pH 7.4)
<i>Macromolecular permeability</i>	
	113.6 mM NaCl
	21 mM NaHCO ₃
	2.4 mM Na ₂ HPO ₄ .12H ₂ O
	0.7 mM NaH ₂ PO ₄ .H ₂ O
	5.4 mM KCl
Standard-Ringer 111	1.2 mM MgCl ₂ .6H ₂ O
	1.2 mM CaCl ₂ .2H ₂ O
	10 mM D(+)-glucose

2.1.6 Plasmids

Plasmids used for stable transfection of shRNA targeting tricellulin are listed in Table 2-6.

Table 2-6. shRNA plasmids.

Plasmid	TRCN	Clone ID	shRNA sequence	Supplier
920	--	SHC001	pLKO.1-puro Empty Vector Control Plasmid DNA Contains no shRNA insert	Sigma- Aldrich, Schnelldorf, Germany
922	000007 2635	NM_14472 4.1- 989s1c1	5'- CCGGGCAGCCATAGTCTATGTGA ATCTCGAGATTCACATAGACTAT GGCTGCTTTTTG-3'	Sigma- Aldrich, Schnelldorf, Germany

923	000007 2633	NM_14472 4.1- 2011s1c1	5'- CCGGGCAGCATCTATCATGTAGA TACTCGAGTATCTACATGATAGA TGCTGCTTTTTTG-3'	Sigma- Aldrich, Schnelldorf, Germany
924	000007 2634	NM_14472 4.1- 1097s1c1	5'- CCGGGCTGCAATGATCTTCCTGT TTCTCGAGAAACAGGAAGATCAT TGCAGCTTTTTTG-3'	Sigma- Aldrich, Schnelldorf, Germany

Plasmids used for stable transfection of angulin-1 sgRNA, CRISPR/Cas9 and HDR are listed in Table 2-7.

Table 2-7. sgRNA, CRISPR/Cas9 and HDR plasmids.

Plasmid	Clone ID	sgRNA sequence	Supplier
CRISPR/Cas9 negative control	--	--	
sgRNA A	sc-401518 A	5'-GAGATCGCCAGTCGTCCTCG-3'	
sgRNA B	sc-401518 B	5'-AAGGACGATGAGCTCTGCGT-3'	
sgRNA C	sc-401518 C	5'-TACGCAGAGCTCATCGTCCT-3'	
HDR plasmid A	sc-401518 - HDR plasmid A	--	Santa Cruz Biotechnology, Inc.
HDR plasmid B	sc-401518 - HDR plasmid B	--	Heidelberg, Germany
HDR plasmid C	sc-401518 - HDR plasmid C	--	

2.1.7 Antibodies

Antibodies used for immunostaining or immunoblotting are listed with catalogue number (Cat. No.) and supplier in Table 2-8. Additionally, the required dilution factors with regard to application are denoted.

Table 2-8. Antibodies.

Antibody (host)	Dilution for immunostaining (in blocking buffer)	Dilution for immunoblotting (in TBST buffer)	Cat. No.	Supplier
<i>Primary antibody</i>				
β-actin (mouse)	--	1:10000	A5441	Sigma-Aldrich, Schnellendorf, Germany
Claudin-1 (rabbit)	1:500	1:1000	51-9000	ThermoFisher Scientific, Waltham, MA, USA
Claudin-2 (rabbit)	1:250	1:1000	516100	ThermoFisher Scientific, Waltham, MA, USA
Claudin-3 (rabbit)	1:300	1:1000	341700	ThermoFisher Scientific, Waltham, MA, USA
Claudin-4 (mouse)	1:300	1:1000	329400	ThermoFisher Scientific, Waltham, MA, USA
Claudin-5 (mouse)	1:300	1:1000	322500	ThermoFisher Scientific, Waltham, MA, USA
Claudin-5 (Rabbit)	1:300	1:1000	341600	ThermoFisher Scientific, Waltham, MA, USA
Claudin-7 (rabbit)	1:300	1:1000	349100	ThermoFisher Scientific, Waltham, MA,

				USA
Claudin-8 (rabbit)	1:300	1:1000	710222	ThermoFisher Scientific, Waltham, MA, USA
Occludin (mouse)	1:250 1:500	--	331500	ThermoFisher Scientific, Waltham, MA, USA
Occludin (rabbit)	1:250 1:500	1:1000	711500	ThermoFisher Scientific, Waltham, MA, USA
Tricellulin (rabbit)	1:500	1:2000	700191	ThermoFisher Scientific, Waltham, MA, USA
Angulin-1 (rabbit)	1:1000	1:3000	HPA007270	Sigma-Aldrich, Schnellendorf, Germany
Angulin-2 (rabbit)	--	1:1000	ARP55751_P050	Aviva Systems Biology Corporation, San Diego, CA, USA
Angulin-2 (rabbit)	--	1:1000	orb518224	Biorbyt LLC, St Louis, MO, USA
Angulin-3 (rabbit)	--	1:1000	HPA012545	Sigma-Aldrich, Schnellendorf, Germany
Angulin-3 (rabbit)	--	1:1000	ARP70574_P050	Aviva Systems Biology Corporation, San Diego, CA, USA
AQP-1 (mouse)	--	1:1500	CF502357	OriGene Technologies GmbH, Herford, Germany
AQP-3 (rabbit)	--	1:1500	LS-B9821/58986	LifeSpan BioScience, Seattle, WA, USA
AQP-4 (rabbit)	--	1:1500	LS-B12547/128405	LifeSpan BioScience, Seattle, WA, USA

AQP-7 (mouse)	--	1:1500	SC-376407	Santa Cruz Biotechnology, Inc. Heidelberg, Germany
SGLT1 (rabbit)	--	1:1000	LS- C179216/71 050	LifeSpan BioScience, Seattle, WA, USA
LI-Cadherin (mouse)	--	1:1000	SC-393533	Santa Cruz Biotechnology, Inc. Heidelberg, Germany
ZO-1 (rabbit)	1:500	--	61-7300	ThermoFisher Scientific, Waltham, MA, USA
ZO-1 (mouse)	1:500	--	610967	BD Biosciences, Heidelberg, Germany
Secondary antibody				
Peroxidase -conjugate affiniPure F(ab')₂ Fragment Goat anti- rabbit IgG (H+L)	--	1:1000	111-036- 003	Jackson ImmunoResearch Laboratories, Cambridge House, UK
Peroxidase -conjugate affiniPure F(ab')₂ Fragment Goat anti- mouse IgG (H+L)	--	1:1000	115-036- 003	Jackson ImmunoResearch Laboratories, Cambridge House, UK
Goat anti- Rabbit IgG (H+L) Highly Cross- Adsorbed, Alexa Fluor	1:500	--	A-11034	ThermoFisher Scientific, Waltham, MA, USA

488				
Goat anti-Mouse IgG (H+L) Highly Cross-Adsorbed, Alexa Fluor 594	1:500	--	A11032	ThermoFisher Scientific, Waltham, MA, USA
DAPI	1:1000	--	--	Sigma-Aldrich Chemie GmbH, München, Germany

2.1.8 Cell lines

Table 2-9 outlines cell lines and the originating species, tissue and cell type.

Table 2-9. Cell lines.

Cell line	RRID	Species/tissue/cell type	Reference/supplier
HT-29/B6	CVCL_LJ30	Human/colon/intermediate-tight epithelial cell line/low transepithelial resistance	(Kreusel et al., 1991; Zeissig et al., 2004)
MDCK C7	CVCL_0423	Dog/kidney/tight epithelial cell line/high transepithelial resistance	(Zak et al., 2000; Wunsch et al., 1995)

2.1.9 Software

Microsoft® Office 2011-2016, GraphPad Prism® 8, Image Studio Lite, image processing packages (ImageJ (Schindelin et al., 2015) and Fiji (Schindelin et al., 2012)), and Zeiss ZEN 2009.

2.2 Cell biological methods

2.2.1 Cell culture

The kidney cell line MDCK C7 (RRID: CVCL_0423) exhibits a very high ratio of paracellular resistance over transcellular resistance as well as very high transepithelial resistance (TER), which therefore makes it an excellent model of a tight epithelium (see Table 2-9). On the other hand, the colon adenocarcinoma cell line HT-29/B6 (RRID: CVCL_LJ30) exhibits a medium-high ratio of paracellular resistance over transcellular resistance as well as an intermediate TER, which therefore makes it an excellent model of an intermediate-tight epithelium (see Table 2-9). Both cell lines were transfected in order to get a knockdown of tricellulin or knockout of angulin-1 (see Chapter 2.2.2).

The transfected cells were incubated at 37°C, and 5% CO₂ in sterilization incubators held. For the cultivation of the cells, sterile culture vessels made of plastic were used. The MDCK C7 cells were cultured in a nutrient medium Earl's salts MEM (minimal essential medium), and HT-29/B6 cells were cultured in RPMI 1640 AQ Media, both supplemented with 10% FCS as well as 100 U/mL penicillin / 100 µg/mL streptomycin and 1.5 µg/mL of puromycin (see Table 2-4). Every second to third day, the medium was changed. The consumption of nutrients generated a change in the color of the medium due to the change in the pH of the indicator.

For protein lysates, water flux measurements and electrophysiological and flux studies, cell monolayers were cultured on porous culture plate inserts (Millicell PCF filters, pore size 0.4 µm, effective area 0.6 cm², Millipore GmbH, Schwalbach, Germany) for 7–10 days before they were used for experiments.

2.2.2 Transfection of cells

Transfection is the transfer of DNA into eukaryotic cells. There are several transfection methods (microinjection, calcium phosphate precipitation, electroporation, liposomes, DEAE-dextran), resulting in handling and transfection efficiency sometimes very different. For transfection with tricellulin shRNA, lipofectamine was used. This transfection reagent consists of liposomes, which pack the DNA in and then into the transport cell via

hydrophobic interaction with the membrane. In the cell, the DNA is transcribed and translated.

For stable tricellulin knockdown, HT-29/B6 and MDCK C7 cells were transfected with pLKO.1-puro vector containing a sequence for shRNA targeting tricellulin or pLKO.1-puro empty vector as a negative control (see Table 2-6). For stable angulin-1 knockout, HT-29/B6 and MDCK C7 cells were transfected with CRISPR/Cas9 plasmids (Santa Cruz Biotechnology, Inc. Heidelberg, Germany) containing three different sgRNA sequences targeting different exons of angulin-1 and their respective HDR plasmids (Santa Cruz Biotechnology, Inc. Heidelberg, Germany) for homologous recombination (see Table 2-7). The CRISPR/Cas9 negative control plasmid (Santa Cruz Biotechnology, Inc. Heidelberg, Germany) was used as a negative control (see Table 2-7).

2.2.2.1 shRNA plasmids

Cells were transfected at high cell density for high efficiency, high expression levels, and to minimize cytotoxicity. One day before transfection, in 6-well plates, 3×10^5 - 5×10^5 cells were seeded in 4 mL of growth medium without antibiotics so that cells will be 50-80% confluent at the time of transfection. On the transfection day, the cells were washing once in 2 mL serum-free medium (\emptyset serum, \emptyset P/S).

For each transfection sample, complexes were prepared as follows:

- 4 μ g of DNA (vector control: pLKO1.puro; tricellulin shRNA: 922, 923, and 924) were diluted in 200 μ L of serum-free medium (\emptyset serum, \emptyset P/S). The solution was mixed gently and incubated for 5 minutes at room temperature.
- 10 μ L of lipofectamine 2000 were diluted in 200 μ L of serum-free medium (\emptyset serum, \emptyset P/S) and incubated for 5 minutes at room temperature.
- After the 5 minutes incubation, the diluted DNA was incubated with diluted Lipofectamine 2000 (total volume = 500 μ L). The complexes were mixed gently and incubated for 30 minutes at room temperature.

The complexes were added to each well-containing cells and medium and mixed gently by rocking the plate back and forth. The medium was changed after 6 hours for medium containing serum and P/S. The cells were incubated at 37°C in a CO₂ incubator for 48

hours prior to testing for tricellulin expression. Forty-eight hours after transfection, the cells were split from one well to four big dishes and resuspended in medium without puromycin. The day after, the media was changed for medium containing puromycin at the appropriate concentration. For effective selection, cells should be subconfluent. Prior to using the puromycin antibiotic, it was titrated to determine the optimal concentration for target cell line. The lowest concentration that kills 100% of non-transfected cells in 3–5 days from the start of puromycin selection was used (2 $\mu\text{g}/\text{mL}$ for HT-29/B6 and 6 $\mu\text{g}/\text{mL}$ for MDCK C7 cells).

For the next two weeks the antibiotic-containing medium was replaced every two to three days (or as needed). During the second week, the cells were monitored for distinct “islands” of surviving cells. Depending on the cell type, drug-resistant clones appeared in 2–3 weeks. Large (500-1000 cells) and healthy colonies were isolated using cloning cylinders and maintained in medium containing puromycin (1.5 $\mu\text{g}/\text{mL}$). Successfully transfected clones were frozen in liquid nitrogen for later analysis. Selected clones were then used for tricellulin KD characterization.

2.2.2.2 sgRNA, CRISPR/Cas9, and HDR plasmids

In a 6-well tissue culture plate, 1.5×10^5 - 2.5×10^5 cells were seeded in 3 mL of antibiotic-free standard growth medium per well 24 hours prior to transfection. The cells were grown to a 50-80% confluency. Healthy and subconfluent cells are required for successful KO and HDR Plasmid transfection.

For each transfection sample, complexes were prepared as follows:

Plasmid DNA/UltraCruz[®] Transfection Reagent amounts: 1 $\mu\text{g}/10 \mu\text{L}$, 2 $\mu\text{g}/10 \mu\text{L}$, and 3 $\mu\text{g}/10 \mu\text{L}$. Because more than one plasmid was transferred (i.e., the CRISPR/Cas9 KO plasmid with the HDR plasmid), the DNA of the plasmids was mixed in equivalent proportions. No antibiotics were added to the plasmid transfection medium (sc-108062).

- Solution A: For each transfection, 1-3 μg of Plasmid DNA were diluted into Plasmid Transfection Medium to bring the final volume to 150 μL . It was pipetted up and down to mix and incubated for 5 minutes at room temperature.
- Solution B: For each transfection, 10 μL of UltraCruz[®] Transfection Reagent were diluted with enough Plasmid Transfection Medium to bring the final volume to 150

μL . It was pipetted up and down to mix and incubated for 5 minutes at room temperature.

The Plasmid DNA solution (Solution A) was added dropwise directly to the dilute UltraCruz[®] Transfection Reagent (Solution B) using a pipette. It was vortexed immediately and incubated for no less than 20 minutes at room temperature. Prior to transfection, the media was replaced with fresh antibiotic-free growth medium. The 300 μL Plasmid DNA/UltraCruz[®] Transfection Reagent Complex (Solution A + Solution B) were added dropwise to every well and mixed gently by swirling the plate. The cells were incubated for 24-72 hours under conditions generally used to culture the cells. No media replacement was necessary during the first 24 hours post-transfection. The media was replaced as needed 24-72 hours post-transfection. Forty-eight hours post-transfection, the cells were split from one well to four big dishes and resuspended in fresh medium. The day after, the cells were resuspended in fresh medium containing puromycin at the appropriate concentration (2 $\mu\text{g}/\text{mL}$ for HT-29/B6 and 6 $\mu\text{g}/\text{mL}$ for MDCK C7 cells). Cell colonies were selected for a minimum of 7–14 days, similar to how it was done for tricellulin KD colonies. Approximately every 2–3 days, the media was aspirated and replaced with freshly prepared selective media (1.5 $\mu\text{g}/\text{mL}$ puromycin). Successful transfection of angulin-1 CRISPR/Cas9 KO Plasmid was confirmed by Western blot.

2.2.3 Cryopreservation and thawing of cells

In addition, the cells must be viable and in exponential growth. The cells were harvested by spinning as gently as possible (speed should not exceed 400 x *g*). The cells were resuspended in growth medium with serum at room temperature to a concentration of 2×10^6 - 2×10^7 cells per mL. To avoid damage to the cell during freezing, DMSO in 7.5% concentration, a cryoprotectant, was added to the growth medium in which the cells were frozen. The cells were slowly frozen at -80°C before being transferred into liquid nitrogen (-140°C to -196°C).

To obtain the best possible survival, the thawing of the cells must be performed as quickly as possible. Once the CryoTube vial was removed from the liquid nitrogen tank, it was placed directly into a 37°C water bath and shaken until it was completely thawed. To avoid transfer of microorganisms from the liquid nitrogen tank or the water bath to the

laminar flow cabinet and subsequently to the culture, the CryoTube vials were soaked in 70% ethanol before they were transferred to the laminar flow cabinet. For cultivation, the cells were transferred into the respective culture medium. In order to avoid physical damage of cells that form a monolayer, such cultures were left untouched in the incubator for at least 16 hours before assessing the result.

2.2.4 Cell passage

To obtain cells from culture bottles, they were first washed with PBS and then treated with trypsin solution. The trypsin activity was at 37°C until all cells detached from the bottom of the flask (about 30-120 min). Then the cells were diluted in 10 mL of medium and potted up with a pipette. The FBS contained in the medium inhibited the trypsin. As needed, the cells were counted in a Neubauer counting chamber (Stone et al., 2009) and then converted to the required volume seeded in new vessels:

- Small bottles (25 cm ²)	450 µL to 7 mL medium
- Medium-sized bottles (75 cm ²)	1000 µL to 19 mL medium
- 6-well plates	350-700 µL to 4 mL/well
- 12-well plates	200 µL to 2 mL/well
- 24-well plates	100 µL to 1 mL/well
- HA filter (0.6 cm ²)	450 µL

After that, the cells were cultured again in the incubator at 37°C / 5% CO₂.

2.2.5 Immunofluorescence labeling and microscopy

Immunofluorescence studies were performed on culture-plate inserts. Confluent monolayers were rinsed with PBS, fixed with 4% paraformaldehyde for 20 min and permeabilized for 10 min with PBS containing 0.5% (v/v) Triton X-100. To block non-specific binding sites, cells were then incubated in PBS containing 1% (w/v) BSA and 5% (v/v) goat serum (blocking solution; Biochrom) for 60 min (see Table 2-5). All subsequent washing procedures were performed with this blocking solution. After blocking, cells were incubated overnight at 4°C with the corresponding primary antibody (see Table 2-8), followed by washing steps and incubation for 60 min at room temperature with the respective secondary antibody (see Table 2-8) and 4',6-diamidino-2-phenylindole (DAPI,

1:1000). Images were obtained with a confocal laser-scanning microscope (LSM 780, Zeiss, Jena, Germany) and processed using ZEN software (Zeiss).

For whole-mount STED imaging, the cell filters were washed gently in PBS, fixed for 20 min in 4% PFA and subjected to the standard IF protocol described previously. Highly cross-absorbed secondary antibody Atto 647N (Active Motif 15038) was used together with Occludin monoclonal antibody, mouse (OC-3F10), Alexa Fluor® 594 conjugate (Invitrogen 331594). Cell membranes were flat mounted in ProLong Gold Antifade Mountant (Invitrogen P36934) to obtain optimal resolution. The STED images of the MDCK C7 cells were taken with a STEDYCON microscope (Abberior Instruments). Dual-color STED imaging was performed by sequential excitation of Occludin-Alexa Fluor® 594 at 590 nm and Atto 647N at 647 nm. For emission depletion, the 775 nm STED laser was used. Time-gated detection was set from 0.3 to 6 ns. Images were sequentially acquired with a HC PL APO CS2 100x/1.40 NA oil immersion objective (Leica Microsystems), and a scanning format of 1024x1024 pixels, 8-bit sampling, 16x line averaging and 6x optical zoom, yielding a voxel dimension of 18.9x18.9 nm. To minimize thermal drift, the microscope was housed in a heatable incubation chamber. Raw data obtained from STED imaging were analyzed by custom macro (ImageJ).

2.2.6 Topology measurements

Morphometric parameters of MDCK C7 and HT-29/B6 cells were obtained from stained cells (tricellulin, angulin-1, occludin, and ZO-1). Epithelial cell membrane images were segmented using a macro written to use in FIJI-ImageJ (Appendix C. Table 7-7). Cells at the edge of the field of view were excluded from the analysis. The number of cells, area, and perimeter were calculated using the Analyze Particles tool. The tTJs were counted manually, and the number of cell sides (vertices) was identified using the “Neighbor analysis” macro from the BioVoxel Toolbox using water shedding and Voronoi analysis.

Using the number of cells counted in each area analyzed, the average cell surface area and cell density was estimated. The total length of TJs within the studied areas was measured and normalized to m/cm^2 . As each bicellular TJ is shared by two cells, TJ length per cell was doubled. For calculating of the TJ length/cell, the total length in m/cm^2 was calculated from cell density. Tricellular contacts were counted and normalized to

within the analyzed area. As each tricellular contact is shared by three cells (very seldom by four contacts), the tricellular contact number was tripled and quadrupled to obtain the average tricellular contact number per cell. These measurements are based on at least three independent seedings of cells (between 3 and 10 immunofluorescence images).

2.2.7 Freeze-fracture electron microscopy

At a confluency of 100%, cells were washed with PBS (containing $\text{Ca}^{2+}/\text{Mg}^{2+}$) and fixed with 2.5% glutaraldehyde at RT for 2 hours. After washing twice with PBS (containing $\text{Ca}^{2+}/\text{Mg}^{2+}$), the cells were stored at 4°C in 0.25% glutaraldehyde. Small rectangles of the bottom of the cell culture filters were cut out, and the attached cells were cryoprotected in 30% glycerol for 30 min, placed between two gold specimen holders and shock frozen in R422D (TEGA GmbH, Würzburg, Germany) cooled by liquid nitrogen (-210°C). The samples were fractured using the freeze-fracture device Denton DV-502 (Denton Vacuum, Moorestown, NJ, USA) at -100°C and 2×10^{-7} mTorr. The samples were vaporized at -150°C (2×10^{-7} mTorr) with a platinum layer and then a layer of carbon. This result in a thin metal film on the broken sample. The replicas were cleaned with 12% sodium hypochlorite, washed several times in ddH₂O, and mounted on a copper mesh grid. The Zeiss 902A electron microscope was used to examine the replicas at 80kV. Magnification between 3000 and 20000 (for thin sections) or 20000 to 50000 (for freeze-fracture) was used.

2.3 Biochemical methods

2.3.1 Preparation of cell lysates

For total protein extraction, cells grown on culture plate inserts were first washed with PBS and then scraped and homogenized in 100 µL lysis buffer (see Table 2-5). The cell suspension was transferred to a 1.5 mL reaction vessel, and after 90 to 120 minutes incubation at 4°C and intermediate vortexing was centrifuged at 15000 g, 4°C for 30 min. The supernatant contained the total protein extract and was stored at -20°C.

2.3.2 Determination of the protein concentration

The principle of Pierce protein concentration determination is the reaction of proteins with copper at alkaline pH, resulting in a colored copper complex, which by absorption

measurement at 562 nm for the calculation of the contained protein concentration is used. This is compared with a calibration series of known protein concentrations. This method is also called BCA assay (Bicinchoninic acid assay) [reagents were purchased from Pierce (Perbio Science, Bonn, Germany)].

The preparation was carried out in microtiter plates, always working in duplicate. One calibration set of 10 μ L BSA solutions each at concentrations of 0.2 mg/mL, 0.8 mg/mL and 1.2 mg/mL, and also 10 μ L of lysis buffer were also presented as the samples to be measured. Upon adding the protein samples (10 μ L), 190 μ L of the BCA solution was added to each batch pipetted and the entire microtiter plate incubated at 37°C for 30 min. After cooling at room temperature, the plate was measured in the Tecan Spectra photometer (Tecan Deutschland, Crailsheim, Germany) at 562 nm, and the concentration can be determined.

2.3.3 Sodium dodecyl sulfate-polyacrylamide gel electrophoresis (SDS-PAGE)

Proteins were separated according to their electrophoretic mobility by one-dimensional sodium dodecyl sulfate-polyacrylamide gel electrophoresis (SDS-PAGE). SDS, an anionic detergent, linearizes the polypeptide and imparts an even distribution of negative charge per mass unit that allows a fractioning by approximate size via electrophoresis. The composition of the stacking, as well as the separation gel, is listed in Table 2-5. The protein probes were incubated with 5x SDS loading buffer (Table 2-5) for 10 min at 95°C and loaded to the SDS-polyacrylamide gel. The separation was performed at 100 V in an SDS-PAGE chamber containing 1x SDS running buffer to the desired running distance; recognizable by the running front of blue of bromophenol contained in the sample buffer. The gel was then removed from the chamber and from the glass plates to be treated further.

2.3.4 Western blotting

Western blot analysis was performed as reported (Amasheh et al., 2002). Aliquots between 10 and 15 μ g protein samples were separated by 12% SDS-polyacrylamide gel electrophoresis and then transferred to a PVDF membrane (Perkin Elmer, Rodgau, Germany) for the detection of different proteins. After blocking for 2 hours in 1% PVP-40

and 0.05% Tween-20, membranes were incubated overnight with the corresponding primary antibody (see Table 2-8) at 4°C. After removing the first antibody and three washing steps, the membranes were incubated for 2 hours with the second peroxidase-conjugated antibody (anti-mouse or anti-rabbit) in 1-2% of milk powder prepared in TBST 1X at room temperature. For detection of the chemiluminescence signal induced by the addition of Lumi-LightPLUS western blotting kit (Roche), a Fusion FX7 (Vilber Lourmat, Eberhardzell, Germany) were used. Densitometric analysis was performed with quantification software (Image Studio™ Lite, LI-COR Biosciences, Lincoln, Nebraska USA). Equal protein loading in each lane was verified by comparison with signals for β -actin (Sigma-Aldrich). For Western blot analysis, lysates of at least three individual cell cultures were used, and one representative experiment is shown.

2.4 Biophysical methods

2.4.1 Transepithelial electrical resistance measurements

Transepithelial electrical measurements permit quantifying ion permeability and barrier function in cell cultures (Yeste et al., 2018). This technique is based on the measurement of the cellular sheet's electrical properties employing extracellular electrodes. In particular, a voltage or current perturbation is applied between electrodes placed on both sides of the barrier. The measurements that give primary information about a cellular barrier are transepithelial voltage (V_{te}), transepithelial resistance (TER), and short-circuit current (I_{sc}) (Yeste et al., 2018).

Transepithelial resistance (TER) was measured at 37°C using chopstick electrodes (STX2, World Precision Instruments, Friedberg, Germany). Electrodes were reproducibly positioned by a semi-automatic motor-driven device and signals were processed by a low-frequency clamp (both own design of Clinical Physiology labs). The bathing solution's resistances and the blank filter support were subtracted from measured values, which were finally converted to $\Omega \cdot \text{cm}^2$.

2.4.2 Dilution potential measurements

Dilution potential measurements for the determination of ion permeabilities were performed in conventional Ussing chambers Water-jacketed gas lifts kept at 37°C were

filled with 10 mL circulating fluid on each side. Bathing solution contained (in mM) 119 NaCl, 21 NaHCO₃, 5.4 KCl, 1.2 CaCl₂, 1 MgSO₄, 3 HEPES and 10 D(+)-glucose (see Table 2-5), and was gassed with 95% O₂ and 5% CO₂ to ensure a pH value of 7.4. All experimental data were corrected for the resistance of the empty filter and the bathing solution. Dilution potentials were measured with a modified bathing solution on the apical or basolateral side of the epithelial monolayer. In the modified bathing solution used for the determination of Na⁺ and Cl⁻ permeability, NaCl was iso-osmotically replaced by mannitol. The ratio of PNa⁺ and PCl⁻ and the absolute permeabilities for Na⁺ and Cl⁻ were calculated as described before (Krug et al., 2012).

2.4.3 Measurement of 4-kDa FITC-dextran flux

Permeability assays consist of tracer diffusion measurements in which the tracers are added in a donor compartment (i.e., the apical or basolateral side) and quantified in a received compartment (i.e., the opposite side) along time (Yeste et al., 2018). This methodology permits to assess the transepithelial transport in both directions, distinguishing between active and passive transport mechanisms (Yeste et al., 2018). To ensure the barrier integrity during permeation assays, especially at the end of the experiments, these studies are usually combined with transepithelial electrical measurements (Yeste et al., 2018).

Flux studies were performed in conventional Ussing chambers under voltage-clamp conditions. Dextran flux was measured in 5 mL circulating 111-Ringer's (see Table 2-5) containing 37 mM unlabeled 4-kDa dextran on both sides of the cells for isosmotic conditions and only on the apical side for osmotic conditions. After the addition of 0.2 mM 4-kDa FITC-labeled dialyzed dextran (Sigma-Aldrich) to the apical chamber (final concentration), basolateral samples (200 µL) were collected at 0, 20, 40, 60, 80, 100, 120- and 140-min. Tracer fluxes were determined from FITC-dextran samples, which were measured with a fluorometer at 520 nm (Spectramax Gemini, Molecular Devices, Ismaning, Germany). Dextran permeability was calculated from $P=J/\Delta c$, where P is the permeability (cm/s), J is the flux (mol·h⁻¹·cm⁻²), and c is the concentration (mol/l).

2.4.4 Measurement of transepithelial water transport

Water flux measurements were performed using a modified Ussing chamber with two glass tubes instead of the gas lifts described before (Figure 2-1) (Rosenthal et al., 2017a; Rosenthal et al., 2019; Rosenthal et al., 2017b; Rosenthal et al., 2010). Throughout these experiments, transepithelial resistance (TER, $\Omega \cdot \text{cm}^2$), short-circuit current (I_{SC} , $\mu\text{A} \cdot \text{cm}^{-2}$), and transepithelial voltage (mV) were recorded routinely by a standard PC with ADC-DAC cards. Pulses of 1 second duration between 1 μA and 30 μA were applied at 25 second intervals to obtain the TER. The resistance of the bathing solution and blank filter support was measured prior to each experiment and subtracted. The stability of transepithelial resistance during the experiment was used as an indicator of cell viability. The transepithelial voltage was clamped to 0 mV to avoid effects on ion fluxes on water flux. It should be kept in mind that our method does not directly discriminate between the pathways for water transport, i.e., transcellular through the cell membranes and paracellular through the bTJ or the tTJ but uses a defined perturbation of tricellulin or angulin-1 to compare the results with that of simultaneously grown control clones of the respective cell line.

Cell filters were mounted in Ussing chambers and perfused with HEPES-buffered solution with the following composition (in mM): 144.8 NaCl, 2.4 Na_2HPO_4 , 0.6 NaH_2PO_4 , 5.4 KCl, 1.2 MgCl_2 , 1.2 CaCl_2 , 10.6 HEPES, 10 D(+)-glucose (see Table 2-5). The pH value of the perfusion solution was pH 7.4. A rotary pump ensured constant circulation of the perfusion solution ($4.0 \text{ mL} \cdot \text{min}^{-1}$) and fast fluid exchange in both hemichambers (volume 500 μL) to avoid the effects of unstirred layers on water permeability. Water flux was induced by a transepithelial osmotic gradient: (i) 100 mM mannitol, (ii), 37 mM 4 kDa-dextran, (iii) 100 mM 4 kDa-dextran, (iv) 5.5 mM 40 kDa-dextran or (v) 2.5 mM albumin. The solution was added to the apical compartment of the Ussing chamber. The dextrans' molecular diameters were estimated using the equation: $d(\text{\AA}) = 0.215 \cdot (\text{MW})^{0.587}$.

The osmolality of the perfusion solutions (mosmol/kg of water, abbreviated mOsm) was determined using a Vapor Pressure Osmometer (5100B, Wescor, Logan, UT) and a freezing point depression osmometer (Osmomat 3000, Gonotec, Berlin, Germany). The osmolality of the HEPES-buffered solutions is annotated in Table 2-10.

Table 2-10. Osmolality of the HEPES-buffered solutions using a freezing point depression osmometer.

		n	Concentration (mM)	Osmolality (mOsm/kg of water) Mean \pm SEM
Tricellulin KD	HEPES	10	--	308.0 \pm 4.4
	Mannitol	10	100 mM	410.3 \pm 1.9
	4-kDa dextran	10	37 mM	396.2 \pm 6.8
	4-kDa dextran	10	100 mM	877.8 \pm 13.7
	40-kDa dextran	5	5.5 mM	390.2 \pm 2.5
	Albumin	5	2.5 mM	340.0 \pm 2.0
Angulin-1 KO	HEPES	17	--	289.0 \pm 13.7
	Mannitol	17	100 mM	391.4 \pm 14.6
	4-kDa dextran	5	37 mM	396.0 \pm 4.5

The fluid level in both glass tubes was monitored by a visual system ColorView XS (Olympus Soft Imaging Solutions GmbH, Münster, Germany), at time 0 min and with intervals of 10 min over a period of 120 min. Transepithelial water flux, given as flux per square centimeter and hour, was calculated from the difference between the menisci at the registration times. Fluxes directed from the basolateral to the apical compartment were defined as positive flux.

At specific and constant gradients, water fluxes are proportional to apparent water permeability, so that conclusions on water permeability can be drawn from measured water fluxes. Water permeability could be calculated from $P=J/\Delta c$, where P is the permeability (cm/s), J is the flux ($\text{mol}\cdot\text{h}^{-1}\cdot\text{cm}^{-2}$), and c is the concentration (mol/l). As water fluxes are the primary measure, these are given in the Results chapter.

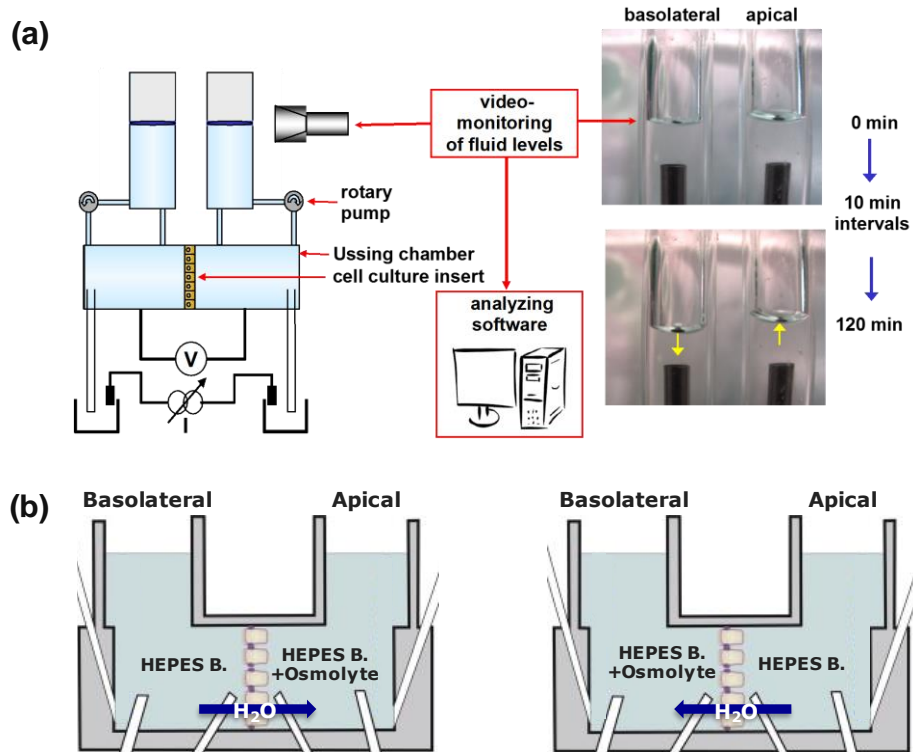


Figure 2-1. Method for analyzing transepithelial water transport (Rosenthal et al., 2017b; Rosenthal et al., 2010). For water transport analysis, **(a)** a modified Ussing chamber with two separated glass tubes in a heated chamber is used instead of gas lifts. Electrophysiological parameters are monitored during the experiment. A rotary pump ensures the constant circulation of the perfusion solution in both chambers to avoid unstirred layer effects. Volume flow induced by a specific osmotic gradient is recorded over 2 hours with intervals of 10 min by a video-optic system recording the height of the menisci on both sides, and water flux is calculated according to the calibration. **(b)** After the cells are mounted, a transepithelial osmotic gradient was induced with different osmolytes (mannitol, 4-kDa dextran, 40-kDa dextran, and albumin) either from the apical or basolateral side. Total transepithelial water transport is measured before and after molecular modification of either the paracellular or the transcellular pathway for transepithelial water transport. As this method does not distinguish technically between trans- and paracellular flux, the contribution of the modified pathway to transepithelial water permeability was determined from the difference between control cells and modified cells.

2.5 Statistics

Graphing and statistics were performed using GraphPad Prism8. Data are expressed as mean values \pm SEM, indicating *n* as the number of single measurements, and *N* is the number of independent experiments, which means independent seeding of cells. Statistical analysis was performed using Student's t-test between the tricellulin KD clone and the corresponding control (KD 23 versus control 2, KD 24 versus control 9 in MDCK

C7 cells). In the tricellulin KD in HT-29/B6 cells and angulin-1 KO in both cell lines, ANOVA one-way and the Tukey and Dunnett adjustment for multiple testing were applied. P values of less than 0.05 were considered significant (*,[#]P≤0.05, **,[#]P≤0.01, ***,^{###}P≤0.001).

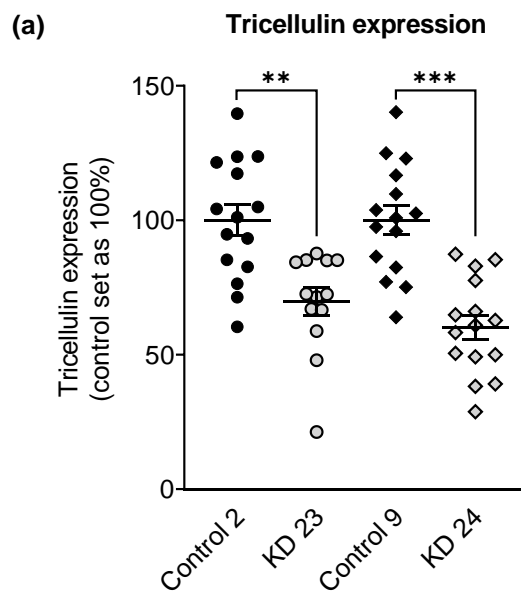
3. Results

3.1 Tricellulin knockdown (KD): MDCK C7 cells

3.1.1 Characterization of tricellulin KD in MDCK C7 cells

In order to investigate the specific role of tricellulin on paracellular water transport in the tight epithelium, the canine kidney cell line MDCK C7 was transfected with shRNA targeting tricellulin (see Chapter 2.2.2.1). Firstly, puromycin-resistant cell clones were screened for tricellulin knockdown by Western blotting (see Chapter 2.3). Two KD clones and two control clones were investigated (KD 23 and its corresponding control 2, and KD 24 and its corresponding control 9). The two KD clones showed a high but different reduction in tricellulin expression: clone KD 23 showed decreased tricellulin by 30%, while clone KD 24 exhibited a drop by 40% (Figure 3-1a, Appendix B. Table 7-1).

On the other hand, the expression and the localization of the remaining tricellulin protein were analyzed after the transfection (see Chapter 2.2.5). The proper localization of tricellulin as dots at TCs was confirmed for the four clones by immunofluorescence confocal laser-scanning microscopy using occludin as a TJ marker (Figure 3-1b).



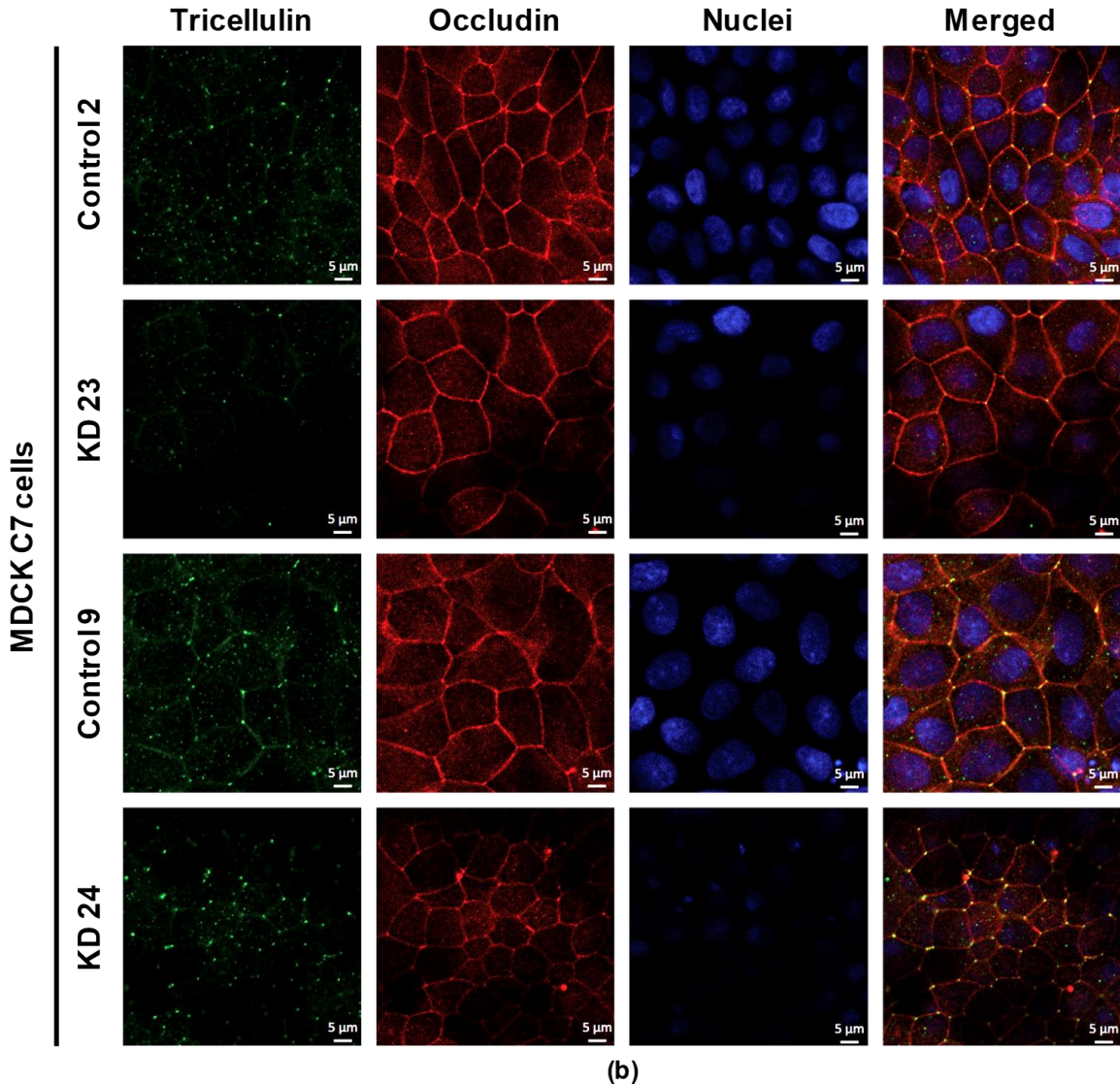


Figure 3-1. Expression and localization of tricellulin in MDCK C7 control and knockdown cells **(a)** Densitometric analysis of tricellulin protein expression levels in stable shTRIC transfectants (KD 23 and KD 24) in comparison to vector-transfected controls (Control 2 and Control 9). shTRIC leads to decreased tricellulin expression ($n=15$, $**P\leq 0.01$, $***P\leq 0.001$). **(b)** Localization of tricellulin in the four clones used throughout this study. In controls and KD clones, tricellulin is localized at tTJ sites. Tricellulin: green; occludin: red; DAPI: blue.

The topology parameters (see Chapter 2.2.6) of fluorescence stained tricellulin knockdown MDCK C7 cells using the program Fiji-ImageJ for estimating the contribution of tricellulin at tTJ to overall permeability are shown in Appendix C. Table 7-5 and Figure 7-3. The most interesting result is that within the analyzed area, the TJ length per cell was

higher in the KD 23 in comparison with its control 2. In contrast, the KD 24 had a lower TJ length per cell than its control 9. On tTJ levels, the tTJ density was reduced in the KD 23 and increased in the KD 24 compared to their respective controls. The higher frequency of tTJ occurrence in the KD 24 monolayers suggests that the tTJ has more impact in that clone than in the KD 23 clone. Concerning the number of vertices or neighboring cells, it was observed that for all clones, there is an average value between 4 and 5 vertices (Appendix C. Figure 7-3), which also corresponds to the calculated number of tTJ per cell (5 tTJ/cell).

3.1.1.1 Effect on the transepithelial resistance (TER)

The transepithelial resistance (TER), a rough indicator for the monolayer's ion permeability, was determined using chopstick electrodes (see Chapter 2.4.1). The data obtained show that the TER was reduced in tricellulin knockdown MDCK C7 cells (Figure 3-2, Appendix B. Table 7-1). KD 24 exhibited a more substantial reduction of tricellulin expression and a stronger TER decrease compared to the corresponding control than KD 23 (75% and 50%, respectively). These results suggest that tricellulin expression is essential for the barrier function against ions in the MDCK C7 cell line.

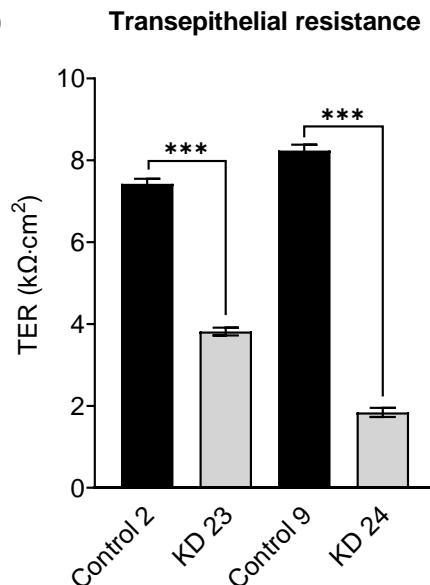


Figure 3-2. Functional analysis of tricellulin knockdown in MDCK C7 cells. Effect of tricellulin knockdown on transepithelial resistance (TER). Tricellulin knockdown decreases TER in MDCK C7 cells. (n=24, ***P≤0.001).

3.1.1.2 Analysis of permeability for sodium and chloride

In order to investigate the ion permeabilities for sodium (P_{Na^+}) and chloride (P_{Cl^-}) in this epithelial cell line, dilution potential measurements were performed (see Chapter 2.4.2). The results showed that in tricellulin-deficient cells the permeability for Na^+ and Cl^- increased compared to their controls cells without any selectivity (Figure 3-3a, Appendix B. Table 7-1). Thus, tricellulin-deficiency has an influence on the paracellular permeability of these monovalent ions without charge preference. The ratio P_{Na^+}/P_{Cl^-} allows a statement on the charge selectivity of an epithelium, which showed no difference between controls and KD clones (Figure 3-3b, Appendix B. Table 7-1).

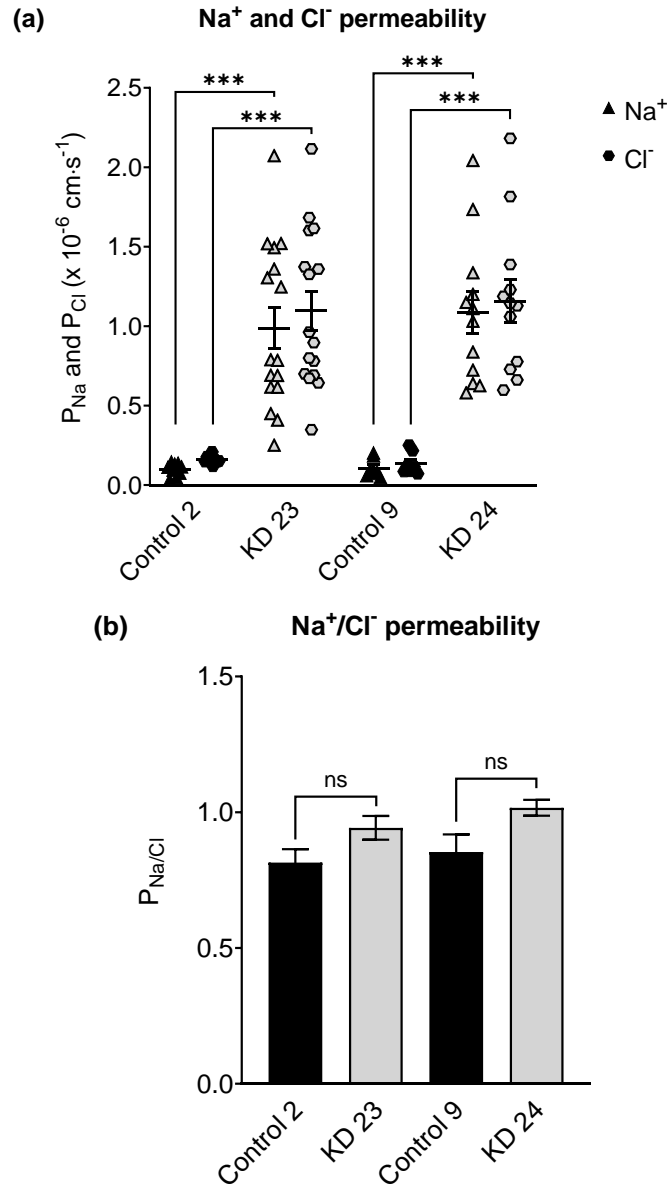


Figure 3-3. Functional analysis of tricellulin knockdown in MDCK C7 cells. **(a)** Effect of tricellulin knockdown on ion permeability. Tricellulin knockdown increases Na⁺ and Cl⁻ permeability to the same extent in MDCK C7 cells. **(b)** Effect of tricellulin knockdown on PNa⁺/PCl⁻. Tricellulin knockdown did not change the Na⁺ over Cl⁻ permeability ratio in MDCK C7 cells. (n=7-16, ns: not significant, ***P≤0.001).

3.1.1.3 Measurement of macromolecule permeability (4-kDa FITC-dextran)

To investigate whether the reduction of tricellulin in tight epithelium has an effect on the paracellular permeability of larger uncharged molecules, flux measurements were performed with 4-kDa FITC-dextran (FD4, 4000 Da) (see Chapter 2.4.3). As a result, FD4

permeability of KD 23 was not significantly different from its control, but that of clone KD 24 exhibited a 5-fold increase (Figure 3-4, Appendix B. Table 7-1). Although clones KD 23 and KD 24 differed only gradually in the reduction of tricellulin expression and TER decrease, the two chosen clones differed basically in macromolecule permeability. These results suggest that tricellulin expression is decisive for barrier function against macromolecules and demonstrates that under an osmotic gradient, macromolecules' permeability is affected by water movement in the opposite direction, significantly when tricellulin levels are reduced.

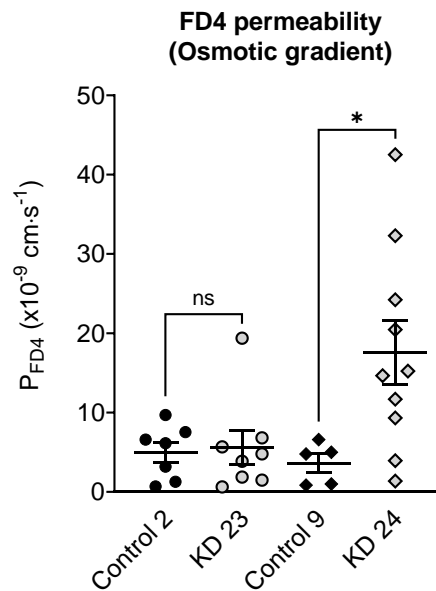
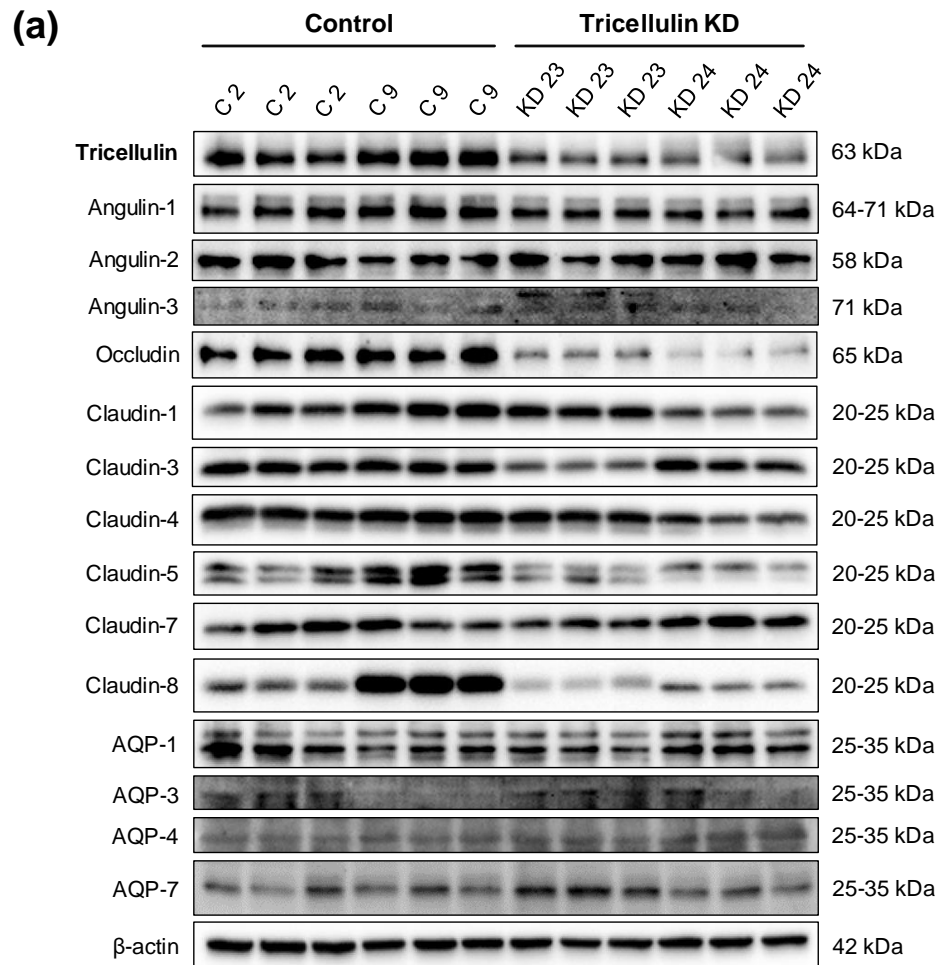


Figure 3-4. Effect of tricellulin knockdown on permeability for 4-kDa FITC-dextran (FD4). Permeability is increased only in tricellulin KD 24 cells under osmotic conditions (see Chapter 2.4.2). (n=5-10; ns: not significant, *P≤0.05).

3.1.2 Effects of tricellulin KD on endogenous proteins of MDCK C7 cells

In order to investigate the possible influence of other tight junction proteins on the results of the functional analyses, controls and tricellulin knockdown clones were examined for expression of other TJ proteins, such as occludin, several claudins, the three angulins, and aquaporin (AQP) water channels, AQP-1, -3, -4 and -7 (Figure 3-5a) (see Chapter 2.3). The densitometric analysis revealed some clonal variability in TJ protein expression between the knockdown clones and the controls. In detail, claudin-1 was increased in the tricellulin KD 23, and occludin, claudin-4, and -8 was decreased in the tricellulin KD 24.

Clonal variability in protein expression was also observed between both control clones and both KD clones. None of the three angulins were significantly altered. Most importantly, the tricellulin knockdown did not affect the expression of the cell membrane water channels expressed in MDCK C7 cells, AQP-1, AQP-3, AQP-4, and AQP-7 (Figure 3-5b).



(b)

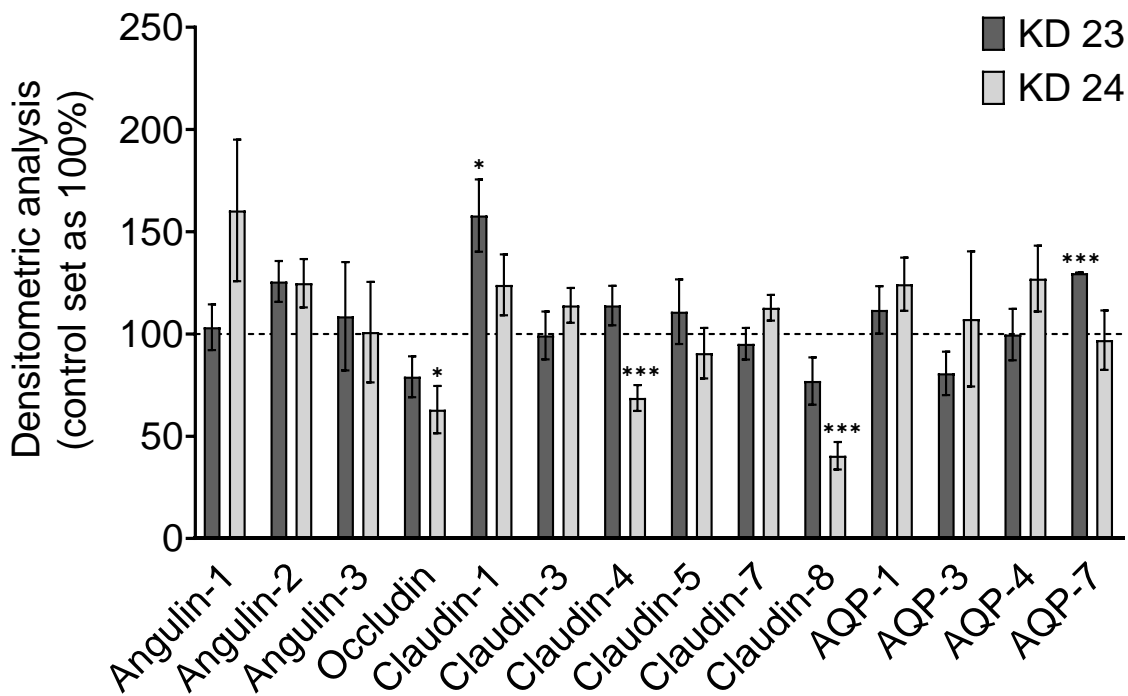
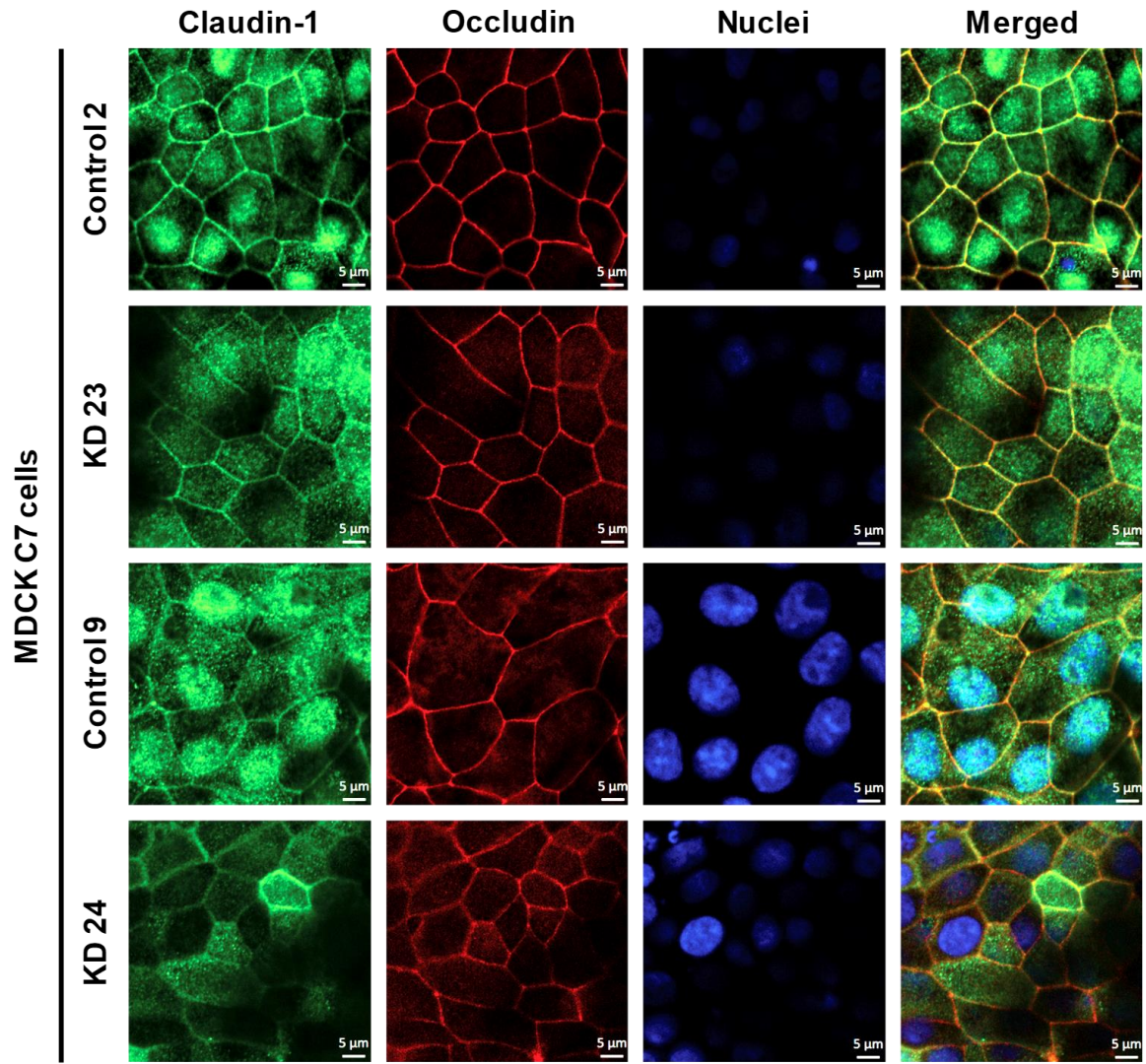
Protein expression profile

Figure 3-5. Claudin, occludin, angulin, and AQP expression in control and tricellulin knockdown MDCK C7 cells. **(a)** Representative Western blots (see Chapter 2.3). **(b)** Densitometric analysis of protein expression levels in tricellulin knockdown clones KD 23 and KD 24 compared to the corresponding vector-transfected controls. β -actin was used as an internal control for normalization to protein content. (n=9-17, N=7; *P \leq 0.05, ***P \leq 0.001).

3.1.3 Effects of tricellulin KD on the localization of other tight junction proteins

Analysis of the apicolateral localization of the TJ proteins that changed their expression (see Chapter 3.1.2) before and after the tricellulin knockdown was investigated by confocal laser-scanning microscopy (see Chapter 2.2.5). The immunofluorescent staining analysis showed a proper localization of claudin-1 inside the tight junction in both KD clones as shown by colocalization with the tight junction marker occludin (Figure 3-6a); nevertheless, it can be seen that it had clearer and stronger signals at the cytoplasm and nuclei. In contrast, claudin-4 localization was diffuse and excluded from the apical membrane in the KD clones and the control cells, although occasional apical junction localization was observed. ZO-1 localization was also perturbed, but the defects were less pronounced (Figure 3-6b).



(a)

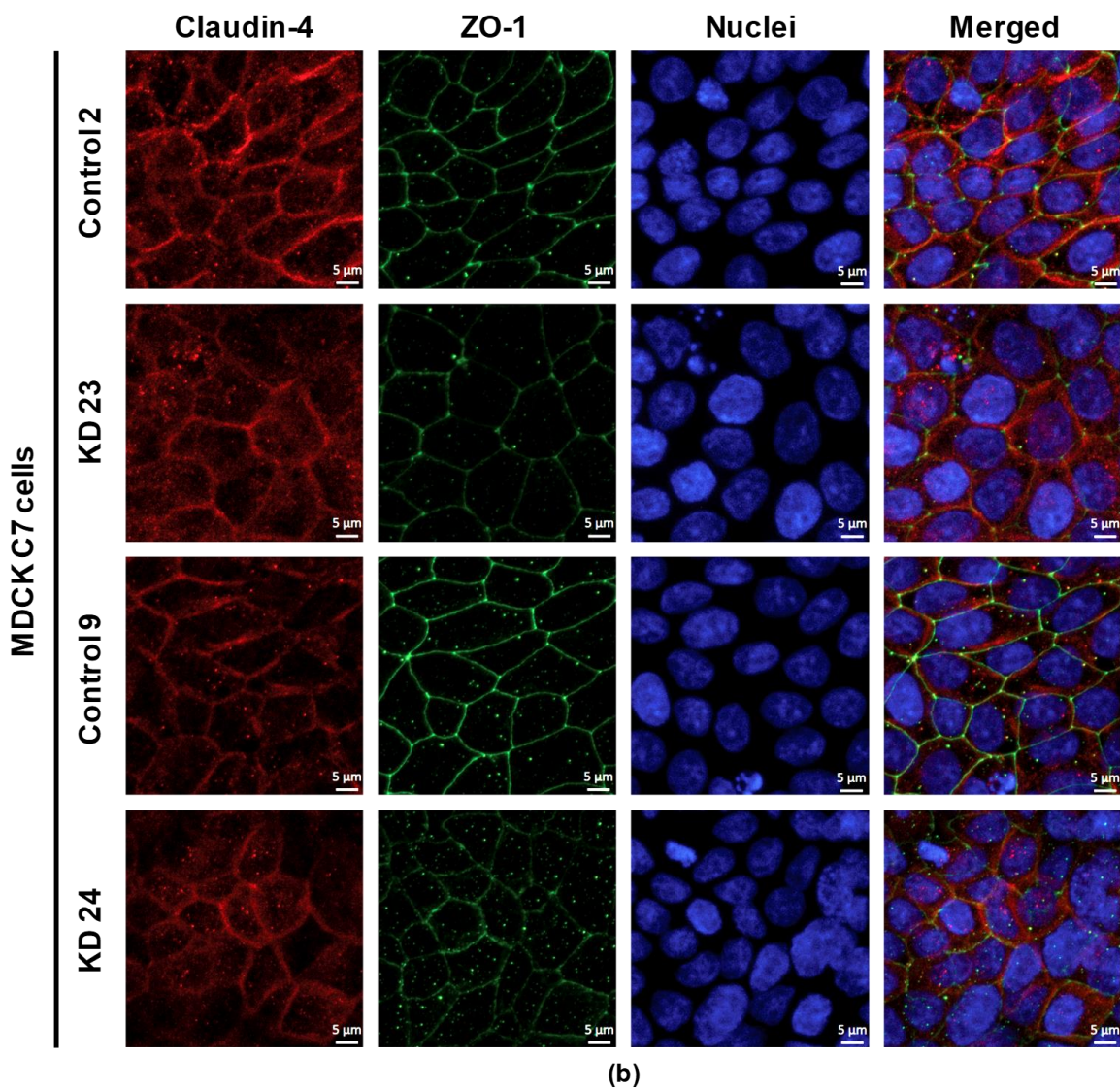


Figure 3-6. Localization of claudin-1 and claudin-4 in MDCK C7 control and tricellulin KD clones. **(a)** Claudin-1 (claudin-1: green; occludin: red; DAPI: blue). **(b)** Claudin-4 (claudin-4: red; ZO-1: green; DAPI: blue).

3.1.4 Effect of tricellulin KD on transepithelial water transport in MDCK C7 cells

To analyze the effect of tricellulin knockdown on water permeability of MDCK C7 cells, water flux was measured after induction with osmotic gradients produced by 100 mM mannitol, by 37 mM 4-kDa dextran, or by 100 mM 4-kDa dextran (Figure 3-7, Appendix B. Table 7-1). These concentrations produced measured osmolality gradients of 100 mOsm for 100 mM mannitol and 37 mM 4-kDa dextran, and 900 mOsm for 100 mM 4-kDa dextran (see Chapter 2.4.4).

Tricellulin KD 23, as well as KD 24, exhibited increased water fluxes compared with their respective vector control clones, but the change obtained by KD 24 was larger under all conditions (Figure 3-7, Appendix B. Table 7-1) (Ayala-Torres et al., 2019). In KD 24, the increase under a mannitol-induced osmotic gradient was 2.6-fold (Figure 3-7a), under a gradient induced by 100 mM 4-kDa dextran the increase was 3.8-fold (Figure 3-7b), and under a gradient induced by 37 mM 4-kDa dextran on the apical side it was 5.2-fold (Figure 3-7c), and on the basolateral side, it was 2.4-fold (Figure 3-7d), compared to 1.5-fold, 2.1-fold, 1.4-fold and 3.4-fold in KD 23, respectively.

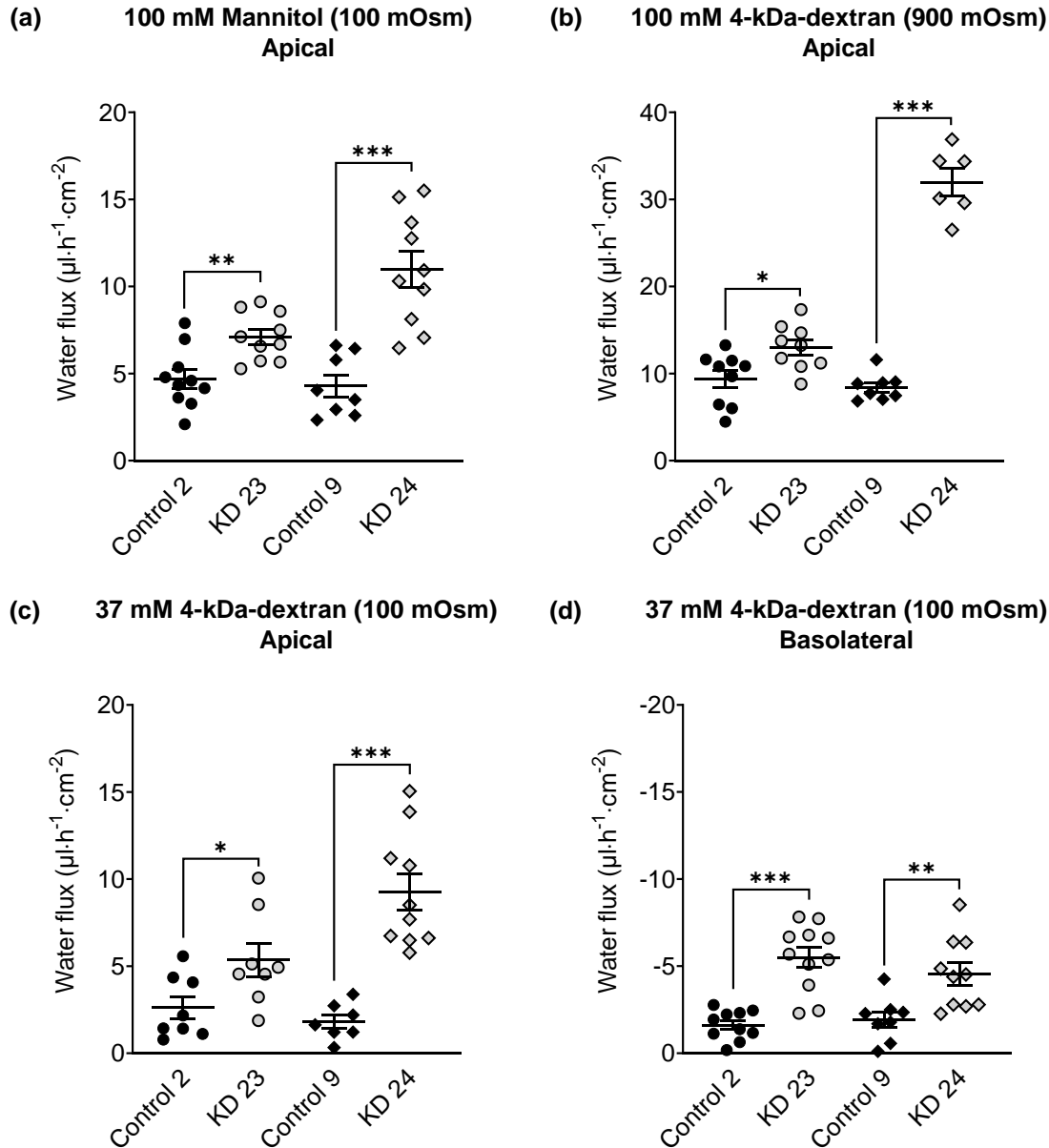


Figure 3-7. Water flux in control and tricellulin knockdown MDCK C7 cells stimulated by an osmotic gradient on the apical side (**a**, **b**, **c**) and on the basolateral side of the cell layer (**d**). Water flux induced by a gradient of (**a**) 100 mM mannitol, (**b**) 100 mM 4-kDa dextran, (**c**) 37 mM 4-kDa dextran/apical and (**d**) 37 mM 4-kDa dextran/basolateral. The transepithelial water flux was increased in both tricellulin knockdown clones, with a stronger increase in clone KD 24 with the higher reduction of tricellulin expression. (n=6-10, *P<0.05, **P<0.01, ***P<0.001).

In the same parallel series of experiments, a 5.5 mM 40-kDa dextran gradient was applied, which produced a measured osmolality gradient of 100 mOsm (see Chapter 2.4.4). In the presence of 100 mOsm 40-kDa dextran, water flux was lower than in the

presence of 100 mOsm mannitol. The 40-kDa dextran gradient did not significantly change water flux in tricellulin KD 24 compared to control, whereas water flux in KD 23 was increased (Ayala-Torres et al., 2019) (Figure 3-8, Appendix B. Table 7-1). This finding indicates that the water flux through the tTJ was inhibited in presence of 40-kDa dextran in the clone with strongest reduction of tricellulin.

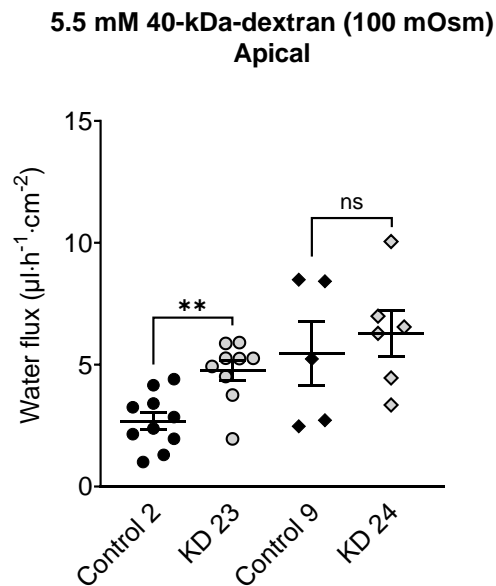


Figure 3-8. Water flux in control and tricellulin knockdown MDCK C7 cells stimulated by an osmotic gradient of 5.5 mM 40-kDa dextran (100 mOsm) on the apical side of the cell layer. No effect could be observed in tricellulin KD 24 cells, whereas in KD 23 with the higher tricellulin expression, the increase was in the same order of magnitude as in the presence of 100 mM mannitol (100 mOsm). (n=6-10, **P≤0.01, ns: not significant).

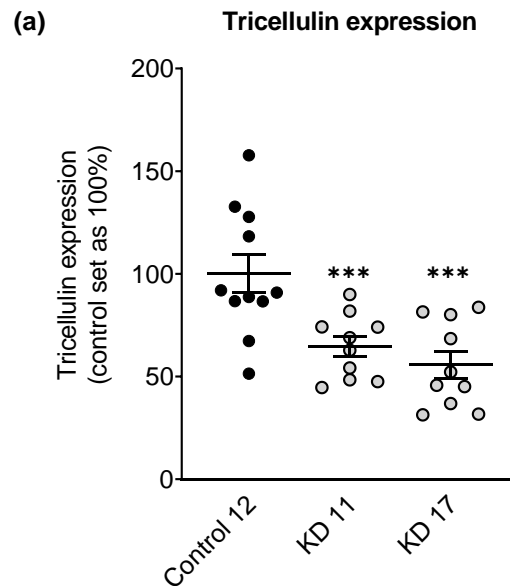
All numerical data can be seen in Appendix B. Table 7-1.

3.2 Tricellulin knockdown (KD): HT-29/B6 cells

3.2.1 Characterization of tricellulin KD in HT-29/B6 cells

Confluent monolayers of the human colon adenocarcinoma cell line HT-29/B6, a well-established model of the intermediate-tight epithelium (Kreusel et al., 1991), were used to analyze the specific role of the human tricellulin protein on the paracellular water transport. The HT-29/B6 cells were transfected with shRNA targeting tricellulin (see Chapter 2.2.2.1). After transfection, puromycin-resistant cell clones were screened for tricellulin knockdown by Western blotting (see Chapter 2.3). In this section, two knockdown clones and their control were investigated (KD 11 and KD 17 and their corresponding control 12). The two KD clones showed a high but different reduction in tricellulin expression: clone KD 11 showed a depression of tricellulin by 35%, while clone KD 17 exhibited a drop by 44% (Figure 3-9a, Appendix B. Table 7-2).

The proper localization of tricellulin as dots at TCs was confirmed for the three clones by immunofluorescence confocal laser-scanning microscopy (see Chapter 2.2.5). ZO-1 served as a TJ marker (Figure 3-9b).



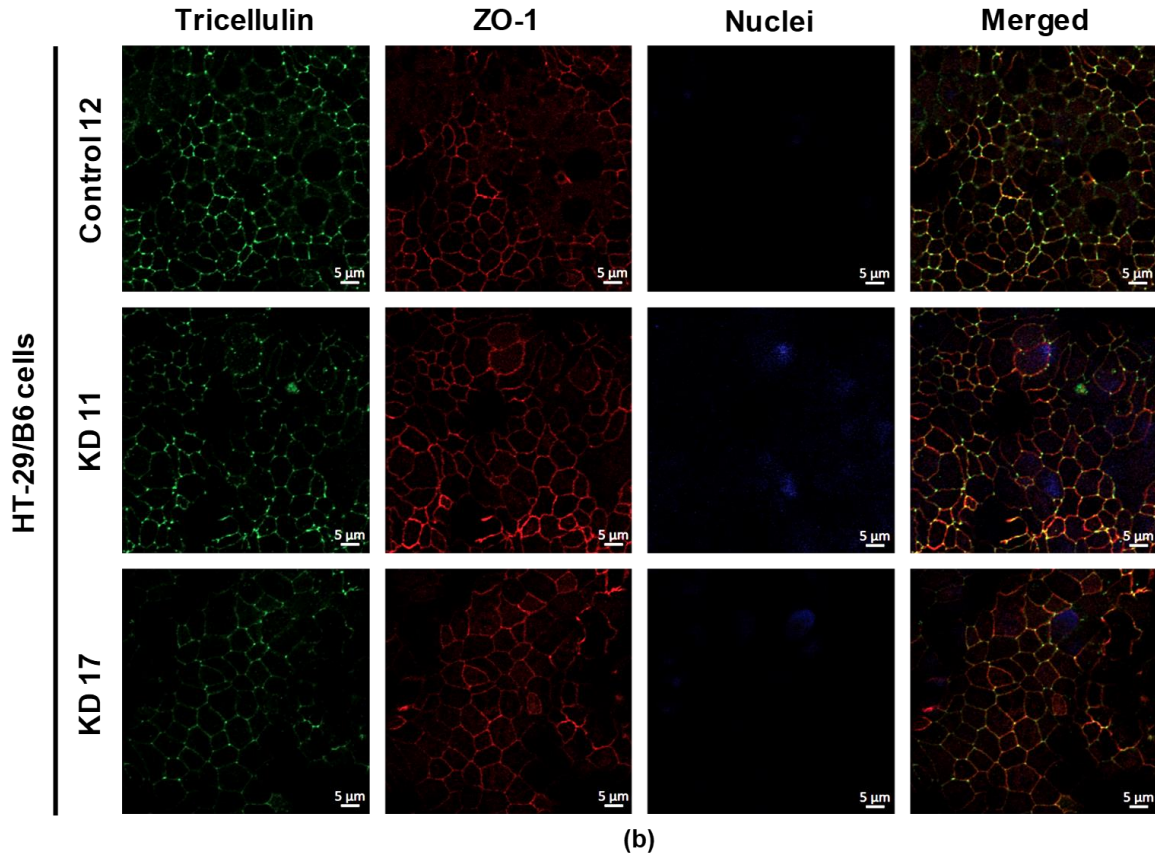


Figure 3-9. Expression and localization of tricellulin in HT-29/B6 cells. **(a)** Densitometric analysis of tricellulin protein expression levels in stable shTRIC transfectants in comparison to vector-transfected controls. shTRIC leads to decreased tricellulin expression ($***P \leq 0.001$) and **(b)** Immunofluorescent staining of HT-29/B6 shRNA targeting tricellulin. Knockdown in HT-29/B6 cells did not affect tricellulin localization, which remained within the tTJ. Tricellulin: green, ZO-1: red, DAPI (nucleus): blue.

The topology parameters (see Chapter 2.2.6) of fluorescence stained tricellulin knockdown HT-29/B6 cells using the program Fiji-ImageJ for estimating the contribution of tricellulin at the tTJ to overall permeability are shown in Appendix C. Table 7-5 and Figure 7-3. The most interesting result is that within the analyzed area, the TJ length per cell was slightly lower in both KD clones; however, the tTJ density was doubled in both KD clones in comparison with their control 12. The higher frequency of occurrence of tTJ in both monolayer KD clones suggests that tricellulin reduction impacts tTJ. In relation to the number of vertices or neighboring cells, it was observed that for all clones, there is an average value between 5 and 6 vertices (Appendix C. Figure 7-3), which also corresponds to the calculated number of tTJ per cell (6 tTJ/cell).

3.2.1.1 Effect on the transepithelial resistance

Since it is known that in HT-29/B6 cells, the tTJ contributes to paracellular ion permeability (Krug, 2017), the effect of tricellulin knockdown on TER was investigated (see Chapter 2.4.1). The TER was reduced in tricellulin knockdown HT-29/B6 cells (Figure 3-10, Appendix B. Table 7-2). KD 17 exhibited a stronger reduction of tricellulin expression than KD11; nevertheless, both KD clones have a strong decrease in TER compared to their control (70% reduction in TER).

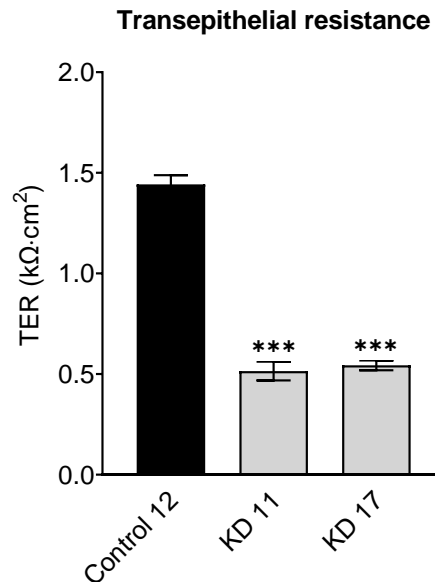


Figure 3-10. Functional analysis of tricellulin knockdown in HT-29/B6 cells. Effect of tricellulin knockdown on transepithelial resistance. Tricellulin KD decreases TER in HT-29/B6 cells. (n=24; ***P≤0.001).

3.2.1.2 Analysis of permeability for sodium and chloride

In order to investigate the ion permeabilities for sodium (PNa⁺) and chloride (PCl⁻) in this epithelial cell line, dilution potential measurements were performed (see Chapter 2.4.2). The results show that in tricellulin-deficient cells the permeability for Na⁺ and Cl⁻ increased compared to their control (Figure 3-11a, Appendix B. Table 7-2). Notably, the ratio PNa⁺/PCl⁻ in the tricellulin KD cells did not change compared to their control, indicating no change in the KD clones' charge selectivity (Figure 3-11b, Appendix B. Table 7-2).

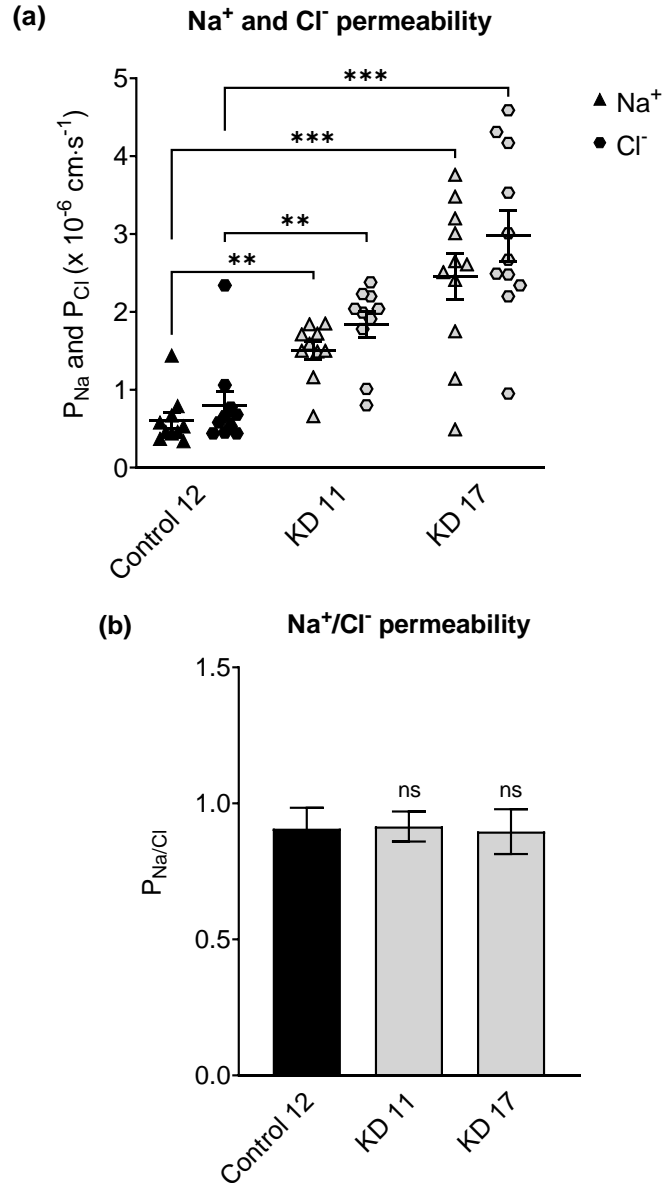


Figure 3-11. Functional analysis of tricellulin knockdown in HT-29/B6 cells. **(a-b)** Effect of tricellulin knockdown on permeability for Na⁺ and Cl⁻. **(a)** Na⁺ and Cl⁻ permeability was increased in both KD clones without any change in selectivity, and **(b)** Ratio Na⁺ over Cl⁻ permeability did not change in KD clones compared with the control. (n=11, ns: not significant; **P≤0.01, ***P≤0.001)

3.2.1.3 Measurement of macromolecule permeability (4-kDa FITC-dextran)

Using the same strategy used for analysis of MDCK C7 cells, the permeability of the three clones to 4-kDa FITC-dextran (FD4) was assessed (see Chapter 2.4.3). As a result, FD4 permeability of KD 11 and KD 17 was higher than their control (Figure 3-12, Appendix B.

Table 7-2). Although KD 11 and KD 17 clones differed only gradually in the reduction of tricellulin expression, the two clones differed strongly in macromolecule permeability, 2.0- and 3.5-times higher than FD4 permeability of the control, respectively.

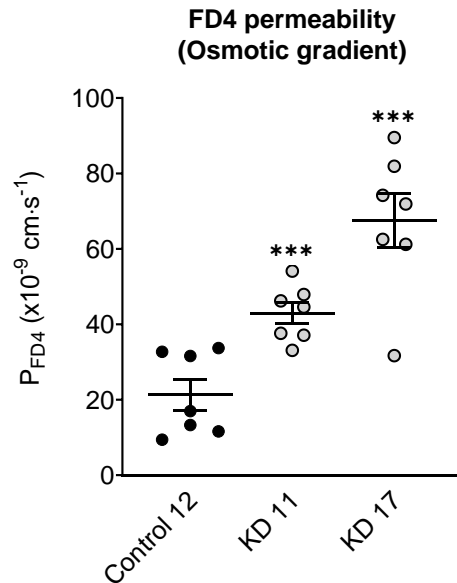
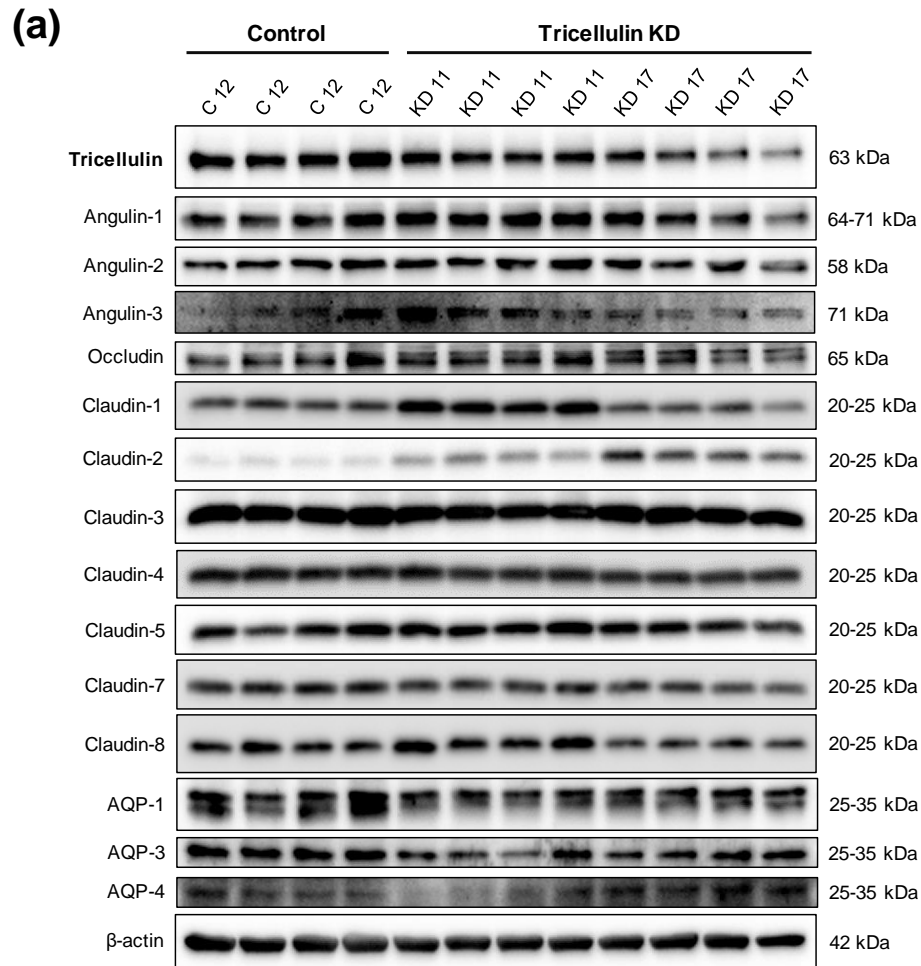


Figure 3-12. Functional analysis of tricellulin knockdown in HT-29/B6 cells. Permeability to 4-kDa FITC-dextran in control cells and tricellulin knockdown clones. Tricellulin knockdown increased the permeability to 4-kDa FITC-dextran under an osmotic condition. (n=7, ***P≤0.001).

3.2.2 Effects of tricellulin KD on other proteins of HT-29/B6 cells

Knockdown of one tight junction protein may cause variation of other proteins; therefore, the levels of occludin, several claudins, the three angulins, and aquaporin-1, -3, and -4 were examined (Figure 3-13a) (see Chapter 2.3). The densitometric analysis revealed some clonal variability in claudin expression between the knockdown clones and their control. In detail, angulin-1, claudin-1, and -8 were increased in the tricellulin KD 11 (Figure 3-13b). The tricellulin KD 17 clone showed an increase in angulin-1, claudin-3 and -8, and AQP-4 and a reduction in AQP-3 (Figure 3-13b). As stated above, angulin-1 was upregulated in both clones possibly as a mechanism of the cells to stabilize the tTJ after tricellulin reduction. Indeed, as most of the claudins present in HT-29/B6 cells seal the barrier in a concerted action, it should be noted that after reducing the tricellulin expression, the set of those claudins increased to keep it in balance. On the other hand, HT-29/B6 cell line expresses the water channel-forming claudin-2, which was upregulated in both KD clones; however, the differences in claudin-2 expression between the clones

had not influence on the selectivity for Na⁺ over Cl⁻ (Figure 3-11), which indicates, that the overexpressed claudin-2 had no functional relevance. Notably, the tricellulin knockdown affected the expression of the membrane water channels expressed in HT-29/B6 cells, AQP3 and AQP4 (Figure 3-13b); AQP3 was downregulated, whereas AQP4 was upregulated. It can be assumed that a compensatory mechanism between these two proteins; thus, the change in AQP expression does not affect the transcellular and transepithelial water flux.



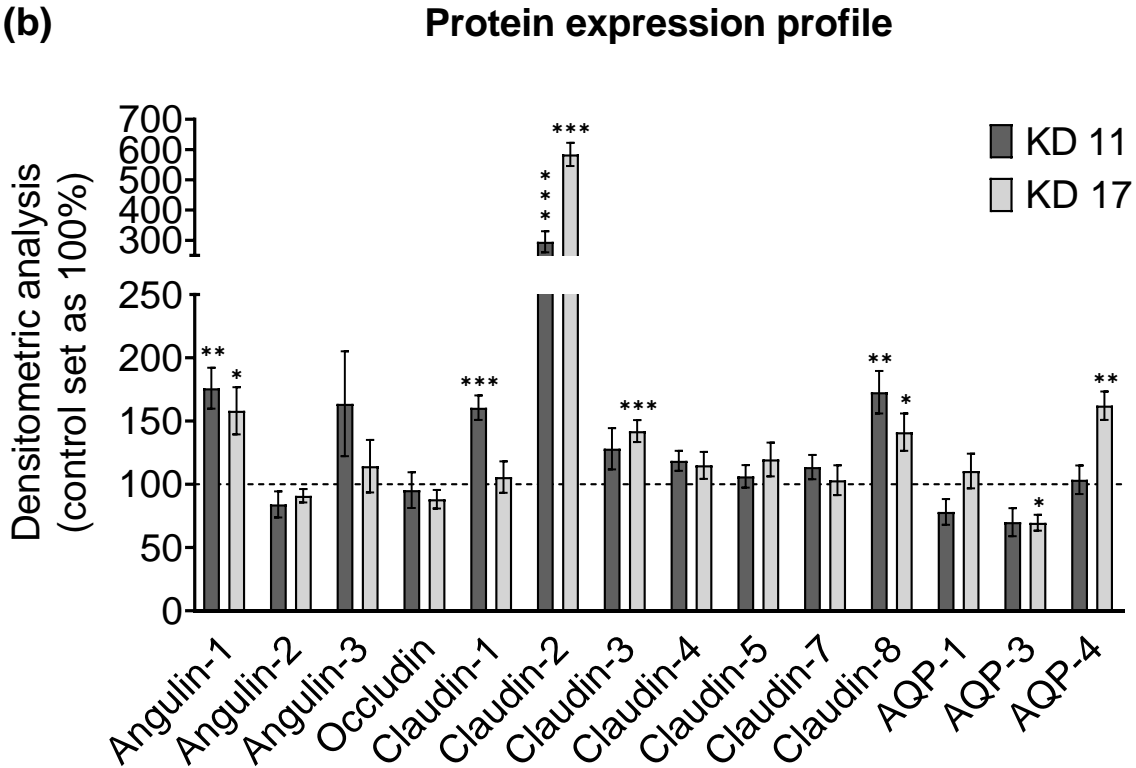
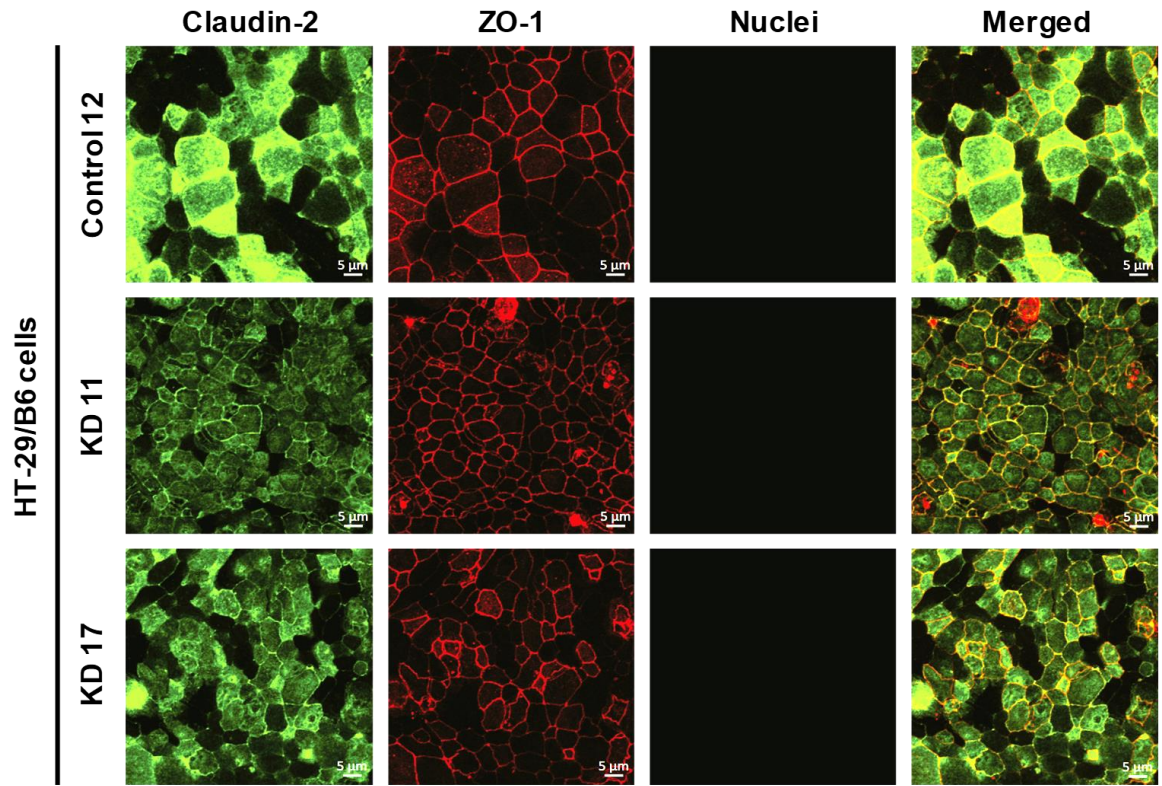


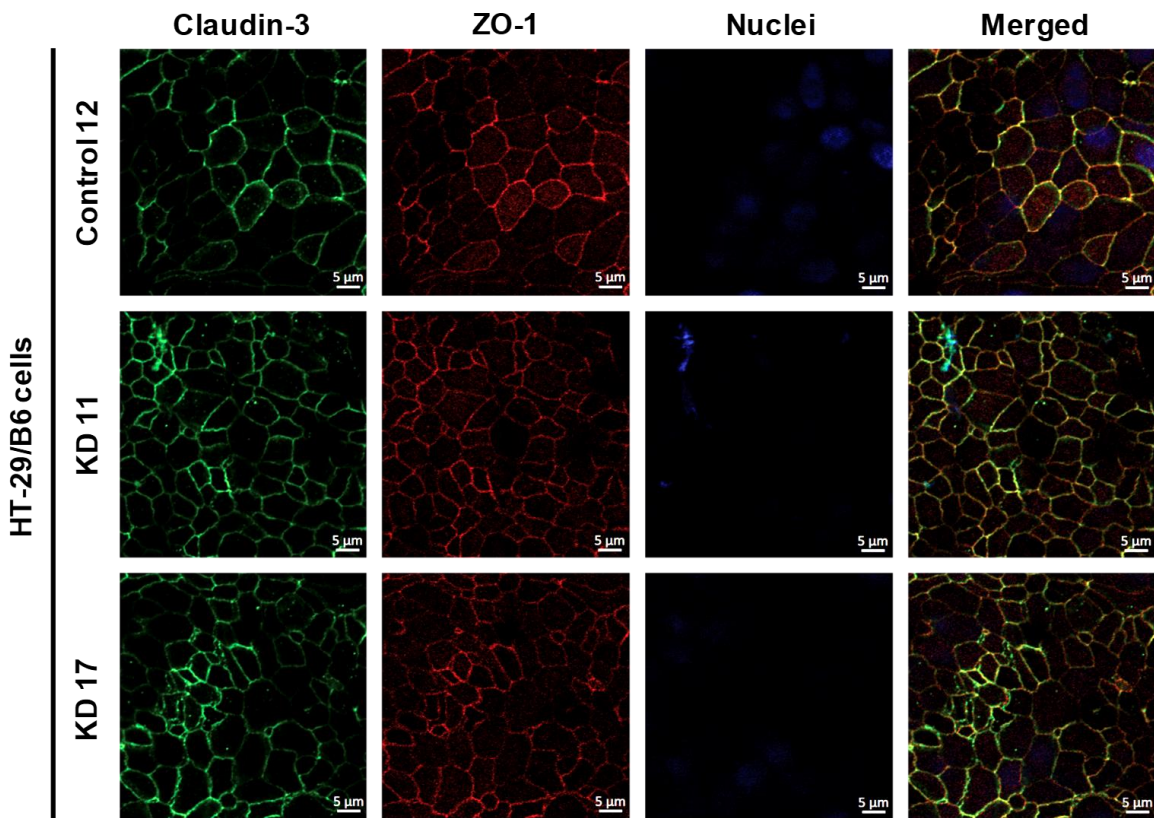
Figure 3-13. Angulin, occludin, claudin, and AQP expression in control and tricellulin knockdown HT-29/B6 cells. **(a)** Representative Western blots. **(b)** Densitometric analysis of protein expression levels in stable shTRIC transfected cells in comparison to the vector-transfected control. β -actin was used as an internal control for normalization to protein content. (n=4-14, N=4, * $P \leq 0.05$, ** $P \leq 0.01$, *** $P \leq 0.001$).

3.2.3 Effects of tricellulin KD on the localization of other tight junction proteins of HT-29/B6 cells

To determine whether tricellulin knockdown altered the localization of the upregulated TJ proteins, angulin-1, claudin-2 and -3, and ZO-1 were analyzed (see Chapter 2.2.5). Immunolocalization in tricellular KD cells revealed that claudin-2 was located at the cell-cell borders; however, this protein was also located intracellularly in all clones, with greater intensity in the control cells, whereas the ZO-1 localization was unaltered (Figure 3-14a). For all of the above, although claudin-2 increased in expression, is not functionally relevant, neither for water permeability nor for ion permeability, which was confirmed by the unchanged $\text{PNa}^+/\text{PCl}^-$. In contrast, no alteration was observed for claudin-3 by colocalization with the tight junction marker ZO-1 (Figure 3-14b). Interestingly, the angulin-1 localized in both bTJ and tTJ did not present significant changes in the KD clones compared to the control cells (Figure 3-14c).



(a)



(b)

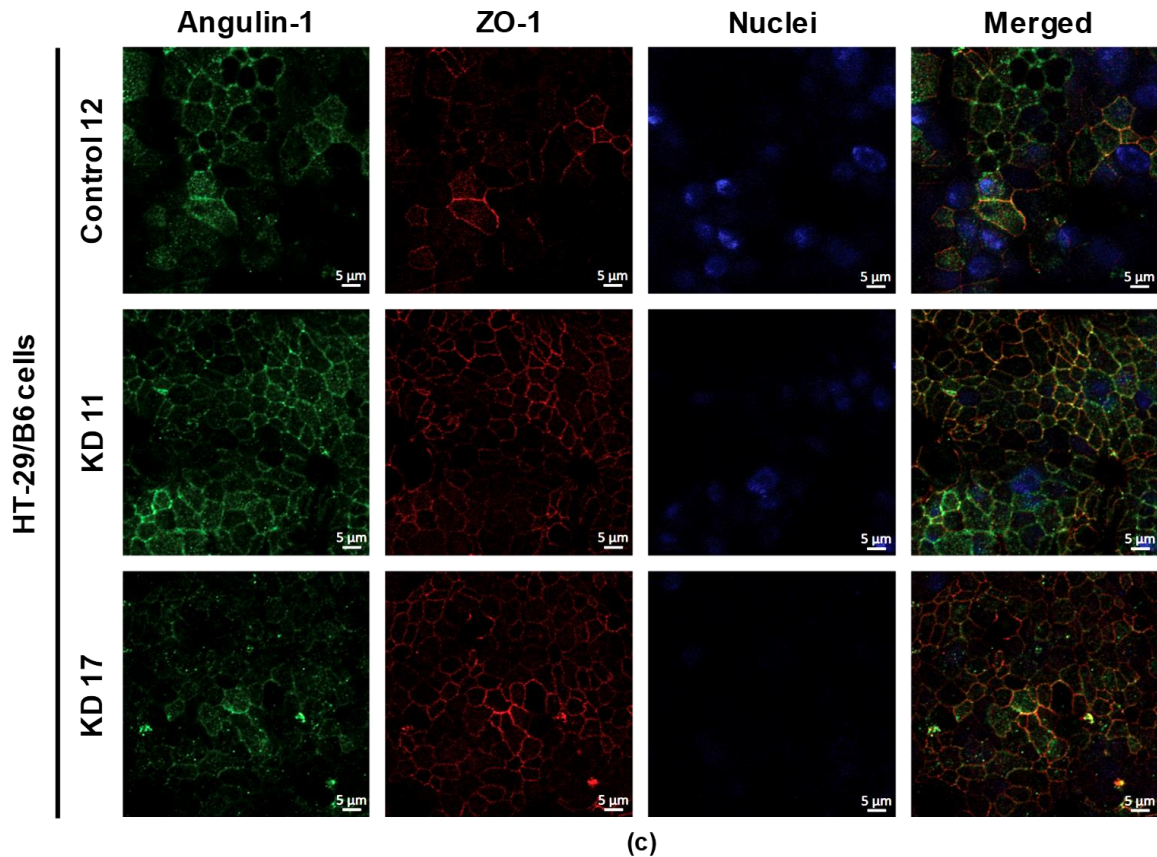


Figure 3-14. Immunofluorescent staining of (a) claudin-2, (b) claudin-3 and (c) angulin-1 in HT-29/B6 control and tricellulin KD cells. Tricellulin knockdown increased the expression of claudin-2; however, its localization was intracellular and subjunctional. (Claudin-2, claudin-3 and angulin-1: green; ZO-1: red; DAPI (nucleus): blue).

3.2.4 Effect of tricellulin KD on transepithelial water transport in HT-29/B6 cells

To analyze the effect of tricellulin knockdown on water permeability of HT-29/B6 cells, water flux was measured after induction of osmotic gradients produced by 100 mM mannitol, by 37 mM 4-kDa dextran, or by 100 mM 4-kDa dextran (Figure 3-15, Appendix B. Table 7-2). These concentrations produced measured osmolality gradients of 100 mOsm for 100 mM mannitol and 37 mM 4-kDa dextran, and 900 mOsm for 100 mM 4-kDa dextran (see Chapter 2.4.4). Transepithelial water flux was 4-fold higher using an osmotic gradient of 900 mOsm.

Tricellulin KD 11 and KD 17 clones did not show significant differences in water flux compared with their vector control. These results confirm the finding that tricellulin is

dispensable for water barrier formation of the tTJ in HT-29/B6 cells. On the other hand, it could be thought that there is a threshold in the expression of tricellulin that was not overcome, and therefore it was impossible to measure differences in water fluxes.

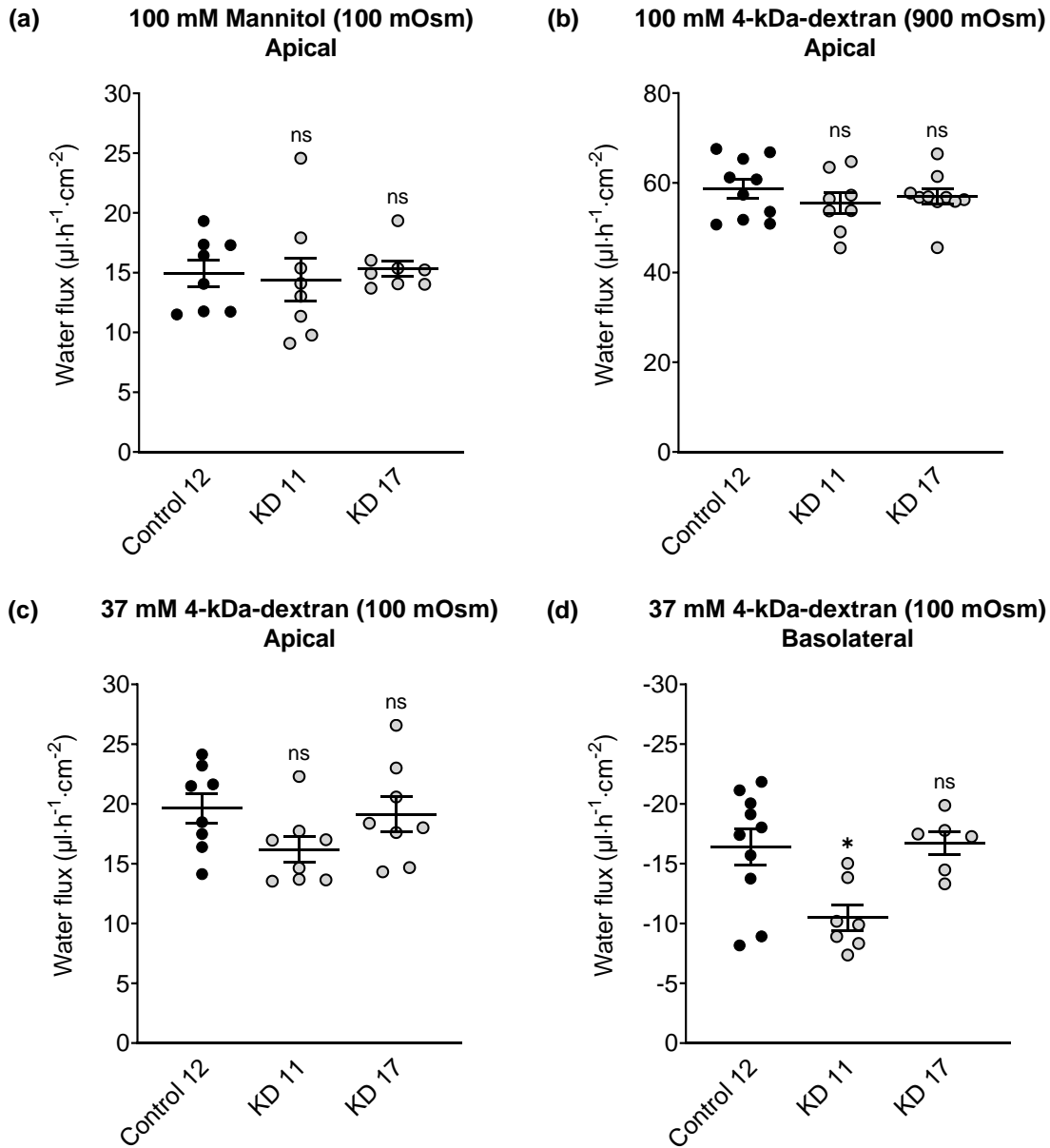


Figure 3-15. Water flux in control and tricellulin knockdown HT-29/B6 cells stimulated by an osmotic gradient. **(a)** Water flux induced by a gradient of 100 mM mannitol on the apical side. **(b)** Water flux induced by a gradient of 100 mM 4-kDa dextran on the apical side. **(c)** Water flux induced by a gradient of 37 mM 4-kDa dextran on the apical side. **(d)** Water flux induced by a gradient of 37 mM 4-kDa dextran on the basolateral side of the cell layer. The transepithelial water transport did not change under any condition between the KD clones and their control. (n=8-10, ns: not significant).

Like that evaluated with 40-kDa dextran, a 2.5 mM albumin gradient was applied, which produced a measured osmolality gradient of 40 mOsm (see Chapter 2.4.4). It is important to clarify that this is the maximum concentration of albumin that could be prepared before this solution became too viscous and impossible to handle in our device. The 2.5 mM albumin gradient did not significantly change water flux in tricellulin KD 11 and KD 17 (Figure 3-16, Appendix B. Table 7-2). This finding could indicate that the water flux was hindered by the flow of big molecules, independent of its chemical nature, like albumin (70 Å in diameter (Tojo and Kinugasa, 2012)), through the tTJ in the opposite direction, in the same way, that 40-kDa dextran affected the transepithelial water transport in MDCK C7 cells.

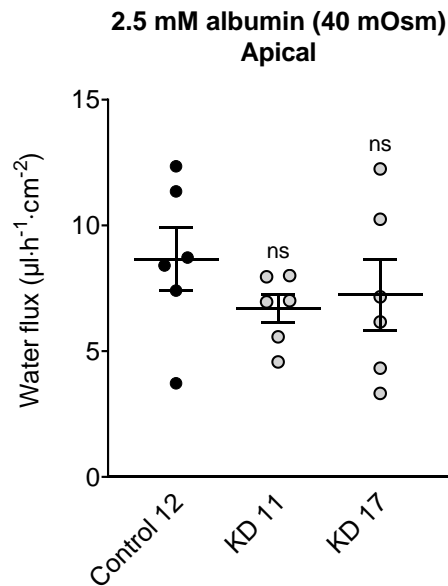


Figure 3-16. Water flux in control and tricellulin knockdown HT-29/B6 cells stimulated by an osmotic gradient of 2.5 mM albumin on the apical side of the cell layer. No effect could be observed in tricellulin KD cells under this osmotic gradient. (n=6, ns: not significant).

All numerical data can be seen in Appendix B. Table 7-2.

3.3 Angulin-1 knockout (KO): MDCK C7 cells

3.3.1 Characterization of angulin-1 KO in MDCK C7 cells

Besides tricellulin, the angulin family proteins also localize at the tricellular tight junction. In order to investigate the specific role of the angulin-1 on the paracellular water transport in a tight epithelium, the angulin-1 gene was inactivated in the canine kidney cell line, MDCK C7, by application of the CRISPR/Cas9 technology. For this purpose, three plasmids obtained from Santa Cruz (Heidelberg, Germany), which contained 3 sgRNA (20 nucleotides each), targeting different exons from the different isoforms of angulin-1 gene (see Table 3-1) and three HDR-plasmids which introduce the puromycin resistance, were used for stable transfection (see Chapter 2.2.2.2).

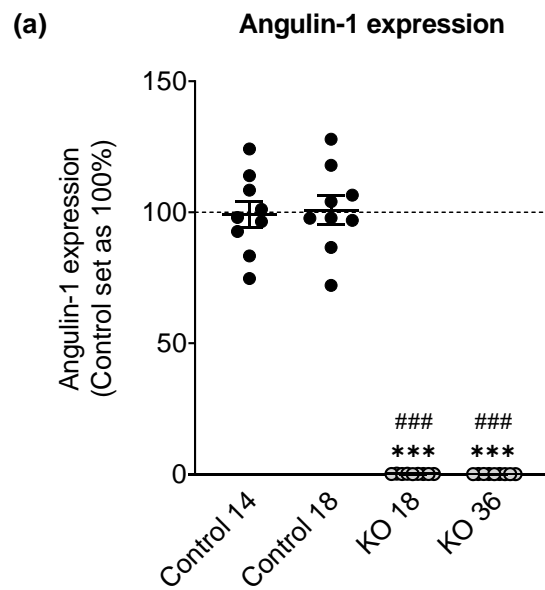
Table 3-1. Angulin-1 isoforms and exons that are targeted by the three sgRNA.

Name	Transcript				Protein			sgRNA (exon target)		
	Transcript ID (ENST00000)	Nucleotides (bp)	Size (aa)	MW (kDa)	Biotype	CCDS	UniProt	A	B	C
212	602122.5	2480	629	--	Protein coding	59376	Q86X29	8	3	3
214	621372.4	2274	649	--	Protein coding	12450	Q86X29	9	3	3
204	361790.7	2210	649	71	Protein coding	12450	Q86X29	9	3	3
202	354900.7	2105	630	70	Protein coding	12449	Q86X29	8	3	3
203	360798.7	1963	581	64	Protein coding	12451	Q86X29	7	3	3
213	605618.5	1885	601	--	Protein coding	--	S4R3V8	9	3	3
201	347609.8	1880	591	66	Protein coding	--	Q86X29	8	3	3
205	427250.5	1606	493	55	Protein coding	--	Q86X29	6	--	--
209	601623.5	530	139	--	Protein coding	--	M0R1W9	--	3	3
208	599658.1	343	114	--	Protein coding	--	M0QZL9	--	2	2
210	602003.1	297	51	--	Protein coding	--	M0R0W1	--	--	--
207	597933.5	873	No protein	--	Processed transcript	--	--	--	--	--
211	602044.2	658	No protein	--	Processed transcript	--	--	--	--	--
206	597446.1	478	No protein	--	Retained intron	--	--	--	--	--

Angulin-1 isoforms and their description were obtained from www.ensembl.org/index.html. The targeting exons were identified using Clustal Omega that uses seeded guide trees and HMM profile-profile techniques to generate alignments between two, three or more sequences (www.ebi.ac.uk/Tools/msa/clustalo/).

Firstly, puromycin-resistant cell clones were screened for angulin-1 knockout by Western blotting (Figure 3-17a, Appendix B. Table 7-3). Two knockout clones and two control clones were investigated (KO 18 and KO 36 and their controls 14 and 18). The two knockout clones are mono-allelic knockouts, as shown by Western blot analyses (Figure 3-17a).

To confirm the efficiency of angulin-1 knockout in MDCK C7 cells, the localization of the angulin-1 protein was analyzed after the transfection. By immunofluorescence confocal laser-scanning microscopy (see Chapter 2.2.5), the proper localization at the TCs in the two control clones and the complete disappearance from the tTJ in the two knockout clones was confirmed using occludin as a TJ marker (Figure 3-17b). Besides, angulin-1 also localized at the bTJ in the control cells, especially in control 14.



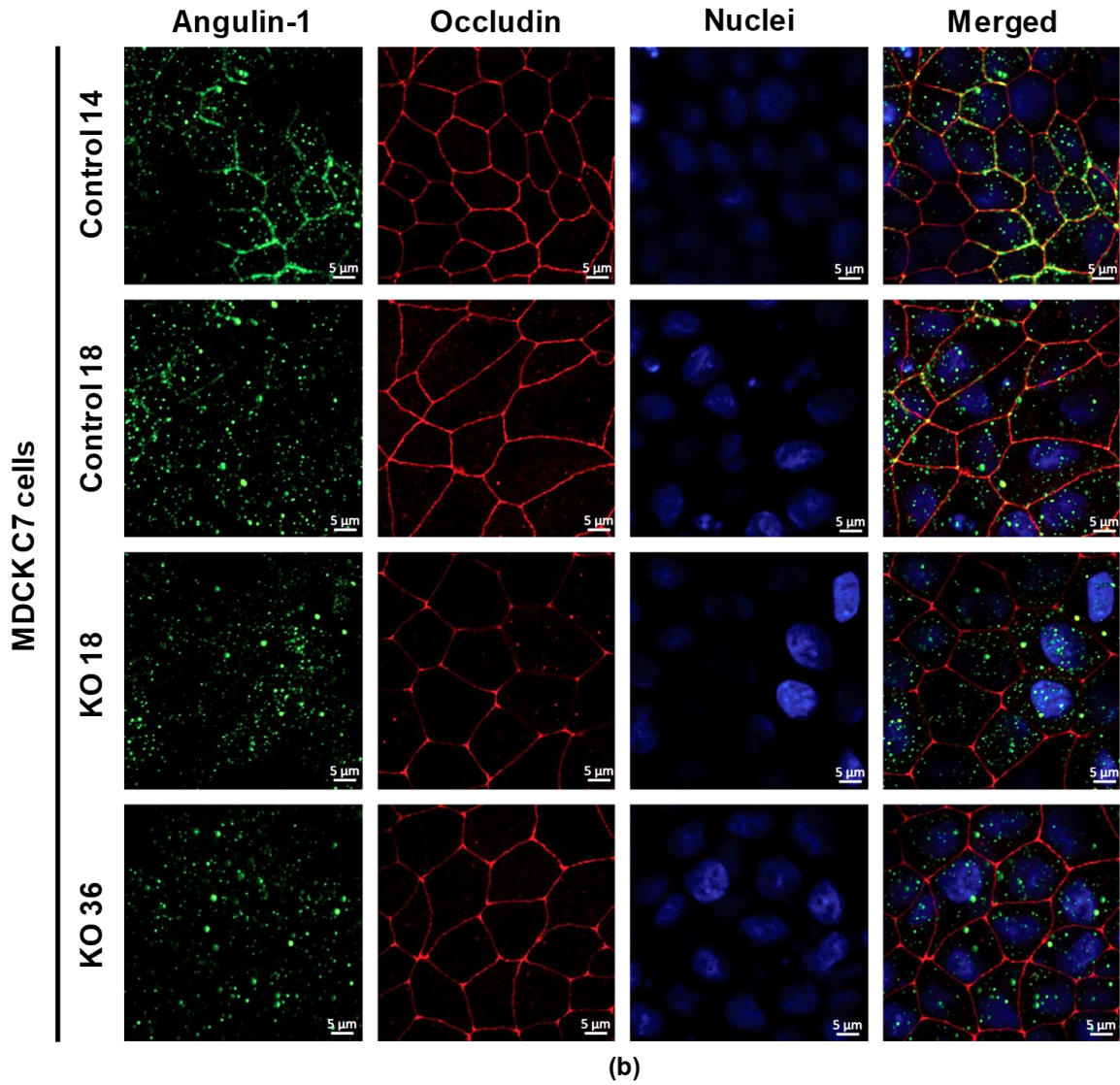


Figure 3-17. Expression and localization analysis of angulin-1 in control and angulin-1 KO MDCK C7 cells **(a)** Densitometric analysis of angulin-1 protein expression levels in stable CRISPR/Cas9 transfectants (KO 18 and KO 36) in comparison to vector-transfected controls (Control 14 and Control 18). sgRNA-CRISPR/Cas9 leads to a complete reduction of angulin-1 expression ($n=9$, $***P \leq 0.001$ with regard to control 14 and $###P \leq 0.001$ with regard to control 18). **(b)** Localization of angulin-1 in the four clones used throughout this study. In the KO clones, angulin-1 is missed at tTJ sites. Angulin-1: green; occludin: red; DAPI: blue.

The topology parameters (see Chapter 2.2.6) of fluorescence stained angulin-1 knockout MDCK C7 cells using the program Fiji-ImageJ for estimating the contribution of angulin-1 at the tTJ to overall permeability are shown in Appendix C. Table 7-6 and Figure 7-4. The

most interesting result is that within the analyzed area, the TJ length per cell was similar in both KO clones in comparison with their controls. On tTJ levels, the tTJ density of the KO 18 was the same compared to its controls; however, the tTJ density of the KO 36 was 1.5-times higher than its controls. The higher frequency of tTJ in the KO 36 clone monolayers suggests an impact of the removal of angulin-1 from tTJ. In relation to the number of vertices or neighboring cells, it was observed that for all clones, there is an average value between 3 and 5 vertices (Appendix C. Figure 7-4), which also corresponds to the calculated number of tTJ per cell (5 tTJ/cell).

3.3.1.1 Effect on the transepithelial resistance and macromolecule permeability

In addition, the barrier function of angulin-1 knockout clones was investigated by determining the transepithelial resistance (TER) (see Chapter 2.4.1). The overall TER values were lower for the knockout cells compared to the MDCK C7 control cells (Figure 3-18a, Appendix B. Table 7-3). In addition to ion permeability, reflected by TER, 4-kDa FITC-labeled dextran's permeability was determined (see Chapter 2.4.3). It was found that although the angulin-1 KO had a high impact on TER, it was nevertheless unable to increase the amount of 4-kDa FITC-dextran transported across the cell layer under isosmotic conditions. In contrast, when an osmotic gradient was applied, the permeability of the KO 18 clone to FD4 increased in comparison to the control 14, probably because in this KO clone the tricellulin delocalization from the tTJ was larger than in the KO 36 clone (Figure 3-18b and 3-18c, Appendix B. Table 7-3).

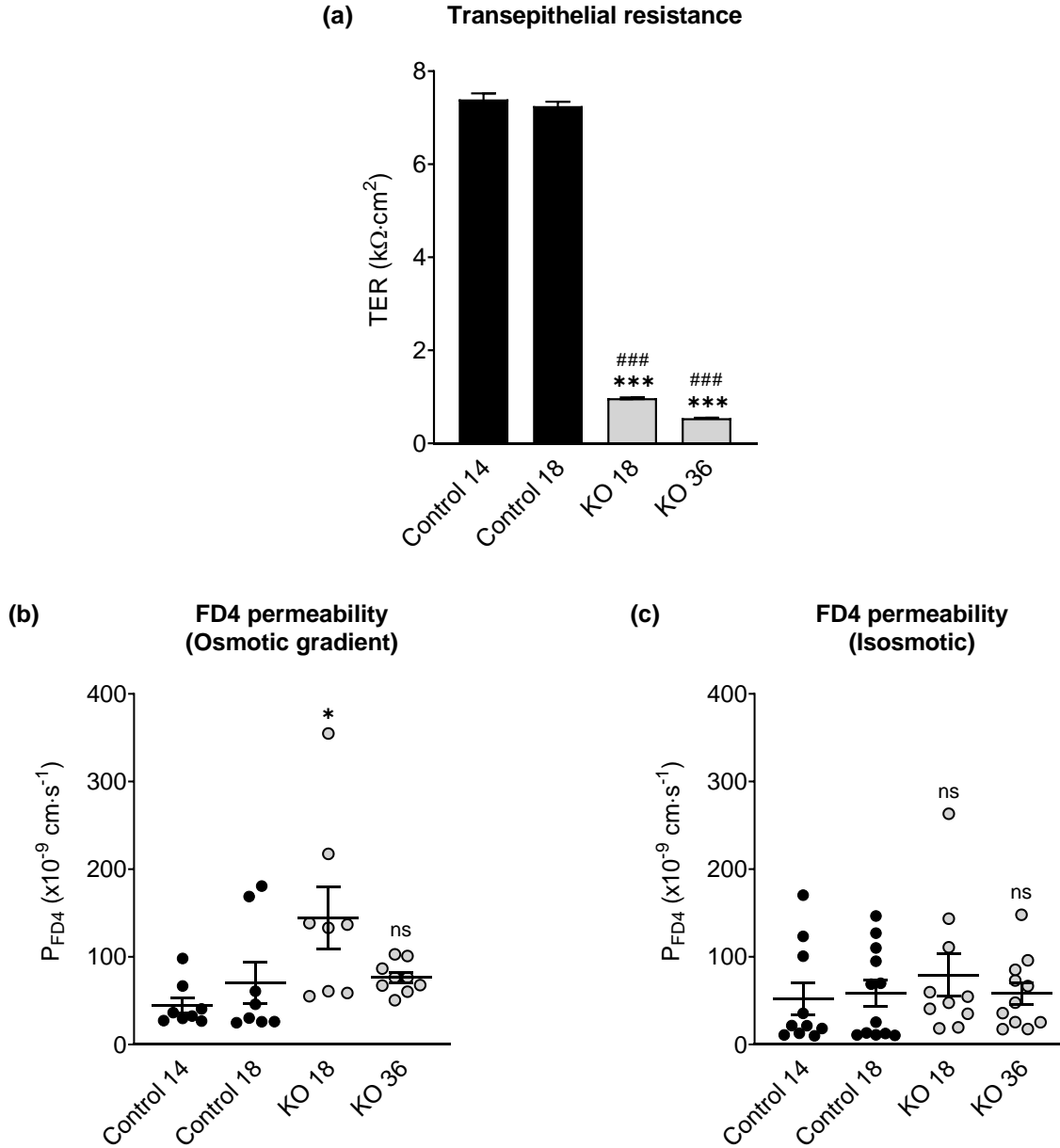
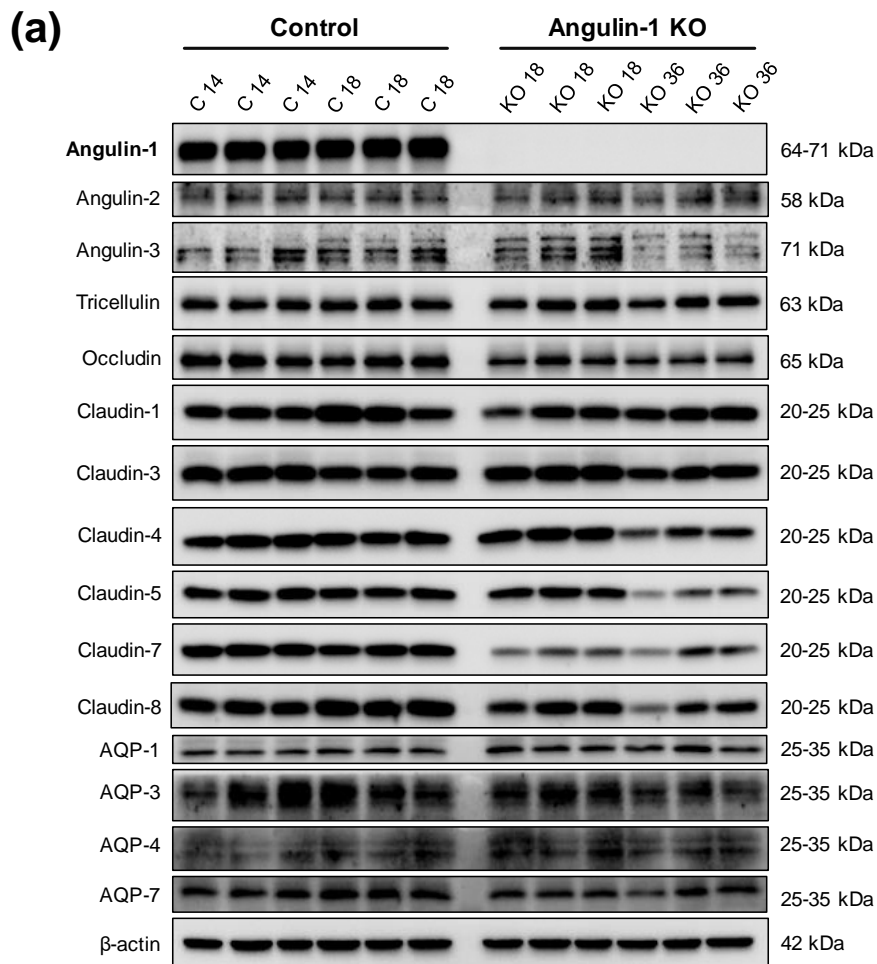


Figure 3-18. Functional analysis of angulin-1 knockout in MDCK C7 cells. **(a)** Effect of angulin-1 knockout on transepithelial resistance (TER). Loss of angulin-1 decreases TER in MDCK C7 cells (N=6, n=60). **(b-c)** Permeability to 4-kDa FITC-dextran under **(b)** osmotic and **(c)** isosmotic conditions. The permeability to FD4 did not change in the angulin-1 KO 36 clone and increased in the KO 18 clone in relation to the control 14 under osmotic conditions. (ns: not significant; * $P \leq 0.05$, *** $P \leq 0.001$ with regard to control 14 and ### $P \leq 0.001$ with regard to control 18).

3.3.2 Effects of angulin-1 KO on other proteins of MDCK C7 cells

Claudins are the major constituents of TJ strands, and the expression pattern of claudins is thought to determine TJs' permeability. Because MDCK C7 cells express the three

angulins, tricellulin, occludin, several tightening claudins, aquaporin-1, -3, -4, and -7, the effects of angulin-1 knockout on the expression levels of these proteins were investigated (Figure 3-19a) (see Chapter 2.3). The densitometric analysis (Figure 3-19b) revealed some clonal variability in claudin expression between the knockout clones and the controls. In detail, occludin, claudin-1, -3, -4, -5, -7 and -8 and AQP-7 were reduced in the angulin-1 KO 36 clone. The angulin-1 KO 18 clone showed a reduction in occludin, claudin-1, -5, and -7 and a slight increase in AQP-1 compare with the controls. Most importantly, the expression of the other angulin proteins (angulin-2 and -3) and tricellulin was not altered. Besides, the angulin-1 knockout did not affect the expression of the other membrane water channels expressed in MDCK C7 cells, AQP-3, -4, and -7. Therefore, the differences in transepithelial water flux are unlikely to be caused by changes in transcellular water flux and can be assumed due to changes in paracellular water flux.



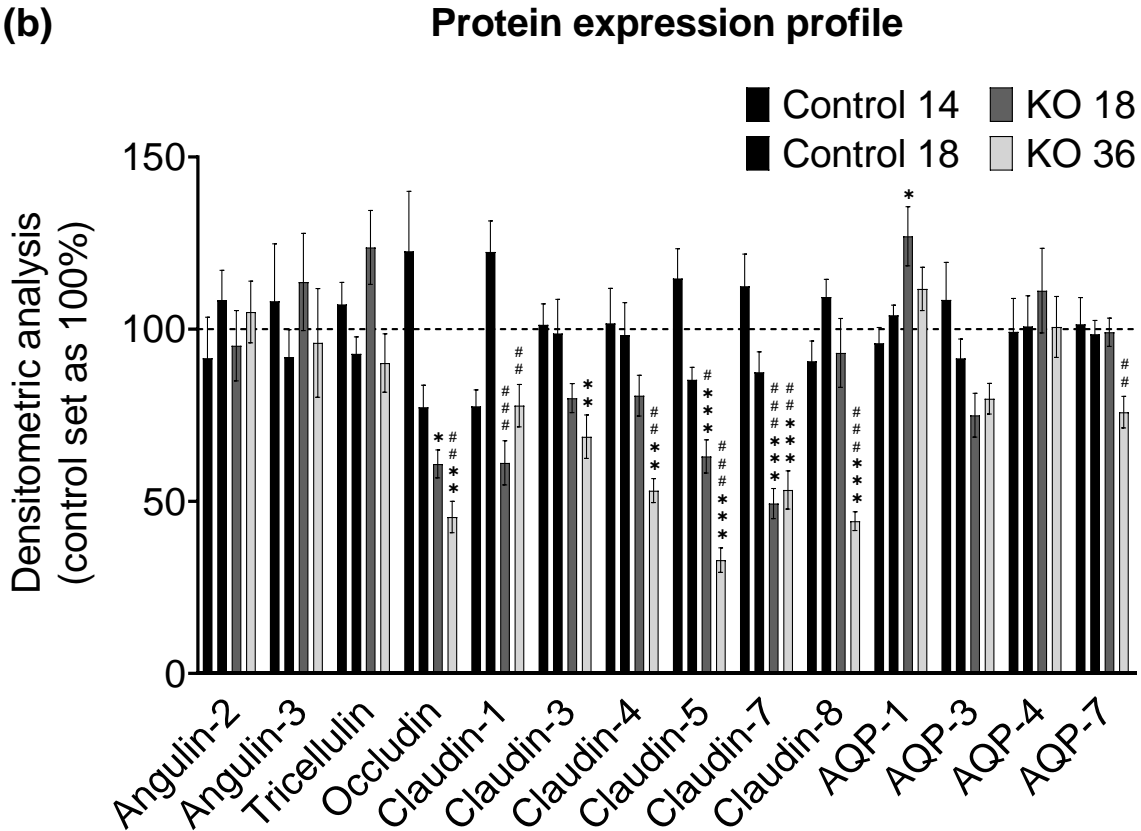
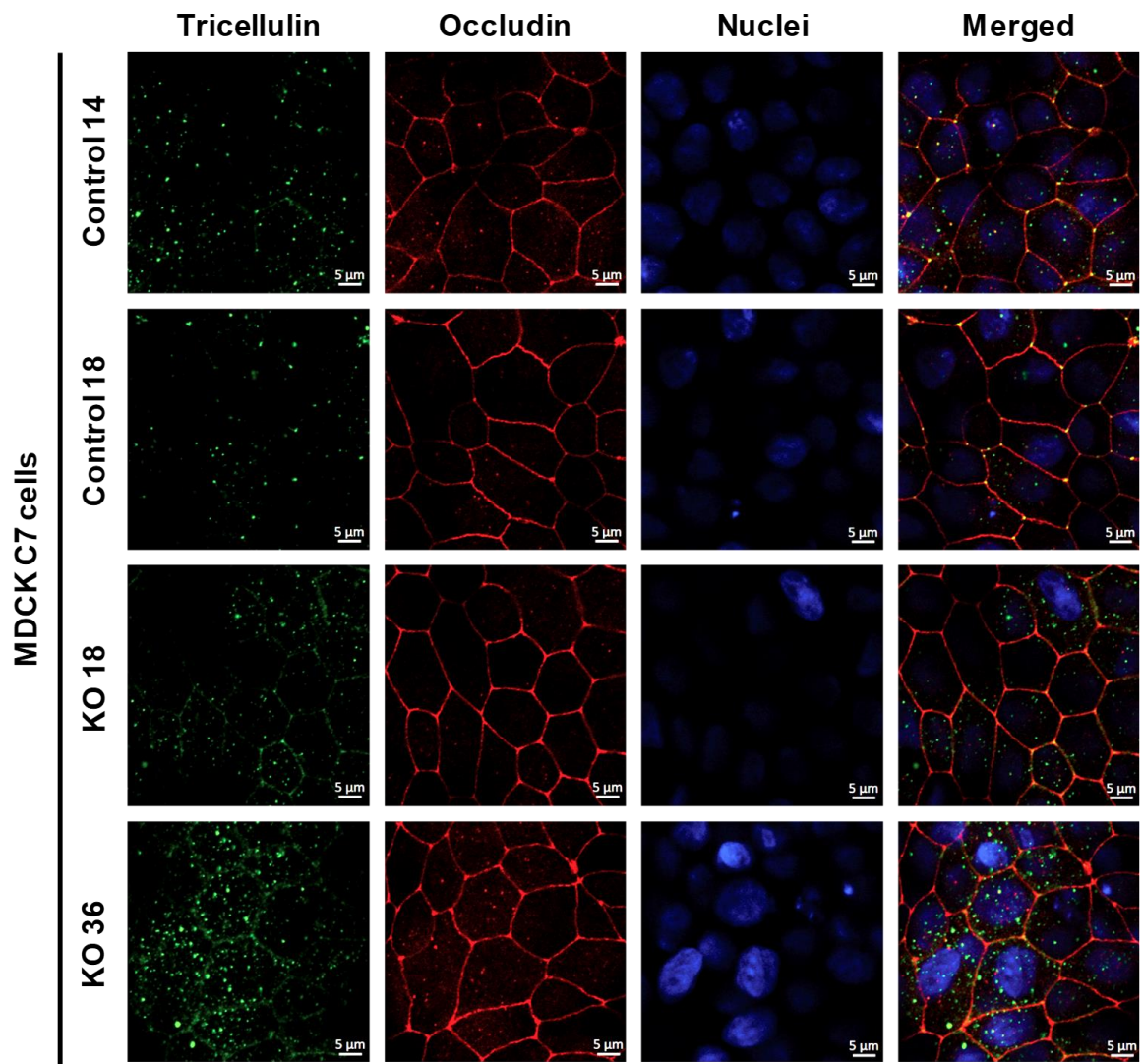


Figure 3-19. Angulin family proteins, tricellulin, occludin, claudins, and AQP expression in angulin-1 knockout MDCK C7 cells. **(a)** Representative Western blots. **(b)** Densitometric analysis of protein expression levels in angulin-1 knockout clones KO 18 and KO 36 in comparison to their vector-transfected controls. β -actin was used as an internal control for normalization to protein content. ($n=9$, $N=3$; * $P\leq 0.05$, ** $P\leq 0.01$, *** $P\leq 0.001$ with regard to control 14 and # $P\leq 0.05$, ## $P\leq 0.01$, ### $P\leq 0.001$ with regard to control 18).

3.3.3 Effects of angulin-1 KO on tricellulin protein localization

Immunofluorescence studies combined with confocal microscopy (see Chapter 2.2.5) revealed a selective delocalization of tricellulin from the tTJs to the bTJ after angulin-1 knockout, whereas occludin was concentrated at the corners of tTJ (Figure 3-20a). In addition, the stimulated emission depletion (STED) microscopy (super-resolution imaging technique) was used to analyze in detail the localization of tricellulin and angulin-1 before and after angulin-1 KO (Figure 3-20b). As can be seen, angulin-1 is located exclusively in the TCs in control 14 cells and disappears entirely in the KO 36 clone. On the other hand, tricellulin appears in the TCs, but its orientation is parallel to the applied plane, perhaps because it connects short strands of TJ to the central sealing elements. After angulin-1 KO, tricellulin partially lost its localization at the TCs (Figure 3-20b).



(a)

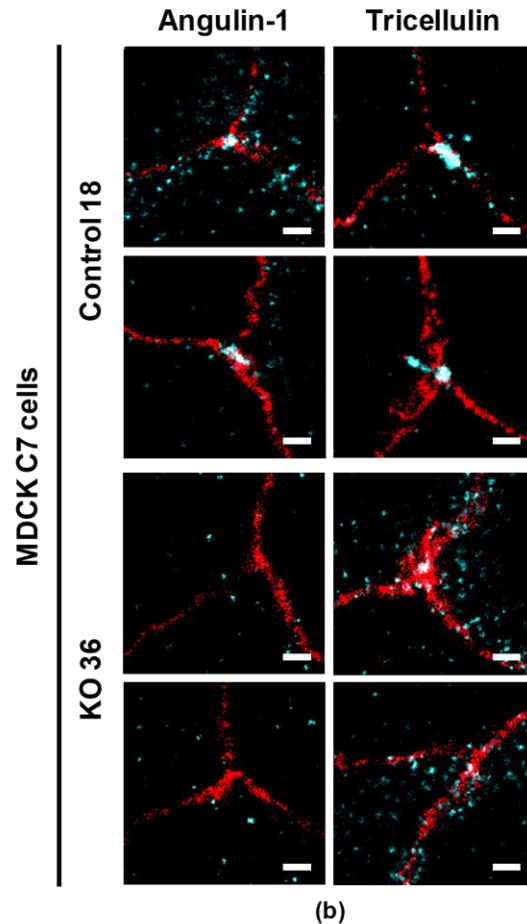


Figure 3-20. Effects of angulin-1 knockout on the localization of tricellulin and occludin. **(a)** Immunofluorescence analysis of tricellulin and occludin in control cells and angulin-1 knockout clones. The localization of these proteins was changed in the angulin-1 knockout clones (Tricellulin: green; occludin: red; DAPI: blue). **(b)** STED microscopy of tTJ of angulin-1 and tricellulin in angulin-1 KO 36 clone in comparison with the control 18 (resolution limit: 20 nm, scale bars: 200 nm) (Tricellulin and angulin-1: cyan; occludin: red; DAPI: blue).

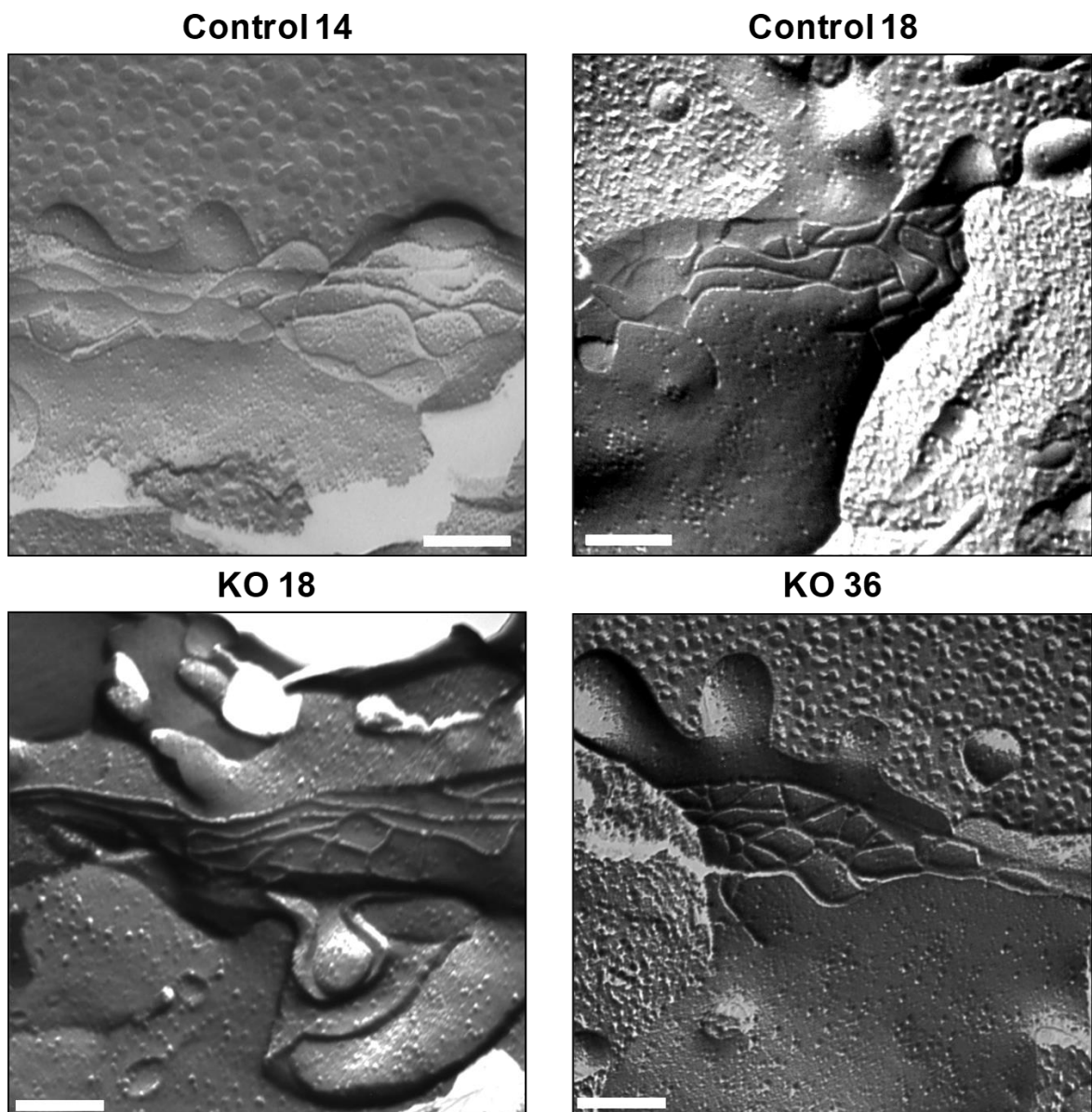
3.3.4 Effect of angulin-1 KO on the ultrastructure of MDCK C7 cells

To obtain insight into whether and to what extent angulin-1 influences the barrier properties of the tight junction in MDCK C7 cells, the ultrastructure of both bTJ and tTJ was analyzed freeze-fracture electron microscopy (Figure 3-21) (see Chapter 2.2.7).

Comparison of the bTJs (Figure 3-21a) of controls and angulin-1 KO clones showed no alteration in the ultrastructure and revealed a regular meshwork. On the other hand, typical tTJs with the central sealing elements and short TJ strands connected to these

elements were observed in the control 14 (Figure 3-21b). In contrast, TCs in angulin-1 KO 36 cells had two vertical TJ strands separated from one another by smooth fracture planes of the plasma membranes (Figure 3-21b); nonetheless, the amount of full tTJs was too low to perform a morphometric analysis. In general, the tTJs were formed as an elongated tubular structure that extends vertically, whose central pore is formed by the tricellular contact between the bicellular tight junction strands (Figure 3-21b).

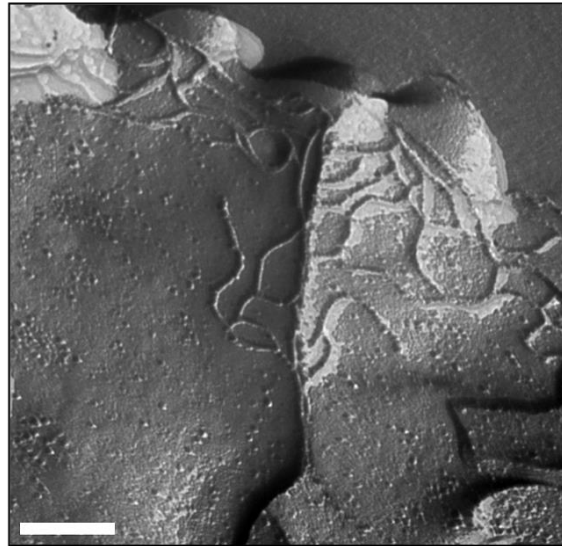
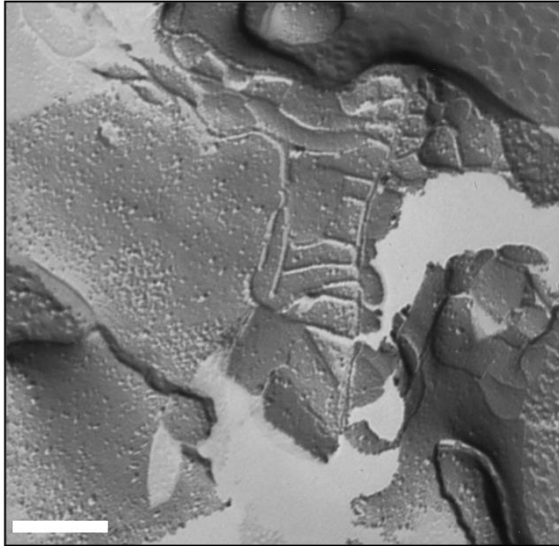
MDCK C7 cells



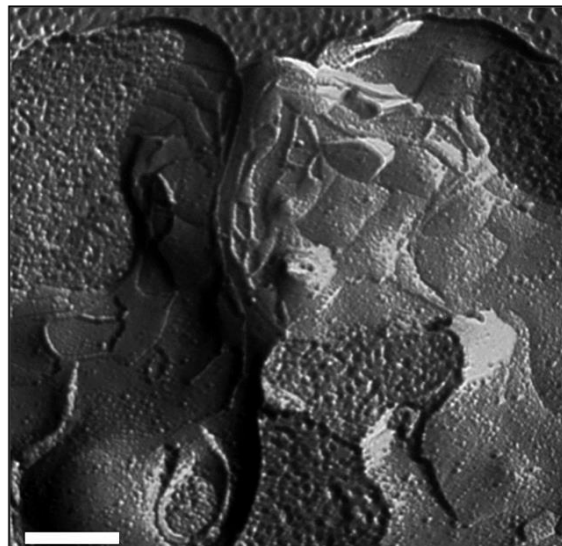
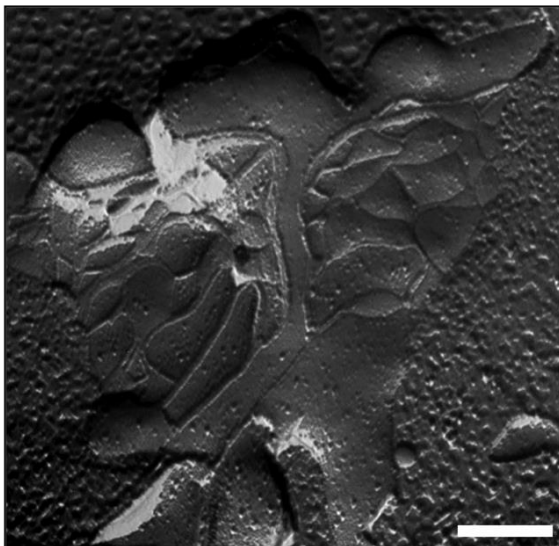
(a)

MDCK C7 cells

Control 14



KO 36

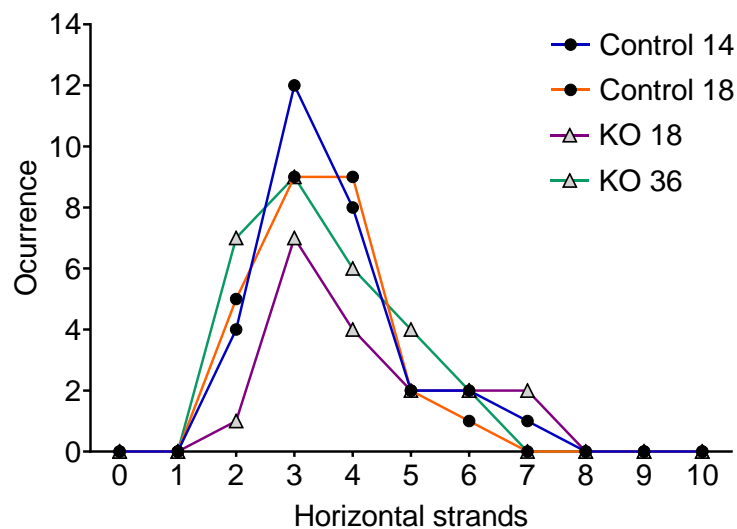


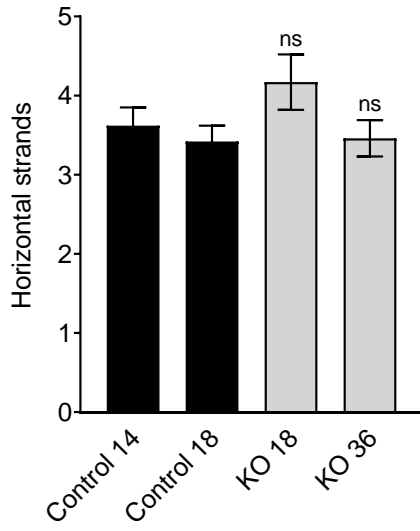
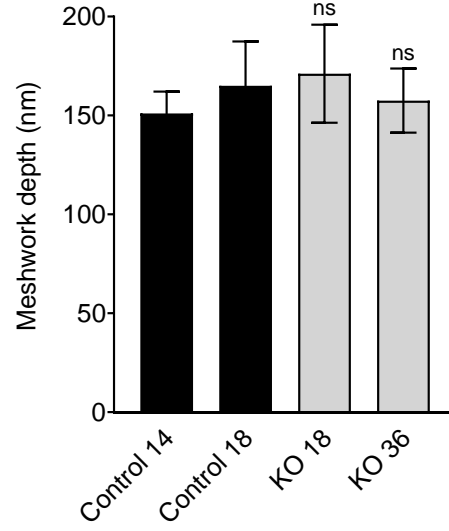
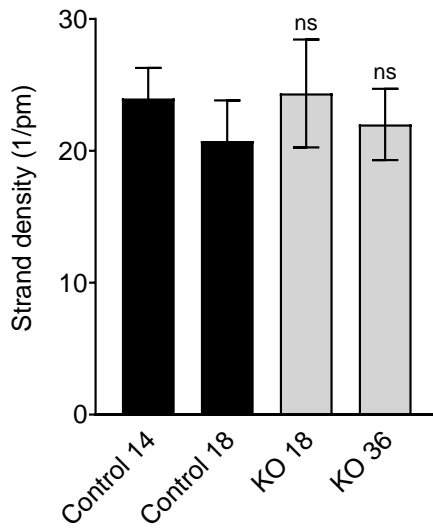
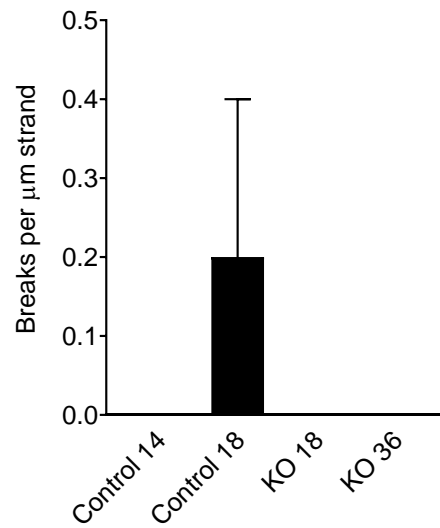
(b)

Figure 3-21. Freeze-fracture electron microscopy of angulin-1 knockout MDCK C7 cells. Photos were taken at x51000; Bars: 200 nm. **(a)** The bTJ strands of the vector-transfected cells and angulin-1 KO clones revealed a regular meshwork, characterized by continuous-type areas, as it is well visible in the magnified detail. bTJs of angulin-1 KO cells show no ultrastructural difference compared with the vector control clones. **(b)** The tTJs of vector-transfected clone 14 are characterized by linear, continuous strands expanding vertically. There is a slight difference in the tTJ width of angulin-1 KO 36 clone and the vector-transfected cells. The linear orientations of TJ strands form a fishbone-like structure.

Regarding bTJs (Figure 3-21a), no alteration was found in the horizontally oriented filaments arranged perpendicular to the paracellular diffusion pathway between the controls and the angulin-1 knockouts, whether analyzed as frequency distribution (Figure 3-22a). Neither the numbers of strands nor the meshwork depth was changed after angulin-1 KO (Figure 3-22b and 3-22c). The network density, which is calculated from the ratio of the number of strands to the network depth, did not differ between controls and angulin-1 knockout clones (Figure 3-22d). The number of breaks (>20 nm) per μm horizontal length of single-strands in bTJ was not significantly different between controls and the angulin-1 KO clones (Figure 3-22e). No breaks were accumulated in a vertical series that could open a complete paracellular path. More importantly, the analysis of strand appearance as either of continuous- or particle- (pearl string) type revealed no changes correlated with the observations reported above. Continuous strands appeared in all of the examined microscopy fields in control clones as well as in angulin-1 KO clones; only 8% of control 18 clone showed particle-type strands (Figure 3-22f). In addition, the tight junctions of the vector controls and the angulin-1 KO clones were composed exclusively of linear strands (Figure 3-22g). Thus, it could be said that any change in water flow in angulin-1 KO clones, compared to control cells, would not be caused by changes in TJ ultrastructure.

(a) Frequency distribution of TJ strand numbers



(b) Number of horizontal strands**(c) Depth of compact meshwork****(d) Density of bTJ strands****(e) Breaks per μm single strand**

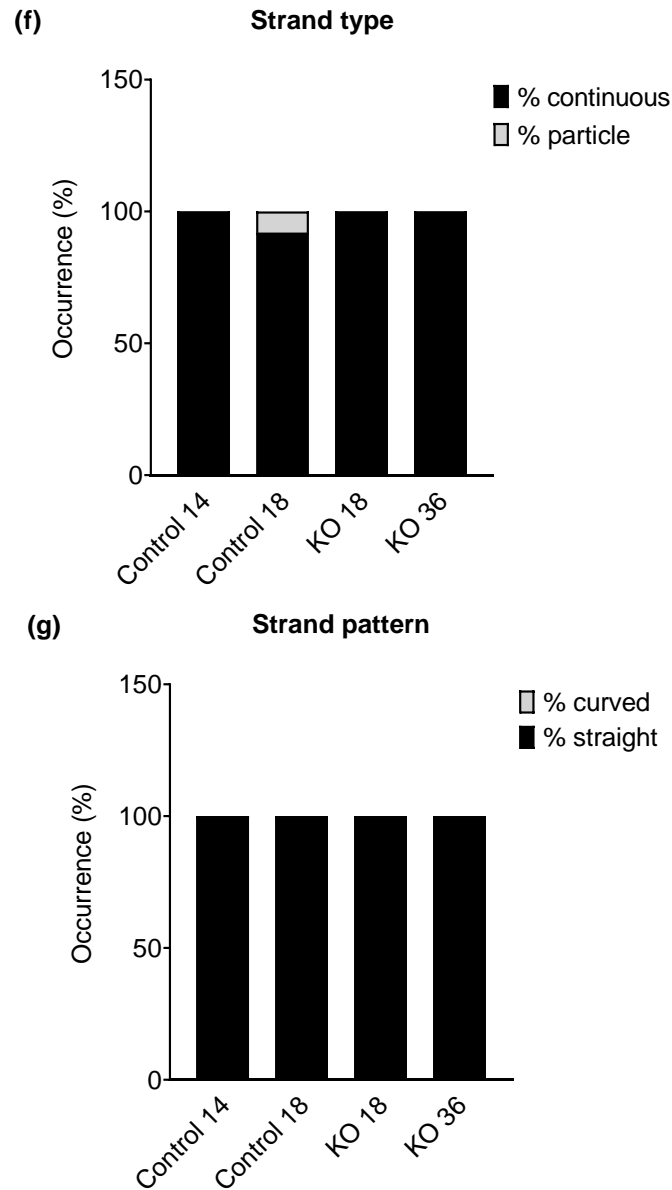


Figure 3-22. Morphometric analysis of TJ ultrastructure of angulin-1 knockout MDCK C7 cells. **(a)** Transfection with CRISPR/Cas9 and sgRNA targeting angulin-1 did not alter the occurrence of strand numbers. **(b)** In bTJs there was no difference in the number of horizontal strands between the vector control clones and the angulin-1 KO cells. **(c)** The vertical depth of the compact meshwork did not change after the removal of angulin-1. **(d)** The strand density did not change between the control and the angulin-1 KO clones. **(e)** The occurrence of breaks >20 nm/m length of single horizontal strands. Knockout of angulin-1 did not modify the occurrence of breaks. **(f)** The occurrence of continuous and particle strand type. Knockout of angulin-1 did not change the strand type compare to their controls. **(g)** Angulin-1 KO had no effect on the characteristically straight strand patterns. (N=2, n=18-29, ns: not significant).

3.3.5 Effect of angulin-1 KO on transepithelial water transport in MDCK C7 cells

To analyze the role of angulin-1 with respect to paracellular water passage, water fluxes were measured after induction of osmotic gradients produced by 100 mM mannitol (100 mOsm) in the vector controls 14 and 18 and in the angulin-1 knockout clones 18 and 36 on the apical and basolateral layer of the cells (see Chapter 2.4.4). The angulin-1-depleted clones showed no difference in water permeability in comparison to control clones with regular angulin-1 expression when mannitol was used as an osmotic gradient (Figure 3-23a and 3-23b, Appendix B. Table 7-3). Nevertheless, the angulin-1-depleted clones showed an increase in water permeability when 37 mM 4-kDa dextran (100 mOsm/Apical side) was used (Figure 3-23c, Appendix B. Table 7-3). This indicates that the removal of angulin-1 from the tTJ had an effect on the passage of water in MDCK C7 cells, which is dependent on the chemical nature of the osmotic gradient.

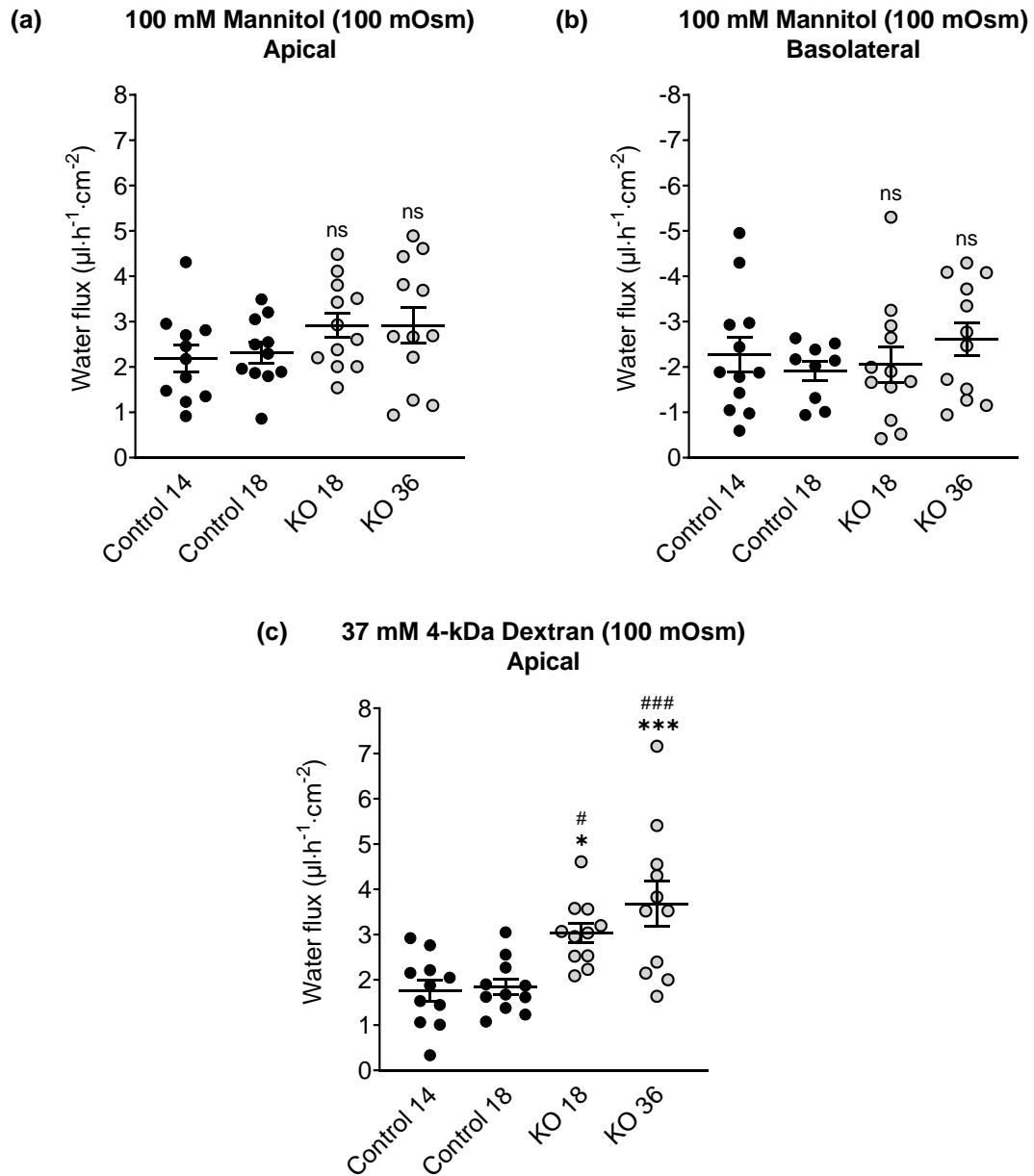
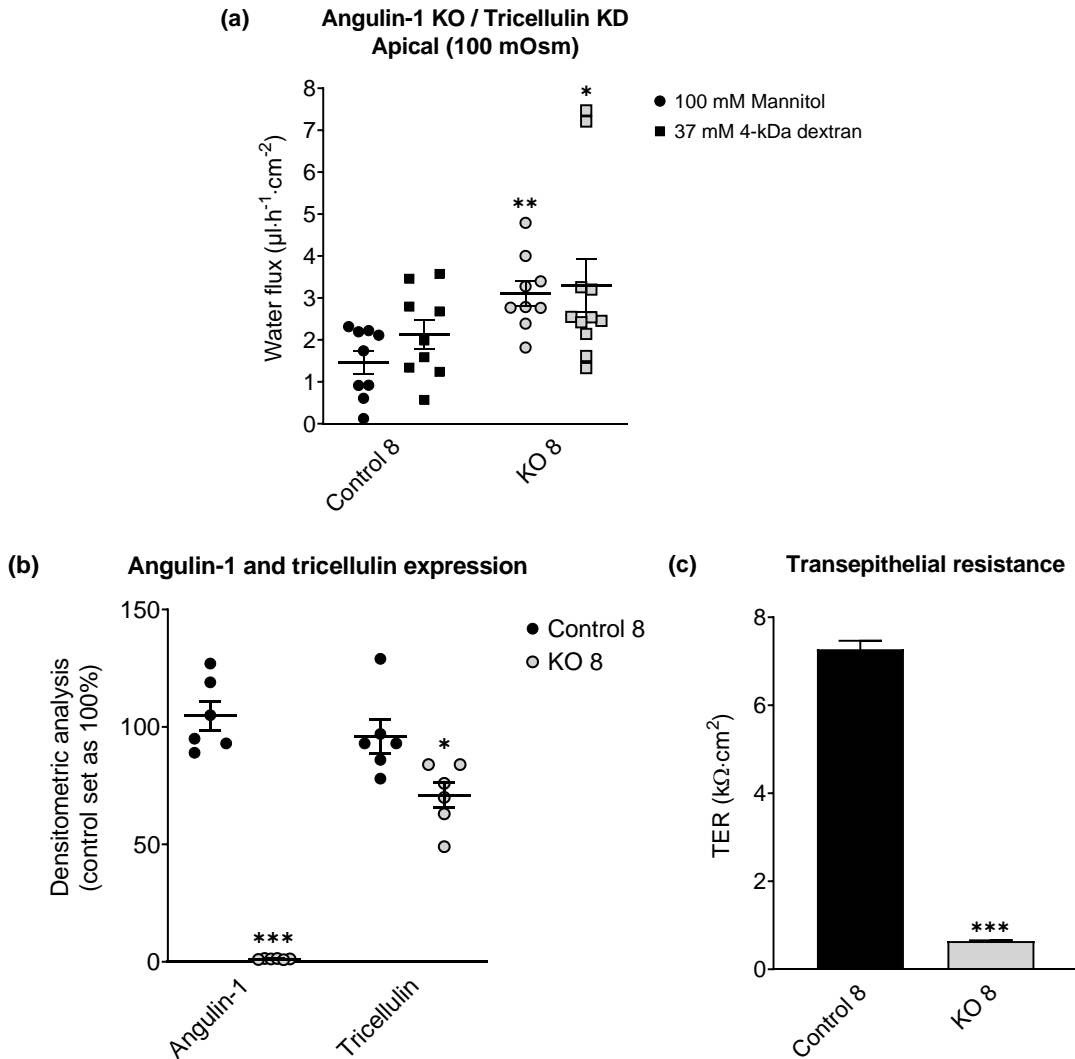


Figure 3-23. Water flux in angulin-1 knockout MDCK C7 cells. Water flux stimulated by an osmotic gradient of 100 mM mannitol **(a)** on the apical side (n=11-12) and **(b)** on the basolateral side (n=9-12) of the cell layer. The transepithelial water flux was unchanged in both angulin-1 knockout clones. **(c)** Water flux induced by a gradient of 37 mM 4-kDa dextran on the apical side (n=10-11). The transepithelial water transport increased in both angulin-1 knockout clones. (ns: not significant, *P≤0.05, **P≤0.01, ***P≤0.001 with regard to control 14 and #P≤0.05, ##P≤0.01, ###P≤0.001 with regard to control 18).

In the same parallel series of experiments, an additional angulin-1 KO clone with a reduction in tricellulin expression and its control were partially characterized (KO 8 and

control 8). The angulin-1 KO 8 clone has a reduction of 25% in tricellulin expression compared with its control 8 (Figure 3-24b). The TER of the KO clone was reduced 90% after angulin-1 KO (Figure 3-24c). The densitometric analysis showed that the expression of occludin, claudin-4, -5, -7, and -8 was reduced except for claudin-3, which was upregulated (Figure 3-24d). Most importantly, no changes in AQPs were found (Figure 3-24d). As for water transport, in the presence of 100 mOsm mannitol and 100 mOsm 4-kDa dextran, the water flux in the angulin-1 KO 8 was higher than in the control 8 (Figure 3-24a). This finding indicates that the water flux through the tTJ is inhibited in the presence of angulin-1 and tricellulin, and when tricellulin is downregulated or delocalized, in this case, due to removal of angulin-1 from the tTJ, the transepithelial water transport increased, similarly to what was found in the tricellulin KD clones.



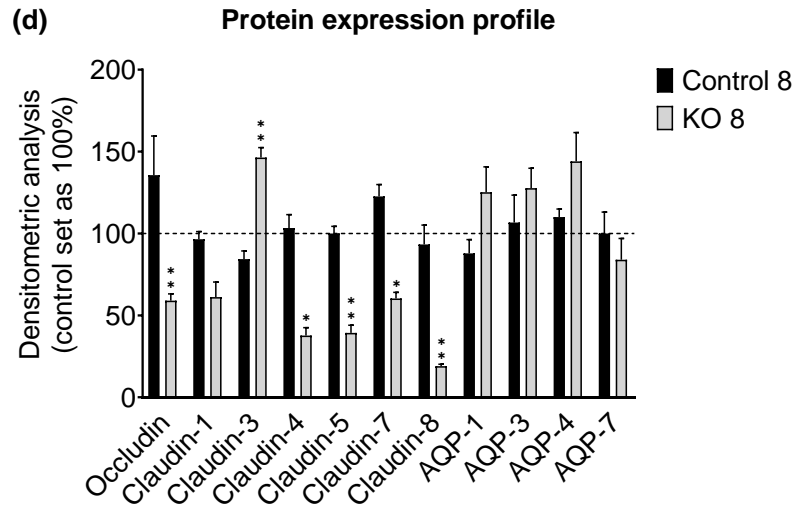


Figure 3-24. Partial characterization of an angulin-1 knockout MDCK C7 clone with a reduction in the expression of tricellulin. **(a)** Water flux stimulated by an osmotic gradient of 100 mM mannitol or 37 mM 4-kDa dextran on the apical side (n=9-11). The transepithelial water flux increased in the angulin-1 KO 8 clone in comparison with its control. **(b)** Densitometric analysis of angulin-1 and tricellulin protein expression levels in stable CRISPR/Cas9 transfectant (KO 8) in comparison to vector-transfected control (Control 8) (N=2, n=6). Angulin-1 KO 8 cells have a 25% reduction in tricellulin expression compare with its control 8. **(c)** Effect of angulin-1 KO/tricellulin KD on transepithelial resistance (TER) (N=6, n=18). Loss of angulin-1 and reduction of tricellulin decreases TER. **(d)** Densitometric analysis of protein expression levels in angulin-1 KO/tricellulin KD clone KO 8 and its vector-transfected control 8 (N=2, n=6). β -actin was used as an internal control for normalization to protein content. The densitometric analysis showed a reduction in the tightening-claudin expression and upregulation of claudin-3. (* $P \leq 0.05$, ** $P \leq 0.01$, *** $P \leq 0.001$).

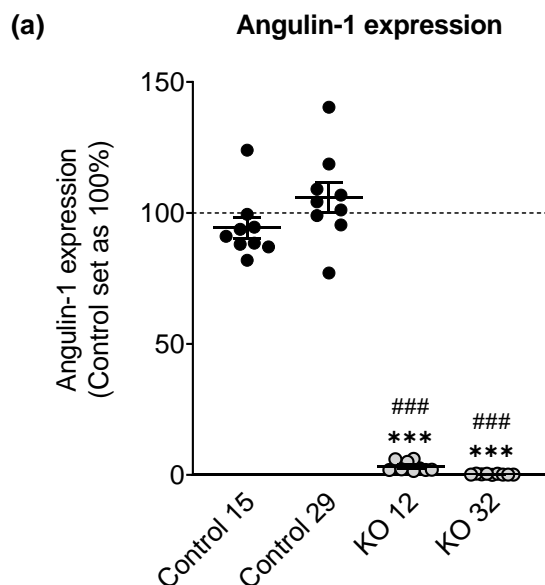
All numerical data can be seen in Appendix B. Table 7-3.

3.4 Angulin-1 knockout (KO): HT-29/B6 cells

3.4.1 Characterization of angulin-1 KO in HT-29/B6 cells

In order to investigate the specific role of the human angulin-1 on the paracellular water transport in the intermediate-tight epithelium, the human adenocarcinoma cell line, HT-29/B6, was transfected with three sgRNA targeting the different isoforms of angulin-1 (see Table 3-1) together with CRISPR/Cas9 and HDR plasmids (see Chapter 2.2.2.2 and 3.3.1). After transfection of HT-29/B6 cells, puromycin-resistant cell clones were screened for angulin-1 knockout by Western blotting (see Chapter 2.3). In this section, two knockout clones and two controls were investigated (KO 12 and KO 32 and their controls 15 and 29). The two knockout clones are mono-allelic knockouts, as shown by Western blot (Figure 3-25a and 3-27a, Appendix B. Table 7-4).

The proper localization of angulin-1 as dots at the TCs in the control cells and their depletion in the knockout cells were confirmed by immunofluorescence confocal laser-scanning microscopy (see Chapter 2.2.5). ZO-1 served as a TJ marker (Figure 3-25b). In addition, it is possible to observe angulin-1 localized in bTJ and also intracellular.



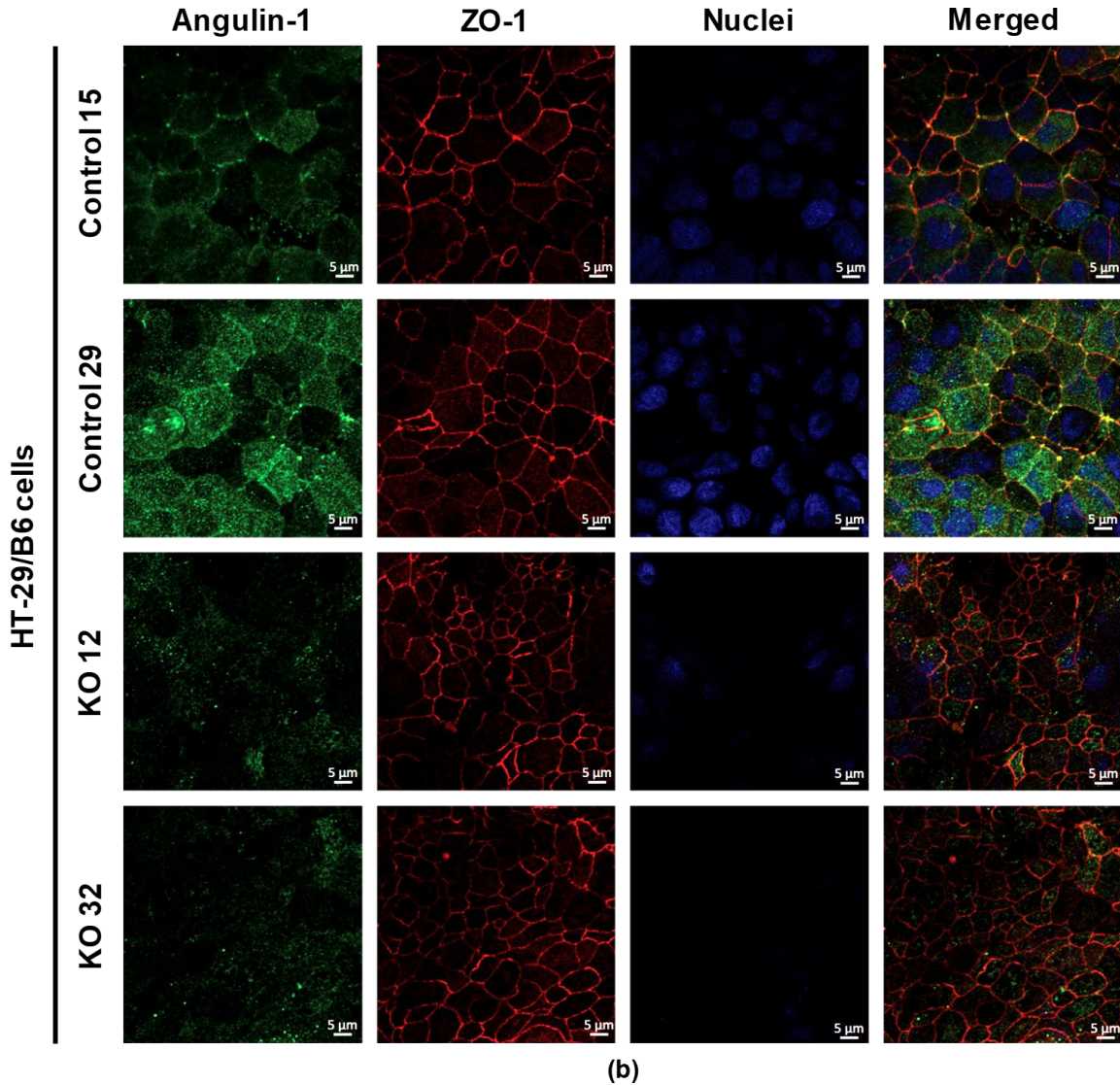


Figure 3-25. Expression and localization of angulin-1 knockout in HT-29/B6 cells. **(a)** Densitometric analysis of angulin-1 protein expression levels in stable CRISPR/Cas9 transfectants in comparison to vector-transfected controls ($n=9$, $***P \leq 0.001$ with regard to control 15 and $###P \leq 0.001$ with regard to control 29) and **(b)** Immunofluorescent staining of HT-29/B6 sgRNA/CRISPR/Cas9 targeting angulin-1. Knockout in HT-29/B6 cells removed angulin-1 compare with the controls where this protein remained within the tTJ. Angulin-1: green, ZO-1: red, DAPI (nucleus): blue.

The topology parameters (see Chapter 2.2.6) of fluorescence stained angulin-1 knockout HT-29/B6 cells using the program Fiji-ImageJ for estimating the contribution of angulin-1 at the tTJ to overall permeability are shown in Appendix C. Table 7-6 and Figure 7-4. The most interesting result is that within the analyzed area, the TJ length per cell was similar

in both KO clones in comparison with their controls. On tTJ levels, the tTJ density of both KO clones also was the same compared to their controls. In relation to the number of vertices or neighboring cells, it was observed that for all clones, there is an average value between 4 and 6 vertices (Appendix C. Figure 7-4), which also corresponds to the calculated number of tTJ per cell (5 tTJ/cell).

3.4.1.1 Effect on the transepithelial resistance and macromolecule permeability

To evaluate the effect of the complete removal of angulin-1 from the tTJ on barrier function, the TER was measured (see Chapter 2.4.1). Angulin-1 knockout reduced the TER between 2- and 4-times in the KO clones compared with their controls (Figure 3-26a, Appendix B. Table 7-4). Besides, to investigate whether angulin-1 was able to prevent tight junction against ions and against larger molecules, flux measurements were carried out with 4-kDa FITC-dextran (FD4, 4000 Da) (see Chapter 2.4.3). In general, the permeability for FD4 was about 7 times higher in the KO clones than in the controls. Also, it can be seen that under isosmotic conditions (Figure 3-26b, Appendix B. Table 7-4), the permeability was higher than under an osmotic gradient (Figure 3-26c, Appendix B. Table 7-4); this is because water flux in the opposite direction possibly inhibits the movement of FD4 when an osmotic gradient is applied.

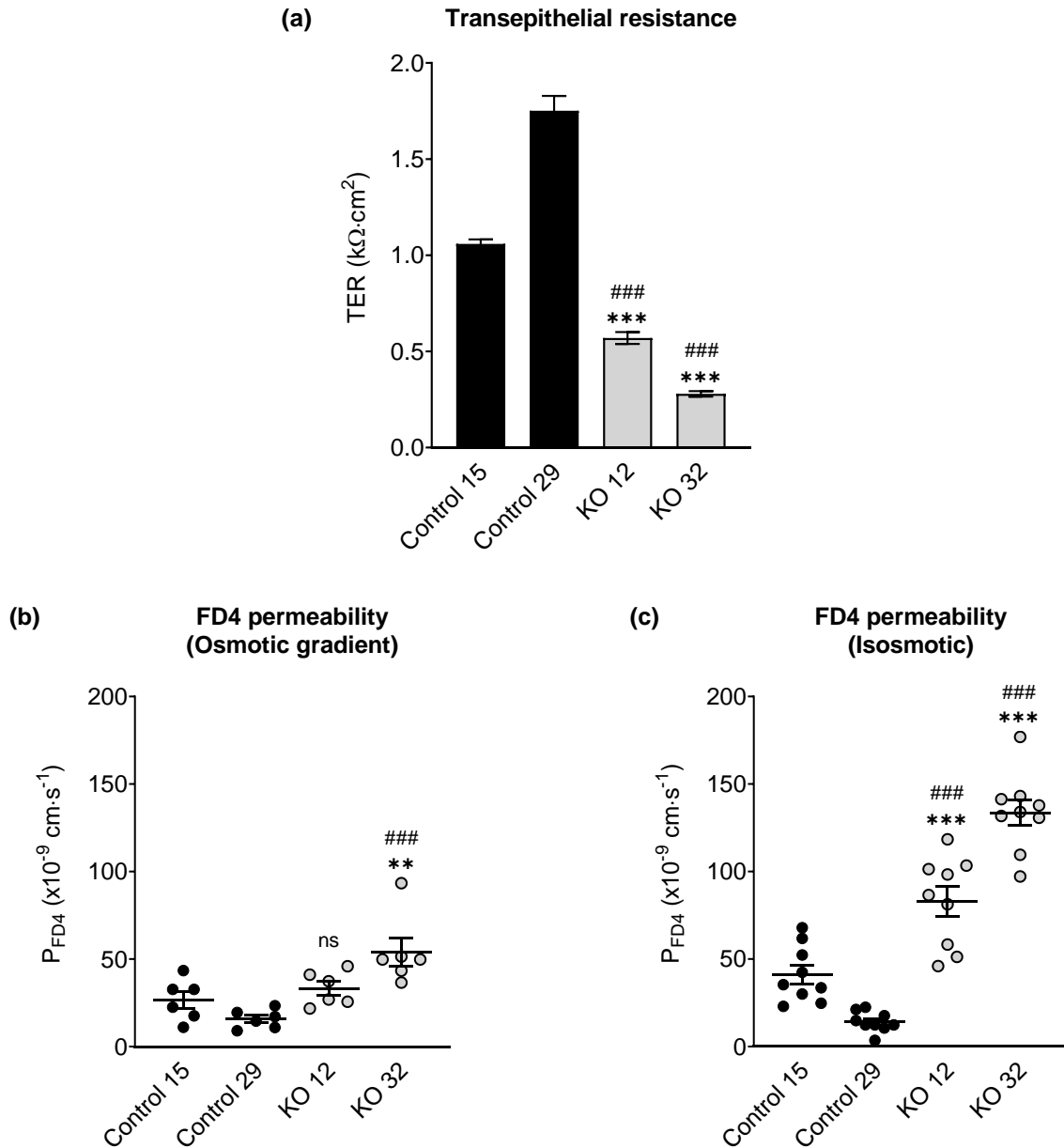
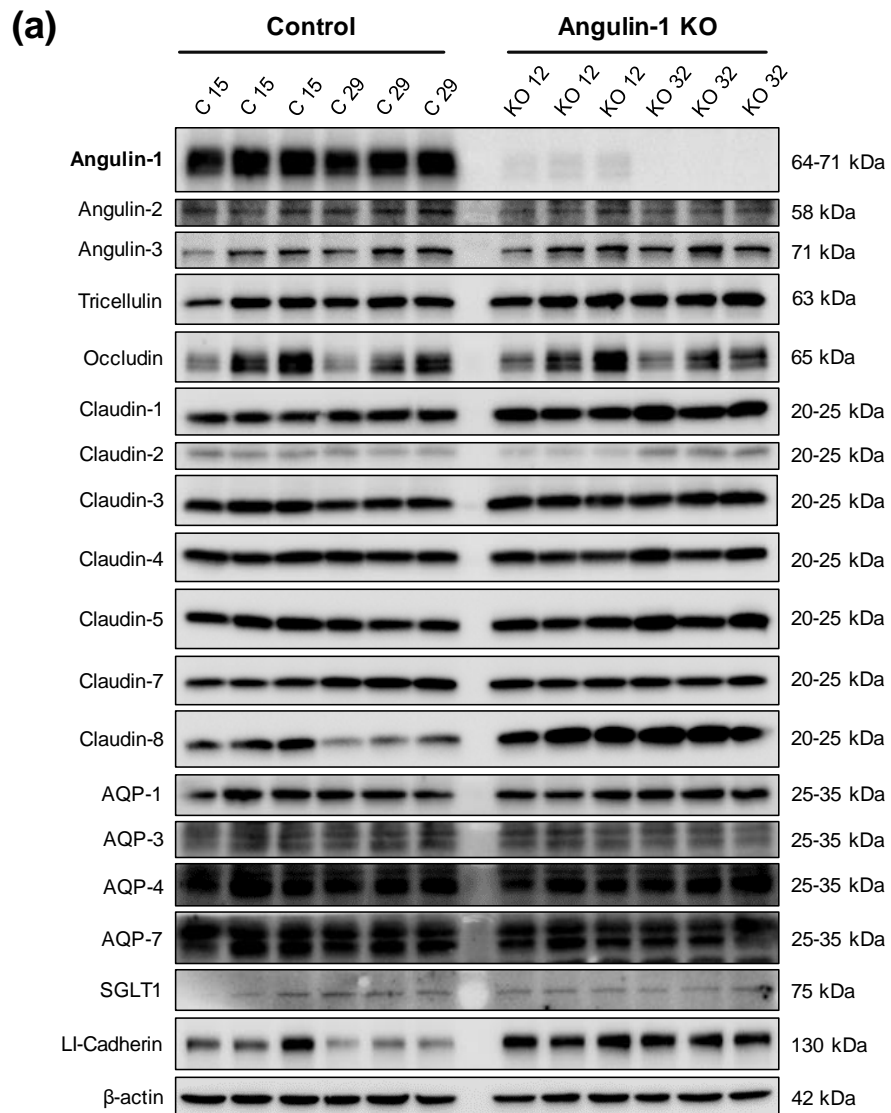


Figure 3-26. Functional analysis of angulin-1 knockout in HT-29/B6 cells. **(a)** Effect of angulin-1 knockout on transepithelial resistance. Angulin-1 KO decreases TER in HT-29/B6 cells ($***P \leq 0.001$ with regard to control 15 and $###P \leq 0.001$ with regard to control 29, $n=43$). **(b)** Effect of angulin-1 knockout on permeability for 4-kDa FITC-dextran (FD4) with osmotic gradient. Permeability is increased only in the KO 32 clone when 4-kDa dextran was added to the apical side ($**P \leq 0.01$ with regard to control 15 and $###P \leq 0.001$ with regard to control 29, ns: not significant, $n=6$). **(c)** Effect of angulin-1 knockout on permeability for 4-kDa FITC-dextran (FD4) without osmotic gradient. Permeability is increased in both KO clones when the osmolality of both sides was equal ($***P \leq 0.001$ with regard to control 15 and $###P \leq 0.001$ with regard to control 29, $n=9$).

3.4.2 Effects of angulin-1 KO on other proteins of HT-29/B6 cells

HT-29/B6 cells express the three angulins, tricellulin, occludin, several claudins, aquaporin-1, -3, -4 and -7, SGLT1 and LI-cadherin, and in further investigations, the effect of angulin-1 knockout on the expression level of these proteins was analyzed (Figure 3-27a) (see Chapter 2.3). The densitometric analysis revealed some clonal variability in claudin expression between the knockout clones and the controls (Figure 3-27b). In detail, tricellulin, claudin-1, -3, -5, -7 and -8, and LI-cadherin were increased in both knockout clones. The water and cation-channel claudin-2 was upregulated in the angulin-1 KO 32 clone and downregulated in the angulin-1 KO 12 clone. Most importantly, the angulin-1 knockout did not affect the expression of the membrane water channels expressed in HT-29/B6 cells, AQP-1, -3, -4, and -7, and the expression of other protein carriers was unchanged, like SGLT1. Thus, the transcellular water flux is unchanged in these cells. It is worth highlighting that for the KO clones, additional proteins were analyzed than in the knockdown clones thinking that the phenotype is much stronger and could modify to a greater extent these proteins related to water transport present in HT-29/B6 cells (AQPs, SGLT1, and LI-cadherin).



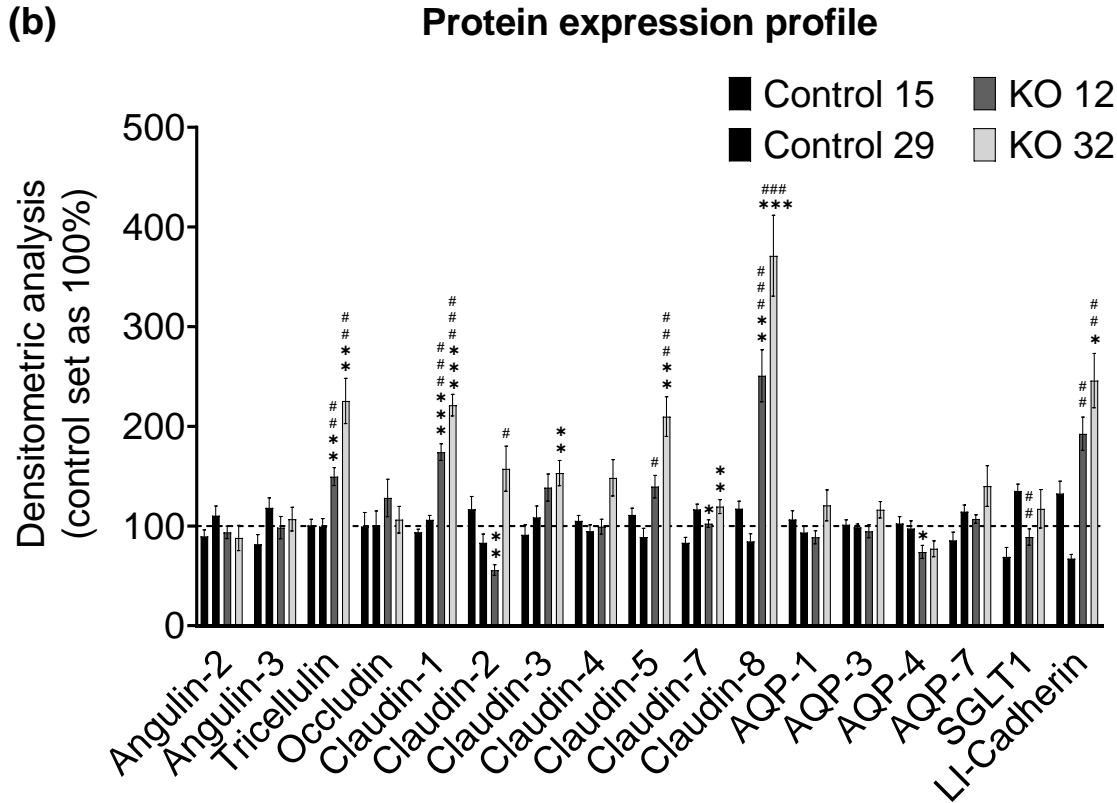
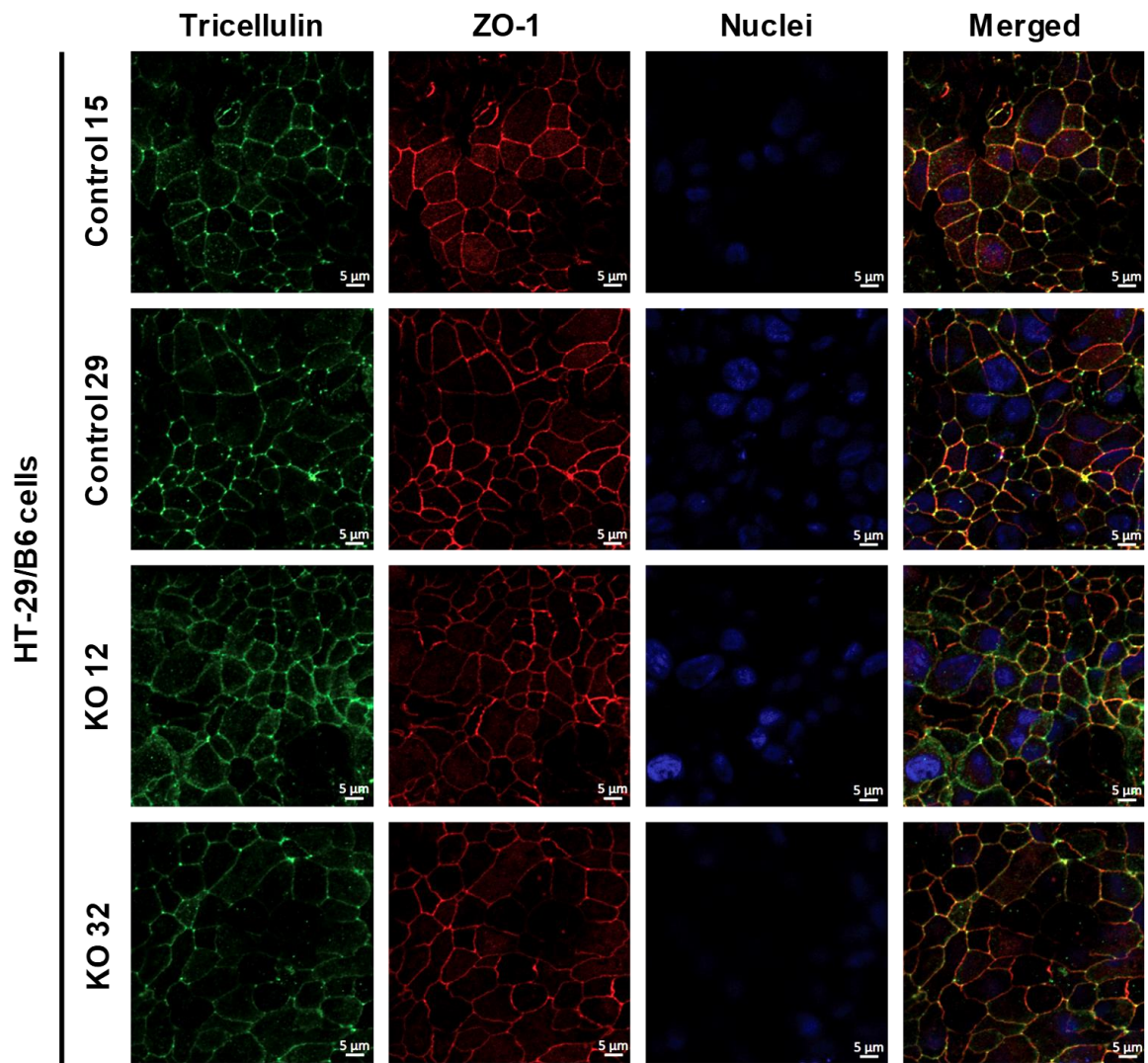


Figure 3-27. Angulin, tricellulin, occludin, claudin, and AQP expression in angulin-1 knockout HT-29/B6 cells. **(a)** Representative Western blots. **(b)** Densitometric analysis of protein expression levels in stable angulin-1 CRISPR/Cas9 transfectants in comparison to their vector-transfected controls. β -actin was used as an internal control for normalization to protein content. ($n=9$, $N=6$, $*P\leq 0.05$, $**P\leq 0.01$, $***P\leq 0.001$ with regard to control 15 and $\#P\leq 0.05$, $\##P\leq 0.01$, $\###P\leq 0.001$ with regard to control 29).

3.4.3 Effects of angulin-1 KO on tight junction protein localization

To investigate whether angulin-1 knockout leads to changed localization of the tTJ proteins tricellulin, immunofluorescence analysis was performed (see Chapter 2.2.5). Knockout of angulin-1 led to lowered localization of tricellulin at tricellular contacts and delocalization into bicellular contacts, whereas localization of ZO-1 (TJ marker) was unaffected (Figure 3-28a).

In the case of claudin-8, one of the most upregulated claudins, its localization seemed to be similar in control and the knockout cells, with the main difference that in knockout clones, intracellular claudin-8 is observed (Figure 3-28b).



(a)

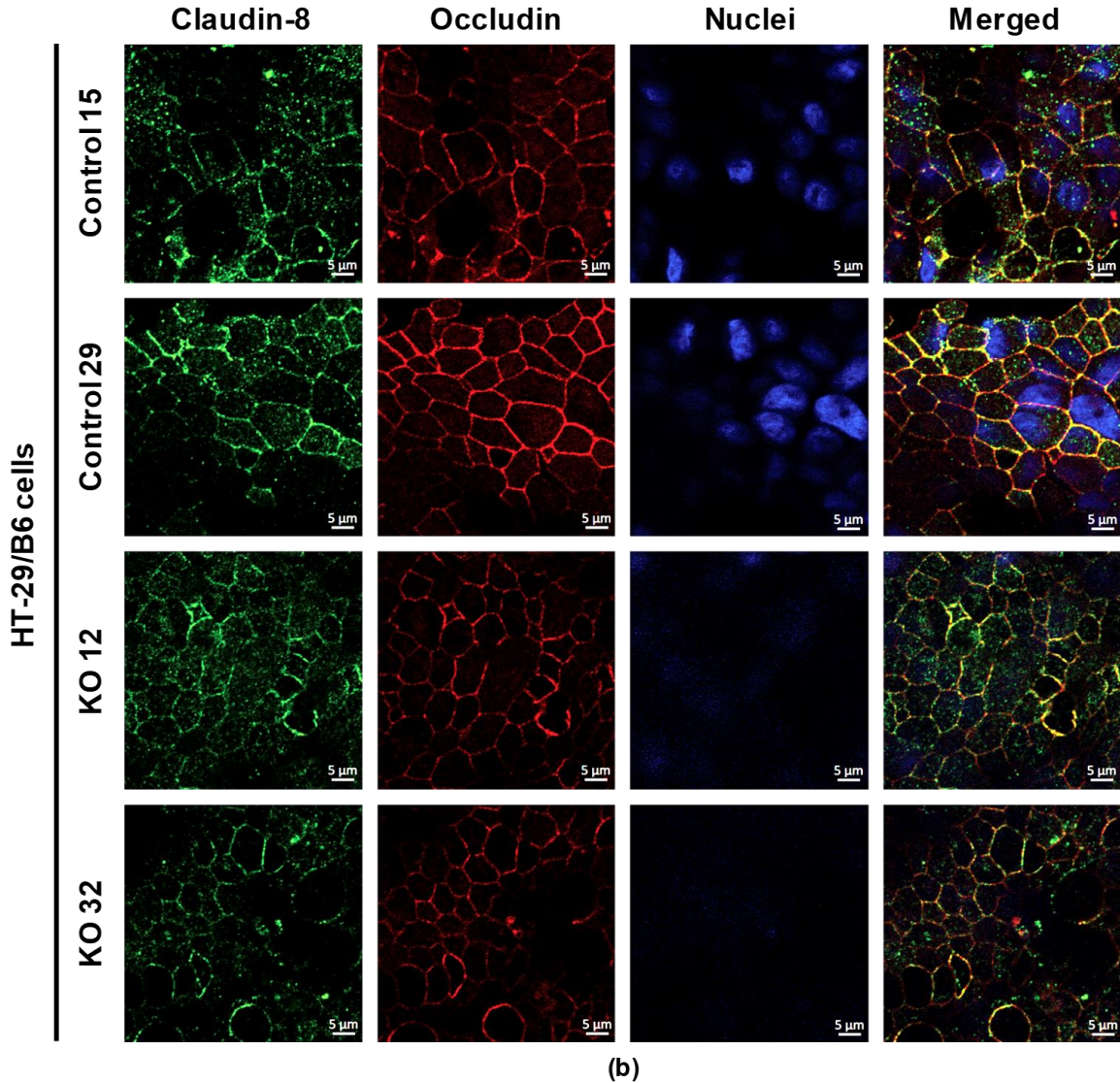


Figure 3-28. Localization of TJ proteins in angulin-1 knockout HT-29/B6 cells. Immunofluorescence analyses of HT-29/B6 control and angulin-1 KO cells. **(a)** Tricellulin. ZO-1 localization was not altered in angulin-1 KO cells. **(b)** Claudin-8. Occludin localization to apical junctions was reduced in angulin-1 KO cells. (Tricellulin, claudin-8: green; occludin, ZO-1: red; DAPI (nucleus): blue).

3.4.4 Effect of angulin-1 KO on the ultrastructure of HT-29/B6 cells

To obtain insight into whether and to what extent angulin-1 influences the barrier properties of the tight junction in HT-29/B6 cells, the ultrastructure of both bTJ and tTJ was analyzed freeze-fracture electron microscopy (Figure 3-29) (see Chapter 2.2.7). Nevertheless, the abundance of tTJs was very low. In addition, they were not complete

and thus not suitable for any measurements. Fortunately, the ones for the knockout clones were not obviously differing from those of the control clones.

HT-29/B6 cells

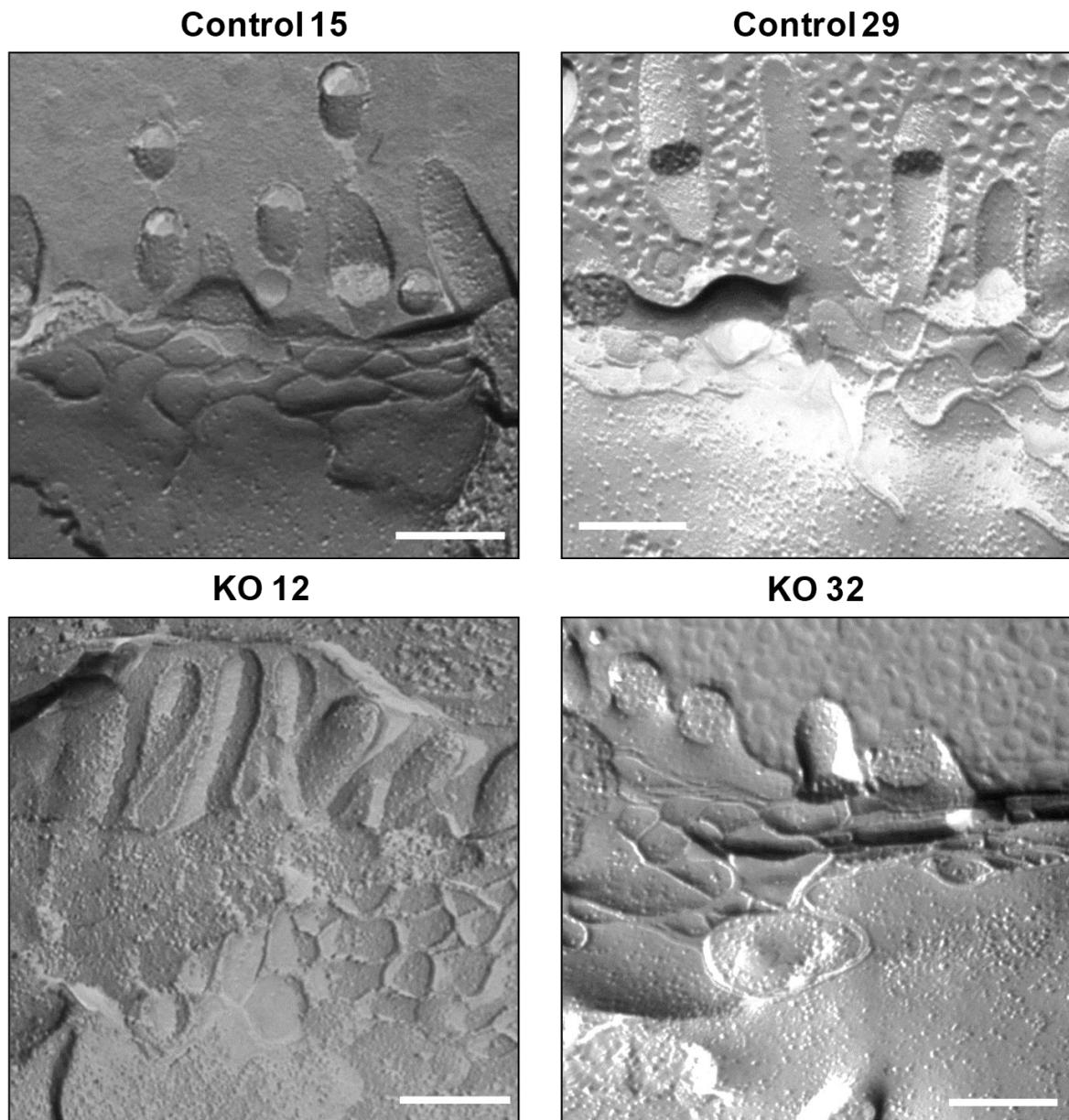
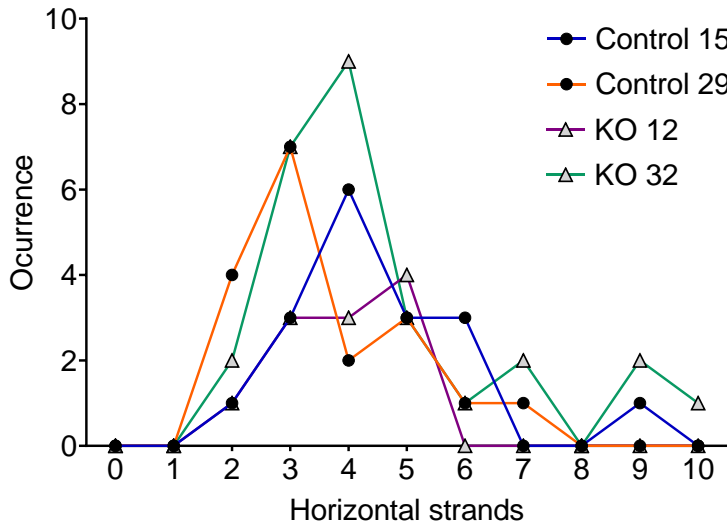


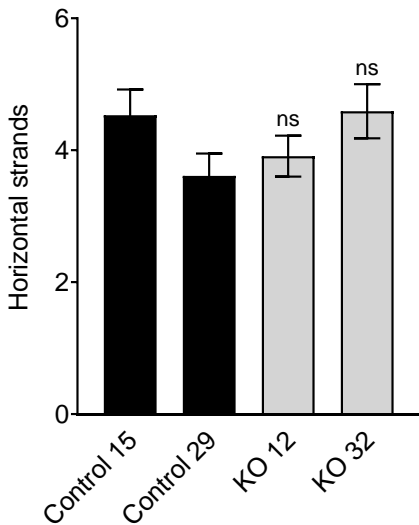
Figure 3-29. Freeze-fracture electron microscopy. Photos were taken at x51000; Bars: 200 nm. The bTJ strands of the vector-transfected cells revealed a regular meshwork, characterized by continuous-type areas, as it is well visible in the magnified detail. bTJs of angulin-1 knockout clones show no ultrastructural difference compared with the vector control-transfected cells.

Regarding bTJs (Figure 3-29), controls and angulin-1 knockouts showed no alteration in the horizontally oriented strands arranged perpendicular to the paracellular diffusion pathway, whether analyzed as frequency distribution (Figure 3-30). As already found for MDCK C7 cells, there is no difference in TJ ultrastructure in HT-29/B6 angulin-1 KO cells compared to their controls (Figure 3-30). Thus, it could be said that any change in water flow in angulin-1 KO clones, compared to control cells, would not be caused by changes in TJ ultrastructure.

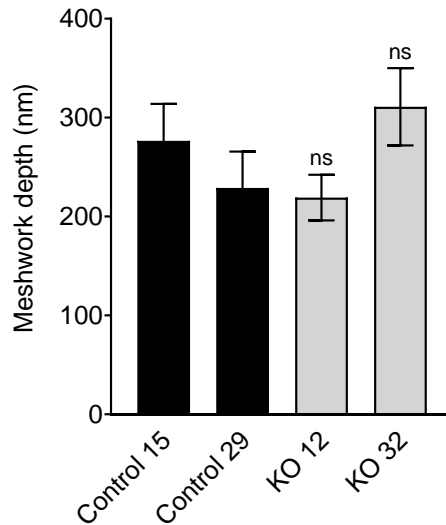
(a) Frequency distribution of TJ strand numbers

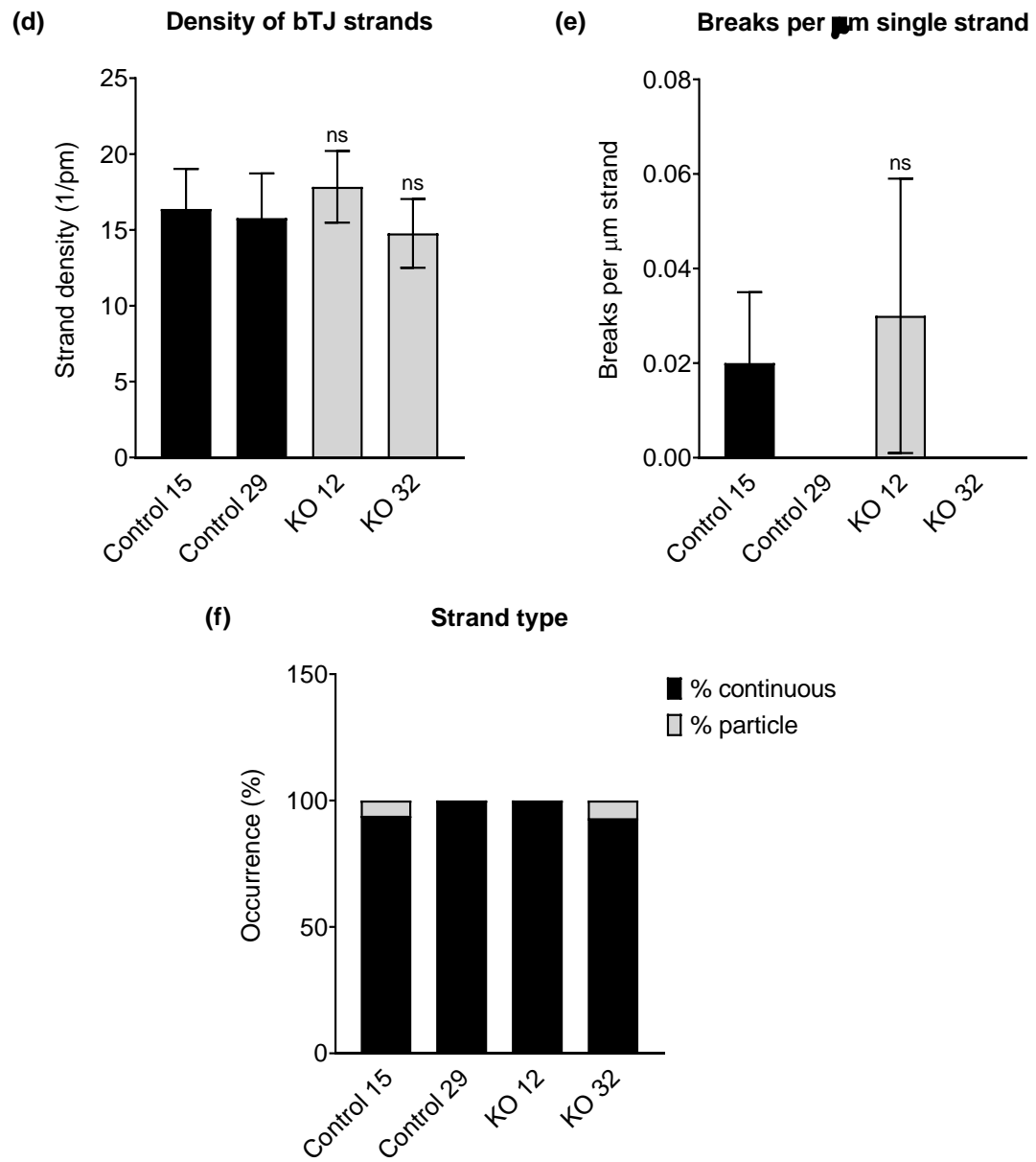


(b) Number of horizontal strands



(c) Depth of compact meshwork





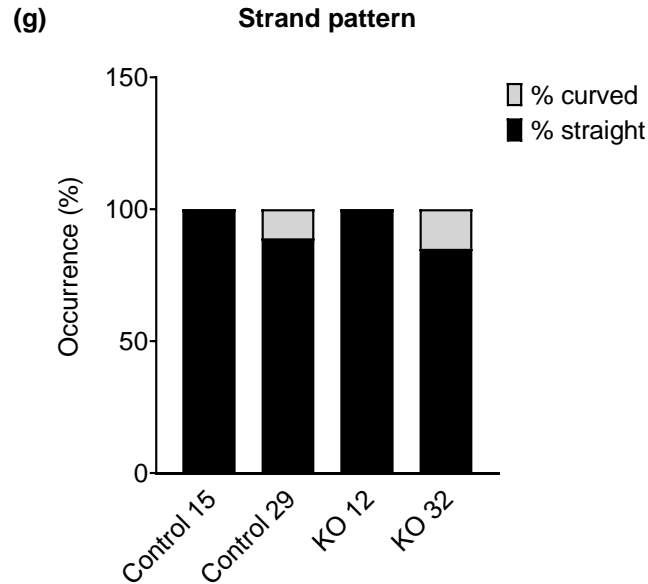


Figure 3-30. Morphometric analysis of TJ ultrastructure of angulin-1 knockout HT-29/B6 cells. **(a)** Transfection with CRISPR/Cas9 and sgRNA targeting angulin-1 did not alter the occurrence of strand numbers. **(b)** In bTJs there was no difference in the number of horizontal strands between the vector control clones and the angulin-1 KO cells. **(c)** The vertical depth of the compact meshwork did not change after the removal of angulin-1. **(d)** The strand density did not change between the control and the angulin-1 KO clones. **(e)** The occurrence of breaks >20 nm/m length of single horizontal strands. Knockout of angulin-1 did not modify the occurrence of breaks. **(f)** The occurrence of continuous and particle strand type. Knockout of angulin-1 did not change the strand type in comparison to the control clones. **(g)** Angulin-1 KO did not affect the characteristically straight strand patterns show in the control cells. (N=2, n=11-27, ns: not significant).

3.4.5 Effect of angulin-1 KO on transepithelial water transport in HT-29/B6 cells

In order to analyze the role of angulin-1 concerning paracellular water passage, water fluxes were measured after induction of an osmotic gradient produced by 100 mM mannitol (100 mOsm) apical and basolateral in the angulin-1 KO clones 12 and 32 and compared with their controls 15 and 29 (see Chapter 2.4.4). As a result, manipulation of angulin-1 expression seemed to exert no effect on transepithelial water transport (Figure 3-31, Appendix B. Table 7-4); in other words, angulin-1 cannot function as a water barrier in the tTJ in HT-29/B6 cells (intermediate-tight epithelium). Water transport was not measured using 4-kDa dextran as an osmotic gradient since the SEM obtained using mannitol was low, and no trend of increased water flow was observed in the KO clones with respect to their controls.

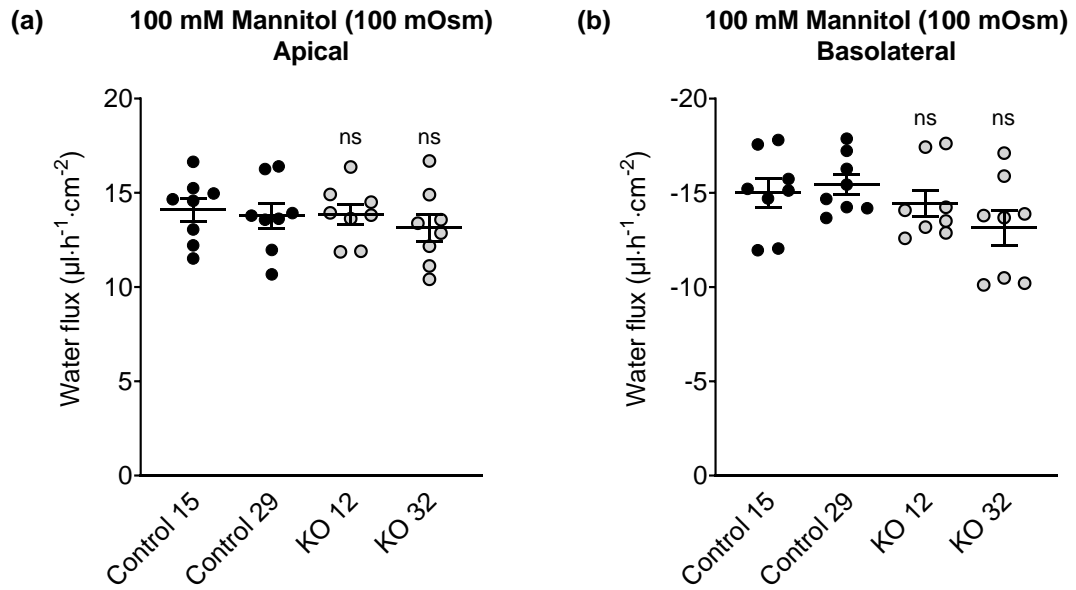


Figure 3-31. Water flux in angulin-1 knockout HT-29/B6 cells stimulated by an osmotic gradient. **(a)** Water flux induced by a gradient of 100 mM mannitol on the apical side. **(b)** Water flux induced by a gradient of 100 mM mannitol on the basolateral side of the cell layer. The transepithelial water flux did not change after angulin-1 KO. (n=8, ns: not significant).

All numerical data can be seen in Appendix B. Table 7-4.

4. Discussion

In the present study, the focus was on elucidating the role of two tricellular tight junction proteins, tricellulin and angulin-1, on the paracellular water permeability. For this, the effect of tricellulin knockdown and angulin-1 knockout was analyzed in two different cell lines, MDCK C7, a tight epithelial cell line, and HT-29/B6, an intermediate-tight epithelial cell line. It was found that tricellulin and angulin-1 are involved in water permeability only in the tight epithelial cell line, while both proteins have no significant effect on water permeability in an intermediate-tight epithelium. These results suggest that the tricellular tight junction is essential for water permeability in the tight epithelium, and it is tricellulin-dependent (Ayala-Torres et al., 2019).

4.1 Tricellulin

Tricellulin was discovered as a transmembrane tight junction protein that is preferentially located at contact sites where three adjacent cells meet (Ikenouchi et al., 2005). The mechanism, which leads to this tricellular arrangement and the role of this tight junction protein in water homeostasis is an important but understudied area. Here, a paracellular water permeation pathway made by the tTJ and regulated by its integral protein, known as tricellulin, was revealed.

Within the scope of this work, the analysis of the intestinal cell line HT-29/B6 (intermediate-tight epithelium) and the renal cell line MDCK C7 (tight epithelium) showed that this tight junction protein is higher expressed in HT-29/B6 than in MDCK C7 cells (Appendix A. Figure 7-1), which might have a large influence on the tTJ and its permeability properties. The above is also supported in bTJ and tTJ topological analysis (Appendix C. Table 7-5 and Figure 7-3), where it can be seen that the density of tTJ and the number of tTJ/cell is higher on HT-29/B6 than on MDCK C7 (control cells).

In this thesis, tricellulin was downregulated in those epithelial cell culture models, and depending on the level of expression, two knockdown clones were selected that showed the most significant reduction in tricellulin expression in both cell lines. Comparing the expression of tricellulin between the clones and the control cell lines showed that after

tricellulin downregulation, the expression level was comparable between MDCK C7 and HT-29/B6 cells (see Chapter 3.1.1 and 3.2.1).

4.1.1 Tricellulin knockdown alters the expression and localization of tight junction proteins in MDCK C7 and HT-29/B6 cells

It has been described that the knockdown of tricellulin influences the organization of tTJ as well as the localization of occludin at bTJ (Ikenouchi et al., 2005). Immunoblots and densitometric analysis demonstrated an apparent reduction of tricellulin expression in both cell lines (Figure 3-5 and 3-13). Nevertheless, the generated tricellulin knockdown clones compared with the controls showed clonal variation in other TJ proteins, which reached significance for occludin, claudin-1, claudin-4, and claudin-8 in MDCK C7 cells, and claudin-1, claudin-2, claudin-3, claudin-8, angulin-1, AQP-3, and AQP-4 in HT-29/B6 cells (Figure 3-5b and 3-13b). The clonal variation also concerns the two control clones in MDCK C7 cells; here, the differences are most prominent for claudin-1, claudin-5, and claudin-8. These claudins seem to have no effect on paracellular water transport, since the water transport of the two control clones did not show any difference (Ayala-Torres et al., 2019).

In the MDCK C7 tricellulin knockdown clones (see Chapter 3.1.2), considering the functional aspects of the variations, it can be said that occludin, which is downregulated only in one of the tricellulin knockdown clones, is assumed to have no effect on TJ barrier function, either genuinely or through compensation of its downregulation by other tight junction proteins (Saitou et al., 2000; Schulzke et al., 2005; Raleigh et al., 2010). In addition to occludin, all claudins present in MDCK C7 cells are known to behave as barrier formers, acting in concert, and compensating for their respective up- and downregulation (Günzel and Yu, 2013). Ion and water channel-forming claudins can be disregarded as they are not genuinely present in MDCK C7 cells. A reduced expression of claudin-4 and claudin-8 and an increased expression of claudin-1 were found in one of the knockdown clones. However, claudin-4 is described as dispensable for TJs' barrier properties in wild-type MDCK II cells (Tokuda et al., 2017).

Furthermore, claudin-1 and claudin-4 were shown to be dispensable for water barrier formation in human submerged keratinocyte cultures (Kirschner et al., 2013), and they are only related to the paracellular pore pathway (Otani et al., 2019). Therefore, we feel safe to conclude that the observed clonal variation of the claudins in sum is balanced and

provides a constant barrier function of the bTJ. Most importantly, the three angulins, as well as the aquaporins AQP-1, -3, and -4, did not change. Thus, the changes in ion, macromolecule, and water permeability found in the knockdown clones can be assumed to be exclusively due to the reduced tricellulin expression in the tTJ; nonetheless, changes in ion permeability could also be affected by the reduction in claudin-4 and -8.

In the case of HT-29/B6 cells (see Chapter 3.2.2), it is important to underline that the change in claudin-2 expression had no functional relevance because a change in Na⁺ permeability would be expected after elevated expression of junctional located claudin-2, which is known to form specific paracellular channels for small cations (Amasheh et al., 2002). Changes in claudin-2 expression in tricellulin KD clones were shown to be without functional relevance because of extrajunctional localization. Interestingly, after tricellulin knockdown, some tightening claudins were upregulated, contrary to MDCK C7 cells. Specifically, claudin-3 and -8 were upregulated. It has been reported that overexpression of claudin-3 in epithelial cells decreases the solute permeability increasing the TER significantly in comparison to the control cells (Coyne et al., 2003; Milatz et al., 2010). In addition, it has been suggested that claudin-8 forms the paracellular barrier to Na⁺ permeation when expressed in MDCK II cells (Yu et al., 2003), and also it is known that barrier improvement by claudin-8 is accompanied by a reduction of endogenous claudin-2 protein at the tight junction (Yu et al., 2003), in this thesis, perhaps the increase in claudin-8 offset the increase in claudin-2, reducing it in TJ, making it non-functional. Lastly, angulin-1 was upregulated in both knockdown clones; this could be due to a compensatory mechanism in the tTJ in response to the absence of tricellulin and also due to the fact that after tricellulin KD the tTJ density increases in the KD clones compared with the control (Appendix C. Table 7-5 and Figure 7-3).

4.1.2 Tricellulin knockdown increases the ion permeability in MDCK C7 and HT-29/B6 cells

Once the change in the protein profile has been analyzed, it is important to analyze the barrier properties (see Chapter 3.1.1.1 and 3.2.1.1). The reduction in tricellulin expression resulted in a lowered transepithelial resistance (TER) in both cell lines, which is in accordance with previous experiments on cell cultures (Krug, 2017; Krug et al., 2013; Krug et al., 2009a; Krug et al., 2018). Since tightening claudins were upregulated in HT-29/B6 knockdown clones, the observed decrease in TER could be attributed to the

absence of tricellulin from the tTJ. In contrast, downregulation of claudin-4 and -8 in MDCK C7 cells could intensify TER's effect after tricellulin knockdown. It is known that overexpression of claudin-4 has been reported to reduce the paracellular permeability specific to Na⁺, and claudin-8 has been suggested to form the paracellular barrier to Na⁺ permeation when expressed in MDCK II cells (Alexandre et al., 2005). Thus, the assumption that tricellulin expression is important for sealing function in HT-29/B6 and MDCK C7 cells could be confirmed (Ayala-Torres et al., 2019).

To describe this barrier in more detail, dilution potential measurements were performed to investigate the influence of ions with different charges (see Chapter 3.1.1.2 and 3.2.1.2). The dilution potential measurements showed an increase of the permeability for Na⁺ and Cl⁻ in the tricellulin knockdown clones. However, since the ratio of Na⁺ to Cl⁻ permeability remained unchanged, tricellulin increase the ion permeability without a change in charge selectivity in both cell lines. In HT-29/B6 knockdown clones, the upregulation of claudin-2 did not increase the PNa⁺/PCl⁻, therefore, it could be said that this increase has no functional relevance in the subsequent analyses, especially in the measurement of transepithelial water transport.

4.1.3 Tricellulin knockdown increases the macromolecule passage in MDCK C7 and HT-29/B6 cells

The present study confirmed that tricellulin plays an important role in regulating paracellular transport of macromolecules in different types of epithelia, and it is related to the content of tricellulin in the tTJ. The permeability to the paracellular marker 4-kDa dextran was increased by tricellulin knockdown in both cell lines as normally this protein is responsible for blocking the passage of macromolecules with diameters from 1.3 to 4.6 nm (0.9 to 10 kDa) (Krug et al., 2009a; Krug, 2017).

In the case of the tight epithelial cell line, it might be surprising that a moderate knockdown of tricellulin by 40% already leads to five times higher permeability for macromolecules (see Chapter 3.1.1.3). This is explained by the fact that normally the permeability for macromolecules is extremely low (in the order of 10⁻¹² cm/s), so that even a slight opening of a pathway for macromolecules causes a significant effect (Krug et al., 2017). Furthermore, the reduction by 30% (KD 23) had no significant effect on macromolecule permeability but ion permeability, indicating that there is already a

significant impairment of the tTJ barrier, which is only affecting small solutes, while 4-kDa dextran is still not able to pass. This leads to the assumption that the varying range of tricellulin expression may lead to different effects. The limit of macromolecule passage seems to range between 30% and 40% reduction of tricellulin, while for small solutes, the regulation is stricter (Ayala-Torres et al., 2019).

In the intermediate-tight epithelial cell line, HT-29/B6, downregulation of tricellulin increases the permeability of the KD clones between two and three times in comparison to their control (see Chapter 3.2.1.3). It is important to consider that this cell line is much less tight (sometimes classified as leaky epithelium), and thus the overall permeability is higher than in MDCK C7 cells. Also, after tricellulin knockdown, further tightening tight junction proteins were upregulated, which may affect the bicellular passage of macromolecules if this exists. Thus, the major way for macromolecules would be the tTJ.

Based on the rareness and the dimensions of tTJs compared with bTJs (Appendix C. Table 7-5 and Figure 7-3) and under the precaution that the dimensions of the central tube of the tTJ are only known roughly, we suggest that macromolecules cross the epithelial layers mainly along the central tube of the tTJ in both cell lines, with an important effect on the HT-29/B6 cells which had more tTJ/cell after the tricellulin KD. Therefore, the existence of narrow points inside the central tTJ tube postulated earlier (Staehelein, 1973), where it is speculated that tricellulin is inserted into the tTJ allowing the branching of TJ strands reducing the diameter of the central tube to a critical size for the passage of the macromolecule, is affected after tricellulin reduction, with greater effect on HT-29/B6, cells with higher TJ length and tTJ density (Appendix C. Table 7-5 and Figure 7-3).

4.1.4 Water transport as driven by different osmotic gradients

It has long been known that water can be transported via the transcellular route. The group of aquaporins that form transcellular water channels is significantly involved in this process (overview in (Gomes et al., 2009)). It was controversially discussed whether water is also transported via the paracellular pathway and to what extent tight junction proteins are involved in this process.

In other studies from this lab analyzing water permeability of claudin channels, mannitol was used for an osmotic gradient since this solute was impermeable and could not pass the claudin channels (Rosenthal et al., 2017a; Rosenthal et al., 2019; Rosenthal et al., 2017b; Rosenthal et al., 2010). In the present study, for the first time, this is different and more complicated. In the tricellulin KD clones, the tTJ central tube is opened, shown by the increased macromolecule permeability, and through this pathway, mannitol can diffuse following its concentration gradient. This has two consequences: First, in the course of the experiment, mannitol may be diluted, and its gradient is reduced. However, this will be below significance because the amount of mannitol in the 9 mL bath solution is high compared to the amount diffusing through the tTJ. Second and more disturbing, mannitol would diffuse through the central tube in opposite direction to the presumed water flux. As long as a molecule like mannitol is small compared to the diameter of the central tube, this may not have a large effect. Anyhow, because this mechanism may alter water transport rates at least slightly, the water permeability coefficients were not calculated in this study, and the data were presented as fluxes only (Ayala-Torres et al., 2019).

In order to investigate the side effect of mannitol diffusion, the data obtained with 100 mM mannitol were compared with those obtained with larger molecules, 37 mM 4-kDa and 5.5 mM 40-kDa dextran in MDCK C7 cells and 2.5 mM albumin instead of 5.5 mM 40-kDa dextran in HT-29/B6 cells (see Chapter 3.1.4 and 3.2.4). For this, dextran concentrations were chosen, which all produced an osmolality of 100 mOsm, as used for mannitol, except for 2.5 mM albumin which its osmolality was 40 mOsm. This resulted in lower nominal concentrations due to a known water-sequestering effect of some macromolecules (Rudan-Tasic and Klofutar, 2004). It turned out that gradients of 100 mM mannitol and 37 mM 4-kDa dextran produced comparable water fluxes and that an elevated 4-kDa dextran concentration (100 mM resulting in roughly 900 mOsm) led to higher water fluxes in both cell lines (see Appendix B. Table 7-1 and 7-2). Since these numbers satisfactorily fit together, this indicates the reliability of the methods used. Lastly, the amount of water flux induced by 4-kDa dextran was independent of the osmotic gradient direction, as seen with 37 mM of 4-kDa dextran, which was added either to the apical or the basolateral side of the cells. Water moved in the opposite direction, but the absolute values for water flux were nearly equal (Ayala-Torres et al., 2019).

The most valuable results should have been obtained with an osmotic gradient obtained by 5.5 mM 40-kDa dextran (measured osmolality 100 mOsm). Surprisingly, this was not the case in MDCK C7 cells: in the presence of 40-kDa dextran, water flux was reduced in the control clones as well as in the knockdown clones compared to water fluxes in the presence of mannitol with the same osmolality (Ayala-Torres et al., 2019). An induction of water flux by a gradient with 40-kDa dextran did not significantly change water fluxes in the KD 24 clone with the stronger tricellulin reduction, whereas KD 23 showed an increased water flux compared to the control clone (see Chapter 3.1.4). As an explanation for this effect, the sizes of the molecule should be related to that of the tTJ central tube. The hydrodynamic radius of the large carbohydrate 40-kDa dextran reportedly amounts 6.6 nm (Wen et al., 2013), while the diameter of the tTJ central tube was assumed to be 10 nm (Staehelin, 1973). We suggest that due to its molecular size, the 40-kDa dextran only barely fits through the central tube or even clogs its entrance so that water is hindered from passing. Thus, water flux was reduced in all clones compared to mannitol-induced fluxes. The strongest reduction was observed in the KD 24 clone with the lowest tricellulin expression and possibly the largest diameter of the tTJ central tube (Ayala-Torres et al., 2019). These assumptions are supported by the findings of Krug *et al.* that the tTJ central tube at low tricellulin levels allows for passage of molecules of 10 kDa but not of 20 kDa (Krug et al., 2009a). This reasoning finds its equivalent in experiments dealing with the bTJ, where a NaCl gradient was used to drive water flux through the claudin-15 channel. Under this condition, claudin-15-mediated water flux was inhibited by Na⁺ diffusion in the opposite direction (Rosenthal et al., 2019).

Interestingly, when albumin, a large protein molecule (3.8 nm in diameter and 15 nm long molecule (Tojo and Kinugasa, 2012)), was used to generate an osmotic gradient in HT-29/B6 cells, the water flux produced did not change in both tricellulin KD clones compared with their control. Therefore, this experiment confirmed that the osmotic gradient's chemical nature did not modify the water transport in HT-29/B6 cells.

4.1.5 Tricellulin knockdown increases transepithelial water transport only in MDCK C7 cells

For the full line of experiments in MDCK C7 cells, two tricellulin KD clones were selected, which differ in the grade of tricellulin reduction, namely by 30% (clone KD 23) and by 40% (clone KD 24) compared to the respective controls. While both KD clones caused a

decrease in TER, only KD 24 produced a slight increase in permeability to a 4-kDa macromolecule and, most importantly, increased water flux driven by different osmotic gradients as discussed above (see Chapter 3.1.4) (Ayala-Torres et al., 2019).

The question arises whether this is an all-or-nothing effect. If yes, one would postulate a threshold of tricellulin depression somewhere between 30% and 40%. In order to have a closer look, an additional experiment was performed employing a clone with tricellulin reduced by 35% (clone KD 22). Being aware that this is based on three points only, resulting water flux appeared to correlate with the tricellulin expression, suggesting that the effect of tricellulin KD depression is gradual, starting at the level found for the controls (Figure 4-1) (Ayala-Torres et al., 2019).

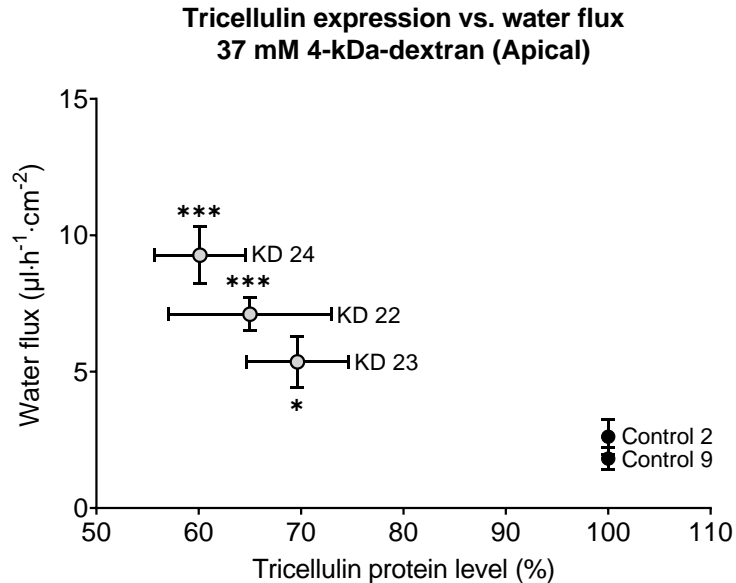


Figure 4-1. Water flux as a function of the level of tricellulin expression in MDCK C7 cells driven by an osmotic gradient of 37 mM 4-kDa dextran (100 mOsm). Tricellulin KD 22 (n=7) is an additional KD clone that was tested only for this purpose (shRNA 22: TRCN0000072635, NM_144724.1-989s1c1, Sigma-Aldrich, Schnellendorf, Germany) and compared with control 9. (* $P\leq 0.05$, *** $P\leq 0.001$).

In the same way, two tricellulin KD clones were selected in HT-29/B6 cells, which differ in the grade of tricellulin reduction, namely by 35% (clone KD 11) and by 44% (clone KD 17) compared to their control. While both KD clones caused a decrease in TER and an increase in permeability to a 4-kDa macromolecule, none of them increased the water flux driven by different osmotic gradients. Since claudin-2 is genuinely expressed in the HT-

29/B6 cells, a large water transport component may have traveled through the bTJ, and a possible contribution from the tTJ may not have reached significant levels (see Chapter 3.2.4). On the other hand, there may be a threshold in the expression of tricellulin, which must be overcome to find significant differences in water transport, which were not reached with the knockdowns generated in this research. In addition, there is a possibility that, in general, the paracellular water flux is lower than the transcellular water flux or that there is a claudin-2-independent paracellular pathway for water. Furthermore, the water movement may cause the accumulation of water between TJ strands because of differences in the water permeability between diffusion across TJ strands and diffusion through the paracellular space between strands (possible bleb formation between TJ strands under hyperosmolality) (Tokuda and Yu, 2019), and this water accumulation may serve as a trigger of cell responses, for example, by increasing the tightening of the intracellular space.

As an overall view, tricellulin is able to regulate osmotically-induced transepithelial water flux in MDCK C7 cells (tight epithelial cell line; for an overview, see Chapter 3.1). This regulation occurs reciprocally, i.e., lowered tricellulin expression causes higher water fluxes (Ayala-Torres et al., 2019). In contrast, the contribution of tTJ central tubes to transepithelial water permeability in HT-29/B6 cells (intermediate-tight epithelial cell line; for an overview, see Chapter 3.2) is neglected, even if maximally conductive. Our findings go hand in hand with what Krug and colleagues found in ulcerative colitis, and HT-29/B6 cells, where there was an increase in the passage of macromolecules caused, at least in part, by the downregulation of tricellulin (Krug et al., 2018). Besides, the role of claudin-2 in IBD has been linked to leak-flux diarrhea as claudin-2 increases permeability for small cations as well as for water, and with our results, it can be said that tricellulin does not have a relevant role in water permeability at the tTJ, which can be masked by claudin-2.

4.2 Angulin-1/LSR

Tricellulin and angulin family proteins, including angulin-1/LSR, angulin-2/ILDR1, and angulin-3/ILDR2, have been identified as molecular constituents of tTJs (Ikenouchi et al., 2005; Masuda et al., 2011; Higashi et al., 2013). Tricellulin and angulins localize along with the central sealing elements of tTJs (Masuda et al., 2011; Ikenouchi et al., 2005). Because angulins recruit tricellulin to TCs, the angulin-tricellulin axis is proposed to play crucial roles in tTJ formation. Angulin-1 may play broader physiologic roles to establish the water homeostasis in different organs, such as the intestine, the skin, lungs, or the kidney, like angulin-2/ILDR1. Here, a paracellular water permeation pathway made by the tTJ and regulated by its integral protein, known as angulin-1/LSR, was disclosed.

In a similar line of experiments conducted to study tricellulin and its role in paracellular water permeability, the intestinal cell line HT-29/B6 and the renal cell line MDCK C7 were investigated concerning angulin-1 expression. It was shown that this tight junction protein is expressed endogenously and in the same proportion in these two cell lines (Appendix A. Figure 7-2). Angulin-1 was removed in those epithelial cell culture models, and for each cell model, the two knockout clones that showed the maximum reduction in its expression were selected (see Chapter 3.3.1 and 3.4.1). The above is also supported in bTJ and tTJ topological analysis (Appendix C. Table 7-6 and Figure 7-4), where it can be seen that the density of tTJ is higher on HT-29/B6 than on MDCK C7 (control cells), nevertheless, the number of tTJ/cell is the same in both cell lines.

4.2.1 Angulin-1 knockout alters the expression and localization of other proteins in MDCK C7 and HT-29/B6 cells

As KD experiments only reduce protein expression, it is not surprising that the null protein phenotypes generated by genome editing yield more severe phenotypes. The expression of several tightening claudins in MDCK C7 cells was reduced in angulin-1 knockout cells, suggesting these claudins were partly removed from the TJ strands in the absence of angulin-1; in contrast, claudins and tricellulin expression were increased after angulin-1 knockout in HT-29/B6 cells, suggesting these claudins were additionally incorporated into TJ strands in the absence of angulin-1. Most importantly, in both angulin-1 KO cell lines, tricellulin was partly removed from the tTJ and detectable in the bTJ as seen before in other cell lines (Masuda et al., 2011).

On one side, angulin-1 knockout in MDCK C7 cells induced a decrease in occludin expression, claudin-1, and -4 (see Chapter 3.3.2). This might affect the barrier function and formation as evidenced by Kirschner *et al.* through different knockdowns of claudin-1 and -4, occludin, and ZO-1 causing increased paracellular permeability for ions and larger molecules (Kirschner *et al.*, 2013). Furthermore, the absence of occludin and claudin-1 in both KO clones prevents the specific localization of tricellulin at tricellular contacts and promotes its localization at bTJ (Ikenouchi *et al.*, 2008; Nakatsu *et al.*, 2019). These observations suggested that the proteins functionally influence each other.

On the other side, angulin-1 knockout in HT-29/B6 cells increased the expression of barrier-forming claudins (Nakatsu *et al.*, 2019) and tricellulin (see Chapter 3.4.2). Therefore, it can be concluded that the observed clonal variation of the claudins and tricellulin in sum is balanced and provides a constant barrier function of the bTJ and tTJ. These results suggested that the effects of angulin-1 and tricellulin relocation from tTJs to bTJs on epithelial barrier function are controversial (Nakatsu *et al.*, 2019). Interestingly, claudin-2 was downregulated in the KO 12 clone and upregulated in the KO 32 clone and appeared not to affect the water permeability. In relation to transcellular water transport, the major aquaporins of the human colon cell line, AQP-1, -3, and AQP-7, were found unchanged or downregulated as in the case of AQP-4; this suggests that an increase in transepithelial water permeability could be attributed to changes in the paracellular pathway generated by the removal of angulin-1 and unlikely due to AQP-4 (Kirschner *et al.*, 2013). Lastly, the expression of LI-cadherin was increased in both KO clones, and this could be important because if LI-cadherin is reduced, water transport from the luminal to the basolateral side could be impaired and even reversed in the case of hypertonic conditions without affecting the tight junctions and therefore not affecting the transport of other molecules (Weth *et al.*, 2017). LI-cadherin might be necessary for water reabsorption of the gut at intraluminal hypertonic conditions by keeping the intercellular cleft narrow and thus preserving a high osmotic gradient driving the water transport (Weth *et al.*, 2017). Thus, the increased LI-cadherin in the KO clones seems to have no effect on transepithelial water flux.

A rather interesting result is that the expression of angulin-2 and -3 did not change after the knockout of angulin-1 as a form of compensation in both cell lines. In this sense, one

might think that just like angulin-1, which is located in bTJ and tTJ (see Chapter 3.3.1 and 3.4.1), these other two angulin proteins could also be located in both TJ, and after the knockout, they simply changed their location from bTJ to tTJ to try to stabilize these junctions without changing their expression levels. However, this is only a hypothesis since antibodies for immunostaining do not work properly. In this same sense of ideas, this result contradicts what has been found in the organ of Corti: normally angulin-1 is not expressed in the organ of Corti; however, its expression is seen when angulin-2 is deficient, and tricellulin is recruited to the tTJ as a result. This clearly demonstrates that compensatory functions exist between the angulin family members. However, the organ of Corti is degenerated even when tricellulin was localized at the tTJ by angulin-1, indicating that there are also functional differences between the angulin family members (Higashi et al., 2015). Recently, Hempstock *et al.* also showed that angulin-1/LSR compensates for the loss of angulin-2/ILDR1 and maintains the epithelia's barrier and function in the large intestine as well as the kidney (Hempstock et al., 2020).

4.2.2 Angulin-1 knockout did not alter the ultrastructure of the bicellular tight junction in MDCK C7 and HT-29/B6 cells

The loss of tricellulin by RNAi led to an unstable ultrastructure of the tight junction, which ultimately caused the junctional complex to collapse completely (Ikenouchi et al., 2005). In both cell lines investigated in this study, the loss of angulin-1 did not modify or alter the bicellular tight junction. Compared to the vector control clones, the number of strands, the network depth, the frequency of strand breaks >20 nm, the continuous-type structures, and the linear strands remains unchanged after angulin-1 knockout in MDCK C7 and HT-29/B6 cells (see Chapter 3.3.4 and 3.4.4).

In the case of HT-29/B6 cells, a similar correlation between strand linearity and paracellular resistance was found in the human colon to be induced by a strong upregulation of claudin-2 in Crohn's disease (Zeissig et al., 2007; Zeissig et al., 2004). It is established that, depending on the presence of claudin-2, strand discontinuities appear or disappear (Furuse et al., 1999). In our study, no discontinuities appear even if claudin-2 is increased in the angulin-1 KO 36 clone, apparently due to tricellulin upregulation. Breaks per se, as rare as found here, may not play a significant role in permeability. In contrast, the angulin-1 knockout did not change the continuous-type strands in the entire meshwork and thus may indeed be related to the observed increase in permeabilities only

due to the tTJ. It is unclear yet, whether strand linearity is a direct determinant of permeability or if it represents an epiphenomenon of an altered composition of proteins within the TJ.

Thus, an increase in ion permeability in both cell lines and an increase in macromolecule permeability in HT-29/B6 cells could be caused by the opening of the tTJ because the only difference between the controls and the angulin-1 KO clones was the width of the central pore. However, the morphometric parameters could not be analyzed because of the low abundance of the same structures in both cell lines. After considering all possibilities, it is concluded that the knockout of angulin-1 did not induce considerable changes in the ultrastructure of bicellular and tricellular tight junctions that could affect water transport.

4.2.3 Angulin-1 knockout increases the ion permeability in MDCK C7 and HT-29/B6 cells

After transfection of both cell lines with CRISPR/Cas9 and sgRNA targeting angulin-1 to eliminate its expression and localization in tTJ, the pore pathway was addressed (see Chapter 3.3.1.1 and 3.4.1.1). Similar to what was observed in tricellulin knockdown cells, the reduction in the expression of angulin-1 resulted in a lowered transepithelial resistance (TER). It is important to note that in MDCK C7 cells, the removal of angulin-1 resulted in reducing the expression of most claudins, while in HT-29/B6, the effect was the opposite. Therefore, it could be said that the reduction in TER on HT-29/B6 cells is due only to the reduction in angulin-1; however, in MDCK C7 cells, the effect could be intensified due to the downregulation of other tightening TJ proteins. It is known that overexpression of claudin-7 resulted in a decrease in the paracellular conductance to Cl⁻ as well as a simultaneous increase in the paracellular conductance to Na⁺ in LLC-PK1 cells (Alexandre et al., 2005). Likewise, it was described that claudin-7 and -8 must interact with each other to regulate the overall paracellular permeability to Na⁺ and Cl⁻ under the normal physiological condition (Alexandre et al., 2005). To conclude, the decrease of angulin-1 within the tTJ also leads to a drop in paracellular resistance which reflects reciprocally the permeability for ions in both cell lines.

4.2.4 Angulin-1 knockout increases the macromolecule permeability only in HT-29/B6 cells

As it is known, knockdown of angulin-1 in the mouse mammary gland Eph4 epithelial cells significantly increased the permeability of macromolecules between 300-Da and 40-kDa (Higashi et al., 2013). Considering the above, the leak pathway was assessed (see Chapter 3.3.1.1 and 3.4.1.1). The present data showed that in an intermediate-tight epithelial cell line, HT-29/B6, a removal of angulin-1 strongly regulates the permeability for 4-kDa macromolecules. Nevertheless, it might be surprising that the same phenotype in MDCK C7 cells only slightly increased macromolecules' permeability in one of the KO clones (KO 18). Considering that HT-29/B6 is an intermediate-tight epithelial cell line and that its tTJ contributes at least 38% to the total paracellular conductance, it can be said that not only did it affect the paracellular passage of the small solutes, including inorganic ions, but also the macromolecules (Krug, 2017). However, the contribution of tTJ in MDCK C7 cells is not yet known, but it would be higher than in HT-29/B6 cells because this cell line is highly tight and, therefore, permeability to FD4 would be higher after angulin-1 knockout (Krug, 2017). This was not the case, perhaps because tricellulin also has an affinity for claudin-based TJ strands within the plasma membrane if it is not directed to tricellular contacts by the angulins (Krug et al., 2017), which could stabilize the tTJ after removal of angulin-1. In addition to the above, occludin was concentrated in the TJ corner after the angulin-1 KO, thus compensating for the partial tricellulin shift. Therefore, one could assume that due to the redistribution of tricellulin into the bTJ, a slight enhancement of bTJ barrier properties against ions could occur (Krug et al., 2017). Finally, according to the estimated topological parameters (Appendix C. Table 7-6 and Figure 7-4), both cell lines had the same number of tTJ/cell; however, the density of tTJ in HT-29/B6 was higher; therefore, a reduction in the expression of angulin-1 would be represented by a strong increase in permeability to macromolecules, in contrast to what was observed in MDCK C7 cells, where the permeability to macromolecules remained almost constant (angulin-1 KO 18 increase but only with respect to control 14, not a generalized behavior as in HT-29/B6 cells).

Additionally, the permeability to FD4 was measured in two different conditions after angulin-1 KO, and as can be seen, in MDCK C7 cells, there are no differences between isosmotic and osmotic conditions (Figure 4-2a). Conversely, in HT-29/B6 cells, it is observed that the permeability to FD4 is higher under isosmotic conditions than under an

osmotic gradient. A possible explanation for this might be that the movement of water in the opposite direction under osmotic conditions inhibits the movement of 4-kDa FITC-dextran, and therefore, a lower permeability was measured (Figure 4-2b). This movement through the tTJ is too small to be detected in the overall transepithelial water flux measured in HT-29/B6 cells.

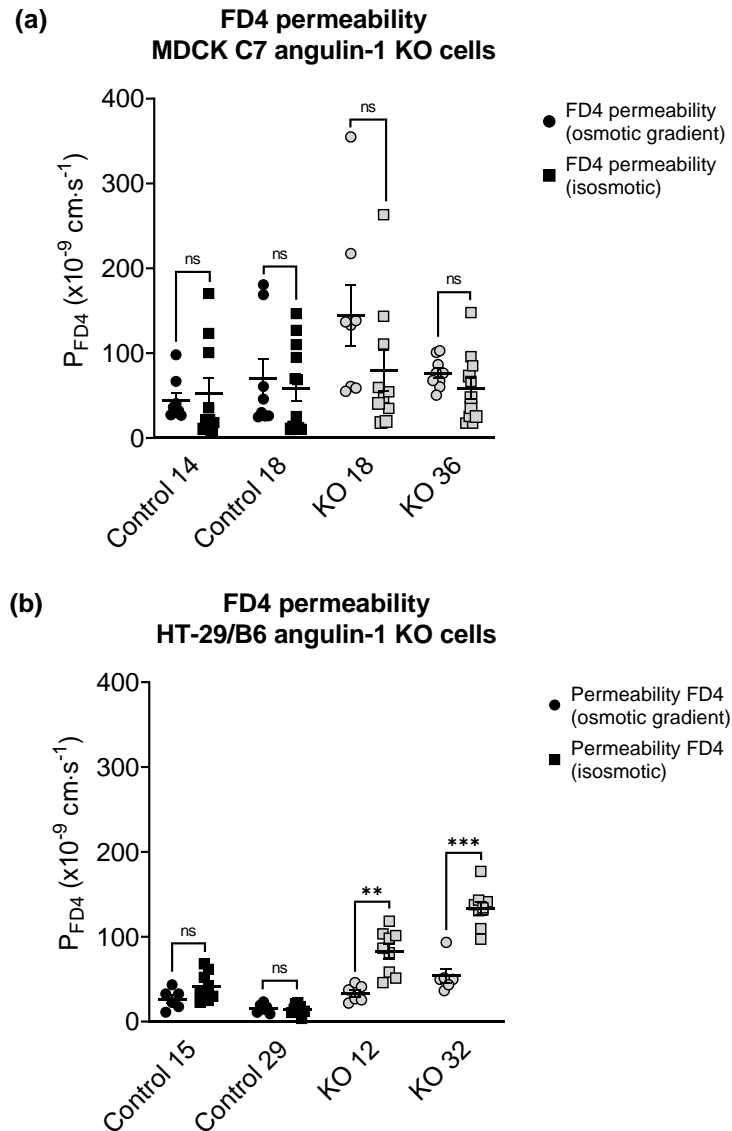


Figure 4-2. Comparison of angulin-1 knockout effect on permeability for 4-kDa FITC-dextran (FD4) under isosmotic and osmotic gradient conditions in (a) MDCK C7 and (b) HT-29/B6 cells. The FD4 permeability was higher under an isosmotic condition than under an osmotic gradient in HT-29/B6 cells, which could indicate an interaction between the movement of water in the opposite direction the movement of dextran in the tTJ. In contrast, no changes were observed in angulin-1 KO MDCK C7 cells. (ns: not significant, ** $P \leq 0.01$, *** $P \leq 0.001$).

4.2.5 Angulin-1 knockout increases transepithelial water transport only in MDCK C7 cells

To complete the tTJ permeability picture, the transepithelial water transport was measured in the angulin-1 KO clones of MDCK C7 and HT-29/B6 cells. As described earlier, while the KO clones caused a decrease in TER in both cell lines, only in HT-29/B6 cells angulin-1 KO increased the permeability to a 4-kDa macromolecule. Interestingly, the angulin-1 KO did not increase the water flux driven by 100 mM mannitol in both cell lines (see Chapter 3.3.5 and 3.4.5), and the total amount of water was independent of the direction of the osmotic gradient. The decision to use 4-kDa dextran was taken due to the dispersion of the values found in MDCK C7 cells when mannitol was used as an osmotic gradient; however, the values obtained with HT-29/B6 cells were more reproducible, and therefore, their study with 4-kDa dextran was obviated. As a result, the water flux increased in the angulin-1 KO clones compare with their controls in MDCK C7 cells when 37 mM 4-kDa dextran was used as an osmotic gradient.

Remarkably, in the case of MDCK C7 cells, an increase in water transport was expected similar to that found after reducing the expression of tricellulin in tTJ (see Chapter 4.1); however, this was not the case when mannitol was used, possibly due to the small diameter of this molecule with respect to the 4-kDa dextran which would facilitate its movement through tTJ reducing its osmotic strength; nevertheless, the osmolality of each solution was measured after the 2-hour experiment, and the values did not differ from the values of the original solutions. It is important to keep in mind that the reduction in the expression of most barrier-forming claudins could influence water transport after angulin-1 KO in MDCK C7 cells. As demonstrated by immunofluorescence confocal laser-scanning microscopy, tricellulin was redistributed from tTJ to bTJ, which could maintain and strengthen the epithelial barrier after the downregulation of several claudins. It should be noted that even a relatively small amount of residual angulin-1 can support the tTJ structure and function to a significant extent and that it masks some phenotypes, for instance, the paracellular water transport mediated by tricellulin. Finally, if we analyze in more detail the preliminary results obtained with the angulin-1 KO 8 (see chapter 3.3.5) which showed a reduction in tricellulin expression of 25% and increased transcellular water transport using mannitol and 4-kDa dextran (Figure 3-24a) compared to its control

8, it can be said that tricellulin is the main protein in tTJ that modulates water transport, in this case through an indirect regulation mediated by angulin-1.

This phenomenon was also observed in HT-29/B6 cells; however, here, the regulation of the tight junction protein expression was the opposite to what we observe in MDCK C7 cells; several claudins were upregulated; nevertheless, no change in water transport could be measured, so that tTJ in intermediate-tight epithelium does not contribute significantly to transepithelial water transport.

In summary, the present study suggests a functional difference between angulin-2/ILDR1 (Hempstock et al., 2020; Gong et al., 2017) and angulin-1/LSR on the paracellular water transport through the tTJs, always taking into account that all experiments were performed in different systems and under different conditions; however, this is an interesting issue for the understanding of tTJ variations. The effects of angulin-1 knockout on the epithelial barrier function of the mammalian epithelial cell sheet vary by cell type and according to the interdependence between different TJ species affecting cell expression, localization, and renewal (For an overview, see Chapters 3.3 and 3.4). The reason could be the differences in angulin-1 interaction partners in bTJs and tTJ. This hypothesis is supported by studies that bTJs and tTJs in each tissue comprise tissue-specific combinations of proteins and that angulin-1 interacts with specific proteins (e.g., occludin) but not others (e.g., MarvelD3) (Higashi et al., 2013; Nakatsu et al., 2019). Therefore, combinations of proteins influenced by angulin-1 knockout in bTJs and tTJ vary by cell type and tissue, and the resulting epithelial barrier function of the mammalian epithelial cell sheet causes cell-specific changes.

Together, our study provides a mechanism of how cells transport water and shows how such a mechanism may be exploited as a therapeutic approach to maintain water homeostasis, specifically in tight epithelium. We disclose a paracellular water permeation pathway made by the tricellular tight junction and regulated by its integral proteins, known as tricellulin and angulin-1. The importance of paracellular water permeability was demonstrated here, supporting the previous results found with angulin-2 and its potential role in causing urinary concentration defects in the kidney (Gong et al., 2017). These proteins may play broader physiologic and pathophysiologic roles to establish the water homeostasis in other organs, such as the skin, lungs, and the intestine. For instance,

though the intestinal barrier is impaired in both Crohn's disease (CD) and Ulcerative colitis (UC), it is known that tricellulin is downregulated in UC but not in CD. However, the predominant localization of tricellulin was shifted toward the surface epithelium in CD, which might indicate that changes in proteins that regulate the correct localization of tricellulin occur in CD, for example, angulin-1 or -2 (Krug et al., 2018). Thus, regulation of tricellulin depends also on other tTJ proteins as described in this thesis, where it is believed that the increase in water transport after angulin-1 KO was possibly due to a partial displacement of tricellulin from tTJ.

5. Conclusion and outlook

The major goal of this research was to clarify whether or not the expression of the tricellular tight junction (tTJ) proteins, tricellulin and angulin-1, is involved in controlling paracellular water transport in cell lines with different level of tightness (HT-29/B6 and MDCK C7 cells). This work supports the previous assumption that tTJs function differentially in distinct epithelial cell lines (Krug, 2017; Krug et al., 2009a; Krug et al., 2009b; Gong et al., 2017; Hempstock et al., 2020; Sugawara et al., 2020). Differences in TJ protein expression of the two cell lines were revealed after tricellulin knockdown and angulin-1 knockout. Likewise, members of the claudin and TAMP family were shown to compensate for each other in expression. It appears that tricellulin or angulin-1 are not the sole determinants of TJ integrity under normal or pathological conditions and that tTJ central tubes may have different permeability depending on the cell line or tissue being analyzed.

In HT-29/B6 cells, representing an intermediate-tight epithelium, tricellulin KD or angulin-1 KO do not significantly alter transepithelial water transport possibly due to: (1) a high contribution of other water-conducting proteins as claudin-2 or SGLT1, (2) or a low contribution of tTJ to transepithelial water transport which is easily masked by paracellular (bTJs) and transcellular water transport. Nevertheless, the tricellulin KD and the angulin-1 KO increase the ion and 4-kDa macromolecule permeability, which means that these proteins can seal off the tTJ and regulate the passage of ions and larger solutes but not water at this point (Figure 5-1 and 5-3). One could say that the existence of a physical pore does not guarantee water permeability, and the electrostatic and steric environment created by the pore-lining residues dictates the water, ion, and macromolecule permeability (Irudayanathan and Nangia, 2020).

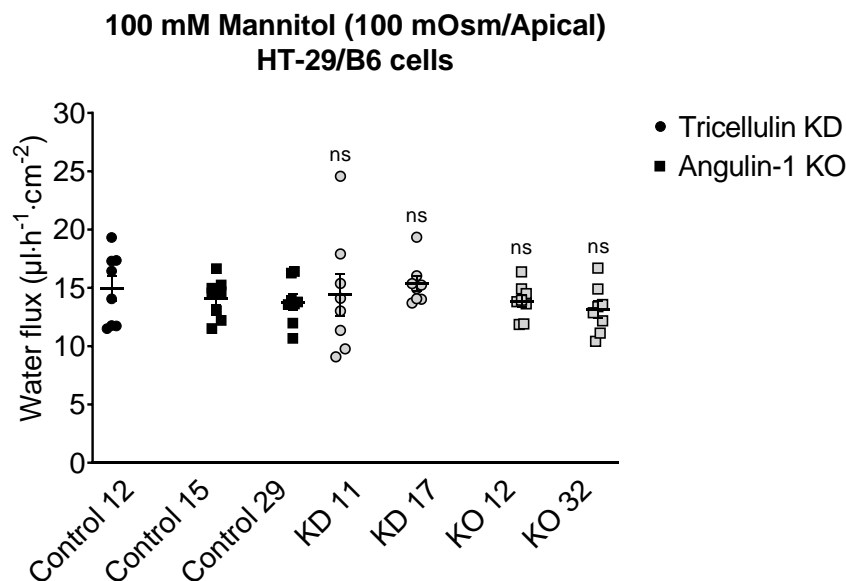


Figure 5-1. Synopsis of tricellulin and angulin-1 effects on osmotically driven water transport in HT-29/B6 cells. Both do not significantly affect the transepithelial water flux in these cells. As a tentative explanation, the transcellular and bTJ pathways of these cells are reasonably permeable, which may cover small changes produced by these two proteins in the tTJ. (ns: not significant).

In contrast, in MDCK C7 cells, which lack the water and cation-channel claudin-2, the transepithelial water transport increases after tricellulin knockdown and angulin-1 knockout and it is controlled by tricellulin expression level and localization. Thus, the contribution of the tTJ to transepithelial water transport depends on the tightness of the epithelium. It could be said that in tight cell lines without claudin-2 and other channel-forming claudins, tricellulin is able to regulate paracellular water permeability through tTJ (Figure 5-2 and 5-3). It should be noted that in the MDCK C7 cell line tricellulin KD and angulin-1 KO increased the ion permeability; nevertheless, the 4-kDa macromolecule permeability increased only slightly in a KO clone with respect to a single control under an osmotic gradient condition, so it could be said that it is not a uniform trend, evidencing once again that permeability at the tTJ depends on the different interactions between tTJ proteins.

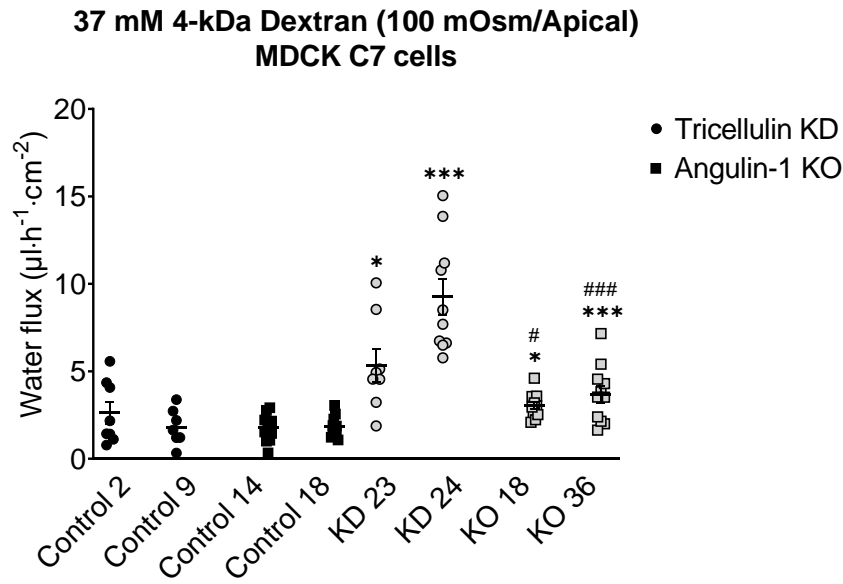


Figure 5-2. Synopsis of tricellulin and angulin-1 on osmotically driven water flux in MDCK C7 cells. Each of them alters the transepithelial water flux (higher water fluxes in the tricellulin KD and angulin-1 KO clones compared to the control clones). As a tentative explanation, the transcellular and bTJ pathways of these cells are of minor permeability, so that changes produced by these two proteins in the tTJ become statistically significant. Tricellulin KD: * $P \leq 0.05$, *** $P \leq 0.001$ with regard to control 2 and 9; Angulin-1 KO: * $P \leq 0.05$, *** $P \leq 0.001$ with regard to control 14 and # $P \leq 0.05$, ### $P \leq 0.001$ with regard to control 18.

Likely, the paracellular transport regulation by the osmolality in each epithelial cell type has respective physiological significance dependent on their organs. Further analysis of the effects of osmolality on the paracellular transport in various cultured cells and animals is required to elucidate the mechanisms and physiological significance of this phenomenon in the transport of water and macromolecules (Tokuda et al., 2016; Tokuda and Yu, 2019). To better understand the implications of these results, future studies could address to experimentally clarify whether (1) the complete removal of tricellulin (KO cells) generates an even stronger increase in water transport (without affecting the integrity of the TJ) than what we found in the present thesis, (2) angulin-3 mediates a direct effect on water permeability independent of tricellulin like angulin-2 in the kidney (Gong et al., 2017), (3) angulin-3 acts indirectly via tricellulin regulation like was demonstrated for angulin-1 in the present research, or (4) angulin-3 has no effect on water permeability like angulin-2 in the intestine (Hempstock et al., 2020).

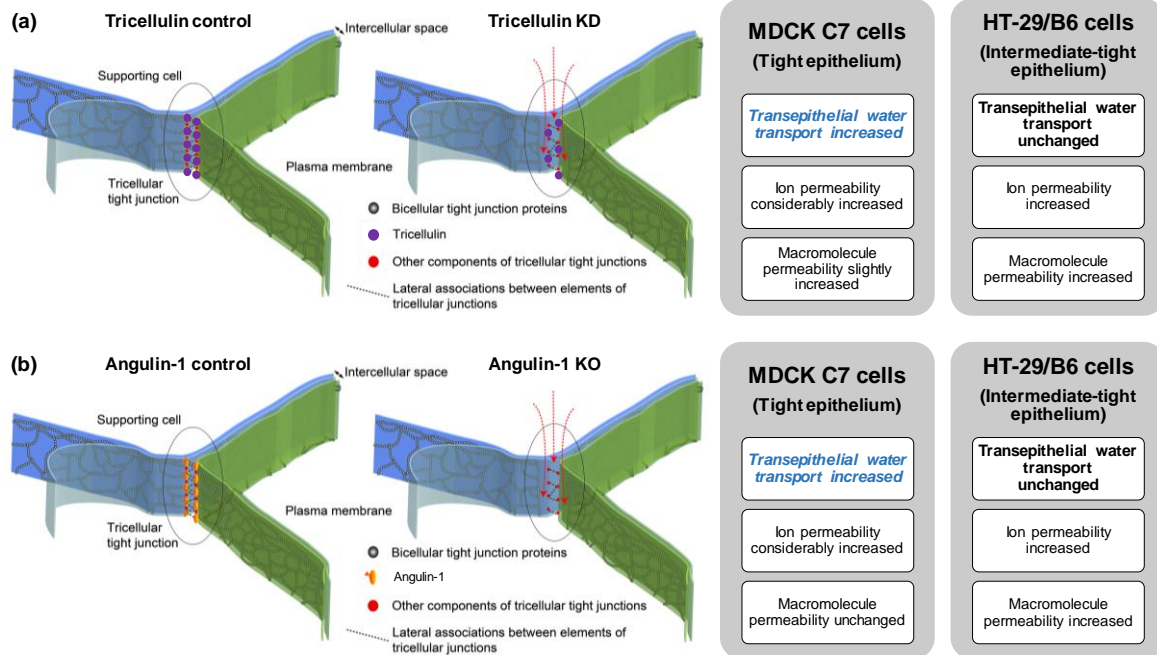


Figure 5-3. Summarizing scheme of water, ion, and macromolecule passage via the tricellular tight junction on epithelial cell lines with different tightness. **(a) Tricellulin effect.** In a tight epithelial cell line (MDCK C7 cells), a partial reduction of tricellulin increased the transepthelial water transport, macromolecule permeability, and ion permeability. In contrast, in an intermediate-tight epithelial cell line (HT-29/B6 cells), the transepthelial water transport was unchanged; nevertheless, the macromolecule permeability and the ion permeability increased. **(b) Angulin-1 effect.** In a tight epithelial cell line (MDCK C7 cells), a complete reduction of angulin-1 increased the transepthelial water transport and slightly increased the macromolecule permeability; nevertheless, the ion permeability was highly increased. Tricellulin levels remained the same; however, its location changed from tTJ to bTJ, which possibly caused the increase in water permeability (this was partially corroborated by the angulin-1 KO clone with a 25% reduction in tricellulin expression, which showed an increase in water flux after an osmotic gradient with mannitol and 4-kDa dextran). Similar to what happened after tricellulin KD, in an intermediate-tight epithelial cell line (HT-29/B6 cells), the transepthelial water transport was unchanged; nevertheless, an increase in the macromolecule and ion permeability was observed. Tricellulin levels increased after the KO, and additionally, its location was also observed in bTJ. (It was adapted from (Nayak et al., 2013)).

6. References

- ADELMAN, J. L., SHENG, Y., CHOE, S., ABRAMSON, J., WRIGHT, E. M., ROSENBERG, J. M. & GRABE, M. **2014**. Structural Determinants of Water Permeation through the Sodium-Galactose Transporter vSGLT. *Biophysical Journal*, 106, 1280-1289.
- ALEXANDRE, M. D., LU, Q. & CHEN, Y. H. **2005**. Overexpression of claudin-7 decreases the paracellular Cl⁻ conductance and increases the paracellular Na⁺ conductance in LLC-PK1 cells. *J Cell Sci*, 118, 2683-93.
- AMASHEH, S., MEIRI, N., GITTER, A. H., SCHONEBERG, T., MANKERTZ, J., SCHULZKE, J. D. & FROMM, M. **2002**. Claudin-2 expression induces cation-selective channels in tight junctions of epithelial cells. *J Cell Sci*, 115, 4969-76.
- ANDERSON, J. M. & VAN ITALLIE, C. M. **2009**. Physiology and function of the tight junction. *Cold Spring Harb Perspect Biol*, 1, a002584.
- AYALA-TORRES, C., KRUG, S. M., SCHULZKE, J. D., ROSENTHAL, R. & FROMM, M. **2019**. Tricellulin Effect on Paracellular Water Transport. *Int J Mol Sci*, 20.
- BEUTEL, O., MARASPINI, R., POMBO-GARCIA, K., MARTIN-LEMAITRE, C. & HONIGMANN, A. **2019**. Phase Separation of Zonula Occludens Proteins Drives Formation of Tight Junctions. *Cell*, 179, 923-936 e11.
- BUCKLEY, A. & TURNER, J. R. **2018**. Cell Biology of Tight Junction Barrier Regulation and Mucosal Disease. *Cold Spring Harb Perspect Biol*, 10.
- BUSCHMANN, M. M., SHEN, L., RAJAPAKSE, H., RALEIGH, D. R., WANG, Y., WANG, Y., LINGARAJU, A., ZHA, J., ABBOTT, E., MCAULEY, E. M., BRESKIN, L. A., WU, L., ANDERSON, K., TURNER, J. R. & WEBER, C. R. **2013**. Occludin OCEL-domain interactions are required for maintenance and regulation of the tight junction barrier to macromolecular flux. *Mol Biol Cell*, 24, 3056-68.
- CHELAKKOT, C., GHIM, J. & RYU, S. H. **2018**. Mechanisms regulating intestinal barrier integrity and its pathological implications. *Exp Mol Med*, 50, 103.
- COLEGIO, O. R., VAN ITALLIE, C., RAHNER, C. & ANDERSON, J. M. **2003**. Claudin extracellular domains determine paracellular charge selectivity and resistance but not tight junction fibril architecture. *American Journal of Physiology-Cell Physiology*, 284, C1346-C1354.
- COLEGIO, O. R., VAN ITALLIE, C. M., MCCREA, H. J., RAHNER, C. & ANDERSON, J. M. **2002**. Claudins create charge-selective channels in the paracellular pathway between epithelial cells. *American Journal of Physiology-Cell Physiology*, 283, C142-C147.
- CORDING, J., BERG, J., KADING, N., BELLMANN, C., TSCHEIK, C., WESTPHAL, J. K., MILATZ, S., GÜNZEL, D., WOLBURG, H., PIONTEK, J., HUBER, O. & BLASIG, I. E. **2013**. In tight junctions, claudins regulate the interactions between occludin, tricellulin and marvelD3, which, inversely, modulate claudin oligomerization. *J Cell Sci*, 126, 554-64.
- CORDING, J., GUNTHER, R., VIGOLO, E., TSCHEIK, C., WINKLER, L., SCHLATTNER, I., LORENZ, D., HASELOFF, R. F., SCHMIDT-OTT, K. M., WOLBURG, H. & BLASIG, I. E. **2015**. Redox Regulation of Cell Contacts by Tricellulin and Occludin: Redox-Sensitive Cysteine Sites in Tricellulin Regulate Both Tri- and Bicellular Junctions in Tissue Barriers as Shown in Hypoxia and Ischemia. *Antioxid Redox Signal*, 23, 1035-49.

- COYNE, C. B., GAMBLING, T. M., BOUCHER, R. C., CARSON, J. L. & JOHNSON, L. G. **2003**. Role of claudin interactions in airway tight junctional permeability. *Am J Physiol Lung Cell Mol Physiol*, 285, L1166-78.
- DAY, R. E., KITCHEN, P., OWEN, D. S., BLAND, C., MARSHALL, L., CONNER, A. C., BILL, R. M. & CONNER, M. T. **2014**. Human aquaporins: regulators of transcellular water flow. *Biochim Biophys Acta*, 1840, 1492-506.
- DIAMOND, J. M. **1974**. Tight and leaky junctions of epithelia: a perspective on kisses in the dark. *Fed Proc*, 33, 2220-4.
- FISCHBARG, J. **2010**. Fluid transport across leaky epithelia: central role of the tight junction and supporting role of aquaporins. *Physiol Rev*, 90, 1271-90.
- FRIEND, D. S. & GILULA, N. B. **1972**. Variations in tight and gap junctions in mammalian tissues. *J Cell Biol*, 53, 758-76.
- FURUSE, M., HIRASE, T., ITOH, M., NAGAFUCHI, A., YONEMURA, S., TSUKITA, S. & TSUKITA, S. **1993**. Occludin - a Novel Integral Membrane-Protein Localizing at Tight Junctions. *Journal of Cell Biology*, 123, 1777-1788.
- FURUSE, M., SASAKI, H. & TSUKITA, S. **1999**. Manner of interaction of heterogeneous claudin species within and between tight junction strands. *Journal of Cell Biology*, 147, 891-903.
- GARCIA-PONCE, A., CITALAN-MADRID, A. F., VELAZQUEZ-AVILA, M., VARGAS-ROBLES, H. & SCHNOOR, M. **2015**. The role of actin-binding proteins in the control of endothelial barrier integrity. *Thromb Haemost*, 113, 20-36.
- GOMES, D., AGASSE, A., THIEBAUD, P., DELROT, S., GEROS, H. & CHAUMONT, F. **2009**. Aquaporins are multifunctional water and solute transporters highly divergent in living organisms. *Biochim Biophys Acta*, 1788, 1213-28.
- GONG, Y., HIMMERKUS, N., SUNQ, A., MILATZ, S., MERKEL, C., BLEICH, M. & HOU, J. **2017**. ILDR1 is important for paracellular water transport and urine concentration mechanism. *Proc Natl Acad Sci U S A*, 114, 5271-5276.
- GÜNZEL, D. & FROMM, M. **2012**. Claudins and other tight junction proteins. *Compr Physiol*, 2, 1819-52.
- GÜNZEL, D. & YU, A. S. **2013**. Claudins and the modulation of tight junction permeability. *Physiol Rev*, 93, 525-69.
- HE, J. & YANG, B. **2019**. Aquaporins in Renal Diseases. *Int J Mol Sci*, 20.
- HEINEMANN, U. & SCHUETZ, A. **2019**. Structural Features of Tight-Junction Proteins. *Int J Mol Sci*, 20.
- HEMPSTOCK, W., SUGIOKA, S., ISHIZUKA, N., SUGAWARA, T., FURUSE, M. & HAYASHI, H. **2020**. Angulin-2/ILDR1, a tricellular tight junction protein, does not affect water transport in the mouse large intestine. *Sci Rep*, 10, 10374.
- HIGASHI, T., KATSUNO, T., KITAJIRI, S. & FURUSE, M. **2015**. Deficiency of angulin-2/ILDR1, a tricellular tight junction-associated membrane protein, causes deafness with cochlear hair cell degeneration in mice. *PLoS One*, 10, e0120674.
- HIGASHI, T. & MILLER, A. L. **2017**. Tricellular junctions: how to build junctions at the TRICKiest points of epithelial cells. *Mol Biol Cell*, 28, 2023-2034.
- HIGASHI, T., TOKUDA, S., KITAJIRI, S., MASUDA, S., NAKAMURA, H., ODA, Y. & FURUSE, M. **2013**. Analysis of the 'angulin' proteins LSR, ILDR1 and ILDR2--tricellulin recruitment, epithelial barrier function and implication in deafness pathogenesis. *J Cell Sci*, 126, 966-77.
- HU, Y. J., WANG, Y. D., TAN, F. Q. & YANG, W. X. **2013**. Regulation of paracellular permeability: factors and mechanisms. *Mol Biol Rep*, 40, 6123-42.

- HUANG, B., WANG, H. & YANG, B. **2017**. Water Transport Mediated by Other Membrane Proteins. *Adv Exp Med Biol*, 969, 251-261.
- IKENOUCI, J., FURUSE, M., FURUSE, K., SASAKI, H., TSUKITA, S. & TSUKITA, S. **2005**. Tricellulin constitutes a novel barrier at tricellular contacts of epithelial cells. *J Cell Biol*, 171, 939-45.
- IKENOUCI, J., SASAKI, H., TSUKITA, S., FURUSE, M. & TSUKITA, S. **2008**. Loss of occludin affects tricellular localization of tricellulin. *Mol Biol Cell*, 19, 4687-93.
- INAI, T., KOBAYASHI, J. & SHIBATA, Y. **1999**. Claudin-1 contributes to the epithelial barrier function in MDCK cells. *Eur J Cell Biol*, 78, 849-55.
- IRUDAYANATHAN, F. J. & NANGIA, S. **2020**. Paracellular Gatekeeping: What Does It Take for an Ion to Pass Through a Tight Junction Pore? *Langmuir*, 36, 6757-6764.
- IVANOV, A. I. & NAYDENOV, N. G. **2013**. Dynamics and regulation of epithelial adherens junctions: recent discoveries and controversies. *Int Rev Cell Mol Biol*, 303, 27-99.
- IVANOV, A. I., PARKOS, C. A. & NUSRAT, A. **2010**. Cytoskeletal regulation of epithelial barrier function during inflammation. *Am J Pathol*, 177, 512-24.
- JOHNSON, L. R. **2012**. *Physiology of the gastrointestinal tract*, Amsterdam, Elsevier/AP.
- KAWEDIA, J. D., NIEMAN, M. L., BOIVIN, G. P., MELVIN, J. E., KIKUCHI, K., HAND, A. R., LORENZ, J. N. & MENON, A. G. **2007**. Interaction between transcellular and paracellular water transport pathways through Aquaporin 5 and the tight junction complex. *Proc Natl Acad Sci U S A*, 104, 3621-6.
- KIRSCHNER, N., ROSENTHAL, R., FURUSE, M., MOLL, I., FROMM, M. & BRANDNER, J. M. **2013**. Contribution of tight junction proteins to ion, macromolecule, and water barrier in keratinocytes. *J Invest Dermatol*, 133, 1161-9.
- KITAJIRI, S., KATSUNO, T., SASAKI, H., ITO, J., FURUSE, M. & TSUKITA, S. **2014**. Deafness in occludin-deficient mice with dislocation of tricellulin and progressive apoptosis of the hair cells. *Biol Open*, 3, 759-66.
- KREUSEL, K. M., FROMM, M., SCHULZKE, J. D. & HEGEL, U. **1991**. Cl⁻ secretion in epithelial monolayers of mucus-forming human colon cells (HT-29/B6). *Am J Physiol*, 261, C574-82.
- KRUG, S. M. **2017**. Contribution of the tricellular tight junction to paracellular permeability in leaky and tight epithelia. *Ann N Y Acad Sci*, 1397, 219-230.
- KRUG, S. M., AMASHEH, M., DITTMANN, I., CHRISTOFFEL, I., FROMM, M. & AMASHEH, S. **2013**. Sodium caprate as an enhancer of macromolecule permeation across tricellular tight junctions of intestinal cells. *Biomaterials*, 34, 275-282.
- KRUG, S. M., AMASHEH, S., RICHTER, J. F., MILATZ, S., GÜNZEL, D., WESTPHAL, J. K., HUBER, O., SCHULZKE, J. D. & FROMM, M. **2009a**. Tricellulin Forms a Barrier to Macromolecules in Tricellular Tight Junctions without Affecting Ion Permeability. *Molecular Biology of the Cell*, 20, 3713-3724.
- KRUG, S. M., BOJARSKI, C., FROMM, A., LEE, I. M., DAMES, P., RICHTER, J. F., TURNER, J. R., FROMM, M. & SCHULZKE, J. D. **2018**. Tricellulin is regulated via interleukin-13-receptor alpha2, affects macromolecule uptake, and is decreased in ulcerative colitis. *Mucosal Immunol*, 11, 345-356.
- KRUG, S. M., FROMM, M. & GÜNZEL, D. **2009b**. Two-path impedance spectroscopy for measuring paracellular and transcellular epithelial resistance. *Biophys J*, 97, 2202-11.
- KRUG, S. M., GÜNZEL, D., CONRAD, M. P., ROSENTHAL, R., FROMM, A., AMASHEH, S., SCHULZKE, J. D. & FROMM, M. **2012**. Claudin-17 forms tight junction channels with distinct anion selectivity. *Cell Mol Life Sci*, 69, 2765-78.

- KRUG, S. M., HAYAISHI, T., IGUCHI, D., WATARI, A., TAKAHASHI, A., FROMM, M., NAGAHAMA, M., TAKEDA, H., OKADA, Y., SAWASAKI, T., DOI, T., YAGI, K. & KONDOH, M. **2017**. Angubindin-1, a novel paracellular absorption enhancer acting at the tricellular tight junction. *J Control Release*, 260, 1-11.
- KRUG, S. M., SCHULZKE, J. D. & FROMM, M. **2014**. Tight junction, selective permeability, and related diseases. *Semin Cell Dev Biol*, 36, 166-76.
- LAGHAEI, R., YU, A. S. & COALSON, R. D. **2016**. Water and ion permeability of a claudin model: A computational study. *Proteins*, 84, 305-15.
- LIANG, G. H. & WEBER, C. R. **2014**. Molecular aspects of tight junction barrier function. *Curr Opin Pharmacol*, 19, 84-9.
- LIU, Y., NIE, H., LIU, C., ZHAI, X., SANG, Q., WANG, Y., SHI, D., WANG, L. & XU, Z. **2017**. Angulin proteins ILDR1 and ILDR2 regulate alternative pre-mRNA splicing through binding to splicing factors TRA2A, TRA2B, or SRSF1. *Sci Rep*, 7, 7466.
- LOHMANN, S., GIAMPIETRO, C., PRAMOTTON, F. M., AL-NUAIMI, D., POLI, A., MAIURI, P., POULIKAKOS, D. & FERRARI, A. **2020**. The Role of Tricellulin in Epithelial Jamming and Unjamming via Segmentation of Tricellular Junctions. *Advanced Science*, 7.
- LOO, D. D. F., ZEUTHEN, T., CHANDY, G. & WRIGHT, E. M. **1996**. Cotransport of water by the Na⁺/glucose cotransporter. *Proceedings of the National Academy of Sciences of the United States of America*, 93, 13367-13370.
- LUETTIG, J., ROSENTHAL, R., BARMAYER, C. & SCHULZKE, J. D. **2015**. Claudin-2 as a mediator of leaky gut barrier during intestinal inflammation. *Tissue Barriers*, 3, e977176.
- MARIANO, C., SASAKI, H., BRITES, D. & BRITO, M. A. **2011**. A look at tricellulin and its role in tight junction formation and maintenance. *Eur J Cell Biol*, 90, 787-96.
- MASUDA, S., ODA, Y., SASAKI, H., IKENOUCHE, J., HIGASHI, T., AKASHI, M., NISHI, E. & FURUSE, M. **2011**. LSR defines cell corners for tricellular tight junction formation in epithelial cells. *J Cell Sci*, 124, 548-55.
- MEINILD, A. K., KLAERKE, D. A., LOO, D. D. F., WRIGHT, E. M. & ZEUTHEN, T. **1998**. The human Na⁽⁺⁾-glucose cotransporter is a molecular water pump. *Journal of Physiology-London*, 508, 15-21.
- MILATZ, S. & BREIDERHOFF, T. **2017**. One gene, two paracellular ion channels-claudin-10 in the kidney. *Pflugers Arch*, 469, 115-121.
- MILATZ, S., KRUG, S. M., ROSENTHAL, R., GÜNZEL, D., MULLER, D., SCHULZKE, J. D., AMASHEH, S. & FROMM, M. **2010**. Claudin-3 acts as a sealing component of the tight junction for ions of either charge and uncharged solutes. *Biochim Biophys Acta*, 1798, 2048-57.
- MINETA, K., YAMAMOTO, Y., YAMAZAKI, Y., TANAKA, H., TADA, Y., SAITO, K., TAMURA, A., IGARASHI, M., ENDO, T., TAKEUCHI, K. & TSUKITA, S. **2011**. Predicted expansion of the claudin multigene family. *FEBS Lett*, 585, 606-12.
- MULLIN, J. M., AGOSTINO, N., RENDON-HUERTA, E. & THORNTON, J. J. **2005**. Keynote review: epithelial and endothelial barriers in human disease. *Drug Discov Today*, 10, 395-408.
- MUTO, S., HATA, M., TANIGUCHI, J., TSURUOKA, S., MORIWAKI, K., SAITOU, M., FURUSE, K., SASAKI, H., FUJIMURA, A., IMAI, M., KUSANO, E., TSUKITA, S. & FURUSE, M. **2010**. Claudin-2-deficient mice are defective in the leaky and cation-selective paracellular permeability properties of renal proximal tubules. *Proc Natl Acad Sci U S A*, 107, 8011-6.

- NAKAMURA, S., IRIE, K., TANAKA, H., NISHIKAWA, K., SUZUKI, H., SAITOH, Y., TAMURA, A., TSUKITA, S. & FUJIYOSHI, Y. **2019**. Morphologic determinant of tight junctions revealed by claudin-3 structures. *Nat Commun*, 10, 816.
- NAKATSU, D., KANO, F., SHINOZAKI-NARIKAWA, N. & MURATA, M. **2019**. Pyk2-dependent phosphorylation of LSR enhances localization of LSR and tricellulin at tricellular tight junctions. *PLoS One*, 14, e0223300.
- NAYAK, G., LEE, S. I., YOUSAF, R., EDELMANN, S. E., TRINCOT, C., VAN ITALLIE, C. M., SINHA, G. P., RAFEEQ, M., JONES, S. M., BELYANTSEVA, I. A., ANDERSON, J. M., FORGE, A., FROLENKOV, G. I. & RIAZUDDIN, S. **2013**. Tricellulin deficiency affects tight junction architecture and cochlear hair cells. *J Clin Invest*, 123, 4036-49.
- O'LEARY, L. F., TOMKO, A. M. & DUPRE, D. J. **2021**. Polarity scaffolds signaling in epithelial cell permeability. *Inflamm Res*.
- OGAMI, A., MIYAZAKI, H., NIISATO, N., SUGIMOTO, T. & MARUNAKA, Y. **2006**. UT-B1 urea transporter plays a noble role as active water transporter in C6 glial cells. *Biochemical and Biophysical Research Communications*, 351, 619-624.
- OTANI, T., NGUYEN, T. P., TOKUDA, S., SUGIHARA, K., SUGAWARA, T., FURUSE, K., MIURA, T., EBNET, K. & FURUSE, M. **2019**. Claudins and JAM-A coordinately regulate tight junction formation and epithelial polarity. *J Cell Biol*, 218, 3372-3396.
- OVERGAARD, C. E., DAUGHERTY, B. L., MITCHELL, L. A. & KOVAL, M. **2011**. Claudins: control of barrier function and regulation in response to oxidant stress. *Antioxid Redox Signal*, 15, 1179-93.
- PRESTON, R. W., T. **2013**. *Lippincott® Illustrated Reviews: Physiology*, Lippincott Williams & Wilkins/Wolters Kluwer.
- RALEIGH, D. R., BOE, D. M., YU, D., WEBER, C. R., MARCHIANDO, A. M., BRADFORD, E. M., WANG, Y., WU, L., SCHNEEBERGER, E. E., SHEN, L. & TURNER, J. R. **2011**. Occludin S408 phosphorylation regulates tight junction protein interactions and barrier function. *J Cell Biol*, 193, 565-82.
- RALEIGH, D. R., MARCHIANDO, A. M., ZHANG, Y., SHEN, L., SASAKI, H., WANG, Y. M., LONG, M. Y. & TURNER, J. R. **2010**. Tight Junction-associated MARVEL Proteins MarvelD3, Tricellulin, and Occludin Have Distinct but Overlapping Functions. *Molecular Biology of the Cell*, 21, 1200-1213.
- RIAZUDDIN, S., AHMED, Z. M., FANNING, A. S., LAGZIEL, A., KITAJIRI, S., RAMZAN, K., KHAN, S. N., CHATTARAJ, P., FRIEDMAN, P. L., ANDERSON, J. M., BELYANTSEVA, I. A., FORGE, A., RIAZUDDIN, S. & FRIEDMAN, T. B. **2006**. Tricellulin is a tight-junction protein necessary for hearing. *American Journal of Human Genetics*, 79, 1040-1051.
- RICHTER, J. F., HILDNER, M., SCHMAUDER, R., TURNER, J. R., SCHUMANN, M. & REICHE, J. **2019**. Occludin knockdown is not sufficient to induce transepithelial macromolecule passage. *Tissue Barriers*, 7, 1612661.
- ROSENTHAL, R., GÜNZEL, D., KRUG, S. M., SCHULZKE, J. D., FROMM, M. & YU, A. S. **2017a**. Claudin-2-mediated cation and water transport share a common pore. *Acta Physiol (Oxf)*, 219, 521-536.
- ROSENTHAL, R., GÜNZEL, D., PIONTEK, J., KRUG, S. M., AYALA-TORRES, C., HEMPEL, C., THEUNE, D. & FROMM, M. **2019**. Claudin-15 forms a water channel through the tight junction with distinct function compared to claudin-2. *Acta Physiol (Oxf)*, e13334.

- ROSENTHAL, R., GÜNZEL, D., THEUNE, D., CZICHOS, C., SCHULZKE, J. D. & FROMM, M. **2017b**. Water channels and barriers formed by claudins. *Ann N Y Acad Sci*, 1397, 100-109.
- ROSENTHAL, R., MILATZ, S., KRUG, S. M., OELRICH, B., SCHULZKE, J. D., AMASHEH, S., GÜNZEL, D. & FROMM, M. **2010**. Claudin-2, a component of the tight junction, forms a paracellular water channel. *J Cell Sci*, 123, 1913-21.
- RUDAN-TASIC, D. & KLOFUTAR, C. **2004**. Osmotic coefficients of aqueous solutions of some poly(oxyethylene) glycols at the freezing point of solution. *Monatshefte Fur Chemie*, 135, 773-784.
- SAITOU, M., FURUSE, M., SASAKI, H., SCHULZKE, J. D., FROMM, M., TAKANO, H., NODA, T. & TSUKITA, S. **2000**. Complex phenotype of mice lacking occludin, a component of tight junction strands. *Mol Biol Cell*, 11, 4131-42.
- SCHINDELIN, J., ARGANDA-CARRERAS, I., FRISE, E., KAYNIG, V., LONGAIR, M., PIETZSCH, T., PREIBISCH, S., RUEDEN, C., SAALFELD, S., SCHMID, B., TINEVEZ, J. Y., WHITE, D. J., HARTENSTEIN, V., ELICEIRI, K., TOMANCAK, P. & CARDONA, A. **2012**. Fiji: an open-source platform for biological-image analysis. *Nat Methods*, 9, 676-82.
- SCHINDELIN, J., RUEDEN, C. T., HINER, M. C. & ELICEIRI, K. W. **2015**. The ImageJ ecosystem: An open platform for biomedical image analysis. *Mol Reprod Dev*, 82, 518-29.
- SCHNOOR, M. & PARKOS, C. A. **2008**. Disassembly of endothelial and epithelial junctions during leukocyte transmigration. *Front Biosci*, 13, 6638-52.
- SCHULZKE, J. D., GITTER, A. H., MANKERTZ, J., SPIEGEL, S., SEIDLER, U., AMASHEH, S., SAITOU, M., TSUKITA, S. & FROMM, M. **2005**. Epithelial transport and barrier function in occludin-deficient mice. *Biochim Biophys Acta*, 1669, 34-42.
- SHEN, L., WEBER, C. R., RALEIGH, D. R., YU, D. & TURNER, J. R. **2011**. Tight junction pore and leak pathways: a dynamic duo. *Annu Rev Physiol*, 73, 283-309.
- SOHET, F., LIN, C., MUNJI, R. N., LEE, S. Y., RUDERISCH, N., SOUNG, A., ARNOLD, T. D., DERUGIN, N., VEXLER, Z. S., YEN, F. T. & DANEMAN, R. **2015**. LSR/angulin-1 is a tricellular tight junction protein involved in blood-brain barrier formation. *Journal of Cell Biology*, 208, 703-711.
- STAEHELIN, L. A. **1973**. Further observations on the fine structure of freeze-cleaved tight junctions. *J Cell Sci*, 13, 763-86.
- STEED, E., RODRIGUES, N. T. L., BALDA, M. S. & MATTER, K. **2009**. Identification of MarvelD3 as a tight junction-associated transmembrane protein of the occludin family. *Bmc Cell Biology*, 10.
- STEWART, M. C., SEO, Y., RAWLINGS, J. M. & CASE, R. M. **1990**. Water permeability of acinar cell membranes in the isolated perfused rabbit mandibular salivary gland. *J Physiol*, 431, 571-83.
- STONE, L. R., GRAY, D. R., REMPLE, K. & BEAUDET, M. P. **2009**. Accuracy and precision comparison of the hemocytometer and automated cell counting methods. *Faseb Journal*, 23.
- SUGAWARA, T., FURUSE, K., OTANI, T. & FURUSE, M. **2020**. Angulin-1 seals tricellular contacts independently of tricellulin and claudins.
- SUZUKI, T. **2013**. Regulation of intestinal epithelial permeability by tight junctions. *Cell Mol Life Sci*, 70, 631-59.
- TAMURA, A., HAYASHI, H., IMASATO, M., YAMAZAKI, Y., HAGIWARA, A., WADA, M., NODA, T., WATANABE, M., SUZUKI, Y. & TSUKITA, S. **2011**. Loss of claudin-15,

- but not claudin-2, causes Na⁺ deficiency and glucose malabsorption in mouse small intestine. *Gastroenterology*, 140, 913-23.
- TAPPENDEN, K. A. **1999**. The human Na⁺ glucose cotransporter is a molecular water pump. *Journal of Parenteral and Enteral Nutrition*, 23, 173-174.
- TOJO, A. & KINUGASA, S. **2012**. Mechanisms of glomerular albumin filtration and tubular reabsorption. *Int J Nephrol*, 2012, 481520.
- TOKUDA, S., HIRAI, T. & FURUSE, M. **2016**. Effects of Osmolality on Paracellular Transport in MDCK II Cells. *PLoS One*, 11, e0166904.
- TOKUDA, S., HIRAI, T. & FURUSE, M. **2017**. Claudin-4 knockout by TALEN-mediated gene targeting in MDCK cells: Claudin-4 is dispensable for the permeability properties of tight junctions in wild-type MDCK cells. *PLoS One*, 12, e0182521.
- TOKUDA, S. & YU, A. S. L. **2019**. Regulation of Epithelial Cell Functions by the Osmolality and Hydrostatic Pressure Gradients: A Possible Role of the Tight Junction as a Sensor. *Int J Mol Sci*, 20.
- TSUKITA, S. & FURUSE, M. **1998**. Overcoming barriers in the study of tight junction functions: from occludin to claudin. *Genes to Cells*, 3, 569-573.
- VAN ITALLIE, C. M. & ANDERSON, J. M. **2006**. Claudins and epithelial paracellular transport. *Annu Rev Physiol*, 68, 403-29.
- VAN ITALLIE, C. M. & ANDERSON, J. M. **2014**. Architecture of tight junctions and principles of molecular composition. *Semin Cell Dev Biol*, 36, 157-65.
- VAN ITALLIE, C. M., FANNING, A. S. & ANDERSON, J. M. **2003**. Reversal of charge selectivity in cation or anion-selective epithelial lines by expression of different claudins. *Am J Physiol Renal Physiol*, 285, F1078-84.
- VAN ITALLIE, C. M., HOLMES, J., BRIDGES, A., GOOKIN, J. L., COCCARO, M. R., PROCTOR, W., COLEGIO, O. R. & ANDERSON, J. M. **2008**. The density of small tight junction pores varies among cell types and is increased by expression of claudin-2. *J Cell Sci*, 121, 298-305.
- VARADARAJAN, S., STEPHENSON, R. E. & MILLER, A. L. **2019**. Multiscale dynamics of tight junction remodeling. *J Cell Sci*, 132.
- VERKMAN, A. S. **2011**. Aquaporins at a glance. *J Cell Sci*, 124, 2107-12.
- WADE, J. B. & KARNOVSKY, M. J. **1974**. The structure of the zonula occludens. A single fibril model based on freeze-fracture. *J Cell Biol*, 60, 168-80.
- WEN, H., HAO, J. & LI, S. K. **2013**. Characterization of human sclera barrier properties for transscleral delivery of bevacizumab and ranibizumab. *J Pharm Sci*, 102, 892-903.
- WETH, A., DIPPL, C., STRIEDNER, Y., TIEMANN-BOEGE, I., VERESHCHAGA, Y., GOLENHOFEN, N., BARTELT-KIRBACH, B. & BAUMGARTNER, W. **2017**. Water transport through the intestinal epithelial barrier under different osmotic conditions is dependent on LI-cadherin trans-interaction. *Tissue Barriers*, 5, e1285390.
- WILMES, A., ASCHAUER, L., LIMONCIEL, A., PFALLER, W. & JENNINGS, P. **2014**. Evidence for a role of claudin 2 as a proximal tubular stress responsive paracellular water channel. *Toxicol Appl Pharmacol*, 279, 163-72.
- WUNSCH, S., GEKLE, M., KERSTING, U., SCHURICHT, B. & OBERLEITHNER, H. **1995**. Phenotypically and karyotypically distinct Madin-Darby canine kidney cell clones respond differently to alkaline stress. *J Cell Physiol*, 164, 164-71.
- YANG, B. & VERKMAN, A. S. **2002**. Analysis of double knockout mice lacking aquaporin-1 and urea transporter UT-B. Evidence for UT-B-facilitated water transport in erythrocytes. *J Biol Chem*, 277, 36782-6.
- YESTE, J., ILLA, X., ALVAREZ, M. & VILLA, R. **2018**. Engineering and monitoring cellular barrier models. *J Biol Eng*, 12, 18.

- YU, A. S., ENCK, A. H., LENCER, W. I. & SCHNEEBERGER, E. E. **2003**. Claudin-8 expression in Madin-Darby canine kidney cells augments the paracellular barrier to cation permeation. *J Biol Chem*, 278, 17350-9.
- ZAK, J., SCHNEIDER, S. W., EUE, I., LUDWIG, T. & OBERLEITHNER, H. **2000**. High-resistance MDCK-C7 monolayers used for measuring invasive potency of tumour cells. *Pflugers Arch*, 440, 179-83.
- ZEISSIG, S., BOJARSKI, C., BUERGEL, N., MANKERTZ, J., ZEITZ, M., FROMM, M. & SCHULZKE, J. D. **2004**. Downregulation of epithelial apoptosis and barrier repair in active Crohn's disease by tumour necrosis factor alpha antibody treatment. *Gut*, 53, 1295-302.
- ZEISSIG, S., BURGEL, N., GÜNZEL, D., RICHTER, J., MANKERTZ, J., WAHNSCHAFFE, U., KROESEN, A. J., ZEITZ, M., FROMM, M. & SCHULZKE, J. D. **2007**. Changes in expression and distribution of claudin 2, 5 and 8 lead to discontinuous tight junctions and barrier dysfunction in active Crohn's disease. *Gut*, 56, 61-72.
- ZEUTHEN, T. **2002**. General models for water transport across leaky epithelia. *Int Rev Cytol*, 215, 285-317.
- ZEUTHEN, T. **2010**. Water-transporting proteins. *J Membr Biol*, 234, 57-73.
- ZEUTHEN, T., GORRAITZ, E., HER, K., WRIGHT, E. M. & LOO, D. D. F. **2016**. Structural and functional significance of water permeation through cotransporters. *Proceedings of the National Academy of Sciences of the United States of America*, 113, E6887-E6894.
- ZEUTHEN, T. & MACAULAY, N. **2012**. Transport of water against its concentration gradient: fact or fiction? *Wiley Interdisciplinary Reviews: Membrane Transport and Signaling*, 1, 373-381.
- ZHOU, T., LU, Y. Z., XU, C. S., WANG, R., ZHANG, L. Y. & LU, P. F. **2020**. Occludin protects secretory cells from ER stress by facilitating SNARE-dependent apical protein exocytosis. *Proceedings of the National Academy of Sciences of the United States of America*, 117, 4758-4769.
- ZHU, S., RAN, J., YANG, B. & MEI, Z. **2017**. Aquaporins in Digestive System. *Adv Exp Med Biol*, 969, 123-130.
- ZUO, L., KUO, W. T. & TURNER, J. R. **2020**. Tight Junctions as Targets and Effectors of Mucosal Immune Homeostasis. *Cellular and Molecular Gastroenterology and Hepatology*, 10, 327-340.

7. Appendices

7.1 Appendix A: Tricellulin and angulin-1 expression (control cells)

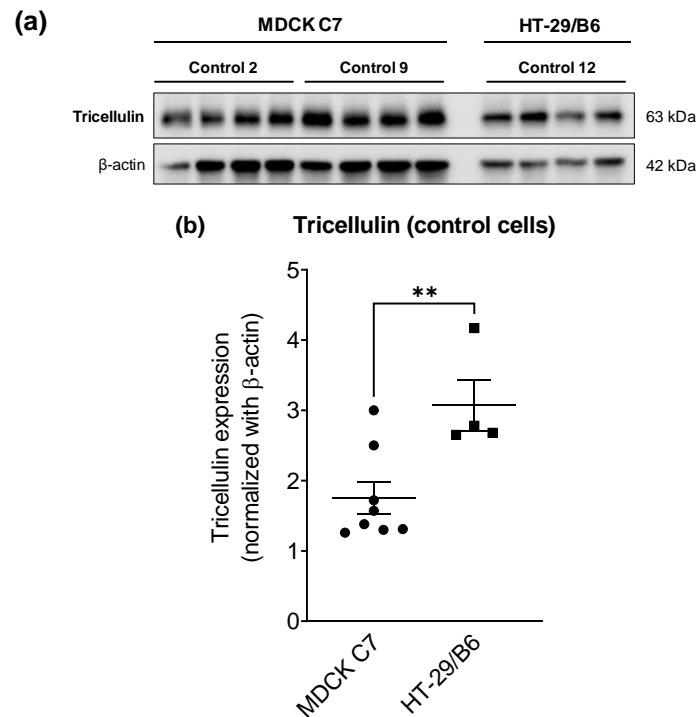


Figure 7-1. Endogenous expression of tricellulin in the epithelial cell lines using in this study. **(a)** Western blot of tricellulin in MDCK C7 and HT-29/B6 control cell lines (15 μ g). **(b)** Densitometric analysis of tricellulin expression using β -actin for normalization. The endogenous expression of tricellulin is higher in HT-29/B6 cells than in MDCK C7 cells. (** $P \leq 0.01$).

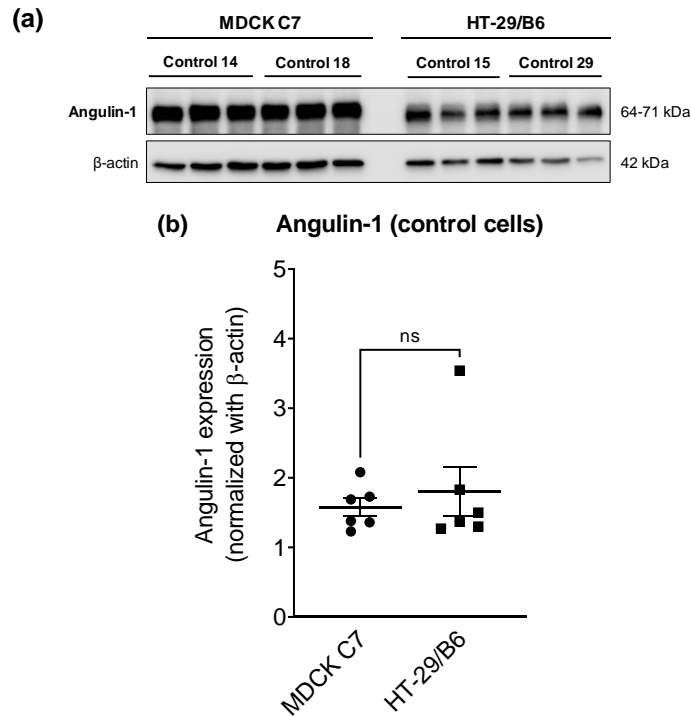


Figure 7-2. Endogenous expression of angulin-1 in the epithelial cell lines using in this study. **(a)** Western blot of tricellulin in MDCK C7 and HT-29/B6 control cell lines (10 μ g). **(b)** Densitometric analysis of angulin-1 expression using β -actin for normalization. The endogenous expression of angulin-1 is similar in both cell lines. (ns: not significant).

7.2 Appendix B: Numerical data

Table 7-1. Characteristics of MDCK C7 tricellulin knockdown clones and the corresponding controls.

		Control 2	KD 23	Control 9	KD 24
Tricellulin expression (%)		100.0 ± 5.6 (n=15)	69.6 ± 5.0 *** (n=13)	100.0 ± 5.2 (n=15)	60.1 ± 4.5 *** (n=15)
TER (kΩ·cm²)		7.4 ± 0.2 (n=24)	3.8 ± 0.2 *** (n=24)	8.2 ± 0.2 (n=24)	1.8 ± 0.1 *** (n=24)
P_{FD4} (×10⁻⁹ cm·s⁻¹)		5.01 ± 1.18 (n=7)	5.56 ± 1.98 (n=8)	3.64 ± 1.03 (n=5)	17.57 ± 3.82 * (n=10)
Osmotic gradient					
PNa⁺ (×10⁻⁶ cm·s⁻¹)		0.10 ± 0.01 (n=9)	0.99 ± 0.13 *** (n=16)	0.11 ± 0.02 (n=7)	1.08 ± 0.13 *** (n=12)
PCl⁻ (×10⁻⁶ cm·s⁻¹)		0.16 ± 0.01 (n=9)	1.10 ± 0.12 *** (n=16)	0.14 ± 0.03 (n=7)	1.16 ± 0.14 *** (n=12)
PNa⁺/PCl⁻		0.81 ± 0.05 (n=9)	0.94 ± 0.04 (n=16)	0.85 ± 0.07 (n=7)	1.02 ± 0.03 (n=12)
Water flux Apical side (μl·h⁻¹·cm⁻²)	100 mM mannitol (100 mOsm)	4.7 ± 0.5 (n=10)	7.1 ± 0.4 ** (n=10)	4.3 ± 0.6 (n=8)	11.0 ± 1.0 *** (n=10)
	37 mM 4-kDa dextran (100 mOsm)	2.6 ± 0.7 (n=8)	5.4 ± 0.8 * (n=8)	1.8 ± 0.5 (n=7)	9.3 ± 1.0 *** (n=10)
	100 mM 4-kDa dextran (900 mOsm)	9.4 ± 1.0 (n=9)	13.0 ± 0.8 * (n=9)	8.4 ± 0.5 (n=8)	32.0 ± 1.4 *** (n=6)
	5.5 mM 40-kDa dextran (100 mOsm)	2.7 ± 0.3 (n=10)	4.7 ± 0.6 ** (n=9)	5.2 ± 1.2 (n=5)	6.3 ± 0.9 (n=6)
Water flux Basolateral side (μl·h⁻¹·cm⁻²)	37 mM 4-kDa dextran (100 mOsm)	-1.6 ± 0.3 (n=10)	-5.5 ± 0.6 *** (n=11)	-1.9 ± 0.4 (n=8)	-4.6 ± 0.7 ** (n=10)

Two tricellulin knockdown clones and their corresponding controls were analyzed in this study (Control 2 and KD 23, Control 9 and KD 24). Data of tricellulin expression have been obtained by densitometric analysis of Western blots using β-actin for normalization. Paracellular permeability measurements for FD4 were carried out in the Ussing chamber. Data of PNa⁺/PCl⁻ permeability and absolute permeabilities for Na⁺ and Cl⁻ (PNa⁺, PCl⁻) were obtained from dilution potential measurements in the Ussing chamber. Water flux measurements were performed in a modified Ussing chamber with water flux induced by different osmotic gradients. Significances refer to respective controls. n number of experiments, *P≤0.05, **P≤0.01, ***P≤0.001.

Table 7-2. Characteristics of HT-29/B6 tricellulin knockdown clones and the corresponding control.

		Control 12	KD 11	KD 17
Tricellulin expression (%)		100.0 ± 8.9 (n=11)	64.6 ± 4.7 *** (n=10)	55.7 ± 6.3 *** (n=10)
TER (kΩ·cm²)		1.44 ± 0.07 (n=12)	0.51 ± 0.03 *** (n=12)	0.54 ± 0.02 *** (n=12)
P_{FD4} (x10⁻⁹ cm·s⁻¹)		21.34 ± 3.80 (n=7)	42.96 ± 2.56 *** (n=7)	67.55 ± 6.54 *** (n=7)
Osmotic gradient				
PNa⁺ (x10⁻⁶ cm·s⁻¹)		0.61 ± 0.10 (n=10)	1.50 ± 0.11 *** (n=10)	2.46 ± 0.30 *** (n=11)
PCl⁻ (x10⁻⁶ cm·s⁻¹)		0.80 ± 0.18 (n=10)	1.84 ± 0.17 ** (n=10)	2.98 ± 0.33 ** (n=11)
PNa⁺/PCl⁻		0.91 ± 0.08 (n=10)	0.92 ± 0.06 (n=10)	0.90 ± 0.08 (n=11)
Water flux Apical side (μl·h⁻¹·cm⁻²)	100 mM mannitol (100 mOsm)	14.9 ± 1.0 (n=8)	14.4 ± 1.7 (n=8)	15.3 ± 0.6 (n=8)
	37 mM 4-kDa dextran (100 mOsm)	19.6 ± 1.2 (n=8)	16.2 ± 1.0 (n=8)	19.1 ± 1.4 (n=8)
	100 mM 4-kDa dextran (900 mOsm)	58.6 ± 2.0 (n=10)	54.0 ± 2.4 (n=9)	56.9 ± 1.6 (n=10)
	2.5 mM albumin (40 mOsm)	8.66 ± 1.14 (n=6)	6.68 ± 0.51 (n=6)	7.24 ± 1.28 (n=6)
Water flux Basolateral side (μl·h⁻¹·cm⁻²)	37 mM 4-kDa dextran (100 mOsm)	-16.4 ± 1.4 (n=10)	-10.5 ± 1.0 * (n=7)	-16.7 ± 0.9 (n=6)

Two tricellulin knockdown clones and its corresponding control were analyzed in this study (Control 12, KD 11 and KD 17). Data of tricellulin expression have been obtained by densitometric analysis of Western blots using β-actin for normalization. Paracellular permeability measurements for FD4 were carried out in the Ussing chamber. Data of PNa⁺/PCl⁻ permeability and absolute permeabilities for Na⁺ and Cl⁻ (PNa⁺, PCl⁻) were obtained from dilution potential measurements in the Ussing chamber. Water flux measurements were performed in a modified Ussing chamber with water flux induced by different osmotic gradients. Significances refer to respective controls. n number of experiments, *P≤0.05, **P≤0.01, ***P≤0.001.

Table 7-3. Characteristics of MDCK C7 angulin-1 knockout clones and the corresponding controls.

		Control 14	Control 18	KO 18	KO 36
Angulin-1 expression (%)		99.2 ± 4.8 (n=9)	100.8 ± 5.1 (n=9)	0.10 ± 0.02 ***,### (n=9)	0.05 ± 0.01 ***,### (n=9)
TER (kΩ·cm²)		7.3 ± 0.2 (n=60)	7.4 ± 0.1 (n=60)	0.96 ± 0.02 ***,### (n=60)	0.53 ± 0.01 ***,### (n=60)
P_{FD4} (×10⁻⁹ cm·s⁻¹)		44.8 ± 8.3 (n=8)	70.4 ± 21.7 (n=8)	144.4 ± 33.6 * (n=8)	76.6 ± 5.5 (n=9)
Osmotic gradient					
P_{FD4} (×10⁻⁹ cm·s⁻¹)		52.4 ± 17.2 (n=10)	58.4 ± 14.1 (n=12)	79.3 ± 22.7 (n=10)	56.5 ± 12.8 (n=10)
Isosmotic					
P_{D4} (×10⁻¹⁰ cm·s⁻¹)		2.41 ± 0.45 (n=8)	3.79 ± 1.17 (n=8)	7.76 ± 1.81 * (n=8)	4.12 ± 0.30 (n=9)
Osmotic gradient					
P_{D4} (×10⁻¹⁰ cm·s⁻¹)		2.82 ± 0.93 (n=10)	3.14 ± 0.76 (n=12)	4.26 ± 1.22 (n=10)	3.12 ± 0.63 (n=11)
Isosmotic					
Water flux	100 mM mannitol (100 mOsm)	2.20 ± 0.28 (n=11)	2.31 ± 0.22 (n=11)	2.92 ± 0.26 (n=12)	2.92 ± 0.38 (n=12)
	37 mM 4-kDa dextran (100 mOsm)	1.76 ± 0.22 (n=11)	1.84 ± 0.17 (n=11)	3.03 ± 0.21 *,# (n=11)	3.68 ± 0.48 ***,### (n=11)
Apical side (μl·h⁻¹·cm⁻²)					
Water flux	100 mM mannitol (100 mOsm)	-2.27 ± 0.37 (n=12)	-1.90 ± 0.20 (n=9)	-2.06 ± 0.37 (n=12)	-2.61 ± 0.35 (n=12)
Basolateral side (μl·h⁻¹·cm⁻²)					

Two angulin-1 knockout clones and their corresponding controls were analyzed in this study (Control 14, Control 18, KO 18 and KO 36). Data of angulin-1 expression have been obtained by densitometric analysis of Western blots using β-actin for normalization. Paracellular permeability measurements for FD4 were carried out in the Ussing chamber. Water flux measurements were performed in a modified Ussing chamber with water flux induced by different osmotic gradients. Significances refer to respective controls. n number of experiments, *P≤0.05, **P≤0.01, ***P≤0.001 with regard to control 14 and #P≤0.05, ##P≤0.01, ###P≤0.001 with regard to control 18.

Table 7-4. Characteristics of HT-29/B6 angulin-1 knockout clones and the corresponding controls.

		Control 15	Control 29	KO 12	KO 32
Angulin-1 expression (%)		94.3 ± 3.8 (n=9)	105.7 ± 5.4 (n=9)	3.2 ± 0.6 ***,### (n=9)	0.2 ± 0.1 ***,### (n=9)
TER (kΩ·cm²)		1.06 ± 0.02 (n=43)	1.75 ± 0.08 (n=43)	0.57 ± 0.03 ***,### (n=43)	0.28 ± 0.01 ***,### (n=43)
P_{FD4} (×10⁻⁹ cm·s⁻¹)		26.7 ± 4.4 (n=6)	15.7 ± 2.0 (n=6)	33.1 ± 3.6 (n=6)	54.0 ± 7.5 **,### (n=6)
Osmotic gradient					
P_{FD4} (×10⁻⁹ cm·s⁻¹)		41.2 ± 5.1 (n=9)	14.1 ± 1.8 (n=9)	82.7 ± 8.0 ***,### (n=9)	133.6 ± 7.0 ***,### (n=9)
Isosmotic					
P_{D4} (×10⁻¹⁰ cm·s⁻¹)		4.28 ± 1.12 (n=6)	2.46 ± 0.57 (n=6)	4.85 ± 0.95 (n=6)	8.25 ± 2.00 # (n=6)
Osmotic gradient					
P_{D4} (×10⁻¹⁰ cm·s⁻¹)		4.08 ± 0.50 (n=9)	1.40 ± 0.18 (n=9)	8.19 ± 0.80 ***,### (n=9)	13.23 ± 0.69 ***,### (n=9)
Isosmotic					
Water flux					
Apical side	100 mM mannitol				
(μl·h⁻¹·cm⁻²)	(100 mOsm)	14.1 ± 0.6 (n=8)	13.8 ± 0.6 (n=8)	13.9 ± 0.5 (n=8)	13.1 ± 0.7 (n=8)
Water flux					
Basolateral side	100 mM mannitol				
(μl·h⁻¹·cm⁻²)	(100 mOsm)	-15.0 ± 0.7 (n=8)	-15.4 ± 0.5 (n=8)	-14.4 ± 0.7 (n=8)	-13.2 ± 0.9 (n=8)

Two angulin-1 knockout clones (KO 12 and KO 32 and their corresponding controls (Control 15, Control 29) were analyzed in this study). Data of angulin-1 expression have been obtained by densitometric analysis of Western blots using β-actin for normalization. Paracellular permeability measurements for FD4 were carried out in the Ussing chamber. Water flux measurements were performed in a modified Ussing chamber with water flux induced by different osmotic gradients. Significances refer to respective controls. n number of experiments, *P≤0.05, **P≤0.01, ***P≤0.001 with regard to control 15 and #P≤0.05, ##P≤0.01, ###P≤0.001 with regard to control 29.

7.3 Appendix C: Topology data

Table 7-5. Morphometric comparison of MDCK C7 and HT-29/B6 cells as models for tight and intermediate-tight epithelia before and after tricellulin knockdown.

	Tricellulin knockdown						
	MDCK C7				HT-29/B6		
	Control 2	KD 23	Control 9	KD 24	Control 12	KD 11	KD 17
n	8	8	10	9	7	7	7
Analyze area (μm^2)	20289	20842	26564	22834	19818	16415	16795
Analyze area (10^{-4} cm^2)	2.0	2.1	2.7	2.3	2.0	1.6	1.7
Counted cells	198	158	209	299	615	739	653
Average cell surface (μm^2)	102	132	127	76	32	22	26
Cell density (10^6 cells/cm^2)	1.0	0.8	0.8	1.3	3.1	4.5	3.9
Total TJ length (μm)	8842	8024	10288	11560	14352	14459	13703
Total TJ length (m/cm^2)	44	38	39	51	72	88	82
TJ length/cell (μm)	89	102	98	77	47	39	42
Counted tTJ	320	210	339	534	915	1617	1381
tTJ density (10^6 tTJ/cm^2)	1.6	1.0	1.3	2.3	4.6	9.9	8.2
tTJ/cell (x3)	5	4	5	5	4	7	6
tTJ/cell (x4)	6	5	6	7	6	9	8

Morphometric parameters of MDCK C7 and HT-29/B6 cells were obtained from occludin and ZO-1 stained cells, respectively, similar to an earlier described approach (Krug, 2017). Cell numbers were counted in each analyzed area, giving average cell surface area and the cell density. Total length of TJs within the analyzed areas was measured and normalized to m/cm^2 . As each bicellular TJ is shared by two cells, TJ length per cell was doubled. For calculation of the TJ length/cell, total length in m/cm^2 was calculated from cell density. Tricellular contacts were counted and normalized to within the analyzed area. As each tricellular contact is shared by three cells and very seldom by four contacts, the tricellular contact number was tripled and quadrupled to obtain the average tricellular contact number per cell.

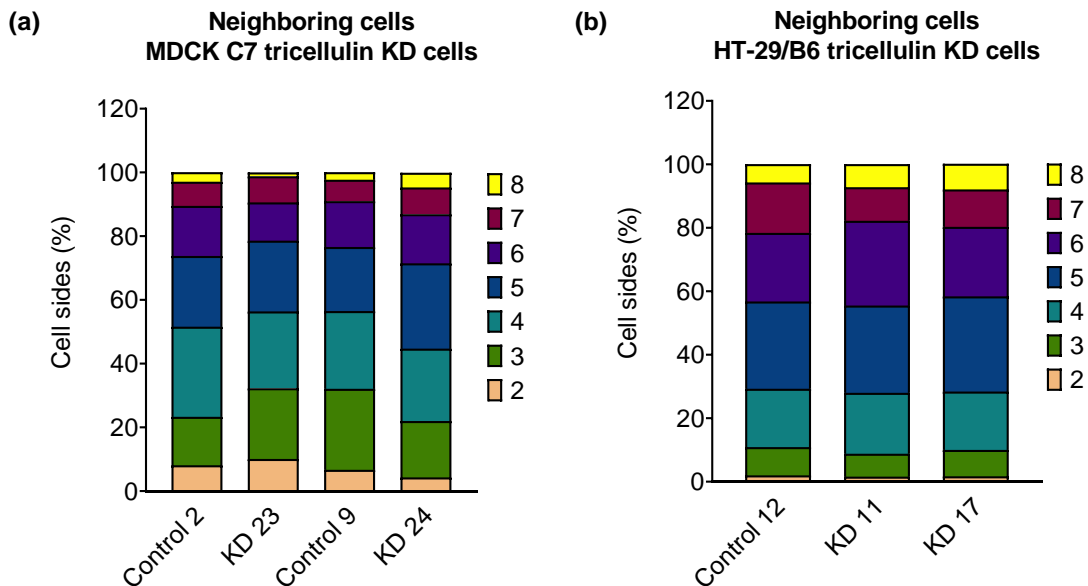


Figure 7-3. Cell geometry analysis. Neighboring cell analysis in tricellulin knockdown on **(a)** MDCK C7 and **(b)** HT-29/B6 cell lines in comparison with their vector controls. In MDCK C7 cells, most cells have between three and six vertices, which can be translated into the number of tTJ. In contrast, in HT-29/B6 cells, most of the cells have between four and six neighbors. In both cell lines, tricellulin KD did not modify the number of vertices (tTJs) in comparison with their controls.

Table 7-6. Morphometric comparison of MDCK C7 and HT-29/B6 cells as models for tight and intermediate-tight epithelia before and after angulin-1 knockout.

	Angulin-1 knockout							
	MDCK C7				HT-29/B6			
	Control 14	Control 18	KO 18	KO 36	Control 15	Control 29	KO 12	KO 32
n	3	3	4	5	4	5	5	5
Analyze area (μm^2)	5410	5547	10820	13455	11139	12792	13360	13667
Analyze area (10^{-4} cm^2)	0.5	0.6	1.1	1.3	1.1	1.3	1.3	1.4
Counted cells	63	66	131	202	243	426	419	384
Average cell surface (μm^2)	86	84	83	67	46	30	32	36
Cell density (10^6 cells/cm^2)	1.2	1.2	1.2	1.5	2.2	3.3	3.1	2.8
Total TJ length (μm)	2497	2615	5134	7059	6765	9904	9918	9553
Total TJ length (m/cm^2)	46	47	47	52	61	77	74	70
TJ length/cell (μm)	79	79	78	70	56	46	47	50
Counted tTJ	107	114	197	369	558	677	756	651
tTJ density (10^6 tTJ/cm^2)	2.0	2.1	1.8	2.7	5.0	5.3	5.7	4.8
tTJ/cell (x3)	5	5	5	5	7	5	5	5
tTJ/cell (x4)	7	7	6	7	9	6	7	7

Morphometric parameters of MDCK C7 and HT-29/B6 cells were obtained from occludin and ZO-1 stained cells, respectively, similar to an earlier described approach (Krug, 2017). Cell numbers were counted in each analyzed area, giving average cell surface area and the cell density. Total length of TJs within the analyzed areas was measured and normalized to m/cm^2 . As each bicellular TJ is shared by two cells, TJ length per cell was doubled. For calculation of the TJ length/cell, total length in m/cm^2 was calculated from cell density. Tricellular contacts were counted and normalized to within the analyzed area. As each tricellular contact is shared by three cells and very seldom by four contacts, the tricellular contact number was tripled and quadrupled to obtain the average tricellular contact number per cell.

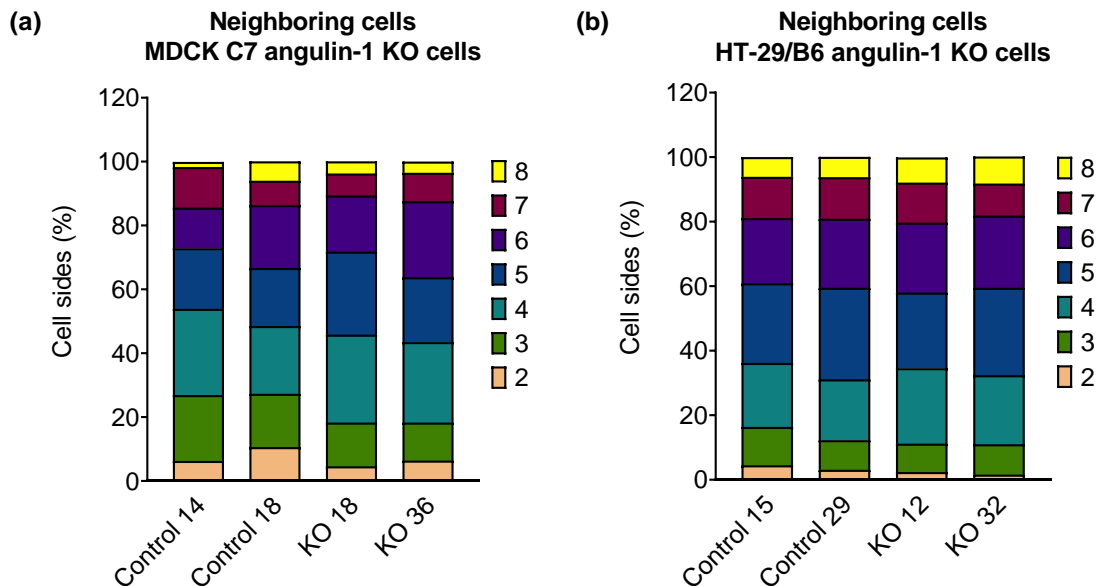


Figure 7-4. Cell geometry analysis. Neighboring cell analysis in angulin-1 knockout on **(a)** MDCK C7 and **(b)** HT-29/B6 cell lines in comparison with their vector controls. In MDCK C7 cells, most cells have between four and six vertices, which can be translated into the number of tTJ. In contrast, in HT-29/B6 cells, most of the cells have between three and six neighbors. In both cell lines, angulin-1 KO did not modify the number of vertices (tTJs) in comparison with their controls.

Table 7-7. Macros for segmentation of epithelial cells depending on the resolution of the fluorescence images obtained.

	Macro
Epithelial Cells - Bad resolution	<pre> //-----macro start original = getTitle(); run("8-bit"); run("Pseudo flat field correction", "blurring=40"); close(original + "_background"); selectWindow(original); run("Median...", "radius=1"); run("Select None"); run("Duplicate...", "title=Background"); background = getTitle(); run("Median...", "radius=40"); imageCalculator("Subtract", original, background); selectWindow(original); run("Enhance Contrast...", "saturated=1.5 normalize"); run("Auto Threshold", "method=Li white"); run("EDM Binary Operations", "iterations=2 operation=close"); run("Analyze Particles...", "size=50-Infinity show=Masks in_situ"); run("Median...", "radius=1"); run("Invert"); run("EDM Binary Operations", "iterations=11 operation=close"); //run("Watershed"); run("Adjustable Watershed", "tolerance=18"); //to be able to use this install the adjustable watershed from https://imagejdocu.tudor.lu/plugin/segmentation/adjustable_watershed/start run("Voronoi"); setOption("BlackBackground", true); setThreshold(1, 255); run("Convert to Mask"); resetThreshold(); run("Invert"); close(background); selectWindow(original); //now run the Neighbor Analysis from the BioVoxel Toolbox to color code your cells //-----macro end </pre>
Epithelial Cells - Regular resolution	<pre> //-----macro start original = getTitle(); run("8-bit"); run("Pseudo flat field correction", "blurring=40"); close(original + "_background"); selectWindow(original); run("Median...", "radius=1"); run("Select None"); run("Duplicate...", "title=Background"); background = getTitle(); run("Median...", "radius=40"); imageCalculator("Subtract", original, background); selectWindow(original); run("Enhance Contrast...", "saturated=1.5 normalize"); run("Auto Threshold", "method=Li white"); run("EDM Binary Operations", "iterations=2 operation=close"); run("Analyze Particles...", "size=50-Infinity show=Masks in_situ"); run("Median...", "radius=3"); run("Invert"); run("EDM Binary Operations", "iterations=11 operation=close"); //run("Watershed"); run("Adjustable Watershed", "tolerance=12"); //to be able to use this install the adjustable watershed from https://imagejdocu.tudor.lu/plugin/segmentation/adjustable_watershed/start run("Voronoi"); setOption("BlackBackground", true); setThreshold(1, 255); </pre>

```
run("Convert to Mask");
resetThreshold();
run("Invert");
```

```
close(background);
selectWindow(original);
```

```
//now run the Neighbor Analysis from the BioVoxel Toolbox to color code your cells
```

```
//-----macro end
```

```
//-----macro start
```

**Epithelial Cells -
Normal resolution**

```
original = getTitle();
run("8-bit");
run("Pseudo flat field correction", "blurring=40");
close(original + "_background");
selectWindow(original);
run("Median...", "radius=1");
run("Select None");
run("Duplicate...", "title=Background");
background = getTitle();
run("Median...", "radius=40");
imageCalculator("Subtract", original, background);
selectWindow(original);
run("Enhance Contrast...", "saturated=1.5 normalize");
run("Auto Threshold", "method=Li white");
run("EDM Binary Operations", "iterations=2 operation=close");
run("Analyze Particles...", "size=50-Infinity show=Masks in_situ");
run("Median...", "radius=2");
run("Invert");
run("EDM Binary Operations", "iterations=8 operation=close");
//run("Watershed");
run("Adjustable Watershed", "tolerance=12");
```

```
//to be able to use this install the adjustable watershed from
```

```
https://imagejdocu.tudor.lu/plugin/segmentation/adjustable\_watershed/start
```

```
run("Voronoi");
setOption("BlackBackground", true);
setThreshold(1, 255);
run("Convert to Mask");
resetThreshold();
run("Invert");
```

```
close(background);
selectWindow(original);
```

```
//now run the Neighbor Analysis from the BioVoxel Toolbox to color code your cells
```

```
//-----macro end
```

```
//-----macro start
```

**Epithelial Cells -
Good resolution**

```
original = getTitle();
run("8-bit");
run("Pseudo flat field correction", "blurring=40");
close(original + "_background");
selectWindow(original);
run("Median...", "radius=1");
run("Select None");
run("Duplicate...", "title=Background");
background = getTitle();
run("Median...", "radius=40");
imageCalculator("Subtract", original, background);
selectWindow(original);
run("Enhance Contrast...", "saturated=1.5 normalize");
run("Auto Threshold", "method=Li white");
run("EDM Binary Operations", "iterations=2 operation=close");
run("Analyze Particles...", "size=50-Infinity show=Masks in_situ");
run("Median...", "radius=5");
run("Invert");
run("EDM Binary Operations", "iterations=4 operation=close");
//run("Watershed");
run("Adjustable Watershed", "tolerance=4");
```

```
//to be able to use this install the adjustable watershed from
```

```
https://imagejdocu.tudor.lu/plugin/segmentation/adjustable_watershed/start
run("Voronoi");
setOption("BlackBackground", true);
setThreshold(1, 255);
run("Convert to Mask");
resetThreshold();
run("Invert");

close(background);
selectWindow(original);

//now run the Neighbor Analysis from the BioVoxel Toolbox to color code your cells
//-----macro end
```

Copyright©, Jan Brocher/BioVoxel. All rights reserved. All Macros/Plugins were written by Jan Brocher/BioVoxel and modified according to the need of this thesis.

7.4 Appendix D: List of publications

7.4.1 Scientific articles

Ayala-Torres C, Krug SM, Schulzke JD, Rosenthal R*, Fromm M* (*shared last authorship) (2019)

Tricellulin effect on paracellular water transport.

Int. J. Mol. Sci. 20(22): 5700 (15 pages)

Rosenthal R, Günzel D, Piontek J, Krug SM, **Ayala-Torres C**, Hempel C, Theune D, Fromm M (2019)

Claudin-15 forms a water channel through the tight junction with distinct function compared to claudin-2.

Acta Physiol. 228(1): e13334 (15 pages)

7.4.2 Presentations at scientific conferences

Carlos Ayala-Torres, Rita Rosenthal, Susanne M. Krug, Jörg-Dieter Schulzke and Michael Fromm

Contribution of tricellulin to paracellular water permeability in two epithelial cell lines of different tightness (Poster)

Experimental Biology (EB) 2020 – Online version, 4th – 7th April 2020

San Diego, California, USA

Carlos Ayala-Torres, Rita Rosenthal, Susanne M. Krug, Jörg-Dieter Schulzke and Michael Fromm

Contribution of tricellulin to paracellular water permeability in epithelia of different tightness (Poster)

Europhysiology 2018, 14th – 16th September 2018

The QEII Centre, London, UK

Declaration of Authorship

I hereby certify that this thesis first submitted has been composed by me and is based on my own work, unless specified otherwise. No other person's work has been used without acknowledgement in this thesis. All references and literal extracts have been cited, and all sources of information, including graphs and data sets, have been specifically acknowledged.

December 2020, Berlin, Germany

Carlos Mario Ayala Torres